Harnessing P450 Enzymes as Biocatalysts for Selective C-H Bond Hydroxylation

Joel Hoong Zhang Lee

Supervisors:

Assoc. Prof Stephen G. Bell

Prof. Andrew D. Abell

Thesis submitted for the degree of Master of Philosophy

THE UNIVERSITY of ADELAIDE

August 9, 2018

School of Physical Sciences

Contents

Abstract

The cytochrome P450 enzyme, CYP101B1 from *Novosphingobhium aromaticivorans* can catalyse the highly efficient and regioselective oxidation of norisoprenoids. However, it has lower affinity towards hydrophobic substrates. Site-saturation mutagenesis of its Histidine85 (H85) residue was carried out as the equivalent tyrosine residue in the sequence of the closely related $P450_{cam}$ enzyme (CYP101A1 from a *Pseudomonas* species) provides hydrophilic interactions with camphor. Mutagenesis of the H85 residue to a phenylalanine residue (H85F) has been reported to increase the enzyme's affinity towards small hydrophobic molecules. Eleven mutants that differ at position 85 were successfully produced and these were incorporated into two separate plasmid vectors for enzyme purification and whole-cell studies. Whole-cell oxidation of the CYP101B1 mutants with various substrates that include norisoprenoids, terpenoids, and hydrophobic molecules of varying sizes were carried out to screen if the mutants have activity towards these substrates. A number of the mutants such as H85V, H85S, H85G and H85I displayed increased product formation and altered product selectivity but most were not as effective as the WT or the H85F mutant in oxidising hydrophobic molecules.

Purification of both the H85A and H85G mutants was also carried out and ferrous-CO assays showed they were functional P450 enzymes. *In vitro* studies with these two mutants demonstrated they have poorer binding affinity and oxidation activity towards phenylcyclohexane when compared to the WT enzyme and the H85F variant.

A mutant library of rationally designed $P450_{cam}$ variants which have been created to increase the affinity and oxidation activity towards the monoterpene, α-pinene, was tested with other monoterpenoids and related compounds. The mutations in this library were incorporated at residues in the active site. The library was screened using a whole-cell system with five substrates of similar size and chemical functionality to camphor and pinene. These were fenchone, fenchyl acetate, isophorone, 1,8-cineole and 1,4-cineole. The screening of these mutants displayed higher selectivity for the oxidations of these substrates compared to the WT. The metabolites were produced in larger quantities for isolation and identification. Fenchone and fenchyl acetate oxidation by different mutants generated a mixture of the C5, C6 and C7 hydroxylation products with the *exo* face being preferred. Isophorone oxidation by the mutants F87W-Y96F-L244A-V247L (WFAL) and F87W-Y96F-L244A (WFA) gave selective formation of (4*R*)-hydroxyisophorone. This product is valuable as a flavouring agent. Several of the mutants also selectively oxidised 1,8- and 1,4-cineole at different C-H bonds. A

desaturation product was observed at the isopropyl group during 1,4-cineole oxidation.

Concurrent studies of isophorone and cineole oxidation by mutants of another enzyme ($P450_{BM3}$) also gave selective transformation of both substrates with high yields in whole-cell turnover systems. The whole-cell oxidation of isophorone and cineole by these $P450_{cam}$ and $P450_{BM3}$ mutants were compared to determine if oxidation activity of the two enzymes were similar. For the isophorone turnovers, the $P450_{cam}$ mutants resulted in greater product yields over the $P450_{BM3}$ mutants, whereby most if not all substrate added was converted to product. In contrast, cineole oxidation by the $P450_{BM3}$ mutants gave higher yields over the $P450_{cam}$ mutants.

As well as oxidising norisoprenoids, CYP101B1 displayed efficient and selective oxidation of monoterpenoid acetates. $P450_{BM3}$ mutants have also been developed to oxidise terpenes and norisoprenoids. A selection of flavour and fragrance compounds with structures similar to norisoprenoids and monoterpenoid acetates were screened both *in vitro* and *in vivo* with CYP101B1 and $P450_{BM3}$-A74G/F87V/L188Q (GVQ). CYP101B1 displayed selective oxidation towards norisoprenoids such as δ- and α-damascone. $P450_{BM3}$-GVQ also showed selective oxidation for acetate compounds such as cuminyl acetate and verdyl acetate. Larger scale turnovers with these two P450 enzymes were carried out and the metabolites were identified. CYP101B1 oxidises norisoprenoids at the ring C3/C4 position and this was preserved in the oxidation of δ- and α-damascone. α-Damascone oxidation by CYP101B1 formed both C3 hydroxy diastereomers and a further oxidation product at the same position. δ-Damascone oxidation occurred across its ring C3/C4 alkene to form the epoxide. $P450_{BM3}$-GVQ oxidised both cuminyl and verdyl acetate at regions distant from the acetate group. Cuminyl acetate oxidation by this mutant also generated a desaturation product at the isopropyl group.

Declaration

I certify that this work contains no material which has been accepted for the award of any other degree or diploma in my name, in any university or other tertiary institution and, to the best of my knowledge and belief, contains no material previously published or written by another person, except where due reference has been made in the text. In addition, I certify that no part of this work will, in the future, be used in a submission in my name, for any other degree or diploma in any university or other tertiary institution without the prior approval of the University of Adelaide and where applicable, any partner institution responsible for the joint-award of this degree.

I give consent to this copy of my thesis, when deposited in the University Library, being made available for loan and photocopying, subject to the provisions of the Copyright Act 1968.

I also give permission for the digital version of my thesis to be made available on the web, via the University's digital research repository, the Library Search and also through web search engines, unless permission has been granted by the University to restrict access for a period of time.

I acknowledge the support I have received for my research through the provision of an Australian Government Research Training Program Scholarship.

Joel Lee

August 9, 2018

Acknowledgements

Many thanks firstly to Associate Professor Stephen Bell for his tireless dedication towards supervising this project and his endless patience in drafting this thesis. Thanks also to Professor Andrew Abell and Associate Professor Tara Pukala for always having an open and welcoming door throughout my time with this project.

I would also like to thank my comrades in the Bell group both in Lab 7 (Tom Coleman, Raihan Sarkar and Matthew Podgorski) and Lab 8 (Stella Child, Sherry Dezvarei, Ian Lau and Natasha Maddigan) for their kindness and fun times over the past two years. I wish all of you the best in your future endeavours. Special thanks towards Tom Coleman, Eunice Lee and Aaron Day for their assistance in drafting this thesis.

Finally, if you are reading this, thank you for taking the time to do so.

Abbreviations

DCM	Dichloromethane
DTT	Dithiothreitol
E.coli	*Escherichia Coli*
EMM	*E.coli* minimal media
EtOH	Ethanol
EtOAc	Ethyl Acetate
FA	Fenchyl Acetate
GC-MS	Gas Chromatography-Mass Spectrometry
GVQ	$P450_{BM3}$-A74G/F87V/L188Q
HCl	Hydrochloric Acid
HPLC	High Performance Liquid Chromatography
HS	High Spin
K_2CO_3	Potassium Carbonate
IPTG	Isopropyl β-D-thiogalactopyranoside
IPA	Isopropyl Alchohol
IS	Internal Standard
LB	Luria-Bertani Medium
LF	$P450_{cam}$-F87L-Y96F
LS	Low Spin
PDB	Protein Data Bank
MeOH	Methanol
NADH	Reduced form of Nicotinamide Adenine Dinucleotide
$NaHCO_3$	Sodium Bicarbonate
NMR	Nuclear Magnetic Resonance
RLYFGVQ	$P450_{BM3}$R47L-Y51F-A74G-F87V-L188Q
RLYFFAIP	$P450_{BM3}$R47L-Y51F-F87A-I401P
SOC	Super Optimal Broth with Catabolite Repression
WT	Wild-Type enzyme
WFA	$P450_{cam}$-F87W-Y96F-L244A
WFAL	$P450_{cam}$-F87W-Y96F-L244A-V247L
WFL	$P450_{cam}$-F87W-Y96F-V247L
TIC	Total Ion Count
VFL	$P450_{cam}$-F87V-Y96F-V247L

List of Figures

List of Tables

This page is intentionally left blank

1 Introduction

1.1 Cytochrome P450s

P450 enzymes are a ubiquitous class of enzymes that exist in all domains of life. They are a superfamily of heme monooxygenases and were first discovered in 1958 by Garfinkel[1] and Klingenberg[2] within pig and rat liver microsomes, respectively. The genomes of species from across all domains in the tree of life contain more than 300,000 cytochrome P450 sequences that further highlights the abundance of P450s in living organisms.[3]

The term P450 was coined after its red pigmentation (P) and the distinctive 450 nm absorption peak generated when the enzyme is reduced and carbon monoxide is added (450).[4] The large number of P450 enzymes has warranted the development of nomenclature to study and categorise them. The members in this superfamily of enzymes are first grouped into a specific family and then subfamily. Family members share $\geq$ 40 % amino acid sequence similarity and subfamily members share $\geq$ 55 % similarity.[5] P450 enzymes are designated by the prefix CYP, that indicates it is a P450 enzyme, followed by its family number. For example, CYP1 - CYP9 are mammalian P450 families, CYP71 - CYP99 are for plant-based P450s and CYP101 to CYP281 are for the bacterial families.[3] Following the family number, its subfamily is denoted by the subsequent letter and number.[5] For example, CYP101A1 from *Pseudomonas putida*,[6] is a member of family 101 and is the first member identified for subfamily A of this family.

1.2 Structure and Catalytic Cycle of P450s

P450 enzymes are involved in a large number of biological oxidative transformations that include, but are not limited to, steroid synthesis and xenobiotic metabolism in eukaryotic organisms. P450 enzymes are responsible for 75 % of all phase 1 metabolism of known human pharmaceuticals.[7,8] These enzymes are monooxygenases that insert a single oxygen atom from atmospheric dioxygen into an inert C-H bond (Equation 1). This occurs often in a regio- and stereospecific manner.

$$\text{R-H} + \text{O}_2 + \text{H}^+ + \text{NAD(P)H} \rightarrow \text{R-OH} + \text{H}_2\text{O} + \text{NAD(P)}^+ \quad (1)$$

P450 enzymes contain an iron protoporphyrin IX (heme) centre that is bound covalently to the rest of the enzyme via a proximal cysteine thiolate ligand.[9,10] The bound thiolate ligand is critical for enzymatic activity and contributes to the unique Soret absorption peak of the CO-reduced enzyme (450 nm).[10,11] The distal side of the heme centre has an iron bound water ligand that is generally observed in substrate free crystal structures of the enzyme superfamily.[9]

The distal water ligand bound to the ferric centre represents the resting state of the P450 enzyme (I) (Figure 1). In most instances, the binding of a substrate causes the water ligand to dissociate and initiates the catalytic cycle. This step is accompanied by a shift in the iron complex from low spin (LS) to high spin (HS) (II). The transfer of the first electron sourced from NADPH or NADH to the iron centre can then occur to produce the ferrous form of the enzyme (III). The binding of molecular oxygen to the free distal site forms the ferrous-dioxy complex (IV).[9]

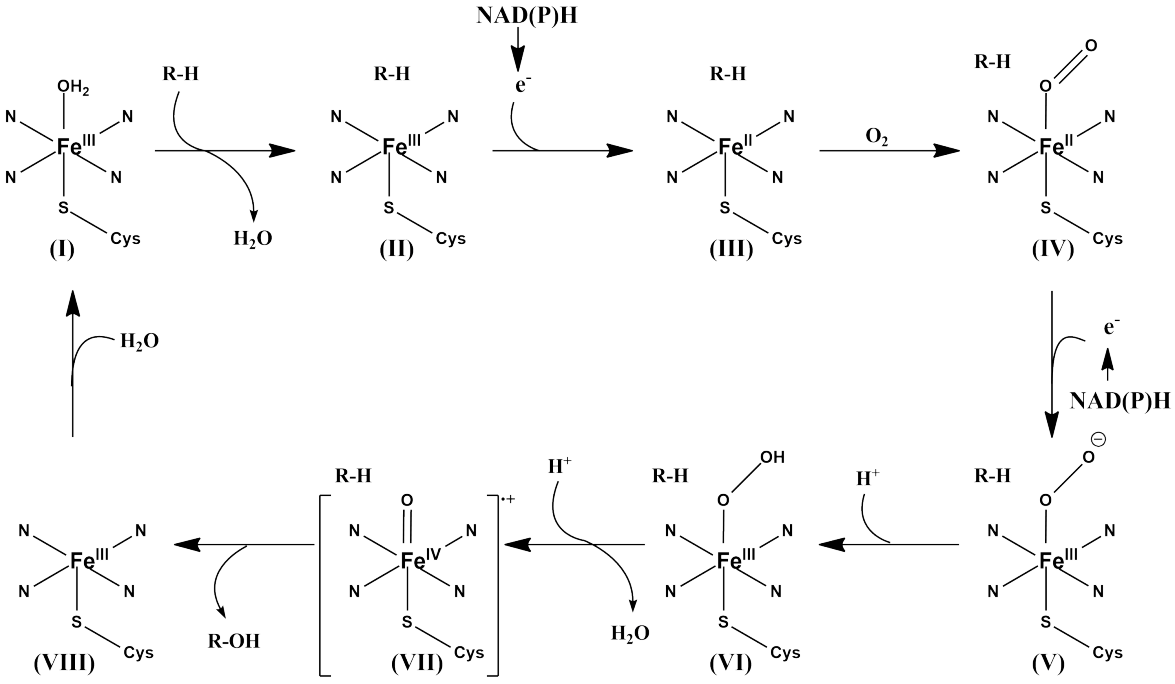

Figure 1: The P450 Catalytic Cycle.

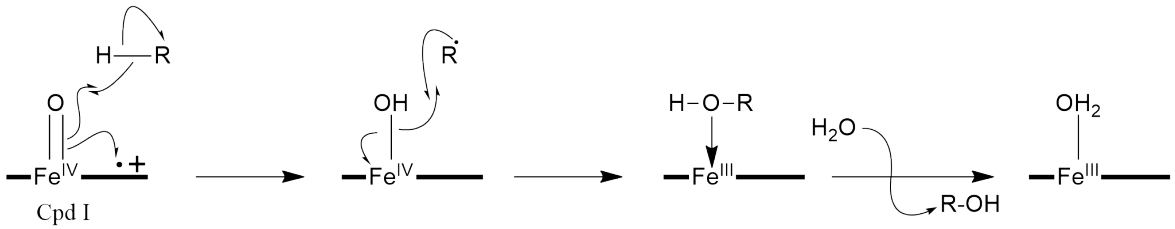

Figure 2: Radical Rebound Mechanism of P450s.

The transfer of a second electron to complex IV forms the ferric-peroxy anion complex (V) . Protonation of complex V forms the ferric hydroperoxo-complex (VI). This sets

the stage for the dioxygen bond to undergo heterolytic cleavage to form the ferryl-oxo porphyrin-cation radical (VII).[12] This highly reactive species is known as Compound I and is the reactive intermediate which undergoes a radical rebound mechanism to introduce a single oxygen atom within the substrate (Figure 2).[8] The oxidised substrate then dissociates from the enzyme (VIII) and a water molecule binds to the iron centre to reform the ferric resting state (I). It has been observed that this catalytic cycle is largely conserved for all members of this superfamily.[13] Specific substrate selectivity and chemical activity of individual P450s arises from the sequential and structural differences in regions around the active site.[14]

As seen in Figure 1, the catalytic cycle requires the transfer of electrons that are sourced from NADH or NADPH using electron transfer systems.[15] These systems consist of electron transfer proteins and the characterised proteins have been divided into ten classes.[16] For example, class I systems which are associated with mitochondrial and bacterial P450s possess two separate redox protein partners.[15] These are an iron-sulfur containing ferredoxin and a flavin containing reductase (FAD). The electron is first received by the reductase, subsequently transferred to the ferredoxin and is finally transferred again to the target P450.[17] P450s that belong to the Class I grouping include CYP101A1 ($P450_{cam}$) and CYP101B1 from *Novosphingobium aromaticivorans.*[18,19]

Class II systems are commonly found in eukaryotes such as P4501A1 in rats. This uses a single membrane-bound NADPH-cytochrome P450 with both FAD and flavin mononucleotide (FMN) domains.[16] Class III systems are similar to class I systems but has a flavodoxin protein similar to FMN instead of the iron-sulfur ferredoxin.[16] $P450_{cin}$ (CYP176A1) from *Citrobacter braakii* utilises this system.[20] Class VIII systems are catalytically self-sufficient enzymes where the P450 is fused to a reductase, which has FAD and FMN domains. CYP102A1 ($P450_{BM3}$) from *Bacillus megaterium* belongs to Class VIII, which are similar to the class II eukaryiotic systems, using both FAD and FMN domains.[16,21,22]

1.3 Utility of P450s for Biocatalytic Synthesis

The ability of P450 enzymes to selectively oxidise a single C-H bond, often in a regio- and stereospecific manner, has drawn significant interest amongst synthetic chemists. Conventional chemistry employs harsh or toxic reactants to achieve the same transformations but in low product yields and with undesirable side-products.[23] The P450 enzymes however can catalyse their reactions under mild ambient conditions utilising molecular oxygen which is abundant, inexpensive and non-toxic to the environment.[24]

The field of bioremediation could also make use of P450s, whereby pollutants generated by industrial processes are metabolised and degraded by these enzymes to provide a safe method for their disposal into the environment.[25–27] The other application that has generated significant interest is using P450 enzymes for the biocatalytic production of fine chemicals.[28–32]

One limitation of using enzymes is that the wild-type (WT) form may have little or no affinity and activity towards their non-physiological substrates. This is an impediment to their use for compound oxidation to yield desirable products. To address this issue, protein engineering of P450 enzymes has been carried out to improve their activity towards non-physiological substrates.

1.4 $P450_{cam}$ Mutagenesis and Biocatalytic Studies

$P450_{cam}$ from the bacterium *Pseudomonas putida* catalyses the conversion of camphor to 5-*exo*-hydroxycamphor in a regio-and stereospecific manner (Figure 3).[33,34] This is the first step in the utilisation of camphor as an energy source by this bacterium.[33,34] The enzyme has been successfully expressed in *E.coli* and was the first bacterial P450 enzyme isolated recombinantly for *in vitro* study.[35,36] The enzyme has also been crystallised in many forms and provided a wealth of information as a model system in determining the general mechanism of P450 catalysis.[37–39] $P450_{cam}$ utilises a Class I electron transfer system with a FAD containing putidaredoxin reductase (PdR) and a [2Fe-2S] putidaredoxin ferredoxin (Pdx) as its electron transfer partners.[16]

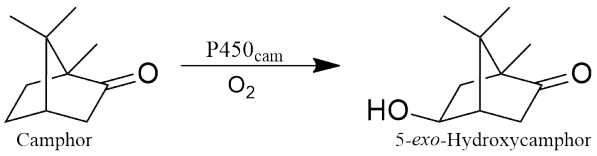

Figure 3: Conversion of camphor to 5-*exo*-hydroxycamphor by $P450_{cam}$.

The available crystallographic data (PDB ID: 3WRH) on $P450_{cam}$ made it an attractive target for protein engineering studies for use in biocatalytic transformations.[40–42] The active site residues of $P450_{cam}$ have been identified from these crystal structures (Figure 4).[43–46] The active site structure of camphor bound $P450_{cam}$ shows that the Tyr96 (Y96) residue forms a hydrogen bond with the camphor carbonyl group.[40] The Phe87 (F87), Leu244 (L244) and Ile395 (I395) residues provide hydrophobic contact with the substrate while Val247 (V247) interacts with the ring carbon methyl group.[46,47] These hydrophillic and hydrophobic residues interact with the substrate and maintain its orientation to allow stereospecific 5-*exo* oxidation.

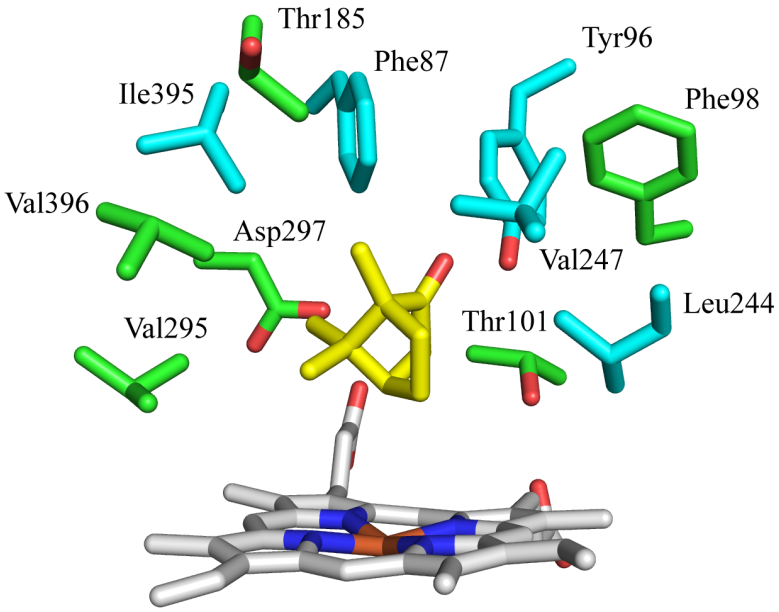

Figure 4: Active site of Cytochrome $P450_{cam}$ with bound camphor (yellow) (PDB ID: 3WRH). Residues of interest in this work are highlighted in cyan.[43]

Tricistronic plasmids (pCWSGB and pSGB) that express $P450_{cam}$ and its electron transfer co-factor proteins have been constructed to yield a functional whole cell *in vivo* oxidation system.[44,46] The *in vivo* system expressing WT-$P450_{cam}$ can catalytically convert 4 mM of camphor to 5-*exo*-hydroxycamphor within 4 h using *E.coli* cells indicating enzyme activity was successfully reconstituted.[44] The system was also reported to be active for at least 48 h if additional aliquots of carbon and nitrogen sources were added.[44]

Mutagenesis of the enzyme by site-directed rational design was carried out to enable the oxidation of (+)-α-pinene (Figure 5). (+)-α-Pinene is a bicyclic 3.1.1 monoterpene compound that is structurally related to camphor, though lacking a carbonyl group. $P450_{cam}$ was mutated at the Y96 residue to a Phe residue (Y96F) to remove the polar phenol group and improve (+)-α-pinene binding by compensating its lack of a carbonyl group.[46] The F87 and V247 residues were also mutated to a Trp residue (F87W) and a Leu residue (V247L) respectively as a way to "fill in" the leftover space caused by the absent carbonyl group and the different ring methyl position to improve enzyme-substrate complementarity.[46] F87L and F87A mutants were also made as a way to investigate the effect of side-chain volume. Finally, the Leu244 residue was mutated to an alanine residue (L244A) to create additional space to further orient (+)-α-pinene to resemble the orientation of camphor in the WT enzyme.[46] A library of $P450_{cam}$ enzymes consisting of different combination of mutants at the F87, Y96, V247, L244 and I395 residues (Chapter 4, Table 10) were tested for the oxidation of (+)-α-pinene.

The mutants in the library all displayed > 70 % conversion to high spin (HS) heme when bound to (+)-α-pinene.[46] Variants that possess an altered F87 residue when combined with V247L and L244A displayed improved oxidation activity and coupling efficiency over the WT enzyme (Figure 5).[46] This indicates that mutagenesis by rational design of the enzyme was successful in improving the oxidation of (+)-α-pinene.

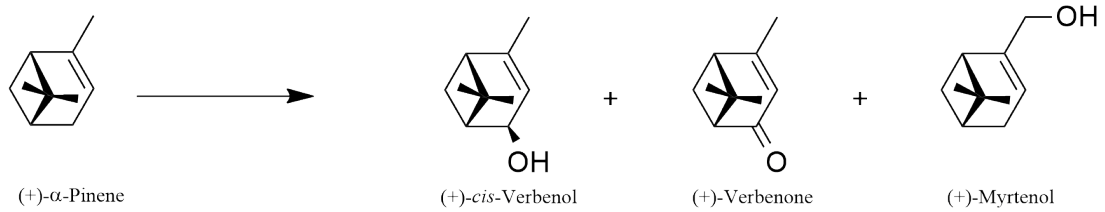

	Product Formation Rate (min^{-1})			
WT	18.6	31 %	10 %	4 %
F87W/Y96F/L244A	120	86 %	5 %	2 %

Figure 5: (+)-α-Pinene oxidation products by WT and a $P450_{cam}$ mutant, F87W/Y96F/L244A (WFA). The remaining products consists of *cis*/*trans* (+)-α-pinene epoxides (WT = 4 %, WFA = 2 %), other monooxygenenated and further oxidation products (WT = 51 %, WFA = 5 %).

WT-$P450_{cam}$ oxidises (+)-α-pinene to form (+)-*cis*-verbenol, an important flavouring precursor material, as the major product (31 %, Figure 5). It also formed other oxidation products (> 51 %), indicating poor selectivity. Amongst the mutants tested, the F87W-Y96F-L244A (WFA) mutant displayed the most selective oxidation of (+)-α-pinene. This generated (+)-*cis*-verbenol in higher yield (86 %), (+)-verbenone (5 %), (+)-myrtenol (2 %) and other oxidation metabolites as minor products (7 %) (Figure 5).[46]

Verbenol, verbenone and myrtenol are all naturally occuring plant fragrances and flavourings. Verbenone and myrtenol are important components in rosemary oil and berry fruits, respectively.[48,49] Verbenone and verbenol can also function as pheromones for pine bark beetles and thus have potential for use as pesticides.[50] Myrtenol has also been reported to display anti-inflammatory activity, indicating possible future pharmaceutical applications.[51]

The Y96F-V247L mutant of $P450_{cam}$ also selectively oxidises *S*-limonene. This mutant has improved binding with 40 % HS (versus 20 % in WT) and a product formation rate of 187 min^{-1} (versus 0.2 min^{-1} in WT).[45] The mutant generates both (*S*)-Isopiperitenol (70 %) and (−)-*trans*-carveol (16 %) (Figure 6) with a limonene epoxide as the minor product (14 %). (*S*)-isopiperitenol is the precursor compound for the production of menthol, an important component of *Mentha* plants, which is responsible for their

minty smell and flavour.[48,52] Carveol is a flavouring agent found in orange peel and has also shown chemoprevention properties in mammary carcinogenesis.[53,54]

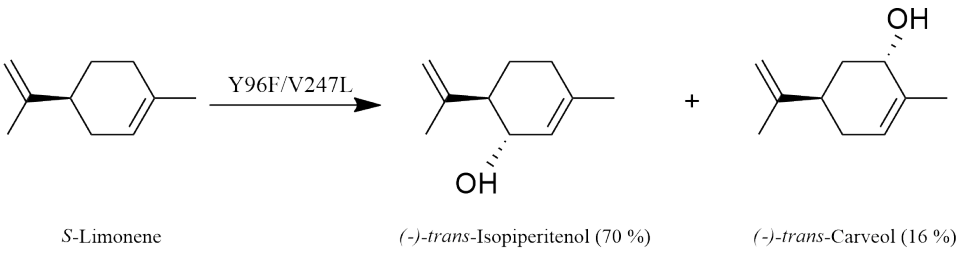

Figure 6: *S*-Limonene oxidation products by a $P450_{cam}$ mutant. The remaining product is limonene ring epoxide (14 %).

$P450_{cam}$ mutants have also been used to enhance the activity of the enzyme towards other hydrophobic substrates. Oxidation of ethylbenzene by $P450_{cam}$ was greatly enhanced with the Y96F-V247L mutant. The product formation rate was 40-fold higher than that of the WT with 1-phenylethanol being generated as the sole product.[44] Ethane, *n*-butane and propane have all been oxidised to their alcohol derivatives by different mutants of $P450_{cam}$ which decrease the size of the active site.[55]

There are likely many substrates which could be oxidised by variants of $P450_{cam}$. The mutant libraries generated for $P450_{cam}$ provide a convenient method to carry out screening for substrate oxidation to generate alternate synthetic pathways for other highly valuable compounds.

1.5 CYP101 enzymes from *N. aromaticivorans.*

Microorganisms that can degrade a wide range of compounds are potential sources of new enzymes for biocatalysis. The oligotrophic bacterium *Novosphingobium aromaticivorans* DSM12444 can degrade a wide range of polyaromatic hydrocarbons, terpenoids and linear alkanes.[56,57] The genome of the bacterium consists of its chromosomal DNA and two circular plasmids. Within the genome, there are a high proportion of genes encoding for oxygenase enzymes.[56,58,59]

Sixteen cytochrome P450s were identified across the chromosomal DNA and one of the plasmids.[57] The large number of P450 genes within *N. aromaticivorans* likely allows it to metabolize a wide variety of environmental xenobiotic compounds and enable it to survive in conditions that offer little support for life.[58] The P450s of this bacterium belong to 10 different families.[57] There are four members of the CYP101 family and one CYP111 family enzyme which use a common class I electron transfer system. This consists of a FAD containing ferredoxin reductase, ArR and a [2Fe-2S] ferredoxin

(Arx).[19] These five enzymes (CYP101B1, CYP101C1, CYP101D2, CYP111A2) were produced with the electron transfer partners in *E.coli* using DUET vectors,[19,57] to generate a whole-cell oxidation system.[19] This enabled the production of hydroxylated metabolites which could be scaled up to a gram-per-litre scale, indicating its viability for use in large scale biocatalysis.[19]

Initial studies with CYP101B1 showed that it can oxidise camphor to form 5-*exo*-hydroxycamphor alongside the formation of four other products (Figure 7a).[19,57] The whole-cell oxidation system containing this enzyme also generated the blue pigment indigo from the P450 catalyzed oxidation of indole (Figure 7b).[19,60] CYP101B1 did however show higher activity and selectivity when oxidising the norisoprenoid, β-ionone (Figure 7c) to form 3-hydroxy-β-ionone (90 %) and one minor product, 4-hydroxy-β-ionone (10 %).[19] In addition, CYP101B1 showed a high binding affinity for β-ionone ($\geq$ 95 % HS, K_d = 0.23 µM) and a fast product formation rate (1010 min^{-1}). This suggests that the physiological substrate of CYP101B1 could be a norisoprenoid compound.[61] The diverse structures of camphor, β-ionone and indole (Figure 7) suggest that CYP101B1 has potential in oxidising a wide range of substrates.

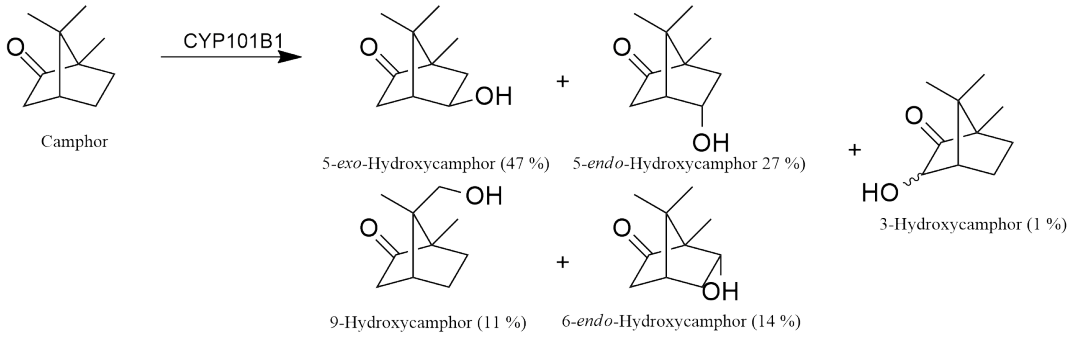

(a)

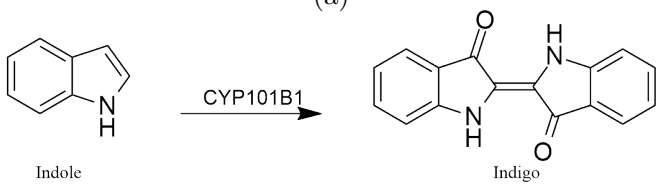

(b)

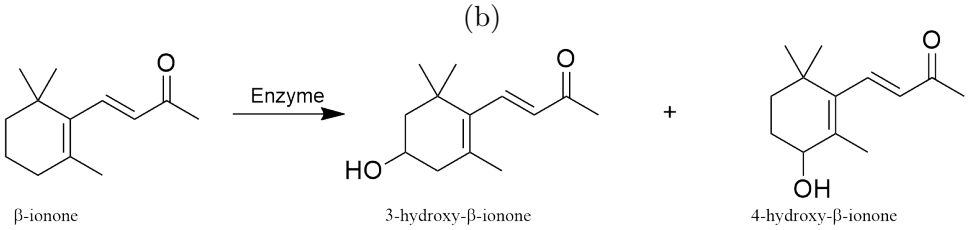

CYP101B1	90 %	10 %
CYP101C1	25 %	75 %

(c)

Figure 7: Oxidation of (a) camphor and (b) indole by CYP101B1 and (c) β-ionone oxidation by CYP101B1 and CYP101C1.

Further screening of CYP101B1 was carried out with a variety of other terpenoid and aromatic compounds.[61] The enzyme displayed high binding affinity for other norisoprenoids such as α-ionone ($\geq$ 95 % HS, K_d = 0.26 µM) and β-damascone ($\geq$ 80 % HS, K_d = 8.3 µM).[61] The hydroxylation of α-ionone was regioselective, producing both *trans*- and *cis*-3-hydroxy-α-ionone in an approximate 2:1 ratio (Figure 8a).[61] Oxidation of β-damascone by CYP101B1 displayed similar regioselectivity to β-ionone, generating 3-hydroxy-β-damascone (86 %) and 4-hydroxy-β-damascone (11 %) (Figure 8b), with lower activity.[61] A third minor product (< 4%) generated was not isolated in high enough yield for characterisation.

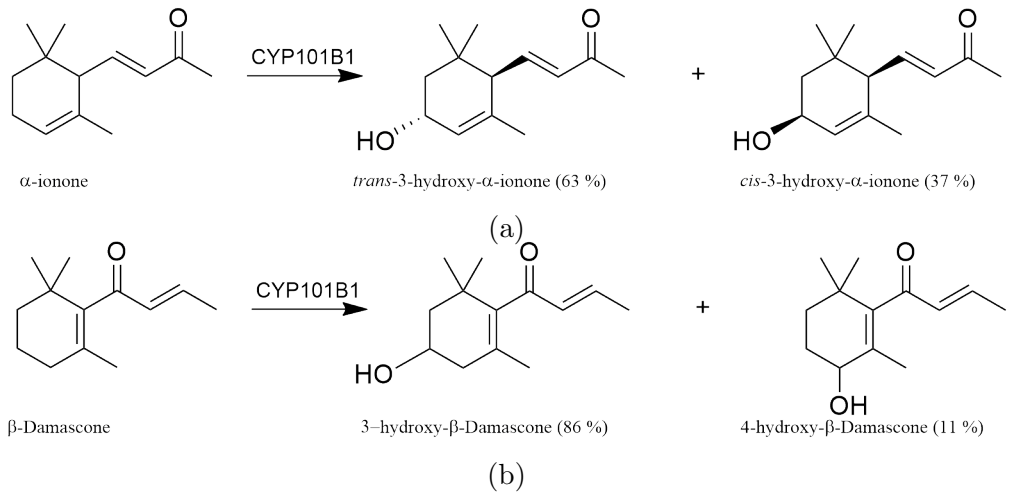

Figure 8: Oxidation of (a) α-ionone and (b) β-damascone by CYP101B1. For β-damascone, a minor metabolite (< 4 %) was not isolated in high enough yield for characterisation.

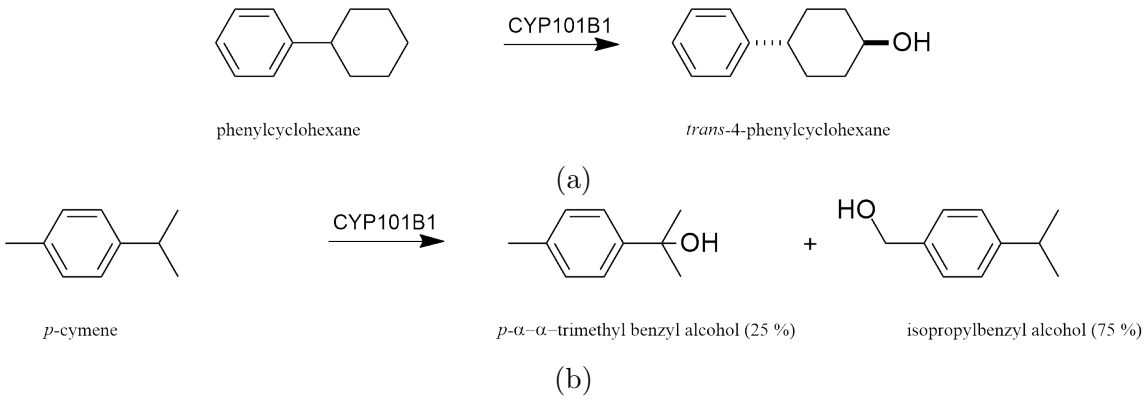

Figure 9: Oxidation of (a) phenycyclohexane and (b) *p*-cymene by CYP101B1.

When screened with aromatic substrates, CYP101B1 was found to be capable of oxidising both phenylcyclohexane and *p*-cymene (Figure 9).[61] Phenylcyclohexane oxidation by the enzyme was regioselective and generated a single product, *trans*-4-phenylcyclohexane (Figure 9a).[61] *p*-Cymene oxidation by CYP101B1 gave a mixture of *p*-α-α-trimethyl benzyl alcohol (25 %) and isopropylbenzyl alcohol (75 %) (Figure 9b).[61] Both induced small spin-state shifts and moderate NADH turnover rates when

compared to norisoprenoids, indicating that they were not as effective as substrates for CYP101B1.[61]

CYP101C1, also from *N. aromaticivorans*, is a homologue of $P450_{cam}$ (CYP101A1) and CYP101B1.[62] The enzyme uses the same Class I electron transfer system as CYP101B1.[63] It displayed no observeable binding or activity with camphor.[57,62] Substrates that are able to bind and be oxidised by CYP101C1 include α-ionone, β-ionone and β-damascone, but all induce low spin-state shifts ($\leq$ 20 % HS).[62] Despite this, CYP101C1 can effectively hydroxylate norisoprenoids, where for example β-ionone oxidation produces 3-hydroxy-β-ionone (25 %) and 4-hydroxy-β-ionone (75 %) (Figure 7c).[62] In contrast, the major product for CYP101B1 is of the C4 oxidation (90 %). α-Ionone oxidation by CYP101C1 resulted in three products.[62] As with CYP101B1, this substrate was oxidised exclusively at the C3 position forming both *cis*- and *trans*-3-hydroxy-α-ionone alongside 3-oxo-α-ionone (Figure 10).[62]

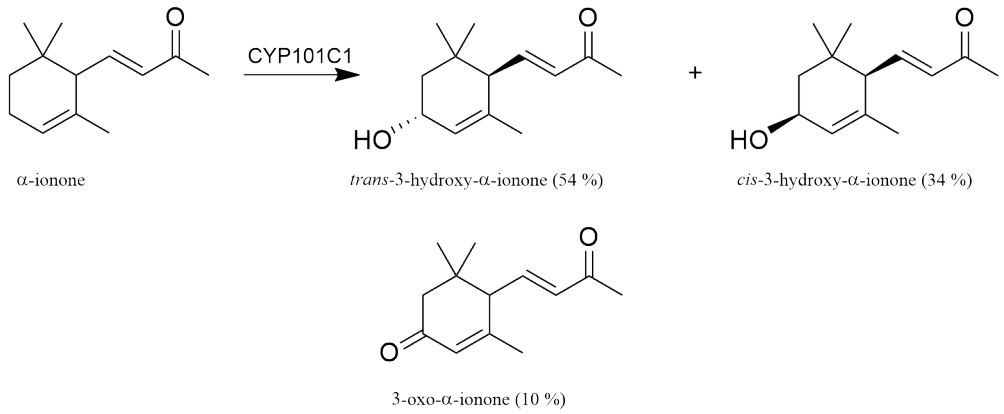

Figure 10: Oxidation of α-ionone by CYP101C1. A minor oxidation product (< 2 %) was not isolated in high enough yield for characterisation.

CYP101B1 and CYP101C1 oxidise norisoprenoids exclusively on the C3 and C4 positions within the aliphatic ring. This implies that the norisoprenoids interact with the enzymes' active site in such a way that it is held with the ring above the heme group for oxidation. The lower spin-state shift with β-damascone and CYP101B1 suggests that the position of the alkene and ketone groups on the butenone side chain are somewhat important for substrate-enzyme binding interactions.[61] The location of the cyclic alkene bond within the ionones and damascones does play a role in the regioselectivity of both CYP101 enzymes. As both enzymes oxidise all norisoprenoids at the C3-position, it is the C3 hydrogens within these substrates that are closest to the heme iron.[61] The oxidation at the C4 position in both β-substrates indicates that the more reactive allylic C4 hydrogens are also close enough to the heme to be oxidised in competition with the C3 hydrogens.[61] The alkene in α-ionone is not oxidised and is presumably too far away for efficient epoxidation.[61] The different selectivities

of CYP101B1 and CYP101C1 with β-ionone could lead to pathways for the selective oxidation of related flavour and fragrance compounds.

1.6 $P450_{BM3}$ Mutagenesis and Biocatalytic Studies

$P450_{BM3}$ was discovered by Fulco et al. in 1974, where it was first identified as a fatty acid hydroxylating enzyme from *Bacillus megaterium*.[64] It exhibited high substrate oxidation activity in the presence of oxygen and NADPH without any other protein partners.[64] This enzyme was capable of exclusively hydroxylating pentadecanoic acid at sub-terminal positions, while also accepting hydroxylated fatty acids, fatty alcohols/amides, and ω-oxo fatty acids as substrates.[64–71]

The enzyme is a single 119 kDa polypeptide that possesses two distinct domains, which are firstly a P450 haem domain (55 kDa) fused to a reductase domain with flavin containing FAD and FMN groups (65 kDa).[21,23] This is a class VIII type electron transfer system that allows $P450_{BM3}$ to be catalytically self-sufficient, as opposed to requiring separate partner proteins to receive electrons such as in class I systems ($P450_{cam}$ and CYP101B1).[16,21,22] The self-sufficent nature of $P450_{BM3}$ provides biocatalytic P450 monooxygenase activity without the need to co-expresss separate protein partners. The heme domain of $P450_{BM3}$ has been structurally characterised, enabling the identification of the active site residues involved in substrate binding (Figure 11, PDB ID: 1FAG).[72,73]

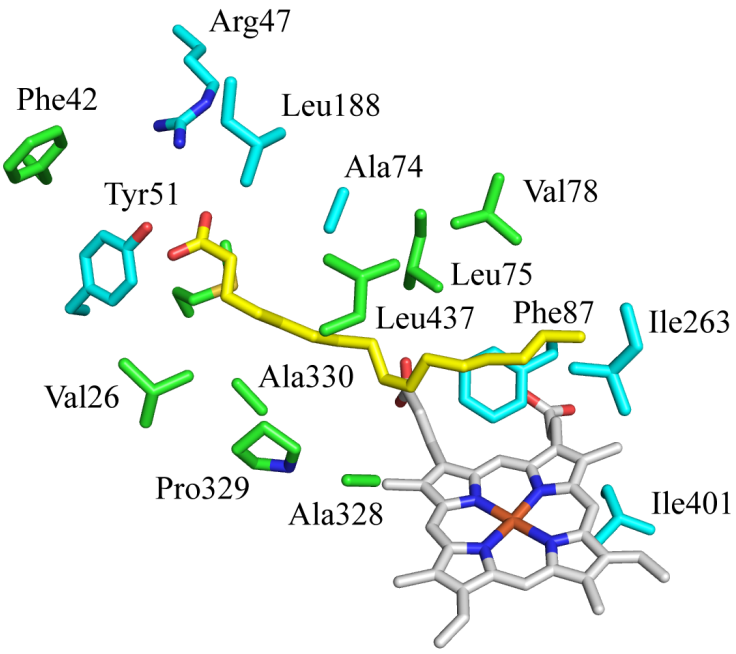

Figure 11: Active site of Cytochrome $P450_{BM3}$ with palmitoleic acid. Residues of interest in this work are highlighted in cyan (PDB ID: 1FAG).[73]

Mutagenesis studies targeting improved activity towards flavour and fragrance molecules have been carried out with $P450_{BM3}$.[74] WT-$P450_{BM3}$ is capable of oxidising β-ionone although it exhibits an extremely poor turnover rate of < 1 min^{-1} and no spin-state shift.[74] Site-directed mutagenesis of $P450_{BM3}$ was carried out to accommodate the bulkier structure of β-ionone compared to fatty acids and move it closer to the heme. Position 87 of the enzyme was the first target for mutagenesis and it contains a Phe residue that sits directly above the heme and is involved with controlling the enzyme's regio- and enantioselectivity.[75,76]

Single mutants at the Phe87 position were tested and it was found that smaller glycine, valine and alanine residues displayed significantly higher oxidation activity towards β-ionone compared to the WT enzyme.[74] The single product arising from the oxidations observed was 4-hydroxy-β-ionone (Figure 12a) and the F87V mutant exhibited the highest product formation rate (115 min^{-1}) among the single mutants.

Further mutagenesis was then carried out at the Arg47 and Tyr51 residues, both which are located at the substrate access channel. Arg47 and Tyr51 were substituted to more hydrophobic substrates of leucine and phenylalanine respectively to allow easier entry of β-ionone into the active site. The R47L and Y51F mutant when coupled with the F87V mutant displayed a significant increase in product formation rate (268 min^{-1}) compared to the WT.[74] This indicates that mutagenesis of $P450_{BM3}$ is also a viable way to develop biocatalysts for the oxidation of norisoprenoids such as β-ionone.

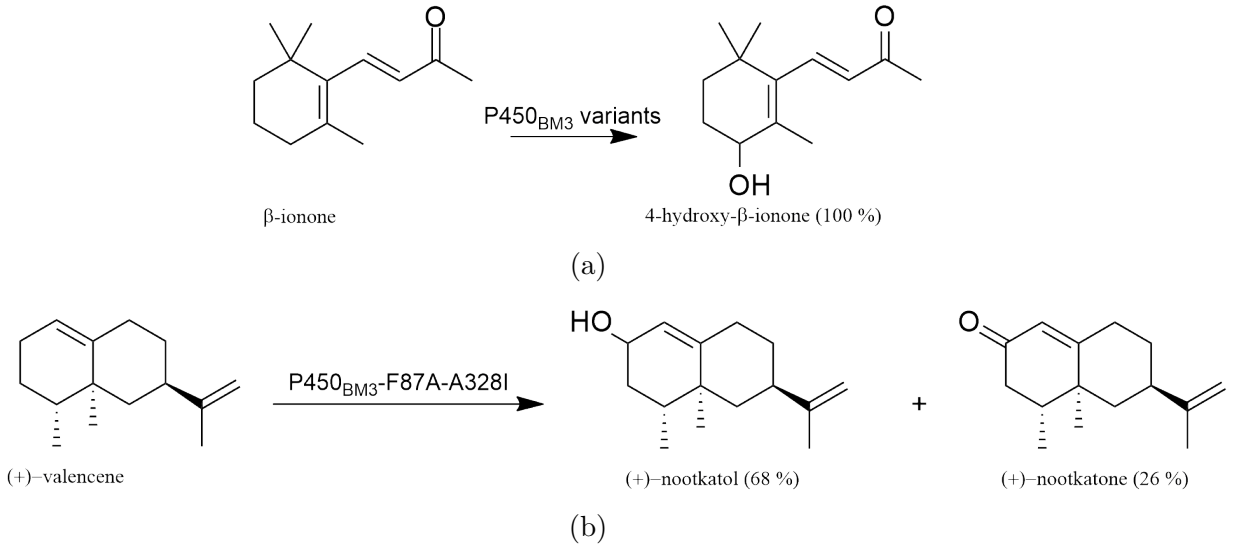

Figure 12: Oxidation of (a) β-ionone and (b) (+)-valencene by $P450_{BM3}$. For valencene oxidation, the remaining minor metabolites (6 %) were unidentified.

In a separate study, the target molecule, (+)-valencene, which is a sesquiterpenoid that is found in orange oil, was oxidised to the ketone derivative, nootkatone, a highly sought after fragrance molecule derived from grapefruit (Figure 12b).[77–79]

WT-P450$_{BM3}$ showed low NADPH oxidation activity (40 min^{-1}) and little to no change in spin-state when (+)-valencene was added.[79] Products formed from the oxidation of (+)-valencene with WT-P450$_{BM3}$ did not contain nootkatone at all but a mixture of five products. One of these was identified as nootkatol (Figure 12b).[79] Nootkatone was succesfully produced when mutations at the Phe87 and Ile263 residues (F87A and I263A) were introduced (Figure 11). The major product was nootkatol and other minor epoxide products (< 10 %).[79] A significant improvement in P450$_{BM3}$'s production of nootkatone was achieved by screening a mutant library containing mutant variants at the Phe87 and Ala328 residues (Figure 11).[23] Three variants containing the A328I mutant and different Phe87 mutant variants were the best, resulting in a high ratio of nootkatone against other metabolites. The F87A-A328I mutant produced the most nootkatone (26 %, Figure 12b).[80]

P450$_{BM3}$ mutants have also been developed to enhance the enzyme's activity for non-natural substrate oxidation while maintaining the WT-enzyme's regioselectivity.[81] These mutants were coined as rate-accelerator variants. These variants include A191T-N239H-I259V-A276T-L353I (KT2), R47L-Y51F-I401P (RLYFIP) and R47L-Y51F-H171L-Q307H-N319Y (R19).[81–84] These mutations are all located outside of the substrate binding pocket. These enzymes are believed to be in a more catalytically ready conformation in the substrate-free form. Substrate induced changes are less important in activating the electron transfer steps and lead to the oxidation of non-natural substrates at increased rates.[81] The R47L-Y51F mutation is also hypothesized to facilitate easier access of small hydrophobic molecules.[26] Substrates that have displayed increased activity with these variants include aromatic compounds such as propylbenzene and napthalene.[82,85]

These mutagenesis studies indicate that P450$_{BM3}$ is a suitable enzyme system for the production of high value compounds. In particular, terpene derivative compounds.

1.7 Producing High Value Compounds with P450s

The creation of new perfume and flavouring agents relies not only on the discovery of new odorous molecules but also the modification of the chemical structures of existing commercial products.[86,87] The second line of research is of interest as the relationship between chemical structure and odor is often unpredictable, whereby molecules with similar structures can possess dissimilar scents and odor thresholds.[88] The alcohol functionality is a prevalent functional group present in flavour and fragrances, making P450 enzymes an ideal method for modifying existing compounds to generate

hydroxylated derivatives with hopefully new olfactory properties.[89] For example, 3-hydroxy-α-ionone possesses a tobacco-like odor that is unlike the floral scent possessed by its parent molecule, α-ionone.[90]

Apcarotenoids or norisoprenoids are derived from the selective oxidative cleavage of carotenoids that are catalysed by carotenoid cleavage dioxygenases.[91] The ionone and damascone C_{13} norisoprenoids (Figure 13) in particular are highly important carotenoid-derived compounds studied within the food and fragrance industry due to their pleasant aromas (Table 1) and low odor thresholds.[92] For example, carotenoid-derived compounds have found wide use in personal care products such as shampoos, body lotions and deodorants.[93,94]

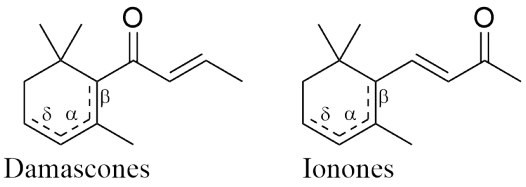

Figure 13: The general structures of damascones and ionones.

Table 1: Norisoprenoids of interest alongside descriptions of their odours.

Norisoprenoid	**Occurrence**	**Odour**
β-Ionone	Carrots, Rose,Blackberries	Floral with fruity and berry notes
α-Ionone	Blackcurrant, Blackberries	Violet and scent with, raspberry notes
β-Damascone	Osmanthus, Rose, Papaya	Fruity and floral scent
α-Damascone	Rose	Rose petals with apple and fruity notes.

Another class of compounds that are of interest are the terpenoids. This class of compounds, which includes their oxygenated derivatives, are produced mainly within herbs and higher plants have been used as flavourants and fragrances for centuries, making them possible targets for P450 oxidations to develop new fragrances.[23,95] Terpenoids have also drawn considerable interest commercially in the prevention and treatment of diseases and use as natural pesticides and antimicrobial agents.[95] Enzymatic enantioselective pathways for the production of hydroxylated derivatives can also provide new sources of chiral intermediates or auxiliaries.[96] Oxidised derivatives of carotenoid and terpenoid compounds have also found use in chemical syntheses as precursors and for pharmaceutical applications, such as the anti-inflammotory activity exhibited by 3-hydroxy-β-damascone.[87,97,98]

1.8 Thesis Objectives

The ability of $P450_{cam}$ and $P450_{BM3}$ variants in oxidising terpenes, terpenoids and norisoprenoids displays a potential for these mutants in oxidising other similar molecules. Small mutant libraries for $P450_{cam}$ and $P450_{BM3}$ have been previously made.[46,84] Selected variants will be screened with a range of terpenes, terpenoids and norisoprenoids to study if new oxidation pathways towards high value hydroxy compounds can be discovered.

CYP101B1 from *Novosphingobium aromaticivorans* has been shown to be a potential biocatalyst for norisoprenoid oxidation. Therefore, it is a viable target for additional substrate screening. A range of different carbonyl containing substrates such as tricyclic and aromatic acetates will be screened with CYP101B1 to investigate if any significant catalytic turnover activity is observed and if new products are formed. Reactions with interesting oxidation patterns or high yield as determined with GC-MS and/or HPLC analysis will be scaled up and the products isolated for characterisation.

Mutants of CYP101B1 will be generated with the aim of improving its activity with hydrophobic substrates. Protein sequence alignment of CYP101B1 with $P450_{cam}$ showed that the 96 residue in the latter was equivalent to the His85 (H85) residue in CYP101B1.[61] The Y96 residue is responsible for the hydrogen bonding interaction with camphor in $P450_{cam}$ (Figure 4) and it is hypothesized that the H85 residue in CYP101B1 may play a similar role and interacts with the carbonyl group of the norisoprenoids. As such it is a suitable target for mutagenesis studies.[47,61] Site-saturation mutagenesis will be carried out on the H85 residue and the variants will be cloned into plasmid systems to enable *in vitro* and *in vivo* screening. Following that, variants with increased activity towards aromatic substrates of different sizes and hydrophobicities will be investigated further.

2 Experimental

2.1 General

General reagents, HPLC solvents, organic substrates and derivatisation agents were purchased from Sigma-Aldrich, VWR, Fluorochem, Acros Organics, Tokyo Chemical Industry or Matrix Scientific. Antibiotics, isopropyl β-D-thiogalactopyranoside (IPTG) and dithiothreitol (DTT) were purchased from Astral Scientific. A racemic mixture of (4*R*)/(4*S*)-hydroxyisophorone was provided by Shaghayegh Dezvarei and A/Prof Stephen Bell of the University of Adelaide using methods previously described.[99] The following fragrance molecules were obtained from Australian Botanical Products:

- α-damascone
- δ-damascone
- cuminyl acetate
- dihydroflorate
- dynascone
- ethyl safranate
- verdyl acetate
- α-methyl ionone

UV/Vis spectra and activity assays were recorded at 30 ± 0.5 °C on a Varian Cary 60 spectrophotometer. NMR spectra were obtained using an Agilent DD2 spectrometer operating at 500 MHz for ^{1}H or 126 MHz for ^{13}C NMR or on a Varian Inova-600 spectrometer operating at 600 MHz for ^{1}H or 151 MHz for ^{13}C NMR. Optical rotations of enantiomeric products were measured using an Anton-Paar MCP 100 Modular Circular Polarimeter.

2.2 Enzymes and Molecular Biology

T4 DNA ligase was purchased from Lucigen and restriction enzymes for molecular biology were from New England Biolabs. General DNA, microbiological experiments and protein purification were carried out by standard methods as described below.[100] Proteins were stored in Tris (50 mM, pH 7.4) containing 50% v/v glycerol at -20 °C

and desalted before use with a PD-10 column (GE Healthcare). DNA for WT-$P450_{cam}$ and $P450_{BM3}$ along with their mutants and whole-cell oxidation systems have been purchased previously.[44–46,82] The media solutions used for cell growths are listed in Table 2.

Table 2: Growth media constituents.

Medium	**Constituents (L^{-1})**
LB	tryptone (10 g), yeast extract (5 g), NaCl (10 g)
SOC	tryptone (20 g), yeast extract (5 g), $MgCl_2$ (1 g), NaCl (0.5 g), KCl (0.2 g), glucose (0.2% w/v)
Trace Elements	Na_2EDTA(20.1 g), $FeCl_3.6H_2O$ (16.7 g), $CaCl_2.H_2O$ (0.74 g), $CoCl_2.6H_2O$ (0.25 g), $ZnSO_4.7H_2O$ (0.18 g), $MnSO_4.4H_2O$ (0.132 g), $CuSO_4.5H_2O$ (0.10 g)
EMM	K_2HPO_4 (7 g), KH_2PO_4 (3 g), $(NH_4)_2SO_4$ (1 g), Na_3Citrate (0.5 g), $MgSO_4$ (0.1 g), 20% glucose (20 mL)

2.2.1 Protein Engineering of CYP101B1

DNA encoding for WT CYP101B1 + Arx in pRSFDUET and WT CYP101B1 in pET22 were available.[101] The gene for CYP101B1 in both vectors was inserted in between the *NdeI* (5') and *KpnI*/*HindIII* (3') restriction sites. The gene contained a *SalI* restriction site at base pair 373 - 378.

A gBlock fragment library for CYP101B1 was purchased from Integrated DNA Technologies which included a nnC triplet codon (n is a random base) incorporated at the His85 position. The nnC codon was used to generate a library of mutants. The gBlock fragment sequence is shown in Figure 14.

atttta**catATG**GAAGCACCAGCTCATGTACCGGCTGATCGTGTCGT**g**GACAT
TGATATCTATATGCCGCCGGGTCTGGCAGAACACGGCTTCCACAAGGCCT
GGTCCGATCTGAGCGCGGGCAACCCGGCTGTTGTTTGGACCCCACGCAAC
GAAGGCCACTGGATTGCCCTGGGCGGTGAAGCCCTGCAAGAGGTTCAGTC
TGACCCGGAGCGCTTCAGCTCCCGTATCATCGTTCTGCCGAAATCCGTTG
GTGAAATG**nnC**GGCCTGATTCCGACCACCATCGATCCGCCAGAACACCGT
CCTTACCGCCAACTGCTGAACGCCCATCTGAATCCGGGTGCTATCCGTGG
TCTGTCTGAAAGCATTCGTCAGACTGCG**GTcGAc**ttaatt

Figure 14: Sequence of the gBlock fragment of CYP101B1 with the nnC codon at the H85 residue (in bold), a *NdeI* restriction site at the 5' terminus and a *SalI* restriction site at 3' terminus (both underlined).

Digestion of the gBlock fragment library and vectors pRSFDUET-Arx and pET22 containing CYP101B1 was first carried out. The digests were prepared using a mixture of the DNA (1 - 1.5 µg) with *NdeI* and *SalI* restriction enzymes (30 units, 1.5 µL) in 10X NEB-Cutsmart® buffer in a volume of 20 µL for the DNA vectors and 50 µL for the gBlock fragment. The digests were incubated at 37 °C for 2 h. Agarose gel electrophoresis was used to purify the required DNA fragment from the digests (Section 2.3). The DNA fragments were excised, whereby the digested vector and cut gBlock fragment were purified with the EZ-10 Spin Column Plasmid DNA Minipreps Kit from Bio Basic Inc.

The mutant gene library (12.5 µL) was then ligated into the digested vectors (12.5 µL) between the *NdeI* and *SalI* restriction sites using T4 DNA ligase (400 units, 1 µL) in 10X T4 DNA Ligase Reaction Buffer (4.5 µL) and H_2O (19 µL). The ligation mixture was incubated at room temperature for 12 h.

The newly ligated DNA vectors were then transformed into competent DH5α *E.coli* cells (35 µL) and incubated at 0 °C for 60 min. This was followed by heat shock at 42 °C for 50 s. After 2 min incubation at 0 °C, SOC media (150 µL) was added to the cells and the resulting culture shaken at 37 °C and 120 rpm for 1 h. The cells were then grown on LB plates containing either 100 µg mL^{-1} ampicillin or 30 µg mL^{-1} kanamycin for the pET22 and pRSFDUET vectors, respectively.

Single colonies were harvested from the plates and used to inoculate a culture of LB (16 mL) with the appropriate antibiotic. The DNA plasmid vectors were purified from the cell pellet of these cultures using the EZ-10 Spin Column Plasmid DNA Minipreps Kit from Bio Basic Inc (2 purification preps for each growth). To confirm if gene fragments were successfully ligated into the desired vectors, the plasmids were digested with *NdeI*/*KpnI* restriction enzymes and analytical agarose gel electrophoresis was carried out to confirm if the insert is of the correct size (Section 2.3). To identify the codon at position 85, the plasmids (900 - 1000 ng in 9 µL) were then sequenced by the Adelaide Genome Research Facility using the T7 promoter primer (3 µL) for pET22 and the DuetUP2 primer (3 µL) for pRSFDUET.

Mutants which were identified in either vector pET22 or pRSFDUET but not the other were first digested with *NdeI* and *KpnI* for cloning into the other vector. Purified fragments were then ligated into desired vectors using T4 DNA ligase and were subsequently transformed into competent DH5α *E.coli* cells. The plasmids were purified and sequenced as described above.

2.3 Agarose Gel Electrophoresis

A 0.8 % w/v agarose gel was prepared by dissolving 0.4 g of agarose in 50 mL of TAE buffer (40 mM Tris, 1 mM EDTA). This was dissolved by heating in a microwave at 10 - 30 sec intervals. The solution was then cooled to 50 °C and 0.5 µL of ethidium bromide solution (10 mg mL^{-1}) was added. The gel was then cast and left to set for 2 h before being immersed in TAE buffer (250 mL) containing 1.5 µL of ethidium bromide (10 mg mL^{-1}).

DNA from restriction digests (15 µL) was mixed with 80 % glycerol (4 µL) and loaded into separate lanes of the gel alongside a molecular weight DNA ladder. The gels were run at 60 V for 1.5 h. The DNA bands were then viewed under UV light and the desired fragments were excised and purified (Section 2.2.1).

Analytical gel electrophoresis was also carried out using the gels that were prepared as above. Gel loading buffer (4 µL of 6 x buffer) was added to the DNA samples before loading into the gels. Gels were run at 100 V for 0.5 h and visualised under UV light.

2.4 Enzyme Purification

2.4.1 Purification of CYP101B1 mutants

The CYP101B1 mutants which were cloned into the pET22 vector (Section 2.2.1) were transformed into BL21(DE3) competent cells and grown on a LB plate containing ampicillin (100 mg L^{-1}). A single colony from the plate was used to inoculate 750 mL of LB in a 2 L shake flask with ampicillin (100 mg L^{-1}) and trace elements (2.25 mL). The culture was allowed to grow at 37 °C and 100 rpm overnight within a shaking-incubator. The incubation temperature was then lowered to 18 °C for 30 min. Benzyl alcohol (0.02 % v/v) and EtOH (2 % v/v) were then added. The culture was allowed to shake for a further 30 min and IPTG (0.1 mM) was added to induce protein expression. The culture was grown for a further 48 h to 72 h and then centrifuged (5000 *g*, 20 min) to collect the cell pellet. The pellet was re-suspended in 200 mL of Buffer T (50 mM Tris, pH 7.4, 1 mM DTT). Sonication was used to lyse the re-suspended cells using an Autotune CV334 Ultrasonic Processor equipped with a standard probe (136 mm x 13 mm; Sonics and Materials, US) using 40 x 20 s pulses with 40 s intervals. Cell debris was then removed using centrifugation (18000 *g*, 30 min, 4 °C). The protein containing supernatant was loaded on to a DEAE Sepharose column (XK50, 200 mm x 40 mm; GE Healthcare) and eluted using a linear salt gradient from 100 mM to

400 mM KCl in Buffer T at a flow rate of 6 mL min^{-1}. Red coloured fractions were combined and concentrated using ultrafiltration (10 kDa exclusion membrane). The concentrated protein was desalted using a Sephadex G-25 medium grain column (250 mm x 40 mm; GE Healthcare) and Buffer T.

The protein once desalted was concentrated again to a volume of 15 mL and loaded on to a Source-Q ion-exchange column (XK26, 80 mm x 30 mm; GE Healthcare) using an AKTA pure and eluted using a linear salt gradient from 0 mM to 250 mM KCl in Buffer T. Fractions with $A_{417}/A_{280} > 2$ were combined and concentrated using ultrafiltration. The protein concentration was determined using ϵ_{417}= 113 mM^{-1} cm^{-1}.[19]

2.4.2 Purification of ArR and Arx

ArR was supplied by Md Raihan Sarkar which was generated and purified using methods previously described.[61,101]

pETDUET containing the Arx gene was transformed into BL21(DE3) competent cells and grown on a LB plate containing ampicillin (100 mg L^{-1}). A single colony from the plate was used to inoculate 8 × 750 mL of LB in 2 L flasks containing 100 mg L^{-1} of ampicillin and trace elements solution (2.25 mL). The cultures were allowed to grow at 37 °C and 120 rpm for 8 h. The incubation temperature was lowered to 18 °C and left for 30 mins before benzyl alcohol (0.02 % v/v) and EtOH (2 % v/v) were added. The culture was left to shake for 30 mins and IPTG (0.1 mM) was added to induce protein expression. The culture was then allowed to incubate for 16 h at 18 °C and 90 rpm. The cells were harvested by centrifugation (5000 *g*, 20 min) and re-suspended in Buffer T (300 mL) that also contained glycerol (10 %), β-mercaptoethanol (3 mL) and Tween (1 mL). The re-suspended cells were mixed with lysozyme (300 mg) and stirred for 30 mins at 0 °C. The cells were then lysed using sonication as per Section 2.4.1 and cell debris removed via centrifugation (18000 *g*, 30 min, 4 °C).

The supernatant was loaded on to a DEAE Sepharose column (XK50, 200 mm x 40 mm; GE Healthcare) and eluted using a linear salt gradient from 200 mM to 400 mM KCl in Buffer T at a flow rate of 6 mL min^{-1}. Brown coloured fractions were combined and concentrated using ultrafiltration (10 kDa exclusion membrane). The concentrated protein was desalted using a Sephadex G-25 Medium grain column (250 mm x 40 mm; GE Healthcare). The protein once desalted was concentrated again to a volume of 15 mL and loaded onto a Source-Q ion-exchange column (XK26, 80 mm x 30 mm; GE Healthcare) using an AKTA pure and eluted using a linear salt gradient from 0 mM to 250 mM KCl in Buffer T. Fractions with $A_{316}/A_{280} > 0.6$ were combined and

concentrated using ultrafiltration. Protein concentration was determined using ϵ_{316}= 12.5 mM^{-1} cm^{-1}.[19]

2.5 P450 Carbon Monoxide Assays

2.5.1 CO Assay of CYP101B1 mutants

The P450 enyme was desalted and diluted with 50 mM Tris to ≈ 1 µM. Its absorbance spectrum was recorded (700 nm - 250 nm) and used to baseline the UV/visible spectrometer. Sodium dithionite (< 1 mg) was then added to the enzyme and its spectrum was used to baseline the instrument again. Carbon monoxide (CO) was bubbled gently through the solution and its absorbance recorded to generate the ferrous-CO bound spectrum.[102]

2.5.2 Quantification of P450 enzymes

A 100 mL growth of *E.coli* cells containing proteins (after induction) was centrifuged (4000 *g*, 15 min) and re-suspended in Tris Buffer (30 mL, 50 mM, pH 7.4). The re-suspended cells were sonicated as per Section 2.4.1 with 5 × 5 s pulses at 10 s intervals. The supernatant (500 µL) was used to measure a CO difference spectrum (Section 2.5.1) to obtain the absorbance at 450 nm. The concentration of P450 enzyme contained within 100 mL of overnight culture was calculated using ϵ_{450}= 91000 M^{-1} cm^{-1}.[102,103]

2.6 Enzyme-Substrate Binding Assays

The purified P450 enzymes were diluted with Tris Buffer (50 mM, pH 7.4) to ≈ 1 µM and their absorbance was recorded using a UV-visible spectrophotometer (700 nm - 250 nm). The substrate (0.5 µL, 100 mM stock in EtOH) was mixed with the enzyme (500 µL) and the spectrum was recorded again. Further 0.5 µL aliquots of substrate were added until the spectrum showed no further observable change. The shift from low spin (LS, 420 nm) to high spin (HS, 390 nm) was then recorded. The percentage of HS enzyme was determined by comparing the enzyme's absorbance spectrum to that of a set of existing spectra generated by the HS and LS forms of $P450_{cam}$ (camphor-bound/free) (Figure 15).

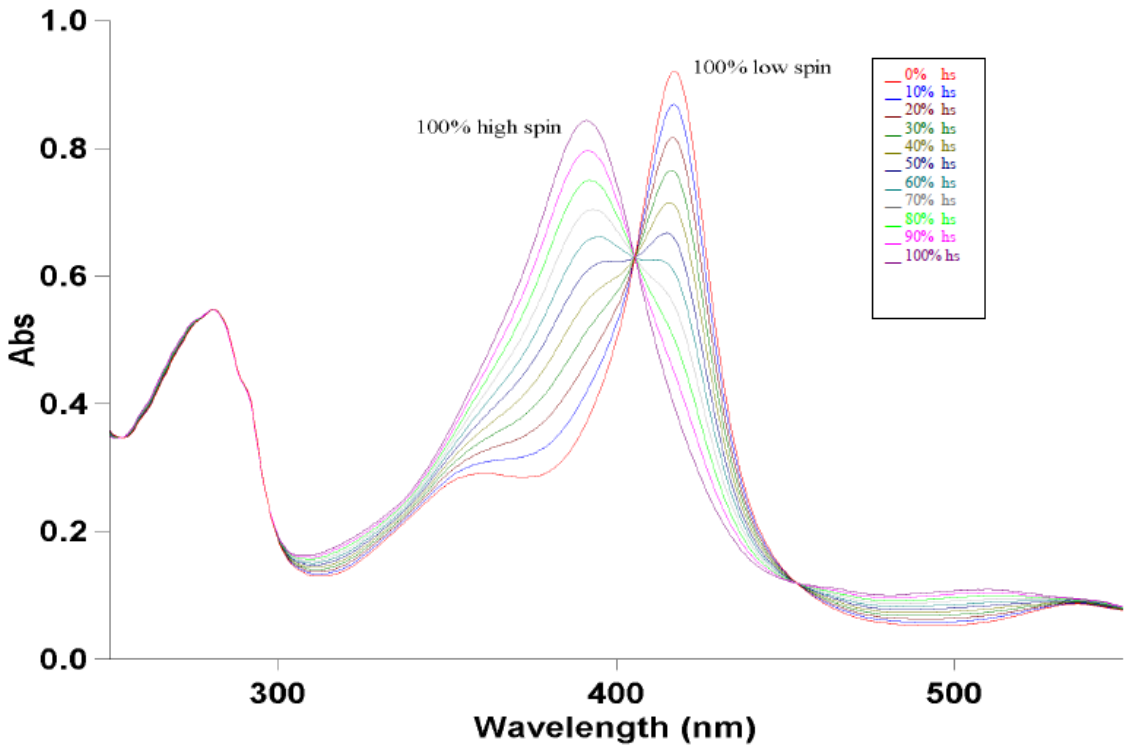

Figure 15: Spin-state diagram for $P450_{cam}$ in camphor free/bound diagrams from 0 % to 100 %.

Dissociation contants (K_d) were measured to determine the affinity of a substrate binding to the enzyme. The enzyme was diluted to ≈ 2 µM using Tris Buffer (50 mM, pH 7.4) and this enzyme was used to baseline the UV/visible spectrophotometer. Aliquots of substrate (1 - 2 µL, 1 mM) were added to the enzyme (2.5 mL) and the difference spectrum after each addition was recorded. After cumulative addition of 10 µL of 1 mM substrate, 1 - 2 uL of 10 mM substrate (up to 10 µL) and then 100 mM substrate were added until the peak to trough difference in absorbance showed no observable change.

The difference in peak to trough absorbance was fitted against the substrate concentration using the following function (Equation 2):

$$\Delta A = \frac{\Delta A_{\max} \times [S]}{K_d + [S]} \tag{2}$$

where ΔA is the peak-trough difference, $\Delta A_{\max}$ is the maximum peak-trough difference and $[S]$ is the substrate concentration.

2.7 Enzyme Activity Assays

2.7.1 *In Vivo* Activity Assays

For the $P450_{cam}$, $P450_{cin}$ and $P450_{BM3}$ systems, the plasmids listed in Table 3 containing the genes encoding these enzymes or their mutants were transformed into competent BL21(DE3) cells and grown on LB plates containing ampicillin (100 µg mL^{-1}) or kanamycin (30 µg mL^{-1}) depending on the vector used.[46,82,104]

The pRSFDUET vector containing WT-CYP101B1 or its mutants and pETDUET containing Arx and ArR (Table 3) were both transformed into competent BL21(DE3) cells and grown on LB plates containing both ampicillin (100 µg mL^{-1}) and kanamycin (30 µg mL^{-1}).[61]

Table 3: Plasmids with P450 *in vivo* systems used.

Plasmid	**Genes Contained**	**Antibiotic**
pCWSGB++	$P450_{cam}$ mutants, Pd, PdR[46]	Amp
pSGBF	WT-$P450_{cam}$, Pd, PdR[46]	Amp
pRSFDUET	WT CYP101B1 or its mutants, Arx[61]	Kan
pETDUET	Arx, ArR[61]	Amp
pET11d	$P450_{BM3}$-GVQ[82] or $P450_{BM3}$-RLYFGVQ[82]	Kan
pET28	$P450_{BM3}$-RLYFFAIP[105]	Kan
pCWori+	$P450_{cin}$, Cindoxin[104]	Amp

A single colony from the plates was used to inoculate 500 mL of LB containing the appropriate antibiotic and 1.5 mL trace elements solution. The culture was then allowed to grow at 37 °C and 120 rpm for 6 h, which was followed by lowering the incubation temperature to 18 °C for 30 min. Benzyl alcohol (0.02 % v/v) and EtOH (2 % v/v) were then added to the culture. The culture was left for 30 min and protein expression was then induced by adding IPTG (0.1 mM). The culture was then left for 16 h at 18 °C and 90 rpm. The cells were harvested via centrifugation (5000 *g*, 15 min) and the wet weight of the cells harvested was recorded.

Small scale turnovers were carried out by re-suspending the harvested cells in 500 mL of EMM and splitting this into either 2 mL, 25 mL or 50 mL aliquots. Substrate (2 mM) was added to the growths and the reactions were then shaken at 180 rpm and 30 °C. A 1 mL aliquot was taken from 25 mL and 50 mL reactions at 3 h and 18 h for analysis. For the 2 mL aliquots, only a 1 mL aliquot was taken at 18 h for analysis.

Large scale turnovers were carried out by dividing the re-suspended cells into 200 mL aliquots (EMM) in 2 L baffled shake flasks. Substrate (1 mM) was added to each reaction and the reactions were then shaken at 150 rpm and 30 °C. Further substrate additions were made at 4 h (1 mM) and 6 h (2 mM). At 6 h, glucose (1 % v/v) and phosphate buffered saline (PBS, 2.5 % v/v) were added and the turnover reaction was left to shake for a further 18 h. The supernatant of the turnover reaction was collected by centrifugation (5000 *g*, 20 min, 4 °C) to remove cell debris before extractions.

2.7.2 *In Vitro* Activity Assays

In vitro NADH activity assays with purified CYP101B1 were carried out by preparing a 1.2 mL mixture of the enzyme (0.5 µM), Arx (5 µM), ArR (0.5 µM), bovine liver catalase (12 µL of 10 mg mL^{-1} stock in glycerol) and oxygenated Tris Buffer (50 mM, pH 7.4). The mixture was equilibrated at 30 °C for 1 min and NADH (≈ 320 µM, $A_{340} \approx 2.0$) was added from a 20 mg mL^{-1} stock. The reaction was monitored at 340 nm using a UV-vis spectrophotometer (Figure 16a). Substrate (1 mM, 100 mM stock in EtOH) was added after 1 min. The gradient of the plot of A_{340nm} against time was used to calculate the rate of NADH consumption using $\epsilon_{340nm} = 6.22$ mM^{-1} (Figure 16a). All *in vitro* activity assays were measured in triplicate.

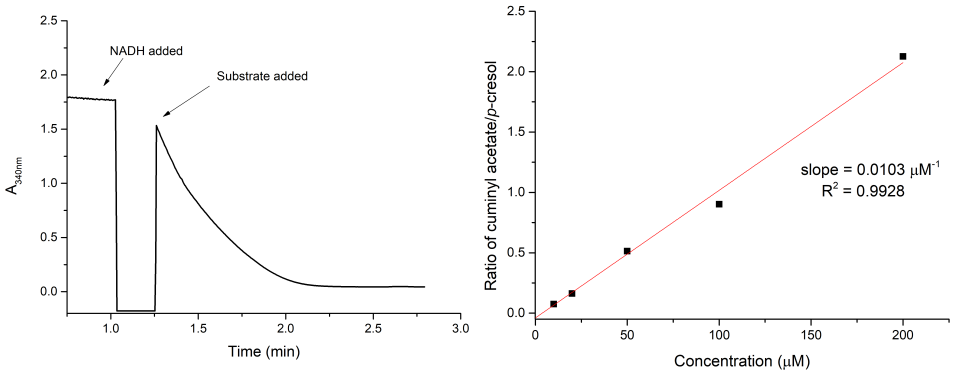

(a) (b)

Figure 16: (a) *In vitro* NADH assay measured and (b) calibration curve for cuminyl acetate.

Table 4: Calibration factors for different substrates and any associated oxidation products. All calibrations were carried out with *p*-cresol as the internal standard.

Compound	**Calibration Factor**
α-Damascone, δ-Damascone	0.0066
β-Ionone, α-Ionone	0.0064
Phenylcyclohexane	0.073
Ethyl Safranate	0.0066
Dynascone	0.066
α-Methylionone	0.072

For $P450_{BM3}$ turnovers, the 1.2 mL turnovers consisted of the enzyme (0.2 µM), bovine liver catalase (12 µL of 10 mg mL^{-1} stock in glycerol), oxygenated Tris buffer (50 mM, pH 7.4) and 1 mM substrate (100 mM stock in EtOH). The mixture was equilibrated at 30 °C for 1 min and NADPH ($\approx$ 320 µM, $A_{320} \approx 2.0$) was added. The reaction was monitored and the rate of NADPH consumption was calculated as above.

In vivo and *in vitro* turnovers were analysed via GC-MS. A 990 µL aliquot of the turnover was taken and *p*-cresol was added as an internal standard (10 µL, 20 mM in EtOH). The mixture was extracted with ethyl acetate (400 µL, EtOAc) and separated by centrifugation. Extracts were analysed via GC-MS/GC-BID analysis.

The concentration of product in an *in vivo* and *in vitro* turnover sample was determined by quantifying the samples against a calibration curve of a known product standard in EtOAc containing the internal standard measured using GC-MS (Figure 16b). If authentic product standards were not available, an isomer or the starting material was used. The concentration of the product in the turnover was divided by the concentration of NADH used to give the coupling efficiency.

The coupling efficiency is defined as the percentage of NADH/NADPH used to successfully oxidise the substrate to generate product. The product formation rate was calculated by multiplying the coupling efficiency by the NADH consumption rate to give the product formation rate.

2.8 Analysis and Identification of Enzymatic Metabolites

Gas chromatography-mass spectrometry (GC-MS) analysis was performed using manual injection on a Shimadzu GC-17A equipped with a QP5050A GC-MS detector and DB-5 MS fused silica column (30 m x 0.25 mm, 0.25 µm). The injector was held at 250 °C and the interface at 280 °C. High throughput GC-MS analysis was carried out with a Shimadzu GC-2010 equipped with a QP2010S GC-MS detector, AOC-20i autoinjector, AOC-20s autosampler and DB-5 MS fused silica column (30 m x 0.25 mm, 0.25 µm). Injection volume used was 1 µL with He as the carrier gas.

For GC-MS analysis with aromatic, norisoprenoid and acetate compounds, the oven temperature was held at 100 °C for 3 min, increased at 14 °C min^{-1} up to 240 °C and held at this temperature for 5 min. For terpenes or terpenoid compounds, the oven temperature was held at 80 °C for 3 min, increased at 10 °C min^{-1} up to 200 °C and was held at this temperature for 5 min.

GC analysis was performed on a Shimadzu TRACERA with a BID detector and Su-

pelcoWax column (30 m x 0.25 mm, 0.25 µm). The injector was held at 250 °C and the interface at 280 °C. For chiral GC analysis, a β-DEX column was used and both the injector and detector were held at 230 °C.

For chiral GC-analysis of the cineole metabolites, the dried samples (2 mg) were derivitised by dissolving them in dichloromethane (500 µL) followed by the addition of trifluoroacetic anhydride (5 µL, TFAA). The mixture was incubated for 2 h at room temperature. Solvent and other volatiles were removed under a stream of nitrogen and the remaining residue re-dissolved in EtOAc (500 µL). The GC oven method used for TFAA-derivitised cineole products was as follows: the oven temperature was held at 60 °C for 3 min, increased at 5 °C min^{-1} up to 140 °C and was held at this temperature for 5 min. The temperature was then increased by 29 °C min^{-1} to 200 °C and this was held for 1 min.

Other chiral products were also analysed via GC or chiral HPLC. The GC method used was as follows: the oven temperature was held at 80 °C for 3 minutes, then increased at 5 °C min^{-1} to 200 °C and held for 3 minutes. The injector and detector temperature were both held at 230 °C.

All high performance liquid chromatography (HPLC) analysis was carried out on a Shimadzu system equipped with a DGU-20A5R degasser, 2 × LC-20AR pumps, SIL-20AC HT autosampler, SPD-M20A photodiode array detector and a CT0-20AC column oven with an Ascentis Si HPLC column (25 cm × 4.6 mm × 5 µm; Sigma-Aldrich). Preparative HPLC was performed using an Ascentis Si HPLC column (25 cm × 10 mm × 5 µm; Sigma-Aldrich). Samples were injected at volumes of 1 - 5 µL and observed at 254 nm. For chiral HPLC analysis, a CHIRALPAK IG column (150 mm × 4.6 mm × 5 µm; Daicel Chemical Industries Ltd.) attached to a CHIRALPAK IG guard column (4 mm × 5 mm × 5 µm; Daicel Chemical Industries Ltd.) was used instead. For chiral HPLC analysis, the chiral compound was eluted in isocratic mode with 5 % IPA in hexane at 0.5 mL min^{-1} for 38 min.

The supernatant from larger scale turnovers containing oxidation products were extracted into EtOAc (3 × 100 mL), washed with brine (100 mL) and dried with $MgSO_4$ followed by solvent removal under reduced pressure. Products were purified on silica with a gradient from 80:20 to 50:50 hexane to EtOAc with a 2.5 % increase every 100 mL. When this was not successful, products were purified using preparative HPLC. They were eluted at 4 mL min^{-1} using a 5 % isocratic run of IPA in hexane for 5 mins before appplying a gradient from 5 % to 10 % for 20 mins. The identities of the products were determined via GC-MS and/or NMR analysis. All NMR samples were dissolved in 600 µL of $CDCl_3$.

3 Site-Saturation Mutagenesis of CYP101B1

3.1 Introduction

CYP101B1 is able to oxidise norisoprenoids such as β- and α-ionone with high regioselectivity for the C3 position with fast product formation rates (> 1000 min^{-1}). In addition, these substrates bind to the enzymes with high affinity (≥ 95 % HS, $K_d < 0.30$ µM).[57,61] The butenone side chain on the ionones is thought to be involved in substrate binding (Figure 17). β-Damascone (Figure 17), which has differing alkene and ketone positions on the butenone, showed lower binding affinity (≤ 90 % HS, $K_d \geq 7$ µM), however the regioselectivity of the oxidation is comparable to β-ionone.[101] Isophorone (Figure 17), which has a ring system similar to the ionones but missing the butenone side chain, displayed only a 40 % shift to the high spin form and slow NADH oxidation rate (75 min^{-1}).[101] Isophorone oxidation by CYP101B1 was unselective, generating 3 metabolites in low yield.

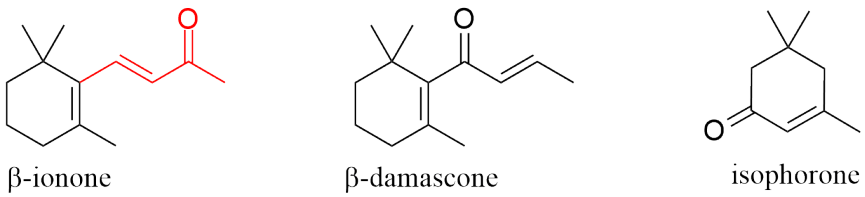

Figure 17: Structures of β-ionone, β-damascone and isophorone. The butenone side chain in β-ionone is highlighted in red.

Terpenoid substrates functionalised with an ester directing group, which mimics the butenone side chain of the norisoprenoids, have also been oxidised with high efficiency and regioselectivity by CYP101B1.[101] As an example, isobornyl acetate showed a 100-fold increase in binding affinity and was oxidised with a nearly 40-fold increase in product formation rate compared to isoborneol. It was also hydroxylated exclusively at the 5-*exo* position (Figure 18), whereas isoborneol was oxidised to three products in low yield.[101] The ester moiety is thought to act as a directing group to anchor the substrate in the active site of the enzyme. These oxidations demonstrate the utility of CYP101B1 in oxidising a wide range of high value compounds that are commonly used as flavourings and fragrances.

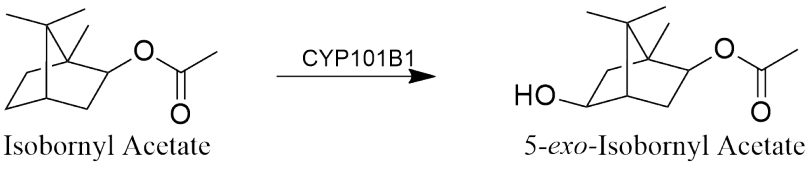

Figure 18: Regioselective oxidation of isobornyl acetate by CYP101B1.

The oxidation of hydrophobic substrates by CYP101B1 was less impressive. Phenylcyclohexane and *p*-cymene oxidations by the enzyme induced moderate (141 min^{-1}) to poor (25.3 min^{-1}) product formation rates.[61] It has also been reported that CYP101B1 was also capable of oxidising alkyl substituted naphthalene and biphenyl molecules with slower product formation rates than that of phenylcyclohexane (< 80 min^{-1}). These substrates also bind with lower binding affinities (≤ 55 % HS, K_d = 17 - 135 µM).[106] The aforementioned studies demonstrate the broad substrate range associated with CYP101B1. The aim of this study is to improve the activity of CYP101B1 towards hydrophobic substrates.

Sequence alignment of the CYP101 enzymes: CYP101B1, CYP101D1, CYP101D2 and CYP101A1 ($P450_{cam}$) show there are several equivalent residues within the active sites of these enzymes.[61] A residue of interest within CYP101B1 was the H85 residue which is equivalent to tyrosine residues in $P450_{cam}$ (Y96), CYP101D1 (Y98) and CYP101D2 (Y96).[61] These tyrosines are conserved in the structures of $P450_{cam}$ and CYP101D1, where they provide the only hydrophilic interaction with camphor as a substrate.[40]

CYP101D1 and CYP101D2 have been structurally characterised by X-ray crystallography.[107,108] CYP101D1 is the closest homolog of CYP101B1 in the Protein Data Bank (PDB) and its camphor-bound structure (PDB ID: 3LXI) was used to model the structure of CYP101B1 using Swiss Model.[109] The modelled active site is shown below (Figure 19).

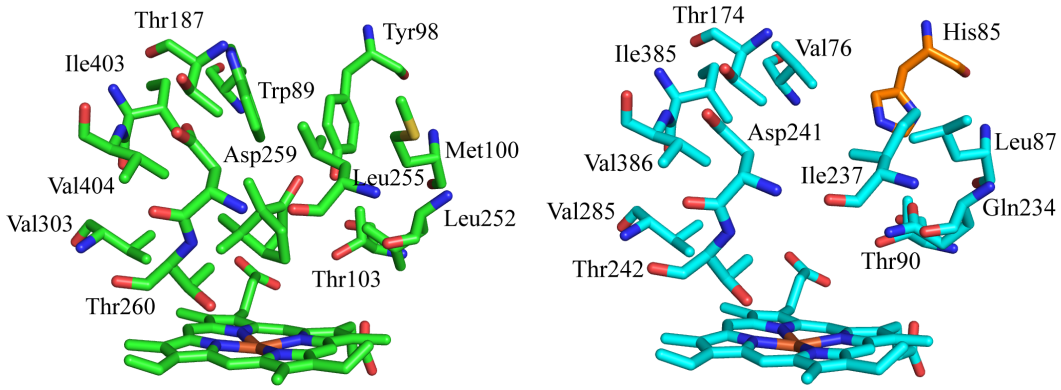

Figure 19: (a) Crystal structure of CYP101D1 with bound camphor (PDB ID: 3LXI).[63] (b) Modelled structure of CYP101B1 using Swiss Model that shows the possible location of the H85 residue (highlighted in orange).[109]

$P450_{cam}$ has been used as a model system to demonstrate how mutations of active site residues allow the enzyme to oxidise non-physiological substrates.[110–112] For example, the Y96 residue of $P450_{cam}$, which interacts with the carbonyl group of camphor via a hydrogen bond interaction, has been mutated to both alanine (Y96A) and pheny-

lalanine (Y96F). These two mutants showed increased binding affinity and oxidation rates towards phenycyclohexane when compared to the WT-enzyme.[110–112] The same mutations of the equivalent tyrosine residue of CYP101D2 also increased the affinity of this enzyme towards hydrophobic substrates.[113]

The H85 residue of CYP101B1 has been previously mutated to a phenylalanine (H85F). This change decreased the binding affinity and activity of CYP101B1 for β-ionone. The H85F mutant also showed improved affinity and activity towards certain hydrophobic substrates, such as acenapthene which showed poor activity with WT-CYP101B1. The binding affinity for this substrate was improved nearly six-fold with the H85F mutant.[114]

The mutagenesis of the H85 residue and subsequent change in enzyme activity showed that the residue plays a role in substrate binding and is likely to be within the active site of CYP101B1. This position is therefore a suitable target for site-saturation mutagenesis. This involves replacing the H85 residue within CYP101B1 with a range of other possible amino acid residues. The mutants generated in this library will then be screened for activity with hydrophobic non-natural substrates. It is hypothesised that changing the steric bulk and hydrophobicity of the H85 residue should allow CYP101B1 to accommodate different substrates.

3.2 Results

Site-saturation mutagenesis was achieved using a gene fragment (gBlock) with a nnC triplet codon (n is a random base) incorporated at the H85 position. The nnC codon would allow the introduction of all possible amino acids with codons ending with cytosine at this position. For example, when the GGC codon is present, position 85 within CYP101B1 would now contain a glycine residue and this mutant is now termed the H85G mutant. A total of 14 possible mutants can be produced with this gBlock fragment. The following table lists all the possible mutants that can be generated with the gBlock gene fragment and the mutants that were successfully produced (Table 5).

Table 5: All possible mutants that can be produced using the gBlock fragment with a nnC codon at the H85 residue. Mutants that were successfully produced and identfied were denoted with 'Y' and mutants that were not produced were denoted with 'N'. The CAC codon which was generated produces a histidine residue which would be the WT enzyme.

Mutant	**nnC**	**Y/N**
H85G	GGC	Y
H85A	GCC	Y
H85T	ACC	Y
H85D	GAC	Y
H85F	TTC	Y
H85V	GTC	Y
H85R	CGC	Y
H85Y	TAC	Y
H85N	AAC	Y
H85S	AGC, TCC	Y
H85I	ATC	Y
H85P	CCC	N
H85C	TGC	N
H85L	CTC	N
H85	CAC	Y

The gBlock fragment was cloned into vectors pET22 and pRSFDUET (Chapter 2, Section 2.2.1). Vector pET22 was used for enzyme production and purification for *in vitro* studies, while vector pRSFDUET which has the Arx gene was used in whole-cell studies with a pETDUET vector containing the ferredoxin reductase, ArR (Chapter 2, Section 2.7.1). The mutants H85P, H85L and H85C were not able to be produced. A total of 11 mutants were generated using this method (Table 5). To confirm whether expression could be achieved, each H85 mutant enzyme within vector pET22 in Table 5 was produced using *E.coli* cells. In all cases, the cell pellets produced were red in appearance, indicating that functional P450s were being generated.

3.2.1 Whole-Cell Studies of CYP101B1 Mutants

The mutants contained in vector pRSFDUET along with the ferredoxin, Arx were co-expressed with a pETDUET vector that contains the ferredoxin reductase, ArR. This generates all three enzymes of the CYP101B1 systems in a single *E.coli* cell and enables whole-cell oxidation. These mutant whole-cell systems were then used for *in vivo* screening with various substrates (Figure 20).

The substrates screened include β-ionone as a control to determine if the mutants altered the oxidation activity. Small and bulky hydrophobic molecules with poor affinity and activity with WT-CYP101B1 were also screened to assess if the mutants have improved oxidation activity. Norisoprenoid and terpenoid compounds such as pseudoionone and 1,8-cineole, were chosen to assess if the mutants improved metabolite yield over the WT enzyme or changed the selectivity of oxidation. The WT enzyme was also screened concurrently with the mutants as a control. Any metabolites previously shown to be generated by the WT enzyme were used to identify products from the mutant.[101,104,106,114]

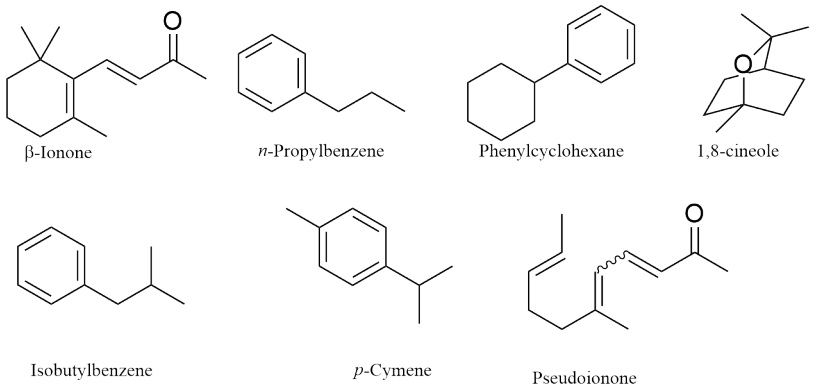

Figure 20: Substrates used for whole-cell *in vivo* screening of CYP101B1 mutants.

The total metabolite yield for β-ionone oxidation with the mutants was lower compared to the WT enzyme. However, the mutants H85G, H85V and H85A all shifted the selectivity of product formation towards the 4-hydroxy metabolite (Figure 21). H85G, H85V and H85A were all mutants containing small hydrophobic residues and these variants favoured oxidation of the more reactive allylic C-H bonds.[114] The altered levels of product formation and change in selectivity provided evidence that the mutant residues were successfully incorporated, and that the H85 residue plays a role in substrate binding.

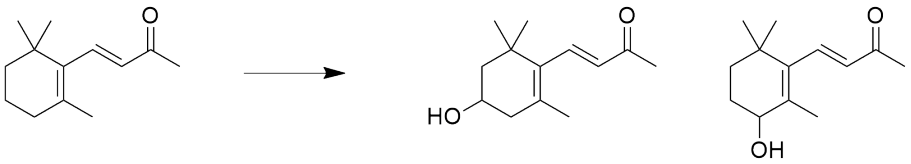

β-ionone | 3-hydroxy-β-ionone | 4-hydroxy-β-ionone

WT	70 %	30 %
H85G	24 %	76 %
H85A	27 %	73 %
H85V	19 %	81 %

(a)

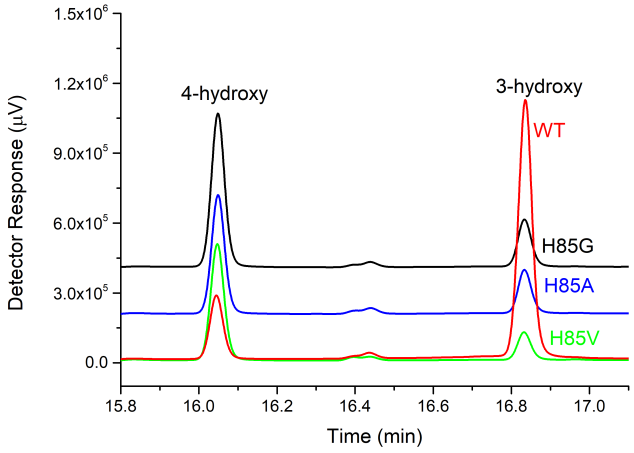

(b)

Figure 21: (a) The oxidation of β-ionone by CYP101B1 mutants. (b) GC-BID analysis of CYP101B1 mutant whole-cell turnovers include the WT (red), mutants H85G (black), H85A (blue) and H85V (green). The remaining mutants that were tested produced lower metabolite yield than the WT. For clarity, the chromatograms were offset along the y-axis.

Phenylcyclohexane is a bulky hydrophobic substrate, and when oxidised by WT-CYP101B1, the sole product was *trans*-4-phenylcyclohexanol (Figure 22).[61] The same product was formed for each of the H85 mutants screened with phenylcyclohexane.

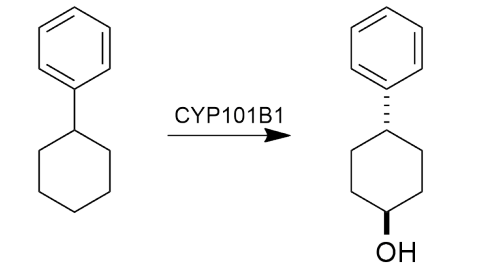

phenylcyclohexane | *trans*-4-phenylcyclohexanol

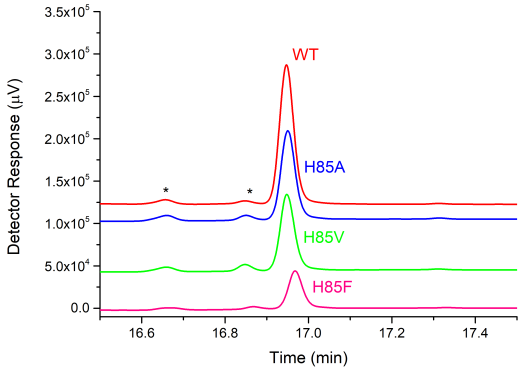

Figure 22: (a) The oxidation of phenylcyclohexane by CYP101B1 mutants. (b) GC-BID analysis of CYP101B1 mutant whole-cell turnovers include the WT (red), mutants H85A (blue), H85V (green) and H85F (pink). For clarity, the chromatograms were offset along the y-axis. Impurities were marked with *.

The product formation levels for all mutants observed were lower than the WT enzyme, even for mutants with smaller residues such as glycine, alanine and valine, which were expected to accommodate the bulkier substrate by virtue of having larger active sites (Figure 22). Potential impurities were also present within the turnovers with phenylcyclohexane but were not identified.

In this study, the metabolites arising from turnovers with isobutylbenzene, *n*-propylbenzene and *p*-cymene and the mutants matched those of the WT-enzyme.[61,114] For all three substrates, the H85F variant generated more product than the WT-enzyme and the other mutants (Figure 23, 24 and 25). This agreed with previous *in vitro* studies of the H85F variant which showed that this mutant increased the binding affinity and oxidation activity of CYP101B1 towards these three substrates.[115]

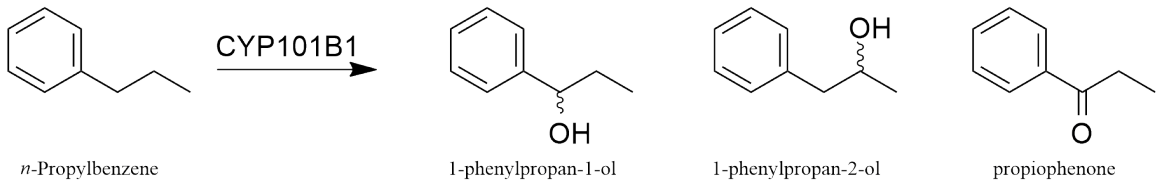

WT	22 %	10 %	70 %

(a)

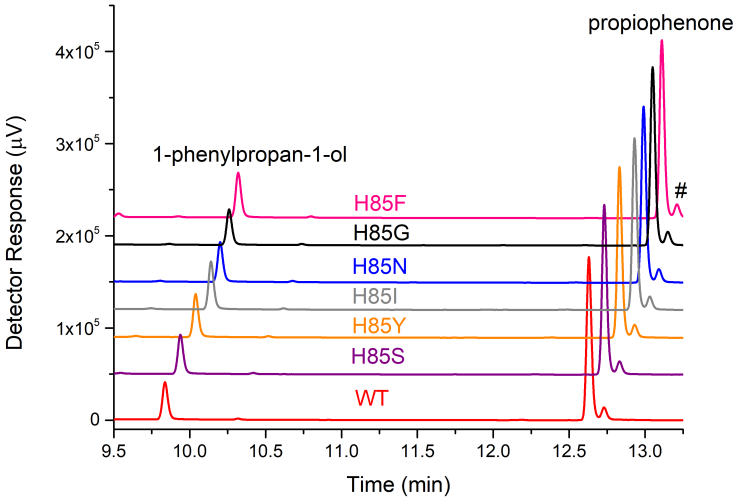

(b)

Figure 23: (a) The oxidation of *n*-propyl benzene by CYP101B1 mutants. (b) GC-BID analysis of CYP101B1 mutant whole-cell turnovers with *n*-propylbenzene. 1-Phenylpropan-2-ol is labelled as #. For clarity, the chromatograms were offset along both axes.

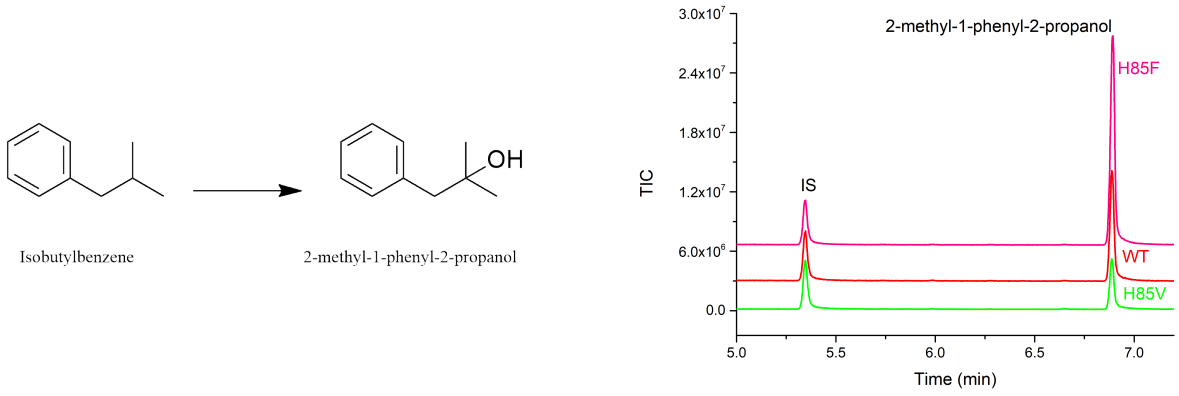

Figure 24: The oxidation of isobutylbenzene by CYP101B1 mutants. GC-MS analysis of the whole cell turnovers of the WT (red) and mutants H85F (pink) and H85V (green). Ratio of the sole product to internal standard (IS): 1.92 (WT), 4.63 (H85F), 1.02 (H85V). For clarity, the chromatograms have been offset along the x-axis.

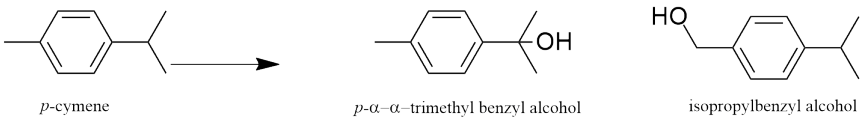

WT	85 %	15 %
H85F	25 %	75 %
H85V	24 %	76 %

(a)

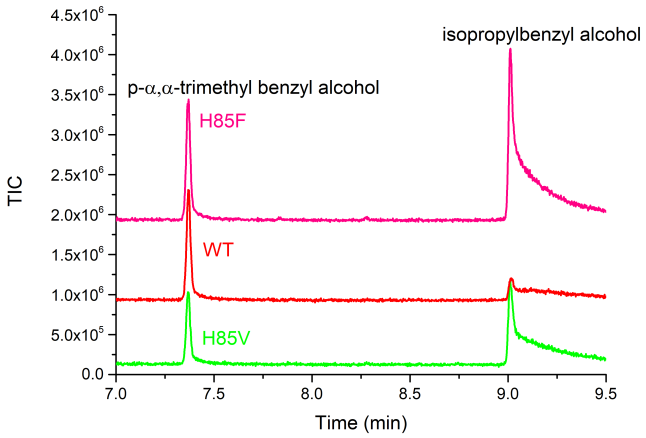

(b)

Figure 25: (a) The oxidation of p-cymene by CYP101B1 mutants. Product distribution was determined via GC-MS analysis. (b) GC-MS analysis of the whole cell turnovers of the mutants including the WT (red), mutants H85F (pink) and H85V (green). For clarity, the chromatograms have been offset along the y-axis.

Amongst the new variants tested, the n-propylbenzene turnovers had seven variants that displayed similar levels of product formation with the WT enzyme (Figure 23). Mutant H85V showed the highest product formation with isobutylbenzene and p-cymene, though the levels were lower than the H85F variant (Figure 24 and 25). The

p-cymene turnovers did display altered product selectivity with the mutants, forming more isopropylbenzyl alcohol, which was less favoured by the WT enzyme (Figure 25).

CYP101B1 oxidises both isomers regioselectively at the alkene furthest from the carbonyl group to yield two epoxide products (*cis*/*trans*, Figure 26).[101] All mutants screened formed the same epoxide products as the WT-enzyme and potential impurities were also present (Figure 26).

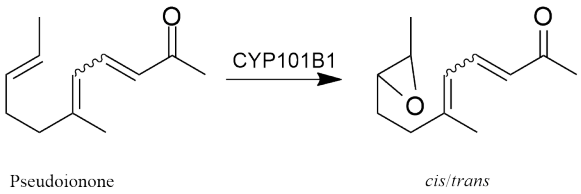

	trans	*cis*
WT	57 %	43 %
H85G	28 %	72 %
H85S	34 %	66 %
H85F	57 %	33 %

(a)

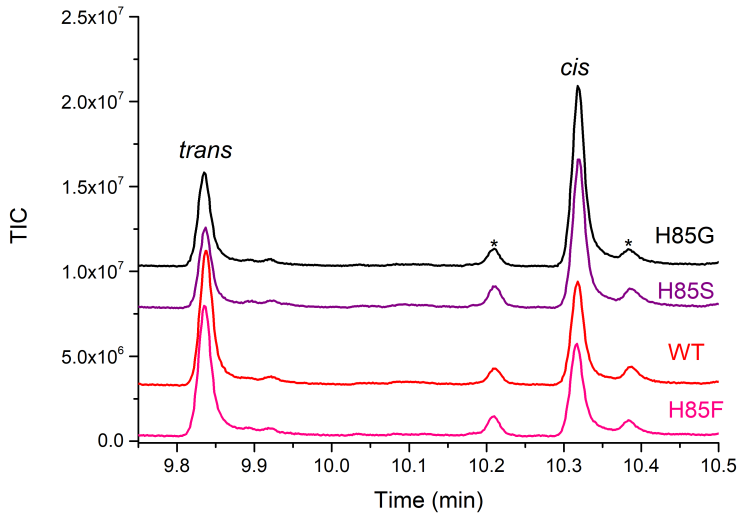

(b)

Figure 26: (a) The oxidation of pseudoionone isomers by CYP101B1. (b) GC-MS analysis of CYP101B1 mutant whole-cell turnovers with pseudoionone include the WT (red), mutants H85S (purple), H85G (black) and H85F (pink). For clarity, the chromatograms have been offset along the *y*-axis. Impurities were marked with *.

Amongst the mutants screened with pseudoionone, H85F generated similar amounts of product compared to the WT-enzyme. The amount of product generated by the mutants H85S and H85G was approximately two-fold higher (Figure 26). WT-CYP101B1

and H85F favoured the formation of the *trans* isomer. Mutants H85G and H85S seems to have shifted the selectivity of CYP101B1 to favour the oxidation of the *cis* isomer instead. There were also impurities present with the pseudoionone turnovers that were not identified (Figure 26b).

1,8-Cineole oxidation by WT-CYP101B1 forms multiple products that have been previously identified as 5-keto-, 5-α-, 6-α-, 6-β- and 5-β-hydroxy-1,8-cineole (Figure 27a).[104] The H85F and H85I mutants generated the highest amount of product and also displayed changes in product selectivity over the WT (Figure 27b). The WT enzyme displayed high selectivity towards towards both 5-keto- and 5-α-hydroxy-1,8-cineole ($>$ 99 %), but the selectivity towards the 5-keto metabolite was decreased with the H85I and H85F mutants (Table 6). The minor metabolites, 6-α-, 6-β- and 5-β-hydroxy-1,8-cineole, which were only produced in small quantities by the WT, were formed in higher yield by these mutant enzymes (Figure 27b, Table 6).

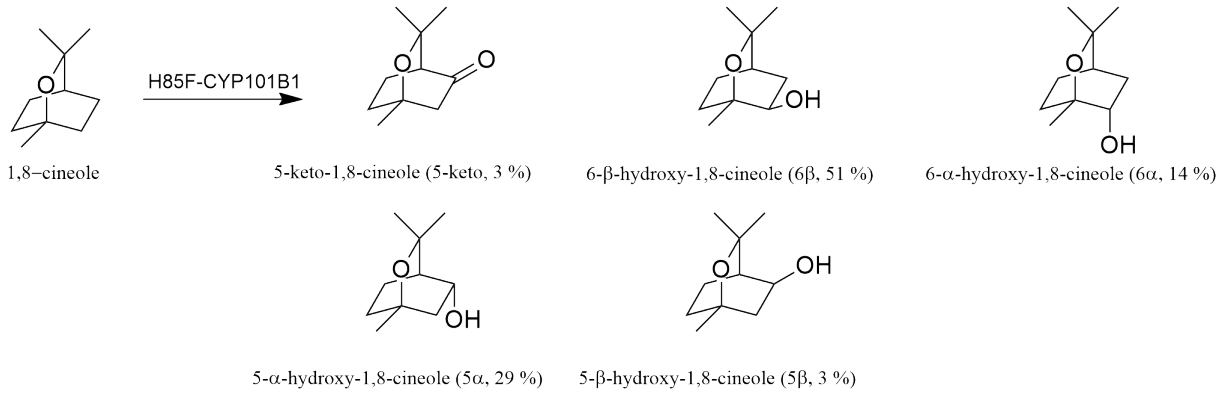

(a)

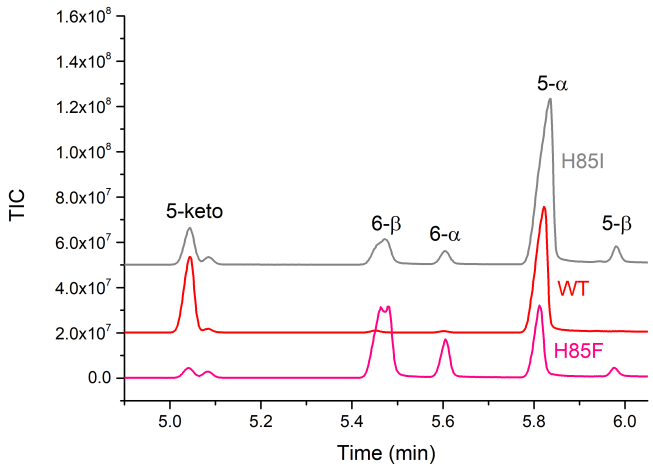

(b)

Figure 27: (a) Products of 1,8-cineole oxidation by CYP101B1. (b) GC-MS analysis of CYP101B1 mutant whole-cell turnovers with 1,8-cineole which include the WT (red), H85I (gray) and H85F (pink).

Table 6: Percentage distribution (%) of 1,8-cineole oxidation products by CYP101B1 and its mutants are listed. See Figure 27 for abbreviations.

	5-keto	6-β	6α	5α	5β
WT	34	< 1	< 1	66	< 1
H85I	11	12	< 1	73	4
H85F	3	51	14	29	3

Initial whole-cell screening of the new CYP101B1 mutants thus showed that altering the H85 residue did not improve or alter the *in vivo* activity of the enzyme with a broad range of substrates. This was in spite of equivalent mutations in other CYP101 family enzymes with higher activity with hydrophobic substrates. Further *in vitro* analysis of the new mutants would be needed to confirm the activity of the mutant enzymes.

3.2.2 *In Vitro* Studies of CYP101B1 Mutants.

This lack of improvement in enzyme activity by the mutant enzymes suggested that the alterations of the H85 residue did not significantly affect the binding and oxidation of CYP101B1. To test this hypothesis, the CYP101B1 mutants H85A and H85G were produced and purified for more detailed *in vitro* investigation (Section 2.4.1).

Mutant H85F and WT-CYP101B1 have been studied previously and have low affinities towards sterically bulky substrates like biphenyls and phenylcyclohexane.[61,106] It was hypothesised that the mutants with less bulky residues such as alanine and glycine would introduce more space within the active site to accommodate these substrates. A similar study employing $P450_{cam}$ was successful in increasing the enzyme's affinity towards bulkier substrates such as phenylcyclohexane and naphthalene.[110,111] Both proteins were purified and the ferrous-CO assay of each variants showed they were functional P450s (Figure 28).[102]

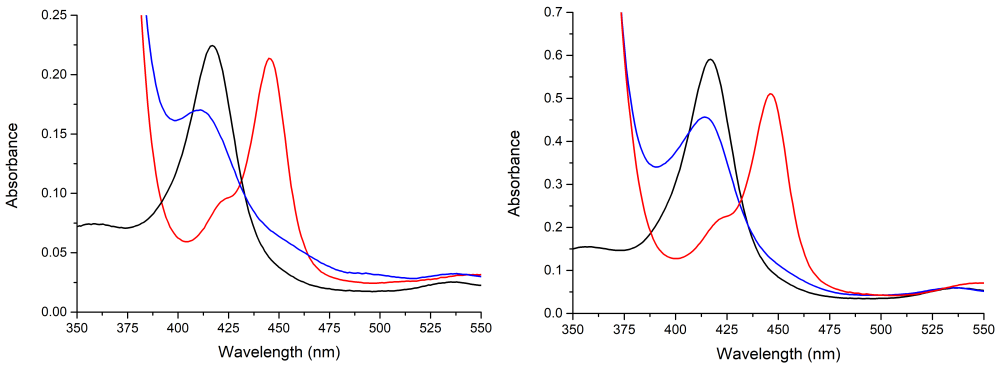

(a) (b)

Figure 28: CO-Assay of CYP101B1 (a) H85A and (b) H85G. The enzyme ferric (black, $\lambda_{max} = 417$ nm), ferrous (blue, $\lambda_{max} = 414$ nm) and ferrous-CO bound forms (red, $\lambda_{max} = 450$ nm) are shown.

WT-CYP101B1 induced a high spin-state shift with both α and β-ionone (> 95 % HS, Table 7).[61] Spin-state shift studies with the H85A and H85G mutants were carried out firstly with these two substrates. The H85A mutant with both ionones displayed large type I spin-state shifts (90 % HS, Figure 29) which were only marginally lower than those observed with the WT enzyme.[61] The spin-state shifts observed for H85G were even lower with β-ionone inducing a 60 % HS shift and α-ionone only inducing a shift to 40 % HS (Figure 30).

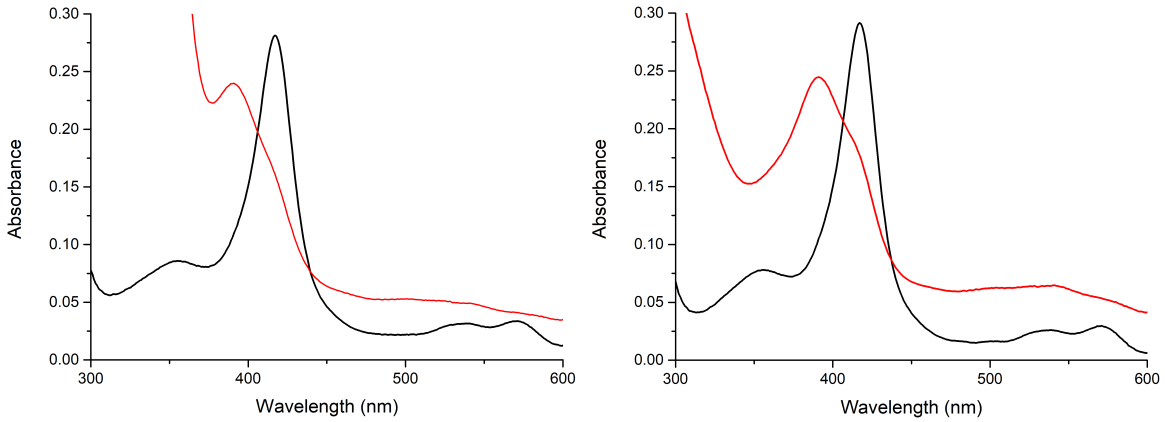

(a) (b)

Figure 29: Spin-state shifts of H85A-CYP101B1 with (a) β-ionone and (b) α-ionone.

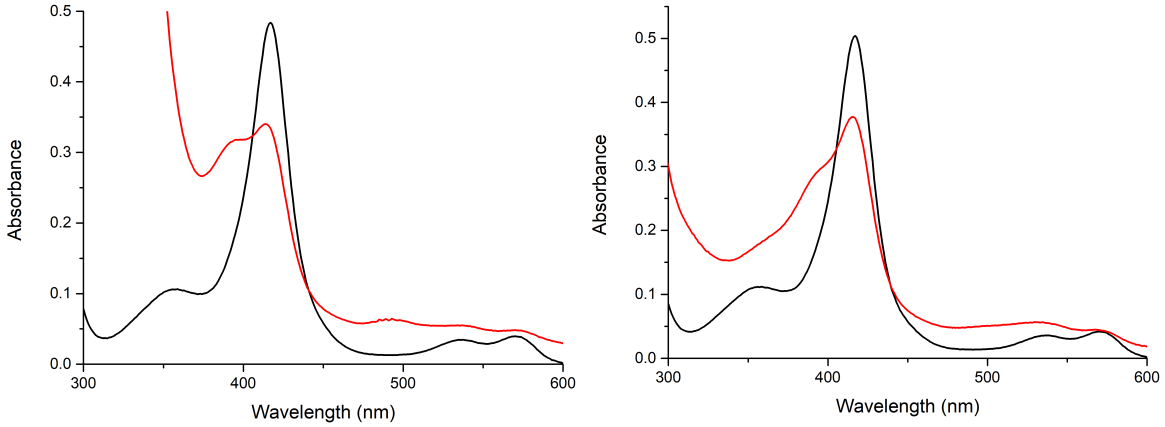

(a) (b)

Figure 30: Spin-state shifts of H85G-CYP101B1 with (a) β-ionone and (b) α-ionone.

The dissociation constants for the mutants towards β-ionone were determined to be 100 $\pm$ 20 µM and 231 $\pm$ 32 µM for H85A and H85G respectively (Figure 31, Table 7). The binding affinity of the WT enzyme with β-ionone was significantly higher (0.23 µM, Table 7). The lower spin-state shifts and weaker dissociation constants observed for both variants indicated that the active site mutants lowered the binding preference of CYP101B1 towards ionones and that this residue is involved in substrate binding.

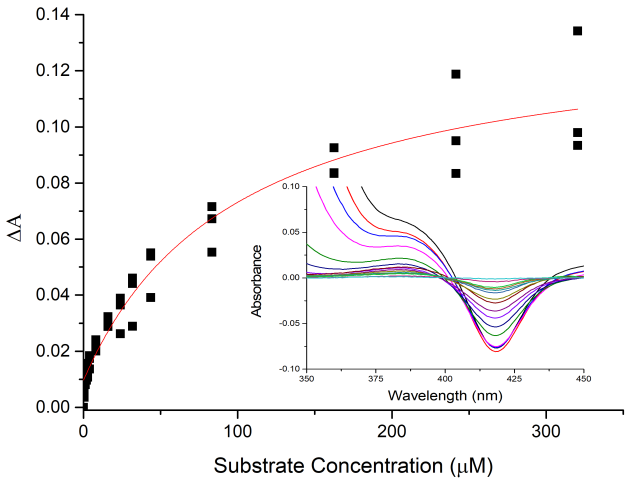

(a)

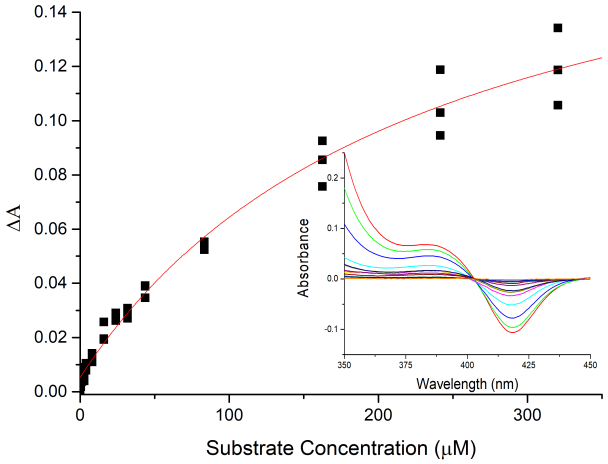

(b)

Figure 31: Dissociation constant analyses of β-ionone with (a) H85A-CYP101B1 and (b) H85G-CYP101B1. Peak to trough used to measure K_d was from A_{420}-A_{600} as β-ionone absorbed strongly below 400 nm.

Table 7: Substrate binding and *in vitro* turnover data for CYP101B1 mutants with different substrates. The data are given as mean ± S.D. with $n \geq 3$. Rates are given as nmol.nmol$_{P450}^{-1}$.min^{-1}.

Mutant	Substrate	% HS	K_d (μM)	NADH	PFR	Coupling
WT[61]	β-Ionone	≥ 95	0.23 ± 0.1	1600 ± 100	1010 ± 60	63
	α-Ionone	≥ 95	0.26 ± 0.04	1380 ± 140	660 ± 60	48
	Phenylcyclohexane	20	7.8 ± 0.9	293 ± 9.0	141 ± 17	48
H85A	β-Ionone[a]	90	100 ± 20	760 ± 7	302 ± 13	40 ± 2
	α-Ionone	90	-[b]	740 ± 16	187 ± 54	25 ± 7
	Phenylcyclohexane	20	15 ± 2	106 ± 5.0	22 ± 1	21 ± 1
H85G	β-Ionone[a]	60	231 ± 32	569 ± 24	185 ± 10	33 ± 1
	α-Ionone	40	-[b]	294 ± 57	22 ± 7	7 ± 3
	Phenylcyclohexane	-[c]	25 ± 6	24 ± 4.0	-[d]	-[d]

[a]Peak to trough used to measure K_d was from A_{420}-A_{600} as β-ionone absorbed strongly below 400 nm. [b]Not measured. [c]No spin-state shift observed. [d]No product formation.

The two mutants were then assayed with phenylcyclohexane to determine if the mutants were better able to accommodate this hydrophobic molecule as hypothesised. The H85A mutant only induced a 20 % HS shift (Figure 32a, Table 7) that was similar to the WT.[61] Addition of phenylcyclohexane to the H85G mutant did not display a significant change in spin-state (Figure 32b, Table 7). The dissociation constants of the mutants (Figure 33) with phenylcyclohexane were measured and found to be 15 ± 2 µM and 25 ± 6 µM for H85A and H85G respectively, which showed that both mutants had weaker binding affinity than the WT (7.8 µM, Table 7).[61]

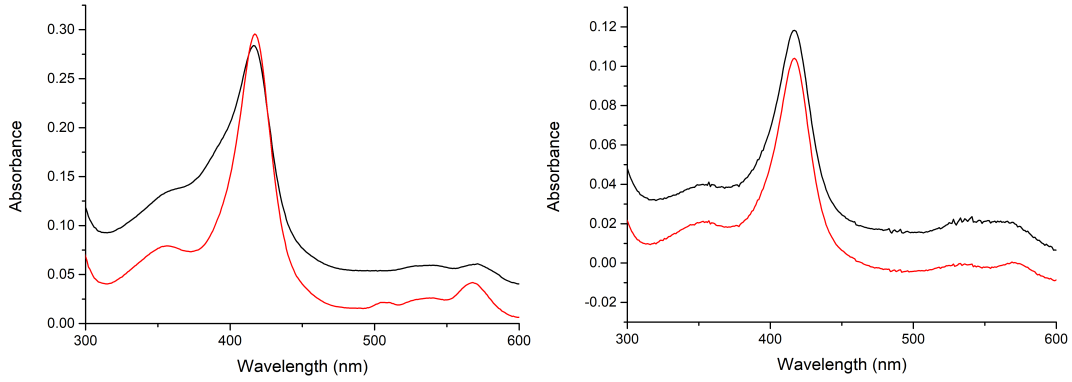

(a) (b)

Figure 32: Spin-state shifts of (a) H85A-CYP101B1 (b) H85G-CYP101B1 with phenylcyclohexane.

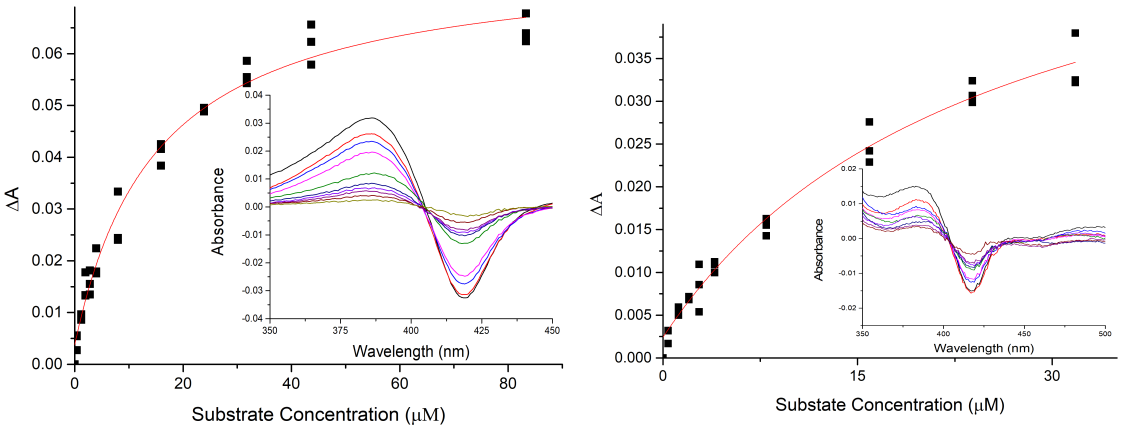

(a) (b)

Figure 33: Dissociation constant analysis of phenycylohexane with (a) H85A-CYP101B1 and (b) H85G-CYP101B1.

The NADH oxidation and product formation rates for both mutants were determined with phenylcyclohexane and β- and α-ionone to measure the catalytic activity of the two mutants towards each substrate (Table 7). The products of each turnover were identified by comparison to the WT-turnover as per the whole-cell screening studies.[61] Products were calibrated against the substrate and this was then used to estimate the concentration of the product peak using GC-MS analysis.

The rates of NADH oxidation with β-ionone were 760 and 569 nmol.nmol$_{P450}{}^{-1}$.min^{-1} (henceforth abbrieviated as min^{-1}) for the H85A and H85G mutant, respectively. These were more than 2-fold slower than that of the WT-enzyme. This result was also consistent with the lower spin-state shifts and binding affinities observed for both mutants with β-ionone. The reduced coupling efficiencies for H85A and H85G (40 % and 33 % respectively) were a result of lower levels of products compared to the WT (Table 7). The product distribution, as determined by GC-MS analysis of the mutant turnovers displayed altered product selectivity by favouring the 4-hydroxy metabolite. This change in selectivity was consistent with the whole-cell oxidation turnovers of the H85A and H85G mutant systems with β-ionone (Figure 21). This was also observed with the H85F variant, where 4-hydroxy-β-ionone was the major product.[19,57,114]

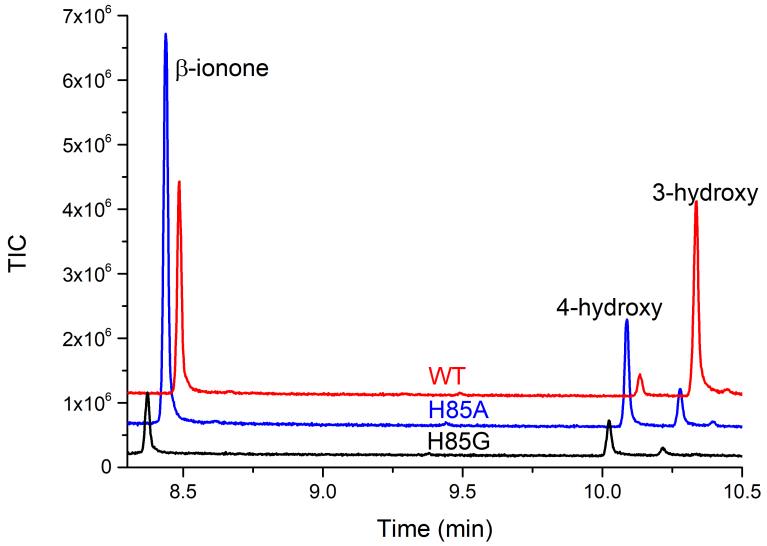

Figure 34: GC-MS analysis of the *in vitro* turnovers of WT-CYP101B1 (red) with β-ionone in comparison to mutants H85A (blue) and H85G (black) with β-ionone. For clarity, the chromatograms have been offset along the x- and y- axes.

The oxidation activity of both mutants with α-ionone showed similar trends as β-ionone. The NADH oxidation activity of both mutants was more than 5-fold slower than the WT-enzyme, and low coupling efficiencies ($\leq$ 30 %) resulted in a significant decrease in the product formation rates ($<$ 200 min^{-1}, Table 7). Both mutant turnovers generated *cis*- and *trans*-3-hydroxy-α-ionone alongside small quantities of 3-oxo-α-ionone (Figure 35). The mutants did not change the product selectivity in comparison to the WT-enzyme, and the *trans*-3-hydroxy diastereomer was the major product for both mutants.

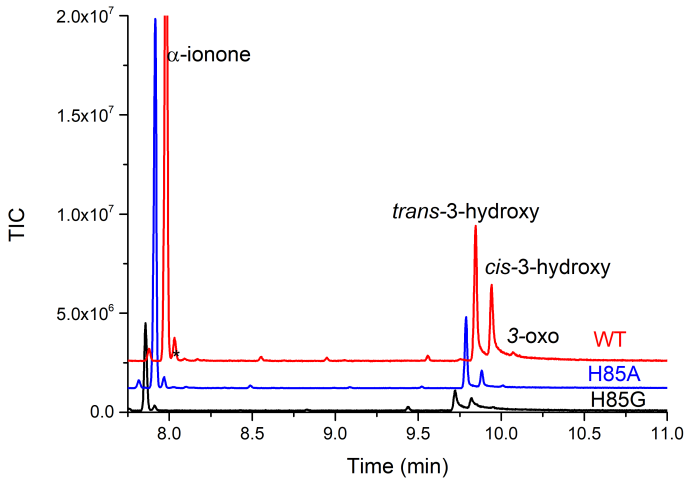

(a)

Figure 35: GC-MS analysis of the *in vitro* turnovers of WT-CYP101B1 (red) with α-ionone in comparison to mutants H85A (blue) and H85G (black) with α-ionone. For clarity, the chromatograms have been offset along the x and y axes.

More surprisingly, the hydrophobic substrate, phenylcyclohexane also displayed low oxidation activity with both mutants (Table 7). The H85A and H85G mutants both displayed slower NADH oxidation rates compared to the WT (293 min^{-1}), with the H85G mutant being reduced by more than 10-fold (24 min^{-1}). The H85A mutant displayed low coupling efficiency (21 %) that resulted in a reduced product formation rate (22 min^{-1}). *trans*-4-Phenylcyclohexane was the sole product (Figure 36).

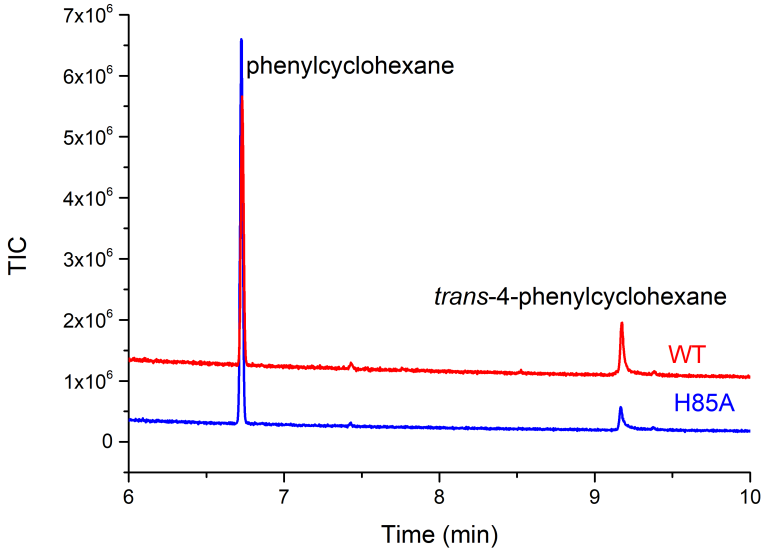

Figure 36: GC-MS analysis of the *in vitro* turnovers of WT-CYP101B1 (red) in comparison to mutant H85A (blue) with phenylcyclohexane. For clarity, the chromatograms have been offset along the x- and y- axes.

The H85G variant did not generate any product formation from monooxygenase ac-

tivity. The weaker binding affinity and slower oxidation activity for both mutants indicates that additional active site volume to accommodate phenylcyclohexane may not have been introduced as initially hypothesized.

3.2.2.1 Spin-State Shift Studies with Mutants H85A and H85G

To further investigate the substrate range of these variants of CYP101B1, spin-state shifts of the H85A and H85G mutants were measured with a wider variety of hydrophobic, terpenoid and norisoprenoid substrates. The highest spin-state shift induced for both mutants was with β-damascone which was 80 % HS for H85A and 50 % HS for H85G respectively (Figure 37). These were on par or lower than the spin-state observed with the WT (80 %).

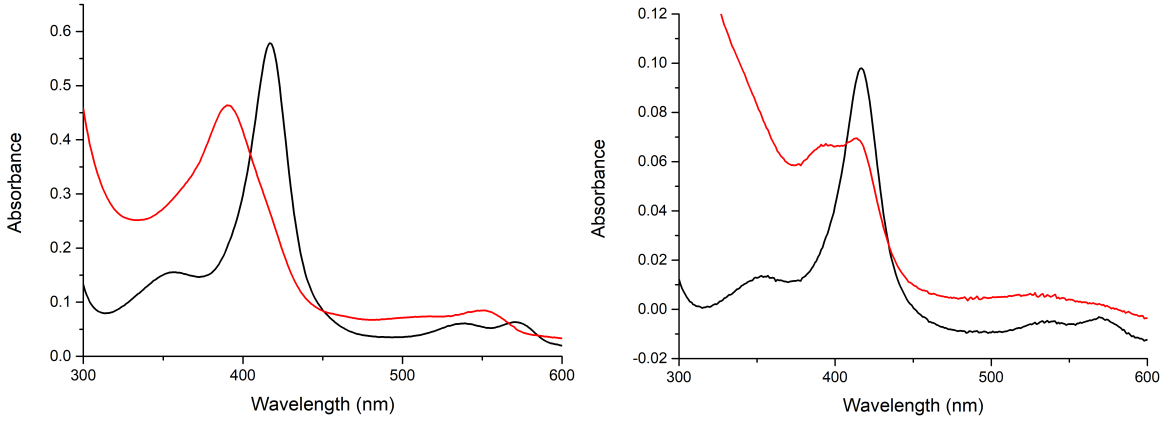

(a) (b)

Figure 37: Spin-state shift studies of β-damascone with CYP101B1 mutants (a) H85A and (b) H85G.

Terpenoids such as 1,8-cineole, *cis*-jasmone, fenchyl acetate, isobornyl acetate, and nopol, induced spin-states that were less than 10 % HS for the H85G mutant (Appendix A1). This contrasted the higher spin-state shifts observed for WT-CYP101B1 with these substrates (45 - 95 % HS).[101] Spin-state shifts of these substrates with H85A were not measured.

A selection of cycloalkanes were also assayed with both mutants. The H85A mutant with cyclodecane displayed the highest spin-state shift (60 % HS), this was followed by cyclooctane (50 % HS) and then cyclododecane (40 % HS, Figure 38). Spin-state shift data for the WT and H85F mutant enzyme with cycloalkanes were also collected for comparison (Table 8). The spin-state of cyclodecane and cyclooctane were greater with the H85F variant (¿ 50 %).

It is worth noting that both the H85A and H85F mutants had higher spin-state shifts induced by cyclodecane and cyclooctane than the WT-enzyme. It appears that hy-

drophobic methyl and phenylalanine residues at the H85 position enhanced the binding of CYP101B1 towards the cycloalkanes. The H85G variant with cyclodecane and cyclododecane had poor spin-state shifts ($\leq$ 10 % HS, Appendix A2), suggesting that smalller residues did not give the same effect. We also note that the larger substrate cyclododecane induced lower spin-state shifts with the H85A variant than cyclodecane or cyclooctane (Table 8).

Table 8: Spin-state shift data for CYP101B1 and its mutants, H85A and H85F, with cycloalkanes.

Mutant	Substrate	% HS
WT[a]	Cyclodecane	40
	Cyclooctane	35
H85F[a]	Cyclodecane	90
	Cyclooctane	80
H85A	Cyclodecane	60
	Cyclooctane	50
	Cyclododecane	40

[a] Data provided by Raihan Sarkar of the University of Adelaide.

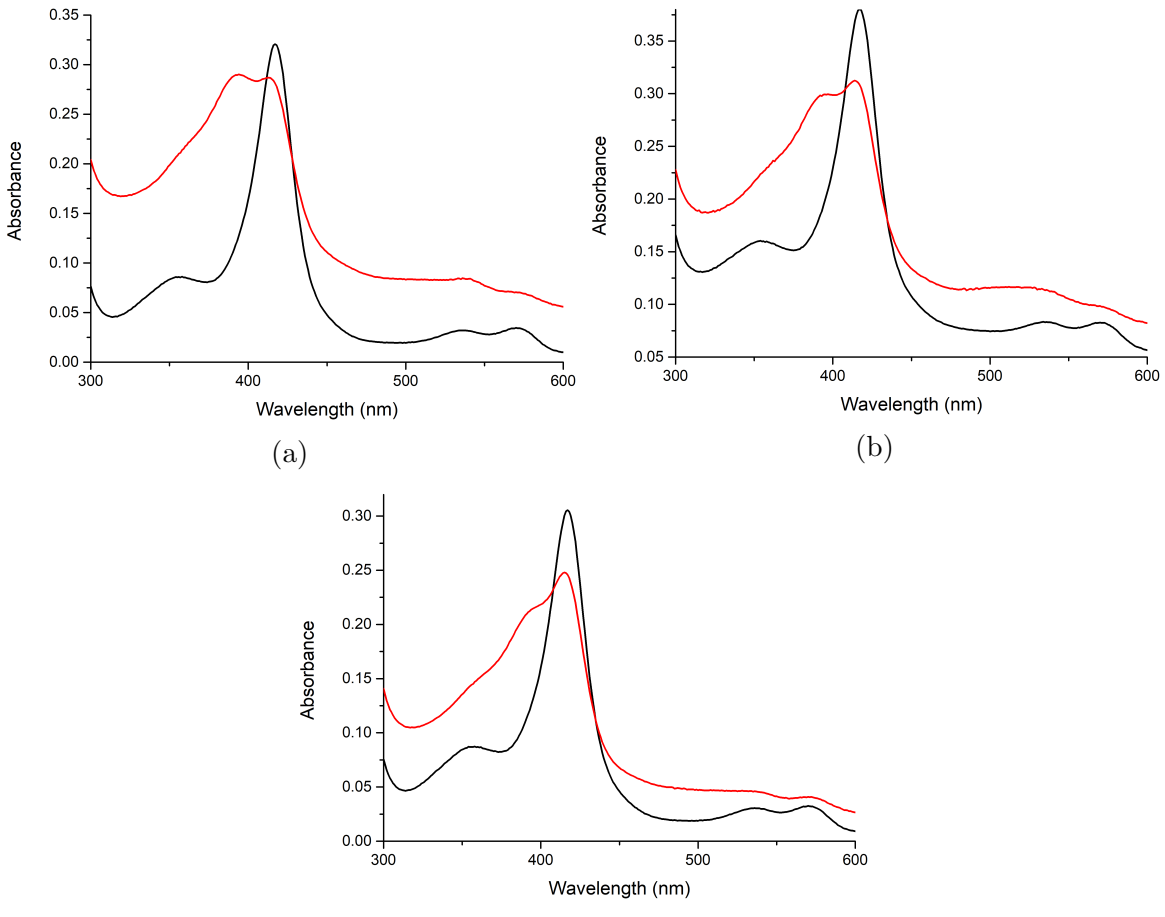

Figure 38: Spin-state shift studies of CYP101B1-H85A with (a) cyclodecane, (b) cyclooctane and (c) cyclododecane.

Additional *in vitro* studies of both mutants with a selection of hydrophobic substrates all consistently gave spin-state shifts lower than 30 % HS irrespective of the substrate size (Appendix A3, A4 and A5). This is a strong indication of poor enzyme-substrate fit and it was likely that the mutants had weak binding affinity with hydrophobic substrates.

3.3 Discussion

We were able to generate eleven mutant forms of CYP101B1 at the H85 position. Ten of the mutants were new variants including Gly, Ala, Thr, Asp, Val, Arg, Tyr, Asn, Ser and Ile residues at position 85 in CYP101B1. The screening using *in vivo* systems showed that some of the mutants had increased product formation and changes in the product selectivity (Figure 21, 26 and 27). However, the majority were less effective than the WT enzyme or the previouly studied H85F variant at oxidising hydrophobic substrates.[61,114] The higher product formation of H85F with *n*-propylbenzene, isobutylbenzene and *p*-cymene was expected, as the mutant showed improved enzyme activity and binding affinity with these three substrates *in vitro* (Figure 23, 24 and 25).[114]

The lack of significant improvement to the enzyme activity of the other mutants with the substrates screened were unexpected. The changes in enzyme activity and selectivity of the mutants with β-ionone is strong evidence that the H85 residue is within the active site or the access channel. It also suggests that this residue has a role in substrate binding. However, the high spin-state shift and enzyme activity induced by β-ionone with the H85A mutant infer that the H85 residue is not the only significant residue involved in substrate binding (Figure 29).

The *in vitro* studies on mutants of CYP101B1 suggests that mutating to smaller residues (alanine and glycine) did not lead to the expected increase in binding affinity or activity with larger hydrophobic substrates. In contrast, $P450_{cam}$ was able to oxidise larger molecules such as diphenylmethane upon the introduction of the Y96A mutant.[112] An important observation is that the Y96A variant of CYP101D2 from *N. aromaticivorans* did not improve the activity towards larger substrates either.[113] Therefore, the enzymes of the CYP101 family from different bacteria seem to display different behaviour upon mutagenesis of equivalent residues. This suggests that these mutations may have an effect on the conformation of these enzymes. The introduction of the mutants may have caused altered interactions between residues within the active site and of those surrounding it, which changes the architecture of the substrate binding pocket and thus affect substrate binding. Crystal structures of CYP101B1 would

be a useful tool in probing the conformation of the enzyme's active site for further study.

There are other residues of interest within the CYP101B1 active site that could be mutated to accommodate larger hydrophobic molecules, including Q234 and I237 that are equivalent to residues L244 and V247 in $P450_{cam}$ (Figure 39).[61] The L244 and V247 residues when mutated were able to increase the activity of $P450_{cam}$ towards non-natural substrates such as valencene and phenylcyclohexane.[79,116,117] However, a similar attempt at mutating equivalent residues within CYP101D2 to increase its binding affinity towards camphor was not successful.[113]

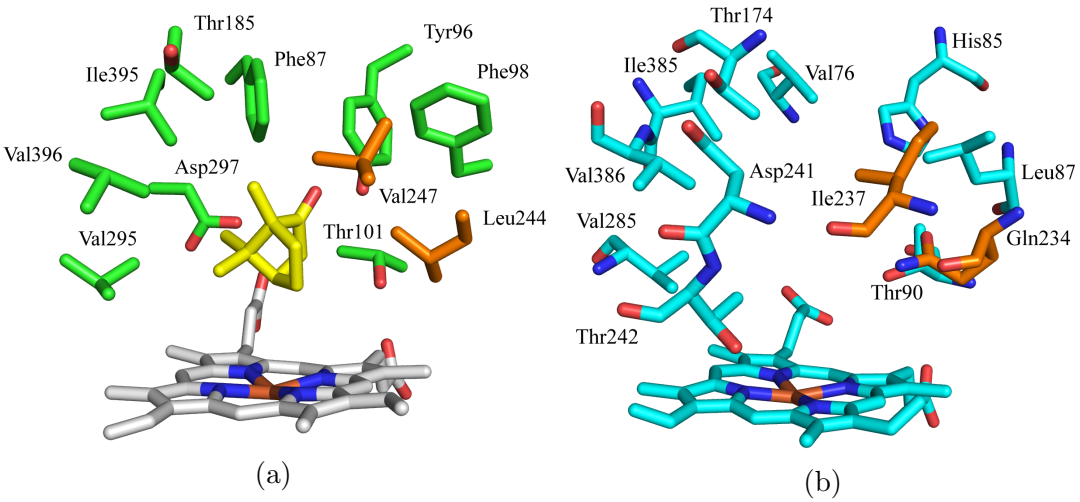

Figure 39: (a) Crystal structure of $P450_{cam}$ with bound camphor (PDB ID: 3WRH). (b) Modelled structure of CYP101B1 using Swiss Model. The L244 and V247 residues of $P450_{cam}$ and the equivalent residues of Q234 and I237 in CYP101B1 are highlighted in orange.

This work provided evidence that P450 evolutionary function and substrate preference does not solely depend on the identity of residues within the first sphere of the active site and their interactions with the substrate. There are likely other unknown factors as well that determine how the identity of the residues affect the overall conformation and subsequently the activity of P450 enzymes.

4 Oxidation of Terpenoids by P450 Mutants

4.1 Introduction

Monoterpenoids are a class of terpenes that are important constituents of plant essential oils.[118] Monoterpenoids consists of a 10 carbon backbone made up of 2 isoprene units.[119] These compounds have found widespread use as flavours, fragrances and pheromones with applications in pesticides, herbicides and as pharmaceutical ingredients.[120–122]

Oxygenated monoterpenes are highly sought after intermediates within commercial industries.[123] The parent monoterpenes can be easily extracted in large quantities from their natural sources but the oxidised variants of these terpenes often exist in lower quantities.[48] P450 catalysed regio- and enantioselective oxyfunctionalisations of these compounds have therefore garnered widespread attention as an important research field[123] New regio- and enantioselective oxidation of existing terpenoids could lead to new fragrances and flavouring compounds with unique sensorial properties.[88,124] Flavouring and fragrance compounds used in commercial products that are generated using chemical synthesis methods also need to be labelled as "nature-identical" under US and European legislation, but the same compounds produced using enzymatic processes can be labelled as "natural" and are more strongly preferred by consumers.[125] The distinct marketing advantage given to products labelled as "natural" has driven significant development for biotechnological processes that also include P450 research into developing novel methods to produce these compounds.[125]

The monoterpenoid, camphor (Figure 40), is the natural physiological substrate of $P450_{cam}$ that stereoselectively hydroxylates this substrate at the 5-*exo* position.[33,34] $P450_{cam}$ therefore serves as a good starting point to develop biocatalysts for the oxidation of terpenes and terpenoids. Mutagenesis of $P450_{cam}$ has generated variants that are capable of oxidising terpene compounds such as α-pinene.[46,74] The aim of this study involves utilising a library of $P450_{cam}$ mutants that have been previously developed for terpene oxidation. This library will be screened against a selection of terpenoids and other similar compounds to selectively generate metabolites (Table 9 and Figure 40).

Table 9: Norisoprenoids of interest alongside descriptions of their odours.

Compound	**Odour**
Fenchyl Acetate	Sweet and pine-like scent
Fenchone	Sweet and camphor-like scent
1,8-Cineole, 1,4-Cineole	Citrus and eucalyptus scent
Isophorone	Sharp and sweet-green camphor-like scent

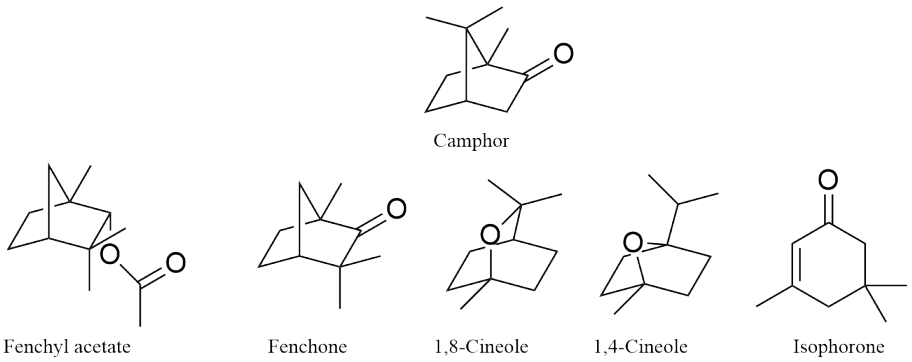

Figure 40: Target substrates used for screening by the library of $P450_{cam}$ mutants.

Fenchone and fenchyl acetate (Figure 40) are both constituents of essential oils from *Foeniculum vulgare*, otherwise known as the common fennel.[126] Fennel oils have exhibited antioxidant and antimicrobial activity and the biotransformation of these two terpenoids could lead to compounds with new biological profiles.[126]

1,8-Cineole is a monoterpenoid that is known trivially as eucalyptol and as the name suggests, the major component of eucalyptus oil.[96] Its isomer, 1,4-cineole (Figure 40), has a similar natural occurrence in many of the same species but often in much lower quantities.[127] The two cineoles are rather chemically inert and require the use of highly reactive reagents to hydroxylate them, often leading to racemic products. The *meso* symmetry of the cineoles allows a single hydroxylation to form at least two chiral centres.[96] These hydroxylated derivatives can be used as chiral auxiliaries in organic syntheses or as synthetic intermediates for herbicides and antimicrobial agents.[96,127,128]

Isophorone is cyclic ketone with a structure similar to the other terpenoids used in Figure 40. It is an important precursor compound for the synthesis of 4-hydroxyisophorone.[129] This compound is an important aroma molecule within saffron,[130,131] and a flavouring agent within tobacco products.[132] It also has applications within the synthesis of pharmaceuticals and natural dye pigments.[133,134]

Variants of $P450_{BM3}$ have also demonstrated the ability to catalyse selective and high yielding oxidation of isophorone and both cineole isomers.[105,135] Therefore, a second aim of this study is to compare $P450_{cam}$ variants to those of $P450_{BM3}$ using whole-cell systems to determine if one enzyme system is more efficient than the other in oxidising these substrates.

It is evident that the oxyfunctionalised derivatives of these compounds have many commercial applications and potential new synthetic pathways towards these compounds would be highly valued. Here, we will screen these terpenoids as substrates against the library of $P450_{cam}$ mutants *in vivo*. Mutants that display high levels of prod-

uct formation will be scaled up accordingly for product isolation and identification. This will potentially provide new biocatalytic pathways towards the synthesis of useful compounds derived from these monoterpenoids.

4.2 Results

Rationally designed mutants of $P450_{cam}$ have been found to increase the enzyme's activity towards (+)-α-pinene while also exhibiting good activity and selectivity towards terpenoid based substrates such as limonene.[45,46] This library of variants consisted of active site mutations at the F87, Y96, L244, V247 and I395 positions (Figure 41, Table 10).[45,46]

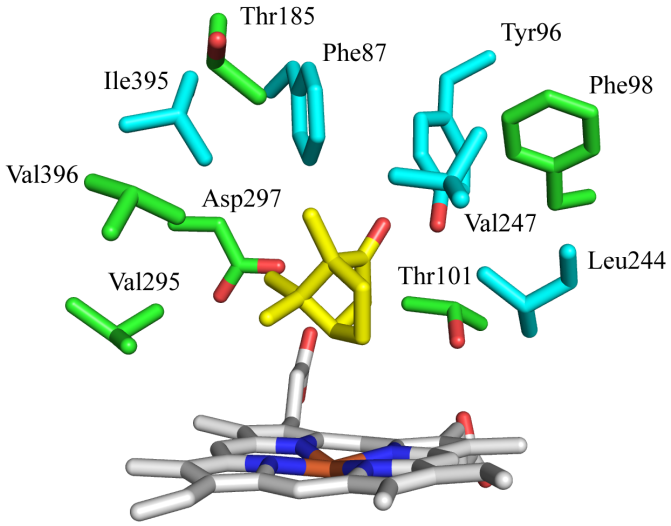

Figure 41: Active site of Cytochrome $P450_{cam}$ with bound camphor (PDB ID: 3WRH). Residues of interest in this work are highlighted in cyan.[43]

Table 10: A list of $P450_{cam}$ mutants tested with monoterpenoid substrates alongside the WT-enzyme. These mutants were cloned into the pCWSGB++ whole-cell expression system and were generated using site-directed mutagenesis.[45]

Mutants		
Y96F-I395G	F87A-Y96F	F87W-Y96F-L244A
Y96F-L244A	F87W-Y96F-V247L	F87L-Y96F-V247L
F87L-Y96F	F87W-Y96F-L244A-V247L	Y96F-L244A
Y96A	Y96L-V247A	Y96F-V247L
Y96F	F87V-Y96F-L244A	

These mutants are therefore suitable for screening with substrates that are of a similar size to (+)-α-pinene.[136] The genes encoding the mutants have been previously cloned into a whole-cell oxidation system alongside the physiological electron transfer partners of $P450_{cam}$, Pdx and PdR.[44]

This library of mutants (Table 10) was transformed into BL21(DE3) competent *E.coli* cells and was screened with fenchone, fenchyl acetate, 1,8-cineole, 1,4-cineole and isophorone (Figure 40) to determine if any of the mutants were able to selectively oxidise these substrates with high levels of product formation. WT-P450$_{cam}$ was screened concurrently with the mutants as a control for comparison. The screening results were analysed with both GC-MS and GC-BID analysis. Mutants that displayed selective oxidations with high yields of product were then scaled up accordingly (200 mL) for product purification and identification.

4.2.1 Fenchone and Fenchyl Acetate Oxidation by P450$_{cam}$ Mutants

Fenchone and fenchyl acetate both possess a bicyclic-2.2.1 structure that is also present in camphor, the natural substrate for P450$_{cam}$. Fenchone and camphor both possess a C2 ring carbonyl. This has been substituted with an acetate moiety in fenchyl acetate. The most significant structural difference between these two substrates and camphor is that the methyl groups within fenchone and fenchyl acetate are located on the C3 carbon instead of the C7 bridge position (Figure 42).

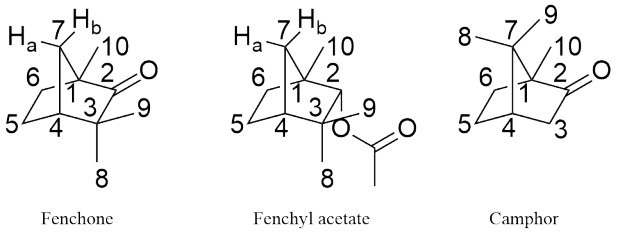

Figure 42: Structures of Fenchone and Fenchyl Acetate in comparison to camphor.

The initial whole-cell oxidation results with fenchyl acetate showed the WT displayed higher levels of product formation compared to the majority of the mutants (Figure 43). The oxidation of fenchyl acetate by WT-P450$_{cam}$ formed three products. Two of the products formed were not fully resolved by GC. The only mutant that exceeded the metabolite formation of the WT was the Y96A variant and this mutant also altered the product distribution (Figure 43).

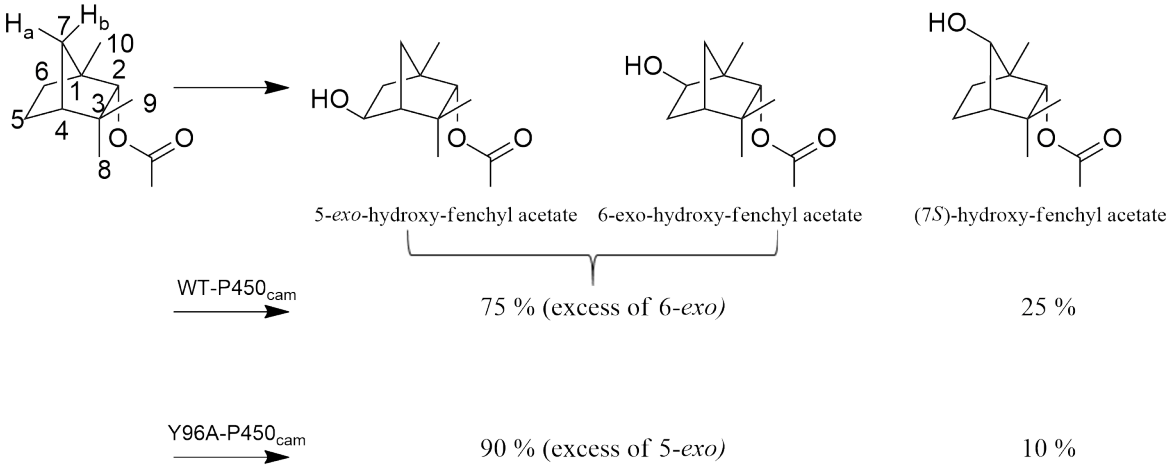

(a)

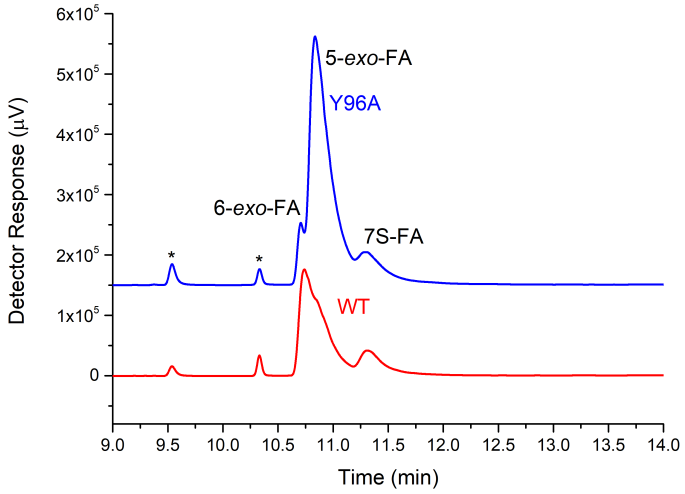

(b)

Figure 43: (a) Product distribution of fenchyl acetate oxidation by $P450_{cam}$ variants and (b) GC analysis of the whole-cell turnovers of fenchyl acetate with WT-$P450_{cam}$ (red) and mutant Y96A-$P450_{cam}$ (blue). The three products present within both turnovers and were identified as 6-*exo*-hydroxyfenchyl acetate (6-*exo*-FA, t_R = 10.75 min), 5-*exo*-hydroxyfenchyl acetate (5-*exo*-FA, t_R = 10.9 min), (7*S*)-hydroxyfenchyl acetate (7*S*-FA, t_R = 11.3 min). It is noted that the product peaks are not resolved completely via GC analysis and therefore the quantifications is an estimate. For clarity, the chromatograms have been offset along the *y*- axes.

A larger scale whole-cell turnover of WT-$P450_{cam}$ and variant Y96A was carried out to generate the metabolites for characterisation. These were extracted and purified by silica chromatography. The major metabolite for the Y96A turnover was identified via ^{1}H NMR and MS analysis as 5-*exo*-hydroxyfenchyl acetate (t_R = 10.9 min, Figure 43). Both the NMR and MS spectra were in agreement with previously reported data (Appendix B1).[101] The C-**H**-OH signal (δ_H = 4.18 ppm, *endo*-H5) displayed a doublet coupling pattern with J = 6.7 Hz (Figure 44). Coupling constants of this magnitude have also been observed in the *endo*-*endo* coupling between the C5 hydrogen to the adjacent C6 hydrogen in the related hydroxylated monoterpenoid, 5-*exo*-hydroxycamphor.[137]

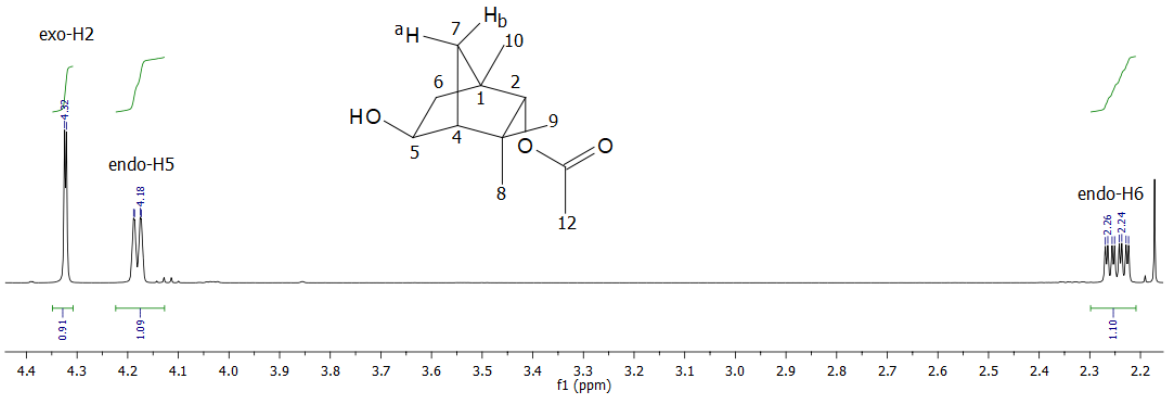

Figure 44: Expansion of the 4.4 - 2.2 ppm region within the ^{1}H NMR spectrum of 5-*exo*-hydroxyfenchyl acetate. The *endo*-H5 signal (4.18 ppm) had a coupling constant of 6.7 Hz that is indicative of *endo*-*endo* coupling to the adjacent H6 hydrogen.

A second minor metabolite from the P450$_{\text{cam}}$-Y96A turnover was isolated and identified as (7*S*)-hydroxyfenchyl acetate (t_R = 11.3 min, Figure 43) based on NMR analysis. This less abundant product displayed an additional 1H signal at δ_H = 3.86 ppm that indicated a CH_2 site was hydroxylated to produce a C-**H**-OH signal (H7, Figure 45a).

This signal displayed no *endo*-*endo*/*endo*-*exo* coupling that is characteristic of C5 or C6 hydroxylation as observed with the 5-*exo* metabolite.[138,139] This leaves the C7 position as the likely oxidation site. The orientation of the hydroxy group was confirmed through ^{1}H-^{1}H ROESY analysis (Figure 45b), whereby a through-space correlation was seen between the remaining H7 signal with the *exo* methyl group (H9) that indicates the hydroxylation occurred on the C7-C6-C5 face.

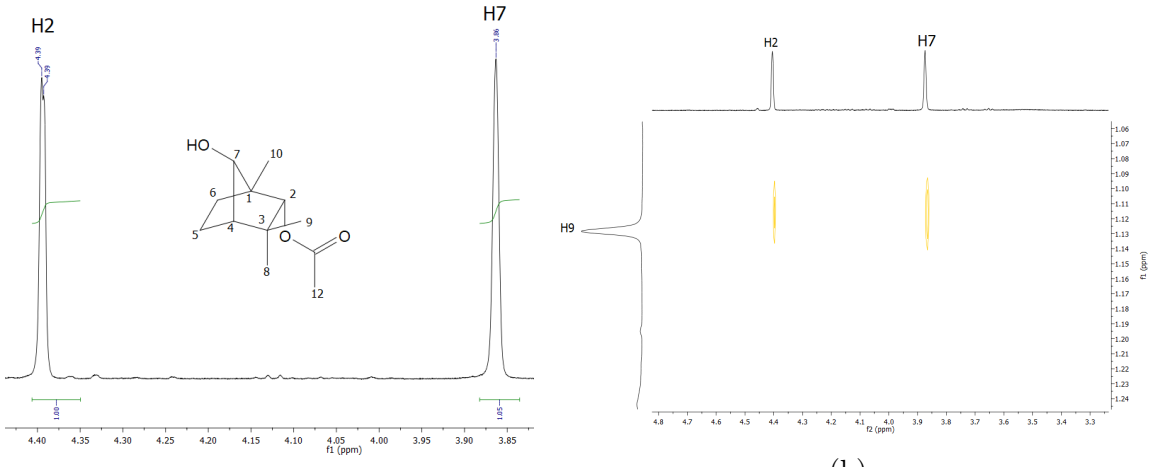

(a) (b)

Figure 45: NMR data for (7*S*)-hydroxyfenchyl acetate that shows (a) an expansion of the ^{1}H NMR data showing the C-**H**-OH signal (H7, 3.86 ppm) and (b) ^{1}H-^{1}H ROESY NMR data showing a through space correlation between H7 with the *exo* methyl group (H9).

Purification of the three metabolites from the WT enzyme turnover was attempted.

The turnover yielded the same (7*S*)-hydroxyfenchyl acetate product as observed with the Y96A variant. The other two metabolites were isolated as a mixture (Figure 46). One of these metabolites was confirmed as 5-*exo*-hydroxyfenchyl acetate and the third product could then be assigned as 6-*exo*-hydroxyfenchyl acetate from NMR analysis of the other signals of this mixture (Figure 46).

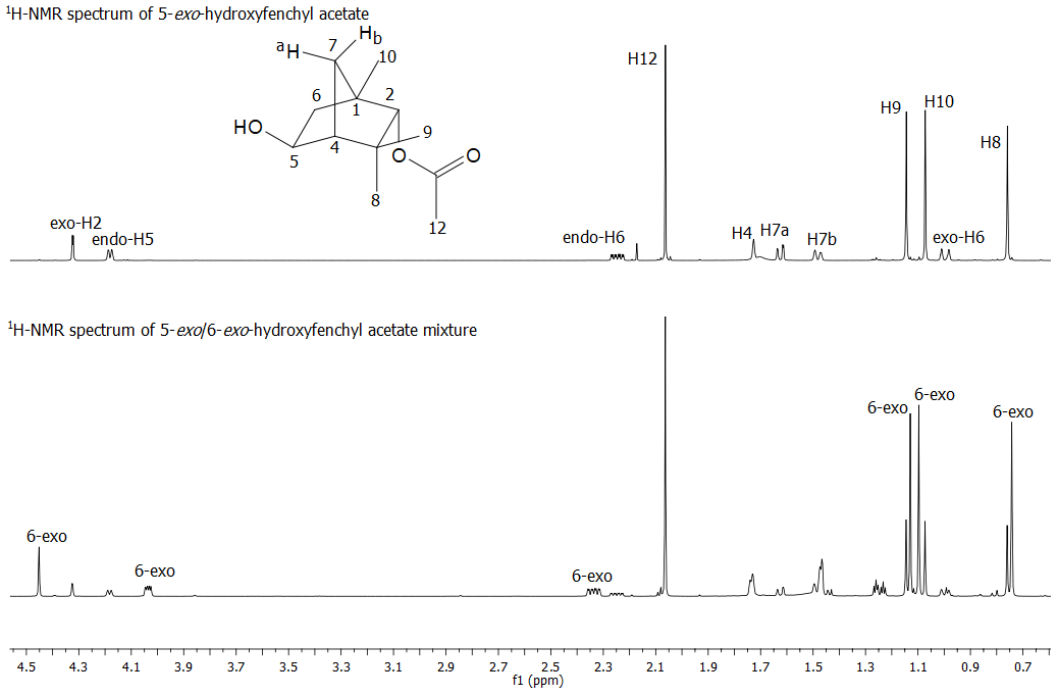

Figure 46: ^{1}H NMR spectrum of the isolated mixture from WT-P450$_{\text{cam}}$ with fenchyl acetate that contains 6-*exo*- and 5-*exo*-hydroxyfenchyl acetate. The NMR of the mixture was overlaid with the ^{1}H NMR spectrum of 5-*exo* hydroxyfenchyl acetate. Signals belonging to be the 6-*exo*-hydroxyfenchyl acetate were labelled in the NMR spectrum of the mixture.

The third product had an additional 1H signal at $\delta_{\text{H}} = 4.03$ ppm upon oxidation that is once again characteristic of a hydroxylation at a CH_2 site (Figure 47a). This signal displayed a dd coupling with $J = 7.1$ and 3.5 Hz. The magnitude of the coupling constants for this signal is indicative of *endo*-*endo* and *endo*-*exo* coupling of the C-**H**-OH signal to the neighbouring CH_2 group. These coupling constants can only arise from oxidation at either the C5 or C6 position as observed with 5-*exo*- and 6-*endo*-hydroxycamphor.[137]

^{1}H - ^{13}C HSQC NMR was used to assign the hydrogen signals within the mixture where possible to their respective carbons. ^{1}H - ^{13}C HMBC analysis (Figure 47b) of the mixture shows a correlation between the hydroxylated (**C**-OH) carbon and the CH_3 methyl hydrogens at the C10 carbon, which places the likeliest hydroxylation site at the C6 position. The lack of any significant W-coupling observed within the C-**H**-OH signal and the *exo*-H2 signal placed the orientation of the hydroxy group in the *exo* position. The third product formed is therefore 6-*exo*-hydroxyfenchyl acetate.

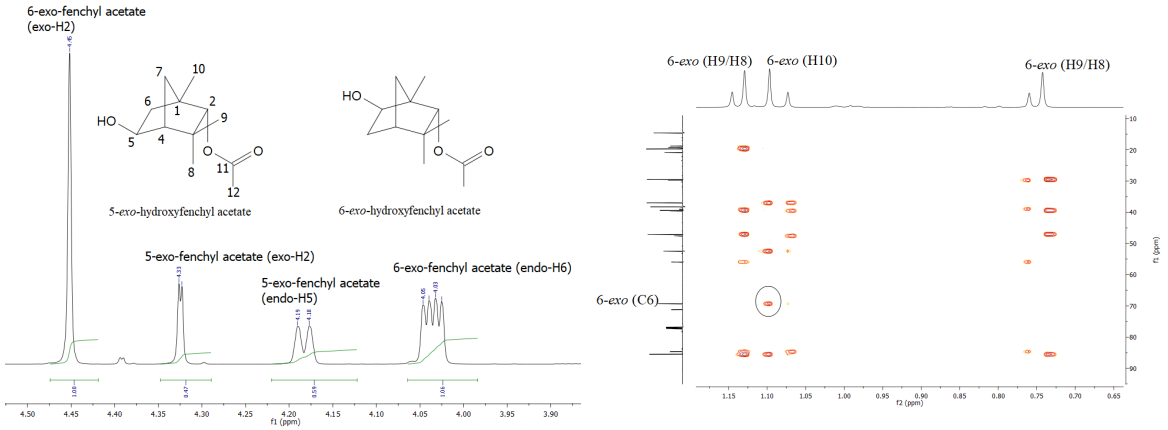

(a) (b)

Figure 47: NMR data for the 5-*exo* and 6-*exo*hydroxyfenchyl acetate mixture that shows (a) an expansion of the ^{1}H NMR data showing the C-**H**-OH signals for both compounds and (b) ^{1}H - ^{13}C HMBC NMR data showing a correlation between the C6 and a CH_3 group (H10) of 6-*exo*-hydroxyfenchyl acetate.

GC-MS co-elution experiments with the purified fenchyl acetate oxidation products and the enzyme turnover confirmed the presence of the products within the whole-cell turnovers (Figure 48). However, the 5-*exo*/6-*exo*-hydroxyfenchyl acetate mixture was not resolved with GC-MS.

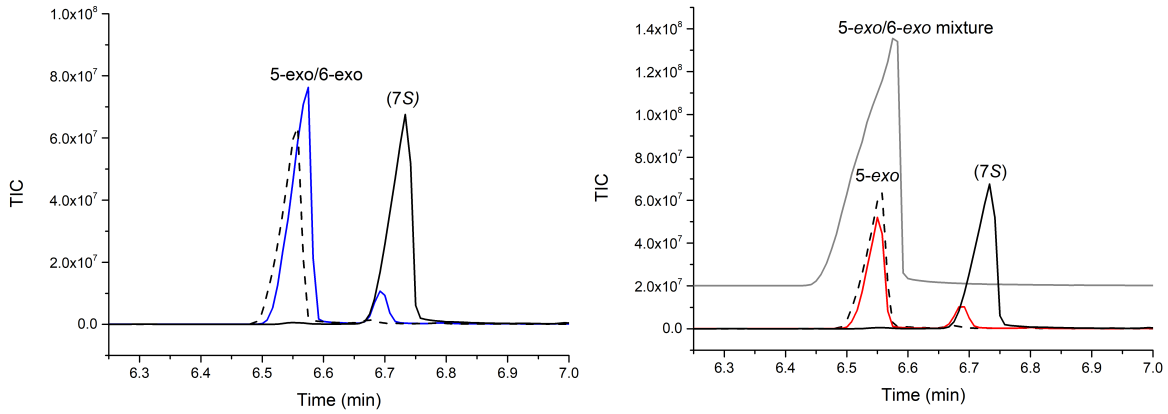

(a) (b)

Figure 48: GC-MS co-elution experiments of fenchyl acetate turnovers using (a) Y96A-P450$_{cam}$ (blue) and (b) WT-P450$_{cam}$ (red). The co-elution was carried out with purified 5-*exo*-hydroxyfenchyl acetate (dashed, t_R = 6.55 min), the 5-*exo*-/6-exo-hydroxyfenchyl acetate mixture (grey, t_R = 6.55 min), purified (7*S*)-hydroxyfenchyl acetate (black, t_R = 6.72 min).

The oxidation of fenchone by the WT enzyme displayed low levels of formation of 4 different products that were detectable by both GC and GC-MS analysis (Figure 49). Of the 14 mutants screened, mutant Y96F generated identical metabolites to the WT but increased the amount of product formed with an altered product distribution (Figure 49b).

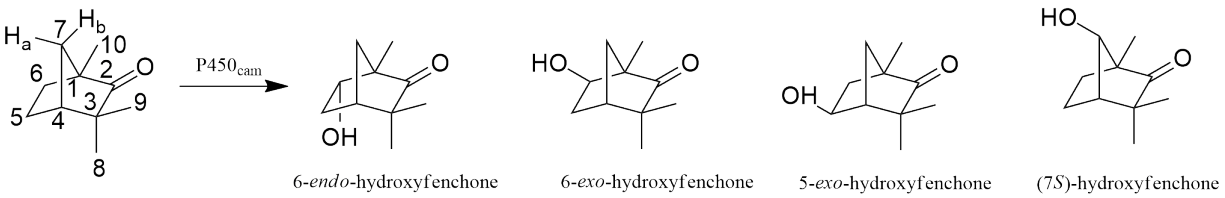

WT	50 %	7 %	28 %	15 %
Y96F	20 %	32 %	29 %	19 %

(a)

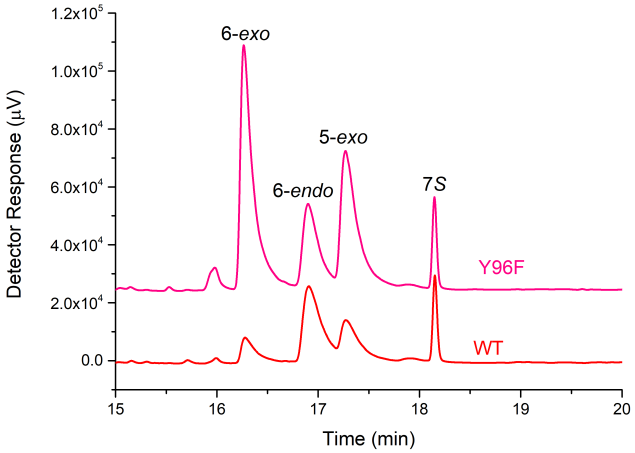

(b)

Figure 49: (a) Product distribution of fenchone oxidation by $P450_{cam}$-Y96F and the WT enzyme. (b) GC-BID analysis of the *in vivo* turnovers of fenchone with WT (red) and Y96F (pink). Products identified were 6-*exo*-hydroxyfenchone (t_R = 16.3 min), 6-*endo*-hydroxyfenchone (t_R = 17.0 min), 5-*exo*-hydroxyfenchone (t_R = 17.25 min), (7*S*)-hydroxyfenchone (t_R = 18.1 min). For clarity, the chromatograms have been offset along the *y*- axes.

A larger scale turnover of the Y96F variant with fenchone was carried out to isolate enough of each metabolite for characterisation. Silica chromatography of the turnover extract isolated one metabolite which NMR matched that of 5-*exo*-hydroxyfenchone (Figure 50).[101]

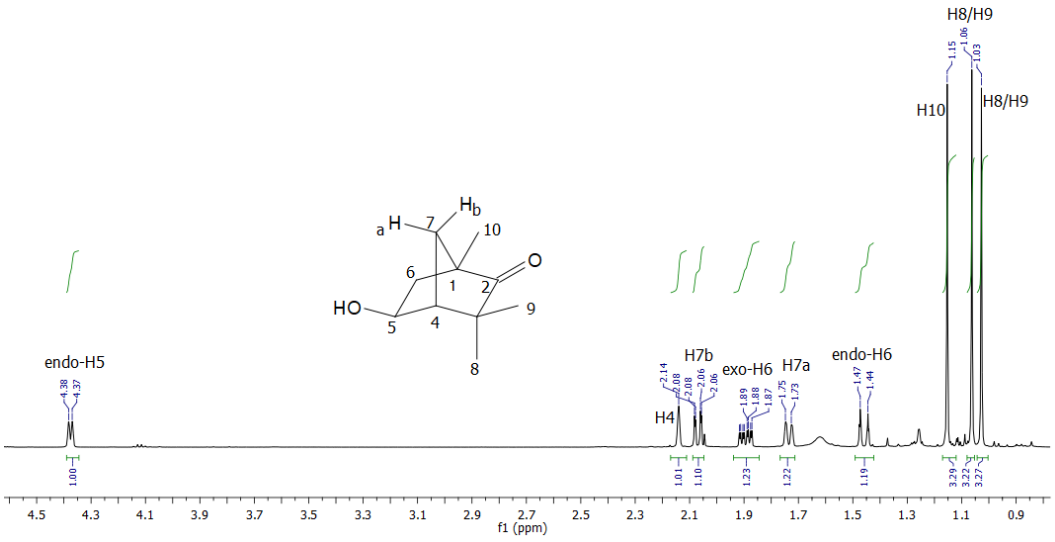

Figure 50: ^{1}H-NMR data 5-*exo*-hydroxyfenchone.

The other three oxidation products could not be separated from each other. Comparison of the GC-MS (Appendix B8) and NMR data (Figure 51 and Appendix B7) of the mixture with those of hydroxyfenchone metabolites in the literature indicated the presence of both 6-*exo*- and 6-*endo*-hydroxyfenchone. The MS and NMR data matched those previously reported in the literature.[140] These two products were identified via their C-**H**-OH peaks : 4.09 ppm for 6-*endo* and 3.62 ppm for 6-*exo*; alongside the three methyl peaks: 1.16, 1.12 and 1.10 ppm for 6-*endo* and 1.14, 1.06 and 0.96 ppm for 6-*exo*.[140]

The fourth product showed a C-**H**-OH signal (δ_H = 4.05 ppm, Figure 51a) with no distinct coupling pattern similar to that observed for the equivalent NMR signal within (7*S*)-hydroxyfenchyl acetate (δ_H = 3.86 ppm, Figure 45a). This metabolite was therefore assigned as (7*S*)-hydroxyfenchone. In addition, there does not appear to be any evidence of carbonyl reduction within the turnover of Y96F with fenchone.

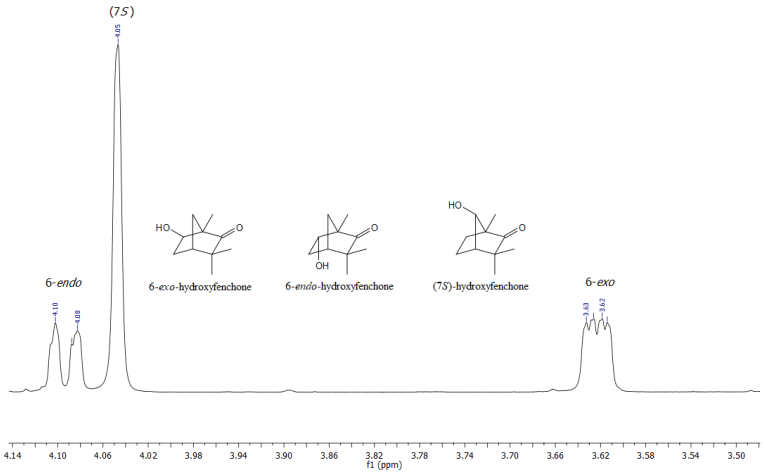

(a)

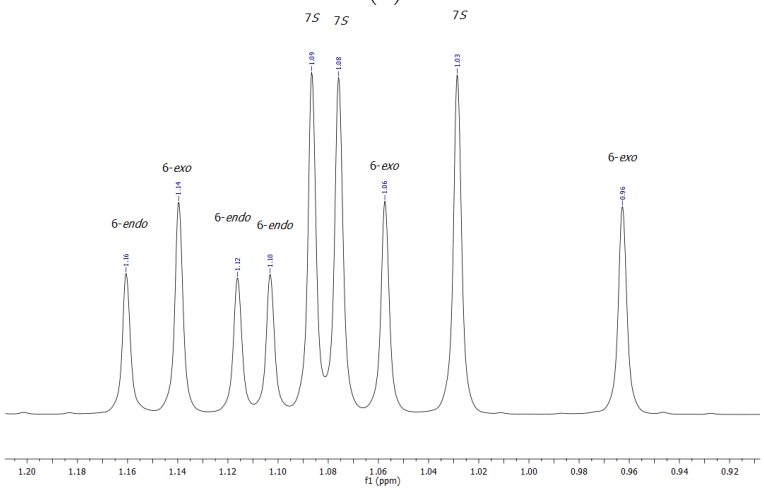

(b)

Figure 51: Selected signals within the NMR data for a mixture of fenchone oxidation products isolated that shows (a) an expansion of the ^{1}H NMR data showing the C-**H**-OH signals and (b) methyl hydrogen signals for 6-*exo*-, 6-*endo* and (7*S*)-hydroxyfenchone.

The presence of all 4 products within the turnover of Y96F-P450$_{\text{cam}}$ with fenchone was confirmed via GC-MS co-elution experiments as shown in Figure 52.

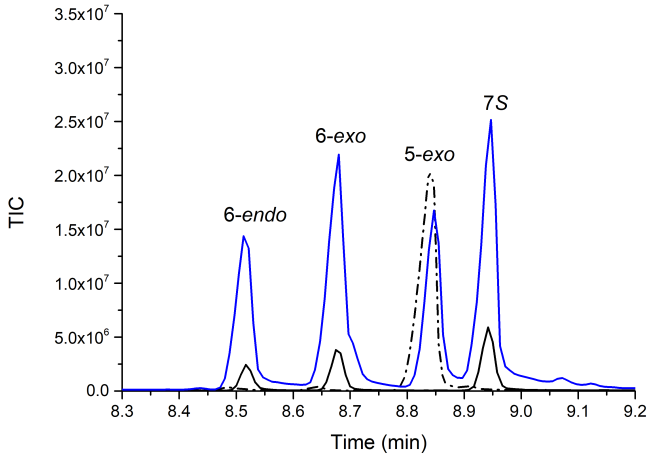

Figure 52: GC-MS analysis of purified 5-*exo*-hydroxyfenchone (dashed), the 6-*endo*-/6-*exo*-/(7*S*)-hydroxyfenchone mixture (black) and the Y96F-P450$_{\text{cam}}$ turnover with fenchone (blue).

4.2.2 Biocatalytic Oxidation of Isophorone by $P450_{cam}$ Mutants

Isophorone is an α, β-unsaturated cyclic ketone. It lacks the bicyclic structure of camphor and contains an additional alkene double bond. It has a similar size and chemical functionality to camphor which makes it a suitable target for screening with the $P450_{cam}$ mutant library (Table 10).

GC analysis of the WT turnover with isophorone showed the formation of two metabolites (Figure 53). One of these metabolites was produced in significant excess by several of the mutants. Amongst the variants screened, the mutants F87W/Y96F/V247L (WFL) and F87W/Y96F/L244A/V247L (WFAL) showed increased product formation and selectivity for this metabolite over the WT enzyme (Figure 53). The other mutants tested all showed lower formations of product and were also less selective.

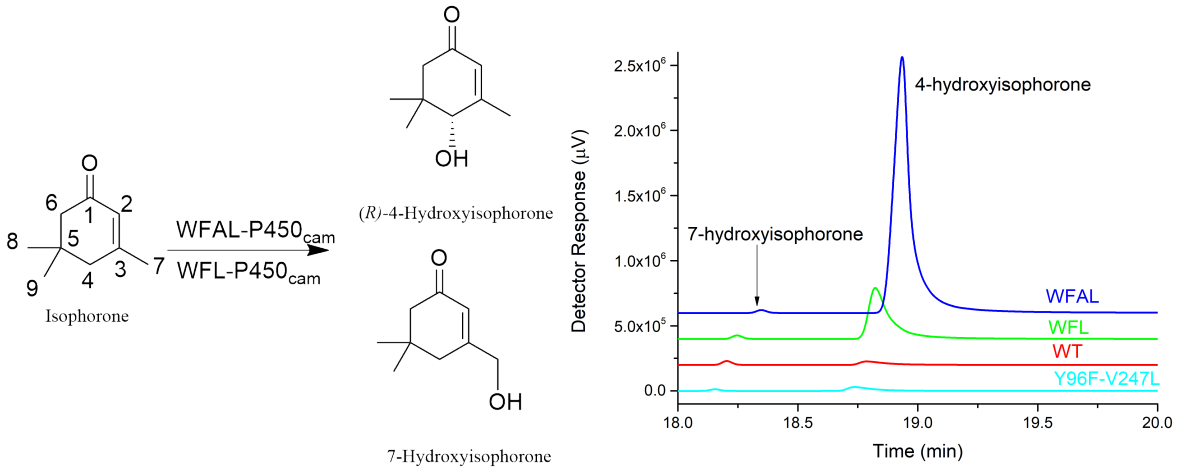

Figure 53: Oxidation products of isophorone by $P450_{cam}$ mutants alongside chiral GC analysis of the whole-cell screening of isophorone with WT (red), F87W-Y96F-V247L (WFL, green), F87W-Y96F-L244A-V247L (WFAL, blue) and Y96F-V47L (cyan). The chromatograms were offset along the x and y axes for clarity. Note the enantiomers of 4-hydroxyisophorone were not separated using this method.

A large scale whole-cell oxidation of isophorone (Figure 56a) with the WFL variant was carried out to isolate the two products formed. The products were purified using silica chromatography. The major product isolated and identified via NMR was 4-hydroxyisophorone (35 mg; Appendix B9). The minor product was characterised as 7-hydroxyisophorone (12 mg; Appendix B12) (Figure 53).

^{1}H NMR data for 4-hydroxyisophorone (Figure 54a) matched previously reported literature NMR data (Table 11).[141] The oxidation site for the major metabolite was identified by the presence of a ^{1}H hydrogen signal at 4.03 ppm that is an indication of a hydrogen attached to a hydroxylated carbon (C-**H**-OH), which suggests a CH_2

group was oxidised. Isophorone possesses two CH_2 groups at the C4 and C6 position. HMBC NMR analysis of the C-**H**-OH signal (4.03 ppm) found it had correlations with the three methyl carbons (C7, C8, C9) and the two alkene carbons (C2, C3). This places the oxidation site at the C4 position which is the only position equidistant to the three methyl and alkene carbons.

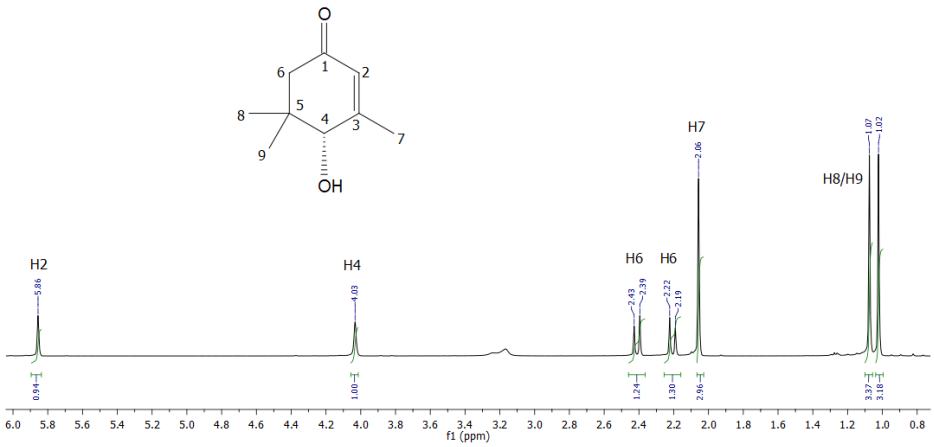

(a)

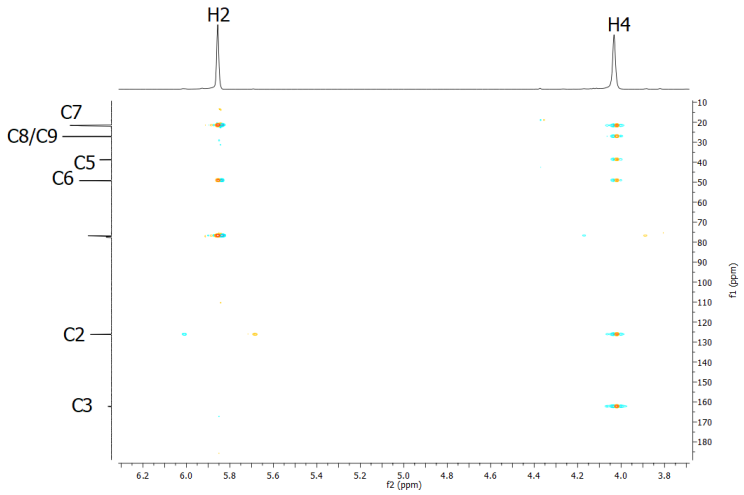

(b)

Figure 54: (a) ^{1}H NMR data and (b) expansion of the HMBC NMR analysis of 4-hydroxyisophorone that shows the correlations of the C-**H**-OH signal.

Table 11: Comparison of Experimental NMR data of 4-hydroxyisophorone to the literature.[141]

Position	Experimental δ_H (ppm)	Literature[141] δ_H (ppm)
H8/H9	1.02	1.02
H8/H9	1.07	1.07
H7	2.06	2.05
H6	2.21 (J = 16.3 Hz)	2.21 (J = 16 Hz)
H6	2.41 (J = 16.3 Hz)	2.41 (J = 16 Hz)
H4	4.03	4.02
H2	5.86	5.82

The oxidation site of the minor metabolite was identified at the C7 position via ^{1}H NMR analysis (Figure 55). The NMR spectrum showed a loss of one methyl signal alongside the presence of a 2H signal at 4.22 ppm that indicates a methyl group was oxidised. The two remaining methyl groups were equivalent as indicated by a large 6H signal at 1.05 ppm. This suggests that the C9 and C8 carbons were not oxidised and therefore the C7 carbon was hydroxylated to generate 7-hydroxyisophorone.

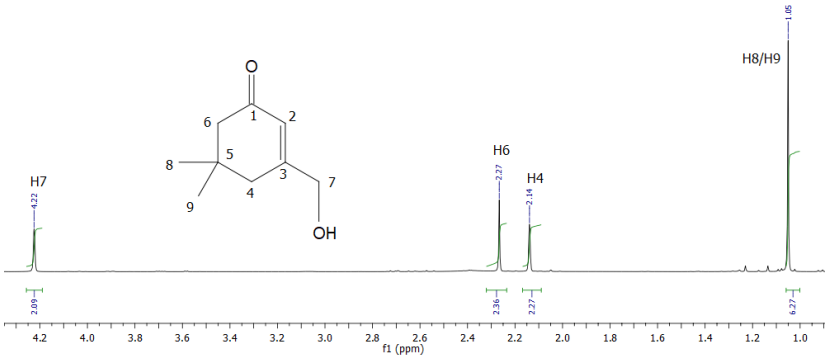

Figure 55: ^{1}H NMR of 7-hydroxyisophorone. The H9/H8 signal (1.06 ppm) had an integration of 6 which indicates symmetry was present.

The oxidation of isophorone to 4-hydroxyisophorone can generate a pair of enantiomers. Chiral GC analysis of the mutant enzyme-catalysed reactions only showed the formation of a single peak (Figure 53). A racemic mixture of 4-hydroxyisophorone was generated via the reduction of 4-ketoisophorone with $NaBH_4$ using a previously described method.[99] This racemic sample was also observed as a single peak by chiral GC, suggesting the enantiomers are not resolved. Chiral HPLC analysis (Figure 56b) of the enzymatic product and the racemic mixture of 4-hydroxyisophorone both displayed two peaks. However, the enzymatic product had one enantiomer produced in much greater excess over the other (99 % e.e, Figure 56b). This indicated that the enzyme-catalysed reactions were enantioselective.

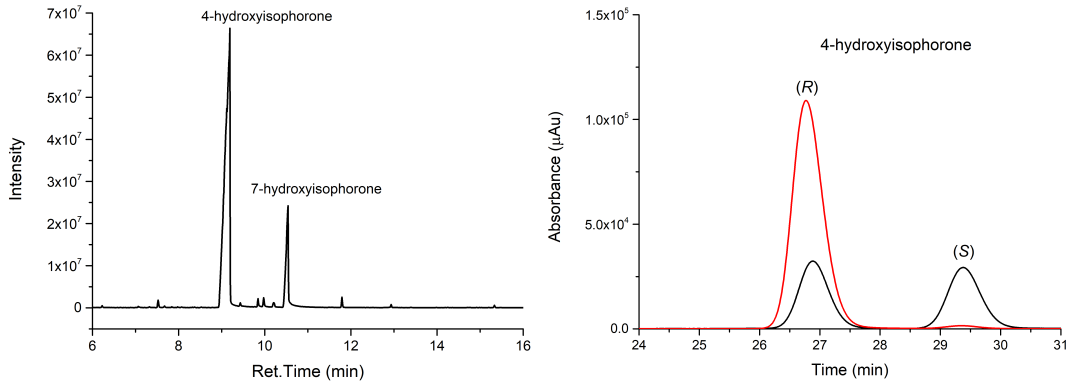

Figure 56: (a) GC-MS analysis of the large scale whole-cell turnover of WFL-P450$_{cam}$ with isophorone and (b) chiral HPLC analysis showing the region of the purified 4-hydroxyisophorone (red) with the racemic product (black). (*R*)-4-hydroxyisophorone was produced with 99 % e.e.

While this work was being undertaken, a separate research group also showed that $P450_{cam}$ mutants stereoselectively generated (*R*)-4-hydroxyisophorone.[142] The pure 4-hydroxyisophorone from the whole-cell turnovers of our study had a specific rotation of $[\alpha]_D{}^{20}$= +113.2 (c= 1.00, MeOH) which agreed with the rotation data of the pure (*R*)-enantiomer previously reported in the literature. This enabled the assignment of the enantiomer.[129,133,142]

4.2.2.1 Comparisons between $P450_{cam}$ and $P450_{BM3}$ Isophorone Oxidation

In a separate investigation, our group has shown that mutants of $P450_{BM3}$ are also capable of oxidising isophorone to form (*R*)-4-hydroxyisophorone as the major product.[135] The formation of other minor metabolites such as 7-hydroxyisophorone and 4-ketoisophorone was also observed with the $P450_{BM3}$ variants.[135] The self-sufficient nature of $P450_{BM3}$ provides easy production and its high enzyme activity makes it a prime candidate for biocatalytic reactions. The $P450_{cam}$ system requires co-expression of electron transfer proteins within the whole-cell oxidation systems but also displayed high oxidation activity.[19,44,143]

$P450_{cam}$'s class I system and $P450_{BM3}$'s class VIII system cannot be compared directly due to the disparate natures of their electron transfer systems (FMN vs ferredoxins), co-factor requirements (NADPH vs NADH) and different plasmid systems used (pET28 vs pCWori). However, we wished to assess if both systems, under the same growth and turnover conditions, would give rise to similar levels of product formation. Two $P450_{BM3}$ mutants which displayed selective and high levels of product formation with isophorone were assessed; A74G/F87V/L188Q (GVQ) and R47L-Y51F-F87A-I401P (RLYFFAIP).

The $P450_{cam}$ variant, WFAL, was compared with the RYLFFAIP and GVQ variants of $P450_{BM3}$ via whole-cell oxidations in *E.coli* BL21(DE3) cells. The two enzyme systems both produced similar amounts of cell biomass (13 - 14 gram cell wet weight per litre of culture, Appendix B1). The P450 concentration detected for the $P450_{BM3}$ variants (88 - 183 nM) were significantly higher than those of the $P450_{cam}$ mutants (25 - 54 nM, Appendix B1).

After the whole-cell reactions were carried out for 7 hours, the RLYFFAIP and the GVQ variants of $P450_{BM3}$ displayed similar levels of product formation ($\sim$ 650 $\pm$ 100 µM, Figure 57 and 58a). However, the GVQ variant formed other metabolites in small amounts. These minor metabolites include 7-hydroxyisophorone, isophorone oxide, 4-ketoisophorone epoxide and levodione.[135] These remaining metabolites were not formed

in significant quantities with the WFAL-P450$_{cam}$ mutant (Figure 57).[135]

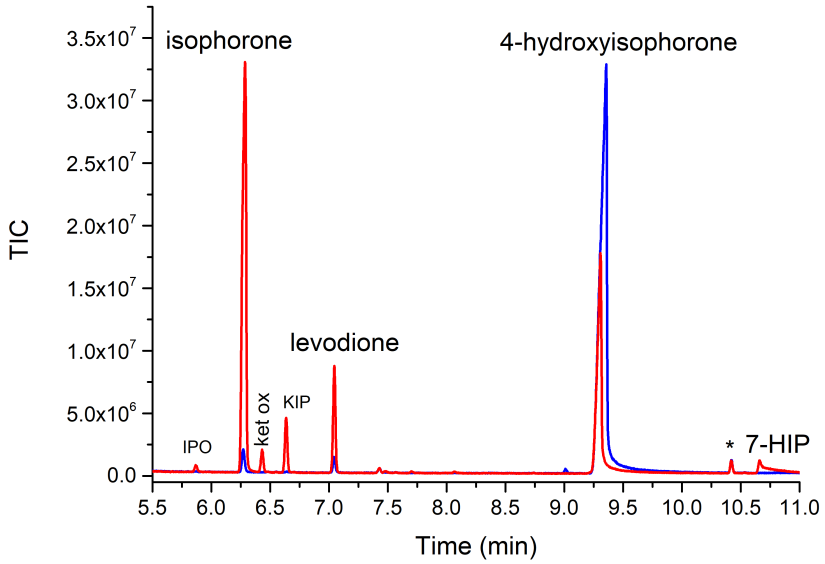

Figure 57: GC-MS analysis of the whole-cell turnover of WFAL-P450$_{cam}$ (blue) and GVQ-P450$_{BM3}$ (red) with isophorone. Peaks shown are isophorone (t_R = 6.25 min), 4-hydroxyisophorone (t_R = 9.25 min), 7-hydroxyisophorone (t_R = 10.6 min). Minor metabolites include isophorone oxide (IPO, t_R = 5.8 min), 4-ketoisophorone epoxide (ket ox, t_R = 6.4 min), 4-ketoisophorone (KIP, t_R = 6.7 min) and levodione (t_R = 7.1 min). Impurities are marked with *.

The WFAL-P450$_{cam}$ variant generated more product than any of the P450$_{BM3}$ mutants at 7 hours ($\sim$ 950 $\pm$ 10 µM). After leaving the samples for a further 13 hours, only the P450$_{cam}$ variant was able to convert the majority of the added substrate (4 mM total) to product (Figure 58b). Both P450$_{BM3}$ mutants displayed lower amounts of product formed after 13 hours ($\sim$ 1200 µM) when compared to the P450$_{cam}$ system. Overall, the P450$_{cam}$ systems provided higher conversions (2.8 - 4 mM of 4-hydroxyisophorone) to product over the P450$_{BM3}$ systems (Figure 57 and 58).

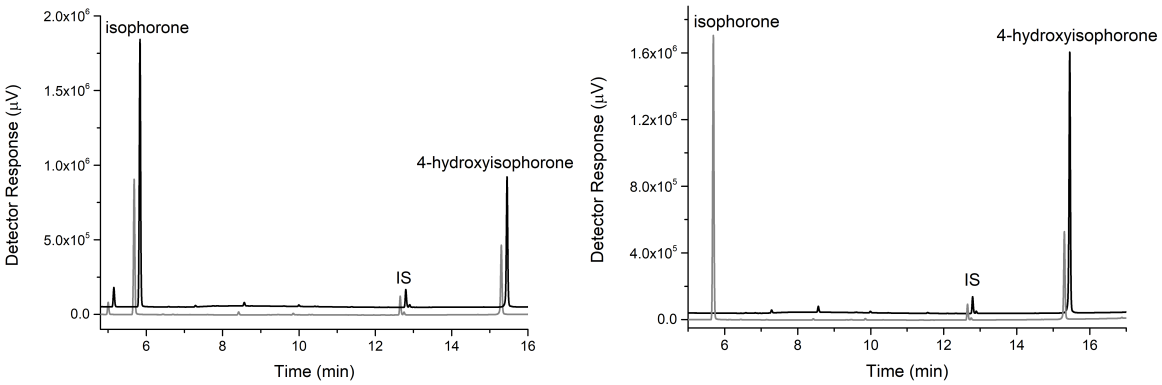

(a) RLYFFAIP (b) WFAL

Figure 58: GC-BID analysis of the *in vivo* turnover of (a) WFAL-P450$_{cam}$ and (b) RLYFFAIP-P450$_{BM3}$ with isophorone at 7h (gray) and 20h (black). For WFAL-P450$_{cam}$, it is apparent that majority of the substrate (4 mM) was consumed after 20 h to show an increase in product levels at 7 h ($\sim$ 970 µM) to 20 h ($>$ 2.5 mM). The isophorone substrate (t_R = 5.8 min), internal standard (IS) (t_R = 12.8) min and 4-hydroxyisophorone t_R = 15.83 min) are shown. The chromatograms have been slightly offset along the x- and y-axes for clarity.

4.2.3 The Oxidation of Cineoles by P450$_{cam}$ Mutants

1,8-Cineole and 1,4-cineole possess bicyclic-2.2.2 and 2.2.1 structures, respectively, that are largely similar in size and shape to (+)-camphor. The two cineoles possess an ether oxygen rather than the carbonyl group found in camphor. For the cineoles, the established literature numbering system for both structures is shown in Figure 59.[96]

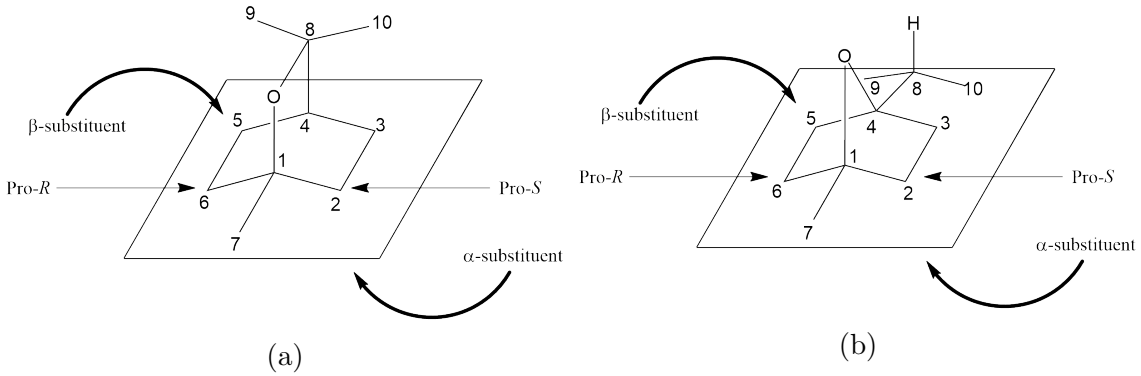

Figure 59: Chemical numbering and stereochemical nomenclature of (a) 1,8-cineole and (b) 1,4-cineole. In order to discuss the stereochemistry of the products formed, the descriptors α and β will be used. The α descriptor is used to define substituents that sit below the plane that passes through the C2, C3, C5 and C6 centres, while β is employed for substituents that sit above this plane. The structure of both cineoles are *meso* and achiral, whereby any functionalisation at either methylene bridge will generate three new stereogenic centres at the C1, C4 and hydroxylated carbon. Therefore, if a carbon after hydroxylation generates the *R*-C1 isomer, it is defined as a pro-*R* carbon and a carbon that produces the *S*-C1 isomer is a pro-*S* carbon.

Previous studies on the oxidation of cineoles by P450s include the enantiospecific hydroxylation of 1,8-cineole by CYP176A1 (P450$_{cin}$) to form (1*R*)-6-β-hydroxy-1,8-cineole. Wild-type P450$_{cam}$ has also been used to oxidise 1,8-cineole, albeit less selectively to form (1*S*)-6-α-, 5-α- and 5-β-hydroxy-1,8-cineole.[104] The latter two products are primarily formed as the (1*S*) enantiomer and the products were made in a 18:68:14 ratio. WT-P450$_{cam}$ and P450$_{cin}$ were screened alongside the P450$_{cam}$ variants.

The P450$_{cam}$ mutant variants were initially screened for 1,8- and 1,4-cineole oxidation using the whole-cell systems with analysis by chiral GC. The variants which displayed high yield and selective formation of products were scaled up accordingly and their metabolites extracted and isolated. Products were identified via MS fragmentation pattern data from previous studies and with comparison to metabolite product standards of the WT-turnover for the 1,8-cineole products.[104]

4.2.3.1 1,8-Cineole Oxidation by P450$_{cam}$ Mutants

The products formed from the WT control include 6-α-, 5-α- and 5-β-hydroxy-1,8-cineole (Figure 60) and the MS fragmentation data matched those previously reported (Appendix B16).[104] It would be expected that the (*S*)-enantioselectivity is also preserved with these metabolites formed. Several of the P450$_{cam}$ mutants displayed altered product distribution for 1,8-cineole oxidation when compared to WT. The metabolites formed were the same as those in the WT. For example, compared to the WT enzyme, the mutant F87V/Y96F/L244A (VFA) showed increased formation of 6-α-hydroxy-1,8-cineole which was the major product (90 %), while 5-α and 5-β hydroxylation products were formed in lower amounts at 8 % and 2% respectively (Figure 60 and 61).

Mutant F87W/Y96F/L244A/V247L (WFAL) had a preference towards 5-α-hydroxy-1,8-cineole (85 %). The other metabolites formed were the 5-β- and 6-α-hydroxy products (Figure 60 and 61). The F87W/Y96F/L244A mutant (WFA) showed an even stronger preference for 5α hydroxylation (90 %) and only the 5β metabolite was produced as the minor product (Figure 60 and 61). However, the product formation level was almost 10-fold lower for the WFA mutant when compared to the WFAL variant (Figure 61). In previous studies with WT-P450$_{cam}$, enantioselective GC was not able to determine the optical purity of the 5-hydroxy-1,8-cineoles formed. Oxidation of the 5-hydroxy variants to 5-ketocineole produced the (1*S*) enantiomer in 86 % e.e., this could also be the enantiomer of the products from the 5-α/5-β hydroxylations for the mutants but this needs to be determined.[104]

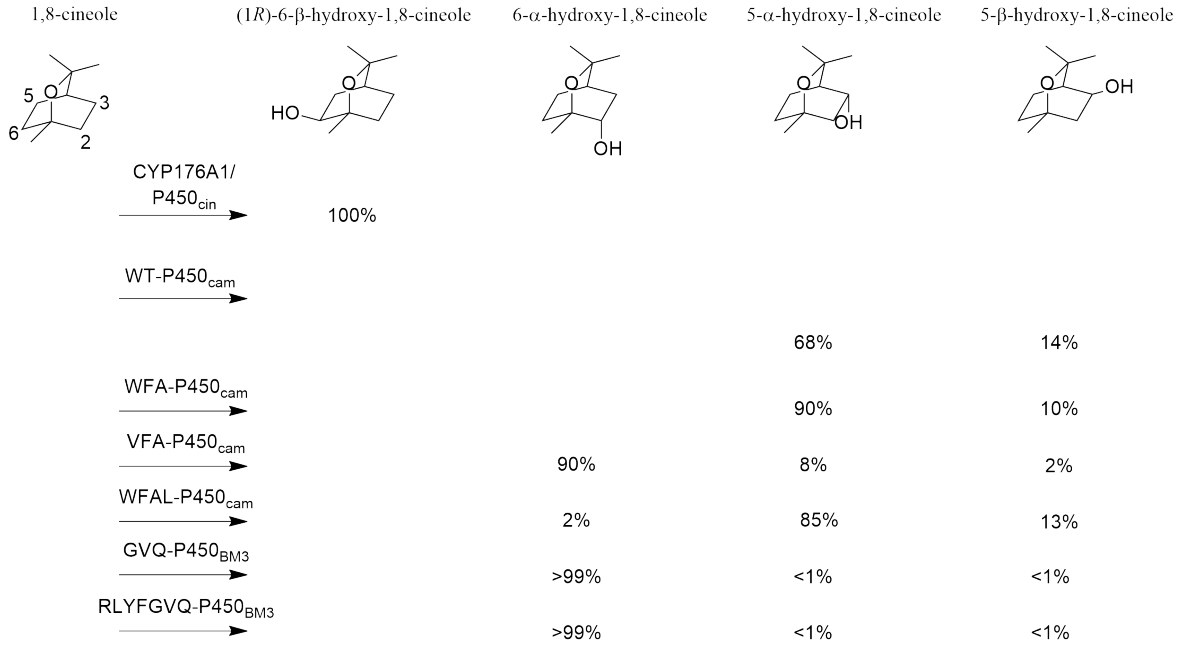

Figure 60: Product distribution of 1,8-cineole *in vivo* turnovers by WT-P450$_{cam}$ mutants. Products from P450$_{cin}$ and P450$_{BM3}$ turnovers are given for comparison.

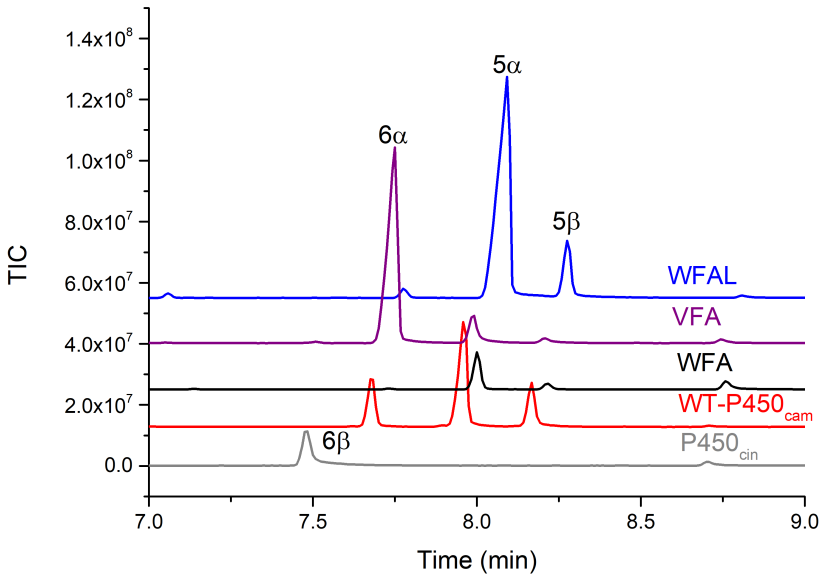

Figure 61: GCMS analysis of 1,8-cineole *in vivo* turnovers by WT-P450$_{cam}$ (red), variants WFAL (blue), VFA (purple), WFA (black) and P450$_{cin}$ (gray). Products shown are (1*R*)-6-β-hydroxy-1,8-cineole (6β, t_R = 7.5 min), 6-α-hydroxy-1,8-cineole (6α, t_R = 7.7 min), 5-α-hydroxy-1,8-cineole (5α, t_R = 7.9 min), 5-β-hydroxy-1,8-cineole (5β, t_R = 8.2 min). For clarity, the chromatograms were offset along the x- and y-axes.

The screening of only a small library of P450$_{cam}$ mutants has allowed for the selective oxidation of different C-H bonds within 1,8-cineole to favour a specific product, i.e. the VFA mutant favours the 6-α- derivative, while WFAL mutant favours the 5-α-derivative instead.

4.2.3.2 1,4-Cineole Oxidation by P450$_{cam}$ Mutants

Screening of the P450$_{cam}$ mutant library with 1,4-cineole was carried out alongside WT-P450$_{cin}$. P450$_{cin}$ was able to oxidise 1,8-cineole in a stereoselective manner (Figure 60), but its oxidation of 1,4 cineole generated multiple products. These were analysed by GC and GC-MS (Figure 62). The MS fragmentation patterns of the major products (Appendix B17) formed were consistent with previously published MS data of 8-hydroxy-, 2-β- and 3-β-hydroxy-1,4-cineole.[144–147] The former two metabolites were the major products formed with WT-P450$_{cin}$. The P450$_{cin}$ turnover also showed low amounts of an additional product (**A**) observed under GC-MS with a retention time close to that of the substrate (1,4-cineole, t_R = 4.15 min; Product **A**, t_R = 4.2 min). The MS spectrum of **A** when compared to the 1,4-cineole substrate (m/z = 154.3) was consistent with a desaturation product being two mass units lower (m/z = 152.1, Appendix B17g).

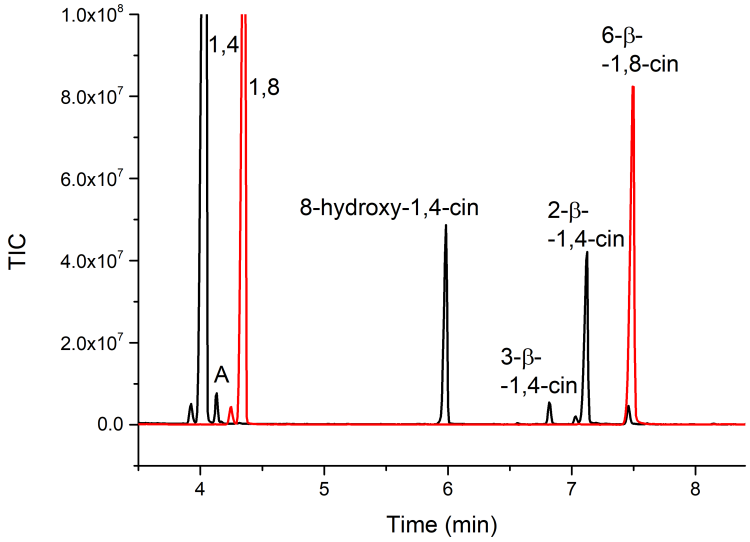

Figure 62: GC-MS analysis of 1,4-cineole (black) and 1,8-cineole (red) *in vivo* oxidation by $P450_{cin}$. Substrates and products are labelled as follows: 1,4-cineole (1,4, $t_R = 4.1$ min), 8-hydroxy-1,4-cineole (8-hydroxy, $t_R = 6.0$ min), 3-β-hydroxy-1,4-cineole (3-β, $t_R = 6.85$ min), 2-β-hydroxy-1,4-cineole (2-β, $t_R = 7.15$ min), 1,4-cineole desaturation product (A, $t_R = 4.15$). 1,8-cineole (1,8, $t_R = 4.3$ min) and its oxidation product, 6-β-hydroxy-1,8-cineole (6-β, $t_R = 7.5$ min) were present as impurities.

The 1,4-cineole sample used was always contaminated with small amounts of 1,8-cineole (Figure 62). Colleagues at the University of Queensland had access to a wide range of hydroxy-cineole metabolites from other studies with $P450_{cin}$ mutants. The extracts from the larger scale turnovers were sent to them for further characterisation. This enabled facile confirmation of metabolites arising from 1,4-cineole oxidation as opposed to those from the 1,8-cineole contaminant (Figure 62).

1,4-Cineole oxidation by WT-$P450_{cam}$ (Figure 63b) resulted in a low yield of metabolites. The major product formed appears to be the 8-hydroxy metabolite and the remaining products were identified as 3-α- and 2-α-hydroxy-1,4-cineole. A number of the $P450_{cam}$ mutants displayed improved product yields and higher regioselectivity in the oxidation of 1,4-cineole (Figure 63b). The variant WFA displayed a strong preference for oxidation at the 3-α- position (90 %) and similar levels of regioselectivity was also observed with the WFAL mutant. The 3-α- product from the WFA turnover was crystallised, which confirmed the relative configuration of the product and determined the absolute configuration as (1*S*).[105] The remaining products from the WFA and WFAL turnovers (Figure 63b) were identified by their MS fragmentation patterns (Appendix B17). These were confirmed either via their NMR spectra and/or GC-MS co-elution with other standards. The other metabolites included 3-β-, 2-β-, 2-α-, 8-hydroxy- and 9-hydroxy-1,4-cineole.[144–148]

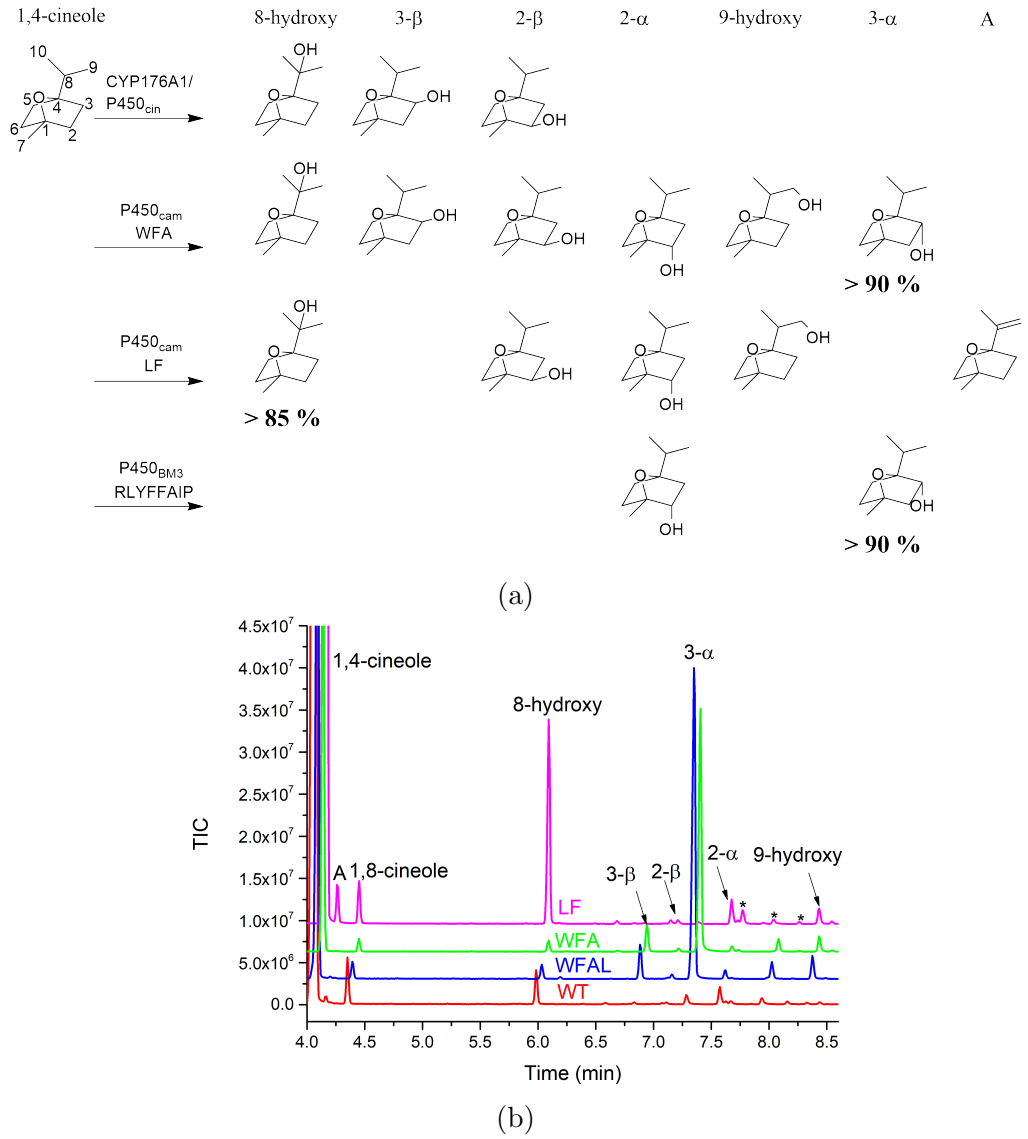

Figure 63: (a) Product distribution and (b) GCMS analysis of 1,4-cineole turnovers by WT-P450$_{cam}$ (red), variants LF (purple), WFA (green), WFAL (blue). Products identified include: 8-hydroxy-1,4-cineole (8-hydroxy, t_R = 6.0 min), 3-β-hydroxy-1,4-cineole (3-β, t_R = 6.85 min), 2-β-hydroxy-1,4-cineole (2-β, t_R = 7.15 min), 3-α-hydroxy-1,4-cineole (3-α, t_R = 7.3 min), 2-α-hydroxy-1,4-cineole (2-α, t_R = 7.65 min), 9-hydroxy-1,4-cineole (9-hydroxy, t_R = 8.25 min). The 1,4-cineole desaturation product was labelled as **A** (t_R = 4.15 min). All 1,4-cineole samples have small amounts of 1,8-cineole and impurities and products arising from 1,8-cineole oxidation are marked with *. For clarity, the chromatograms were offset along the x- and y-axes.

The mutant F87L/Y96F (LF) favoured hydroxylation on the isopropyl moiety to give rise to 8-hydroxy-1,4-cineole (85 %) with product formation levels of this product far exceeding those observed with WT-P450$_{cam}$ by approximately 10-fold (Figure 63). Minor products observed include 2-β-, 2-α- and 9-hydroxy-1,4-cineole (Figure 63). The LF variant also generated increased levels of the desaturation product **A** at 4.15 min. There appeared to be a trend in the increase of product **A** with the increasing levels of 8-hydroxy-1,4-cineole amongst the mutants tested (Figure 63). The desaturation product **A** likely has an alkene between the C8 and C9 carbons of the isopropyl moiety of 1,4-cineole and hence has been assigned as such (Figure 63a).

4.2.3.3 Comparison between Different Bacterial P450 systems for Cineole Oxidation

Separate investigations into the use of $P450_{BM3}$ mutants for the selective oxidation of the two cineoles identified several mutant enzyme systems that can oxidise both substrates in a regioselective manner.[105] For 1,8-cineole oxidation, mutants GVQ and R47L-Y51F-A74G-F87V-L188Q (RLYFGVQ) were able to oxidise 1,8-cineole selectively to form 6-α-hydroxy-1,8-cineole (Figure 60). For 1,4-cineole oxidation, mutant RLYFFAIP was selective for 3-β-hydroxy-1,4-cineole (Figure 63a).[105] A comparison between both P450 *in vivo* systems was carried out to compare the relative amounts of product formed between the most selective cineole oxidation systems. P450 mutants of both systems relevant to cineole oxidation were transformed into *E. coli* BL21(DE3) cells. All systems generated similar levels of cell biomass (13 - 17 gram of cell wet weight per litre of cell culture, Table B1). The $P450_{cam}$ systems again displayed lower levels of the P450 (10 - 98 nM) compared to the $P450_{BM3}$ mutants (86 - 108 nM).

In contrast to the isophorone oxidations, the $P450_{BM3}$ mutants displayed higher levels of product formation for both cineoles. GVQ and RLYFGVQ were able to produce 2.26 mM $\pm$ 0.4 mM of 6-α-hydroxy-1,8-cineole after 16 h from the addition of 4 mM of 1,8-cineole (Figure 64a and 64b).

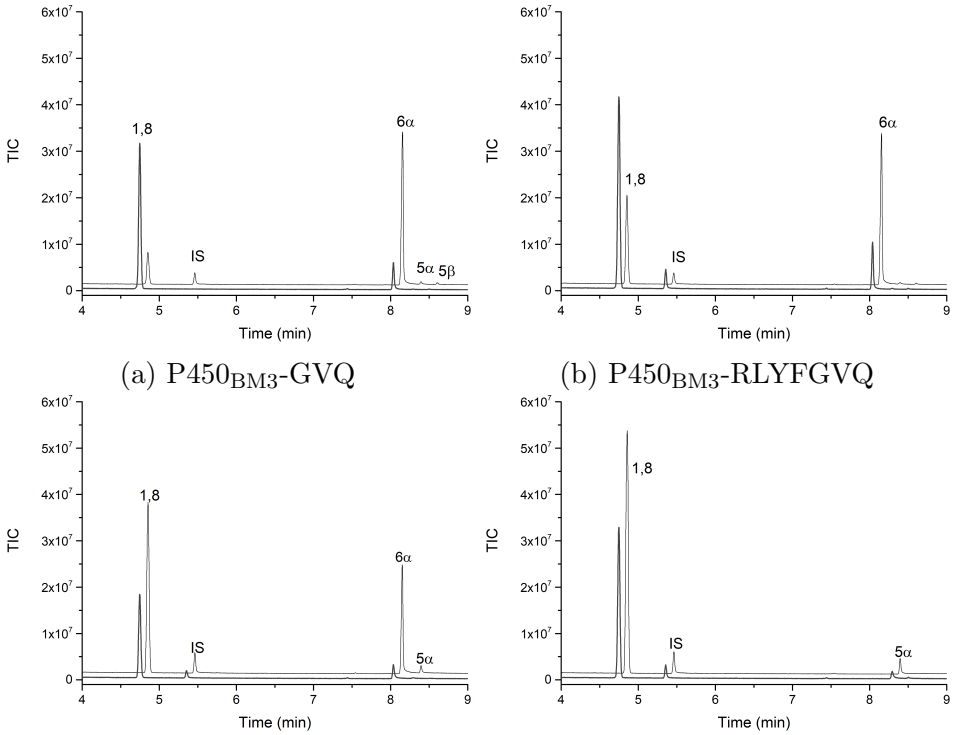

(a) $P450_{BM3}$-GVQ (b) $P450_{BM3}$-RLYFGVQ

(c) $P450_{cam}$-VFA (d) $P450_{cam}$-WFA

Figure 64: Whole cell turnovers of (a) $P450_{BM3}$-GVQ and (b) RLYFGVQ, (c) $P450_{cam}$-VFA and (d) WFA with 1,8-cineole at 6 h (black) and 16 h (grey). Products observed include 6-α-hydroxy-1,8-cineole (6α, t_R = 8.01 min), 5-α-hydroxy-1,8-cineole (5α, t_R = 8.4 min) and 5-β-hydroxy-1,8-cineole (5β, t_R = 8.52 min). For clarity, the chromatograms were offset along the x- and y-axes.

1,8-Cineole oxidation by the VFA mutant also produced 1.0 ± 0.4 mM of 6-α-hydroxy-1,8-cineole but the WFA variant gave even lower yields of 5-α-hydroxy-1,8-cineole (Figure 64c and 64d). For the 1,4-cineole turnovers, the RLYFFAIP mutant generated high amounts of 3-α-hydroxy-1,4-cineole (2.0 ± 0.1 mM) under the same conditions (Figure 65a). The yields for the $P450_{cam}$ systems were consistently lower than $P450_{BM3}$ for both cineoles (Figure 64 and 65) and appeared to be in agreement with the lower amounts of P450 detected for this system. Mutant WFA was still capable of generating approximately 1.0 ± 0.4 mM of 3-α-hydroxy-1,4-cineole (Figure 65c). The LF variant only produced 470 µM of 8-hydroxy-1,4-cineole alongside the 2-α-hydroxy metabolite (Figure 65b). Unknown oxidation products were also present for mutants RLYFFAIP (\$, m/z = 170.15, Appendix B18) and LF (#, m/z = 168.15, Appendix B18).

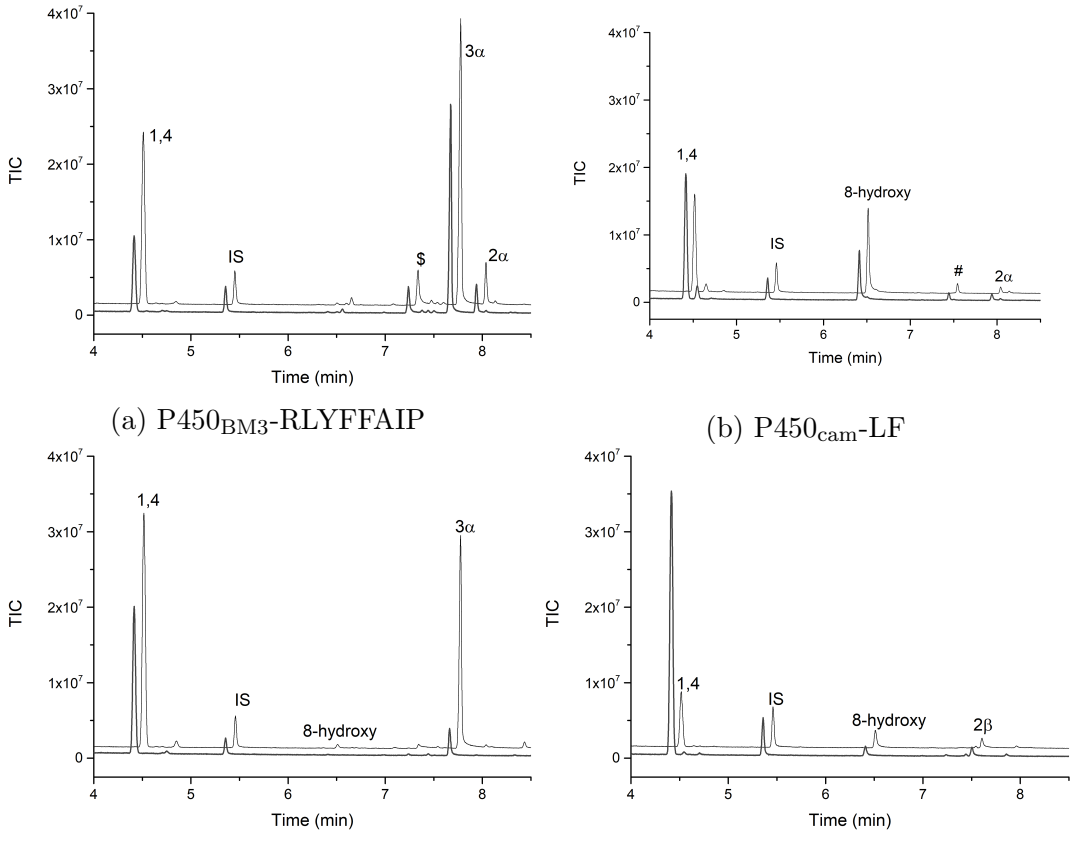

(a) $P450_{BM3}$-RLYFFAIP

(b) $P450_{cam}$-LF

(c) $P450_{cam}$-WFA

(d) $P450_{cin}$

Figure 65: Whole cell turnovers of (a) $P450_{BM3}$-RLYFFAIP, (b) $P450_{cam}$-LF and (c) WFA, (d) $P450_{cin}$ with 1,4-cineole at 6 h (black) and 16 h (grey). Unknown oxidation products were labelled as # and \$. Products observed include 8-hydroxy-1,4-cineole (8-hydroxy, t_R = 6.4 min), 2-α-hydroxy-1,4-cineole (2α, t_R = 7.8 min), 2-β-hydroxy-1,4-cineole (2β, t_R = 7.5 min) and 3-α-hydroxy-1,4-cineole (3α, t_R = 7.6 min). For clarity, the chromatograms were offset along the x- and y-axes.

The $P450_{BM3}$ mutant systems overall provided better biocatalytic conversions of the cineoles compared to the $P450_{cam}$ systems in these whole-cell turnovers. In spite of this, the WT-$P450_{cam}$ system was able to unselectively convert 1,8-cineole (4 mM total) to its three hydroxy products at levels similar to the $P450_{BM3}$ mutants (> 2.0 mM) (Figure

66). The higher yields of WT-P450$_{cam}$ and the high *in vivo* product formation for isophorone with P450$_{cam}$ systems tested previously, suggests that further optimisation of the systems could be used for larger scale production of these metabolites in a selective manner. Further investigation into the *in vitro* activity and binding properties of the P450$_{cam}$ variants would also provide insights into how these systems could be improved.

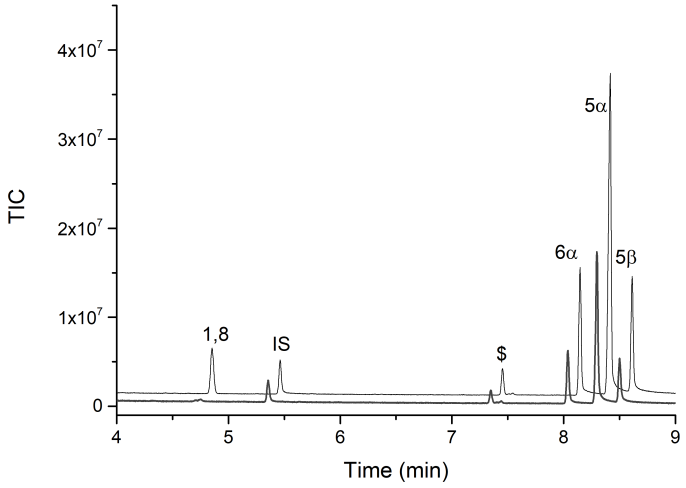

Figure 66: Whole-cell turnover of WT-P450$_{cam}$ with 1,8-cineole, where the samples were taken at 6 h (bottom) and 16 h (top). It can be seen after 16 h, a majority of the substrate was converted to products. Products identified include 6-α-hydroxy-1,8-cineole (6α, t_R = 8.01 min), 5-α-hydroxy-1,8-cineole (5α, t_R = 8.4 min) and 5-β-hydroxy-1,8-cineole (5β, t_R = 8.52 min). A possible further oxidation ketone product was labelled as \$ at t_R = 7.35 min. For clarity, the chromatograms were offset along the x- and y-axes.

The enantioselectivity of both P450$_{BM3}$ and P450$_{cam}$ mutants were assessed. To better resolve any hydroxy cineole enantiomers via chiral GC analysis, the metabolites were derivatised to their corresponding trifluoroacetate esters and the enantioselectivity was analysed for each turnover (Figure 67 and 68).[96,104]

Mutants P450$_{BM3}$-GVQ and RLYFGVQ produced the same major product (6-α-hydroxy-1,8-cineole) as mutant P450$_{cam}$-VFA. GC-chiral analysis of their derivitised turnover extracts showed that the 6-α-hydroxy metabolite of the P450$_{cam}$-VFA turnover was resolved into one peak (Figure 67c). The two P450$_{BM3}$ mutants resolved the same metabolite into a smaller product peak alongside the major product (6-α, Figure 67a and 67b, t_R = 12.25 - 12.45 min)). This inferred that the product of the P450$_{cam}$ mutant had higher e.e. than P450$_{BM3}$ and therefore was more enantioselective. For 1,4-cineole oxidation, both P450$_{BM3}$-RLYFFAIP and P450$_{cam}$-WFA were selective for the formation of 3-α-hydroxy-1,4-cineole (Figure 68, t_R = 10.85 min). GC-chiral analysis showed the derivitised major product peak for both mutant enzymes resolved into

one peak, this also suggests a high e.e. was possible for these mutants, though the peak may not have been resolved by chiral GC. Further studies with comparisons to synthesised racemic and chiral standards would be required to confirm the enantioselectivity of these mutants with the cineoles.

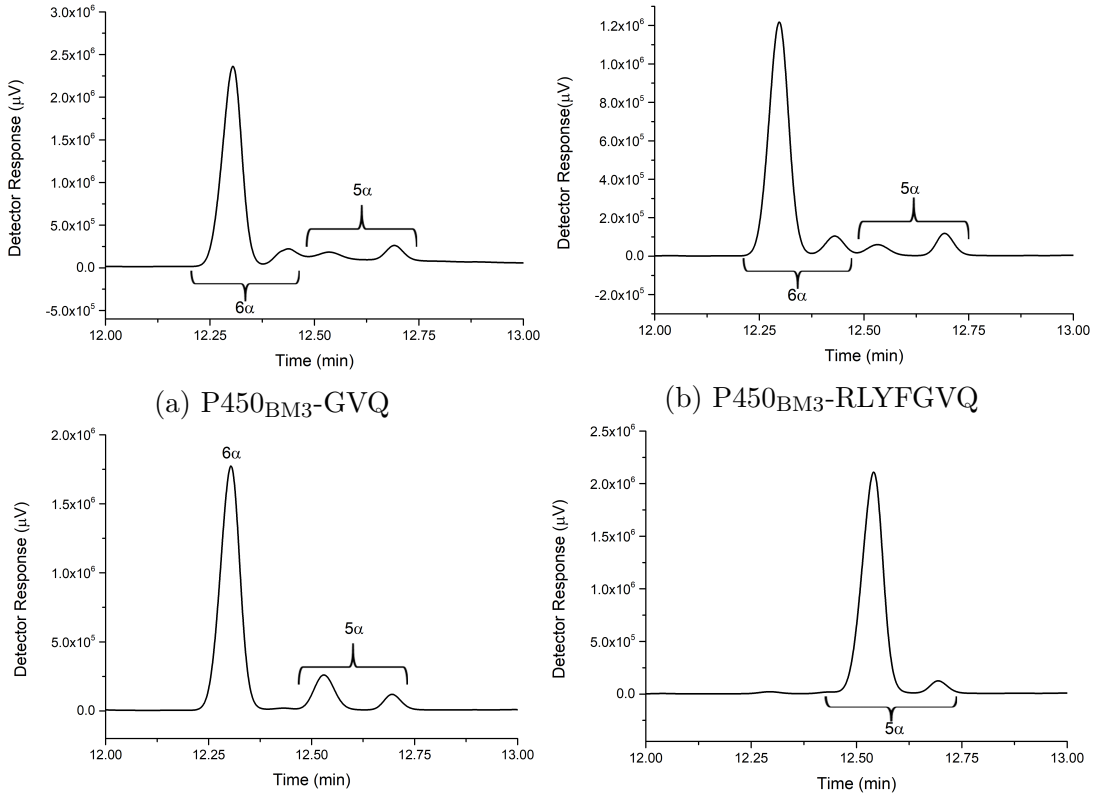

(a) $P450_{BM3}$-GVQ (b) $P450_{BM3}$-RLYFGVQ

(c) $P450_{cam}$-VFA (d) $P450_{cam}$-WFAL

Figure 67: GC-chiral analysis of trifluoroacetate derivitised 1,8-cineole turnovers with (a) $P450_{BM3}$-GVQ and (b) $P450_{BM3}$-RLYFGVQ, (c) $P450_{cam}$-VFA and (d) $P450_{cam}$-WFAL. Possible derivitised enantiomers include 6-α-hydroxy-1,8-cineole (6-α, t_R = 12.25 - 12.45 min) and 5-α-hydroxy-1,8-cineole (5-α, t_R = 12.5 - 12.7 min).

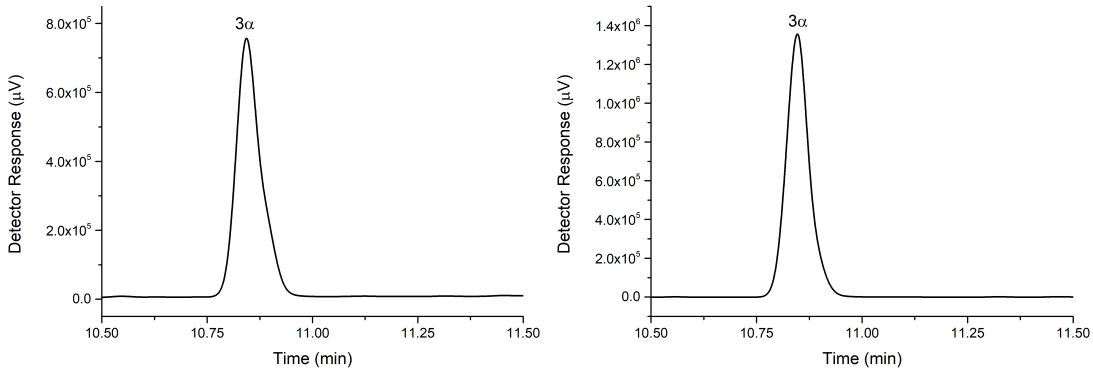

(a) $P450_{BM3}$-RLYFFAIP (b) $P450_{cam}$-WFA

Figure 68: GC-chiral analysis of trifluoroacetate derivitised 1,4-cineole turnovers with (a) $P450_{BM3}$-RLYFFAIP and (b) $P450_{cam}$-WFA. Possible derivitised enantiomer include 3-α-hydroxy-1,4-cineole (3-α, t_R = 10.85 min).

4.3 Discussion

Fenchone, fenchyl acetate, isophorone, and 1,8- and 1,4-cineole are molecules that possess similar sizes and chemical functionalities to both camphor and pinene. The *in vivo* screening of only a small library of $P450_{cam}$ mutants, designed primarily to oxidise pinene, allowed for selective transformations of these substrates to produce their oxy-metabolites in improved yield relative to the WT.[46] Several of the oxidations have also been shown to be enantioselective when this was determined.

Fenchone and fenchyl acetate oxidation by mutants Y96F and Y96A was selective for the C5-C6-C7 face of both molecules. The carbonyl and acetate groups likely acted as an anchor within the enzyme active site to bias this face towards the heme centre. The introduction of alanine and phenylalanine mutations to the Tyrosine96 residue of $P450_{cam}$ seem to have increased the product yield over the WT. A possible explanation is that the less bulky residues provided more active site volume to accommodate the larger fenchyl acetate and the different shape of fenchone compared to camphor.

There was greater selectivity with the Y96A variant in oxidising fenchyl acetate. This mutant selectively hydroxylated the *exo* face of fenchyl acetate. Both *exo* and *endo* hydroylation products were observed with fenchone oxidation by Y96F. Fenchone has been oxidised to form the 6-*endo*, 6-*exo*, 10-hydroxy and 5-*exo* hydroxy products by various organisms, including the bacterial organism, *Salmonella typhimurium* and the common cutworm, *Spodoptera litura*.[101,149,150] It has also been metabolised by human microsomal CYP2A6 to form 6-*endo*, 6-*exo* and 10-hydroxyfenchone.[140] Fenchyl acetate oxidation has only been reported with CYP101B1 and forms the 5-*exo* hydroxy product. For both substrates, the formation of the 7-hydroxy product via biotransformation using a P450 enzyme or otherwise has not previously been reported.

The enantioselective production of (*R*)-4-hydroxyisophorone in high yield was achieved using two $P450_{cam}$ mutants, WFL and WFAL, with the latter displaying the highest yield of the desired product. Isophorone differs from the other substrates tested here in that it lacks a bicyclic structure and possesses an alkene moiety. The oxidation of isophorone by the WFAL mutant has also been studied concurrently in a separate investigation by Turner et al. and our results agree with their findings.[142] Their docking studies with the WFAL mutant and isophorone have suggested that the L244A mutation introduces additional space to accomodate the dimethyl groups, while the longer side chain of the V247L residue might push the bound isophorone closer to the heme centre.[142]

4-Hydroxyisophorone is of considerable commercial value as a flavouring agent and an

intermediate for the synthesis of natural dye pigments.[133,134] The ability to produce this compound via whole-cell biocatalysis would enable it to be generated on a large scale.[130–133] A study by Kaluzna and colleagues has already successfully scaled up a turnover of WT-P450$_{BM3}$ with isophorone in a fermentor system.[129] They successfully produced 10 g L^{-1} of 4-hydroxyisophorone with cell densities 30 times than those used in our experiments and space-time product yields of 1.5 g L^{-1} h^{-1}. However, the *in vivo* reaction of isophorone and WT-P450$_{BM3}$ has been observed to give low yields and activity,[135] and the availability of more efficient and high yielding P450 systems such as those reported here is encouraging for the scale up of this reaction.

The P450$_{cam}$ mutant library has also exhibited a diverse array of predominantly regioselective oxidations of 1,8- and 1,4-cineole. These were also enantioselective in some cases and this provides a significant development towards new enantio- and regioselective hydroxylation pathways for cineoles. This circumvents the need for reactive chemical reagents to functionalise the inherently chemically inert bonds of both compounds.[96] The selective formation of one cineole oxidation product in higher yield will also aid in the isolation and purification of said product.

P450$_{cin}$ from *Citrobacter braakii* selectively produces (1*R*)-6-β-hydroxy-1,8-cineole from 1,8-cineole.[104] The same reaction has also been reported with a *Rhodcoccus* bacterium.[20,96] 1,4-Cineole oxidation by P450$_{cin}$ (Figure 62) was not as selective as its 1,8 analogue. The preference for 1,8-cineole by P450$_{cin}$ despite their similar structures indicates P450$_{cin}$ has evolved specifically to oxidise 1,8-cineole to form the hydroxy metabolite. This is unsurprising, as the hydroxylation of its substrate is the first step of 1,8-cineole metabolism within *C.braakii*.[151] The complementary (1*R*)-6-α-hydroxy metabolite was reported to be a biotransformation product of 1,8-cineole by *Bacillus cereus*.[96] Oxidation products at the C2, C3, C4, C7 and C8 positions have also been produced from the metabolism of various organims such as rabbits and human microsomes, though in an unselective manner.[96,152,153]

A number of P450$_{cam}$ mutants within the library were able to hydroxylate 1,4-cineole with high selectivity at either the C3 and C8 positions. 1,8-Cineole was hydroxylated at the C5 and C6 positions. These metabolites have been produced previously in other organisms, though mostly in a less selective manner as minor products.[101,104,144–146] The selective nature of the P450$_{cam}$ mutant oxidations greatly expands the range of metabolites that can be generated from 1,8- and 1,4-cineole. The P450$_{cam}$ mutants also seem to favour the *endo* (α) face of the cineoles that would be sterically less hindered than the *exo* (β) face. P450$_{cin}$ showed a very strong preference for the *exo* face. The orientation of 1,8-cineole within P450$_{cin}$ is biased through a hydrogen bonding interac-

tion between Asparagine242 (N242) and the cineole's ether oxygen that orientates the 5-*exo* hydrogen above the heme for hydroxylation (Figure 69).[154] An alanine mutation introduced at N242 (N242A) was able to decrease the product selectivity and oxidation from the *endo* face was significantly increased.[104,154]

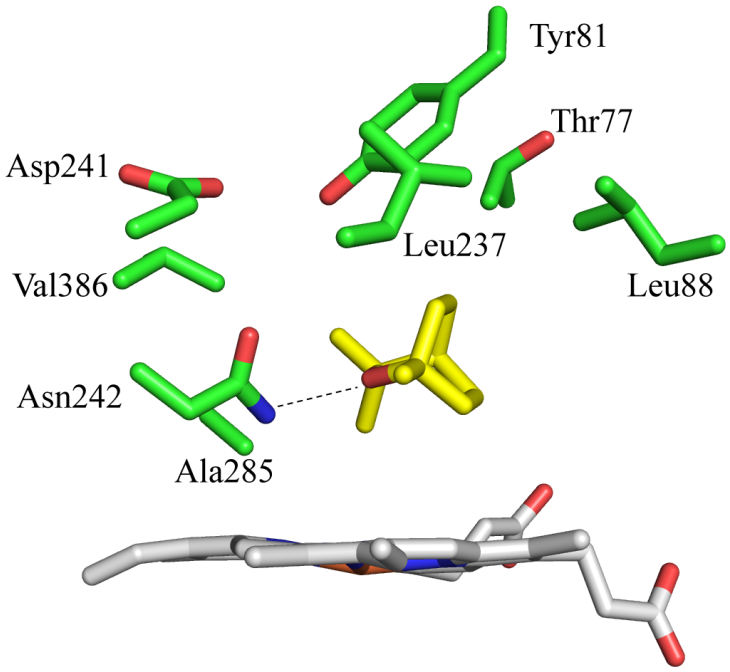

Figure 69: Active site of Cytochrome $P450_{cin}$ with bound 1,8-cineole (PDB ID: 1T2B). The Asn242 residue has a hydrogen bonding interaction with the ether oxygen of 1,8-cineole.[154]

WT-$P450_{cam}$ was previously reported to be selective for (1*S*)-6-α-hydroxy-1,8-cineole and this metabolite was also produced by mutant VFA when oxidising 1,8-cineole.[104] The mutant formed one enantiomer of the 6-α metabolite with high e.e. based on the single peak resolved via GC-chiral analysis of the trifluoroacetate ester derivative as according to previous methods (Figure 67c).[104] The identity of this enantiomer is likely to be in the (*S*) configuration as the WT but comparison to known chiral standards would be needed to confirm this. The 3-α enantiomer formed by $P450_{cam}$-WFA oxidation of 1,4-cineole also appeared to be formed with high e.e. based on GC-chiral analysis (Figure 68). It was crystallised by our colleagues with a (1*S*) absolute configuration.[105]

The 1,8-cineole hydroxy products were easily identified as they were already metabolites generated by WT-$P450_{cam}$. However, the mutant enzymes altered the selectivity of the 1,8-cineole oxidation and this was exemplified by the WFA and VFA mutants which catalysed the selective production of the 5α and 6α isomers respectively ($\geq$ 90 %). The production of the desaturated alkene metabolite of 1,4-cineole was greatest for the LF mutant and this could be potentially used to investigate this unusual P450

transformation.

Comparisons of the whole-cell systems between $P450_{cam}$ and $P450_{BM3}$ displayed contrasting behaviours for isophorone and cineole oxidations. The cell wet weights per litre for P450 systems used were largely consistent across all mutant $P450_{cam}$ and $P450_{BM3}$ systems but the enzyme concentrations detected were lower for $P450_{cam}$ systems. $P450_{BM3}$ is a single species fused to its electron transfer partner. However, $P450_{cam}$ must be produced with its two electron transfer partners which could decrease the yield.

Despite the low P450 concentration, $P450_{cam}$ systems displayed greater product yields for isophorone oxidations over a longer period of time. However, the $P450_{BM3}$ mutants gave greater product yields with cineoles using similar conditions. This could suggest that the cineoles were better substrates for $P450_{BM3}$ systems and isophorone was more suited for the $P450_{cam}$ systems instead. However, direct comparison between two P450s from widely different electron transfer systems, i.e. three component Class I versus fused Class VIII systems respectively is not trivial. This is because $P450_{BM3}$ may also require different cellular NADPH concentrations and possess different co-factor regeneration rates against that of the NADH used by $P450_{cam}$.[155–158] *In vitro* studies would be needed to confirm the preference of each system for these substrates.

Regardless, it has been shown that functional whole-cell oxidation systems for both $P450_{cam}$ and $P450_{BM3}$ mutants are capable of oxidising a variety of monoterpenoids in good yield. These systems were scaled up for product isolation in a non-optimised manner in shake flasks and it is likely these oxidations can be made more efficient with further study. The oxidations here were found to be regioselective through the use of mutant enzymes. Therefore it is possible that further protein engineering of these enzymes could increase the activity of these or other P450 enzymes towards the biotransformation of monoterpenoids and other related compounds.

5 Oxidation of Fragrance Compounds by P450s

5.1 Introduction

The potential of developing new aroma compounds from the biocatalytic oxidation of existing fragrances makes P450 enzymes especially valuable. P450 enzymes such as CYP101B1 are capable of hydroxylating compounds that include ionones and damascones with high efficiency.[61,62] Monoterpenoid acetates have also been hydroxylated with high activity by CYP101B1. The presence of the acetate moiety in these substrates is hypothesised to mimic the butenone side chain in norisoprenoids.[101]

Mutant variants of $P450_{BM3}$ have also been observed to oxidise ionones and terpenes in a selective manner.[74] For example, $P450_{BM3}$ mutant variant GVQ has been developed for α-pinene oxidation and mutant R47L/Y51F/F87V can oxidise β-ionone with high selectivity.[74,159]

A selection of fragrance compounds will be screened for selective and high yield generation of metabolites with CYP101B1 and $P450_{BM3}$-GVQ (Figure 70) . These compounds possess molecular architectures similar to the above mentioned substrates that can be efficiently oxidised by these enzymes.

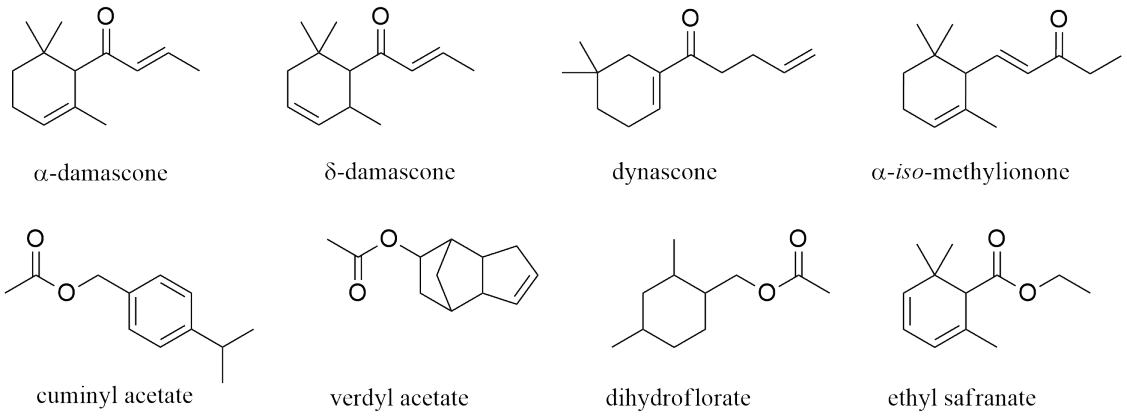

Figure 70: Fragrance compounds with norisoprenoid and acetate structures.

The norisoprenoid compounds, α-damascone, δ-damascone, dynascone and α-*iso*-methylionone have similar structures to β-ionone (Figure 70). All four of these compounds possess pleasant floral and fruity aromas that have considerable commercial value.[160] The damascones are known to possess potent odour blocking properties and are important components in deodorants and perfumes.[161,162] The key structural differences between these compounds compared to β-ionone is the differing alkene and carbonyl positions on the side chain. Dynascone and α-*iso*-methylionone also possess longer alkyl side chains. The alkene position on the ring also differs between the

four compounds and this alongside the altered side chains could have an effect on the binding to and oxidation by P450 enzymes.

Monoterpenoid acetate esters have also been oxidised with high yield and efficiency by CYP101B1.[101] Therefore a selection of acetate and ester compounds with ring and side chain moieties similar to ionones and monoterpenoids will also be screened with the aforementioned P450 enzymes. These substrates include cuminyl acetate, verdyl acetate, dihydroflorate and ethyl safranate. They all possess a 6-membered ring and a carbonyl moiety within their structure. For example, ethyl safranate possesses an ethyl formate group attached to a ring structure with two ring alkenes and methyl substitutions in the same positions as the norisoprenoids (Figure 70). As with the norisoprenoids, these acetate compounds also possess pleasant aromas and the oxidised derivatives of these compounds may also provide new sensory properties.

In vitro and *in vivo* screening of these substrates with CYP101B1 and $P450_{BM3}$-GVQ will be carried out. Whole-cell turnovers that displayed selective oxidation profiles and high conversion/yield will be scaled up as before. The products of these high yielding turnovers will be isolated and characterised.

5.2 Results

Initial *in vitro* binding studies of CYP101B1 were first carried out on the chosen substrates (Figure 70). Amongst the substrates tested, the norisoprenoid derivatives, δ- and α-damascone, dynascone and α-*iso*-methylionone induced the highest changes in spin-state with CYP101B1 (65 - 95 %, Table 12, Figure 71). The similarity in structure between these substrates and β-ionone would be expected to enable them to bind to the active site pocket of CYP101B1 with high complementarity.

Table 12: Spin-state shift data for CYP101B1 and $P450_{BM3}$ with different substrates.

Enzyme	Substrate	% HS
CYP101B1	δ-Damascone	65
	α-Damascone	80
	Dynascone	60
	α-*iso*-methylionone	$\geq$95
	Ethyl safranate	60
	Dihydroflorate	90
	Cuminyl acetate	10
	Verdyl acetate	-[a]

[a]No spin-state shift observed.

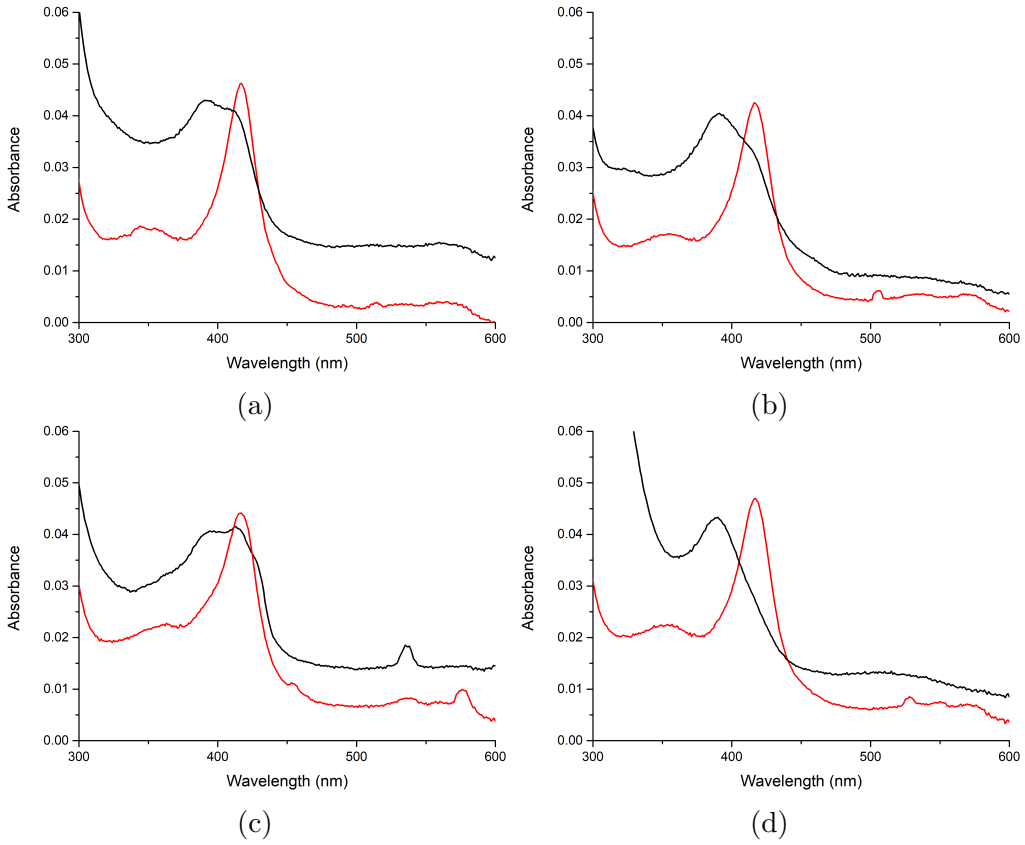

Figure 71: Spin-state shift studies of WT-CYP101B1 with (a) δ-damascone, (b) α-damascone, (c) dynascone, (d) α-*iso*-methylionone.

Addition of ester compounds, ethyl safranate and dihydroflorate to CYP101B1 also generated a significant spin-state shift (60 - 90 % HS, Figure 72).

The remaining ester compounds, cuminyl and verdyl acetate showed minor changes in the spin-state when added to CYP101B1 (Table 12). Ethyl safranate and dihydroflorate both possess an ethyl formate side chain that is comparable in length to the butenone moiety in the norisoprenoids. They also contain ring structures which are similar to the norisoprenoids. Ethyl safranate has an additional ring alkene while dihydroflorate has a saturated ring system. The similar ring structure and side chains of these substrates are likely to contribute to the greater spin-state shift observed with CYP101B1 compared to cuminyl and verdyl acetate.

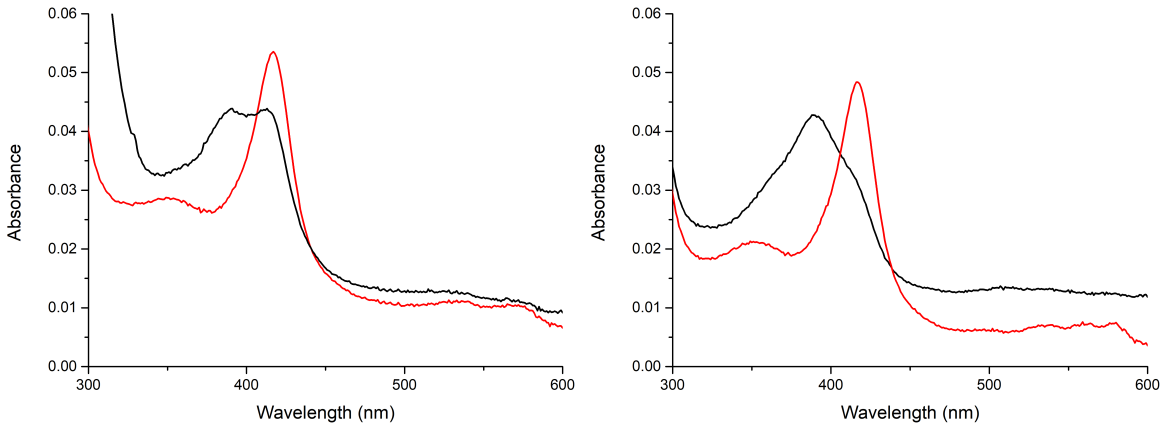

Figure 72: Spin-state shift study for (a) ethyl safranate and (b) dihydroflorate with WT-CYP101B1.

Next, the turnover of the compounds by the complete CYP101B1 system were assessed to determine the catalytic activity and production formation, where oxidation products were identified using GC-MS analysis based on the change in mass ($\Delta m/z$) compared to the substrate. The NADH oxidation rate of CYP101B1 with dihydroflorate (1235 min^{-1}) was comparable with the oxidation of β-ionone[61] (1600 min^{-1}) but resulted in low levels of product formation (Figure 74). This is reflected in a low coupling efficiency (24 %).

GC-MS analysis of the dihydroflorate turnover showed the formation of three products that all show MS spectra consistent with substrate oxidation ($m/z = 200$, $\Delta m/z = +16$, Appendix C.1). The three products formed are presumed to correlate with the three substrate peaks (D1, D2, D3) observed by GC-MS (Figure 74). The dihydroflorate sample supplied displayed three peaks by GC-MS analysis. All three peaks in the supplied dihydroflorate possessed similar mass spectra (Appendix C.1). Dihydroflorate possesses three chiral centres and the sample could contain different diastereomers (Figure 73).

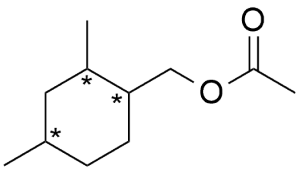

Figure 73: Structure of dihydroflorate where chiral centres are marked with *.

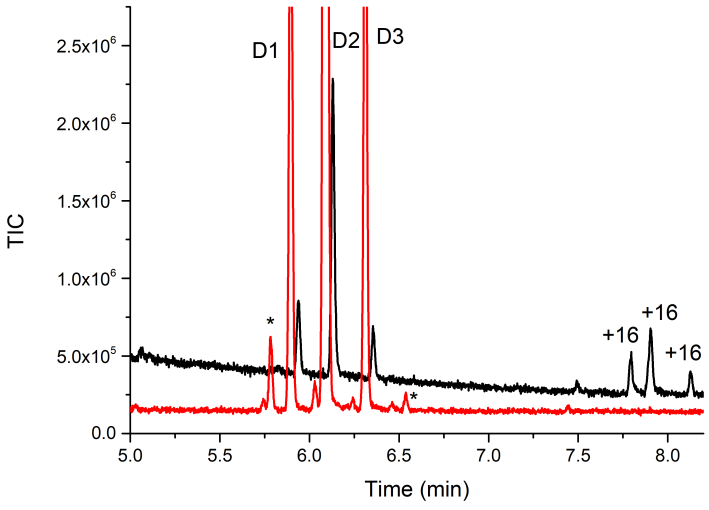

Figure 74: GC-MS analysis of the *in vitro* turnover of dihydroflorate ($m/z = 184$) with WT-CYP101B1 (black) with substrate control (red). Products at t_R = 7.75, 7.85 and 8.08 min had mass spectra consistent with an addition of an oxygen atom ($m/z = 200$, $\Delta m/z = +16$). Dihydroflorate has three chiral centres and could be composed of different diastereomers as evidenced by the 3 peaks (D1, D2 and D3). These had similar mass spectra which were consistent with isomers of dihydroflorate.

Addition of ethyl safranate also induced a high NADH oxidation rate in the CYP101B1 system (837 min^{-1}). Higher levels of product formation compared to the dihydroflorate turnover were observed and were reflected in the coupling efficiency of the turnover (32 %). The supplied ethyl safranate also possessed three peaks that had similar mass spectra (Appendix C.2). Ethyl safranate is known to be produced commercially as a mixture of its α, β and γ-isomers, where the ratio between them depends on the reaction conditions used to generate the sample (Figure 75).[163,164] At least six metabolites (Figure 76) could be assigned as oxidation products (m/z = 200, $\Delta m/z$ = +16) based on their mass spectra detailed in Appendix C.2. The presence of two alkenes within the ethyl safranate ring structure would likely favour epoxidation by CYP101B1 (see δ-damascone in Chapter 5.2.1.1) and the multiple products formed could be diastereomers of these epoxides.

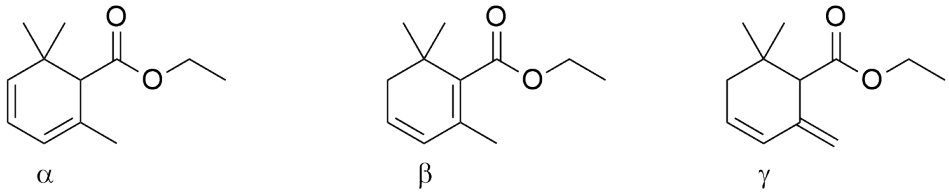

Figure 75: Different isomers of ethyl safranate.

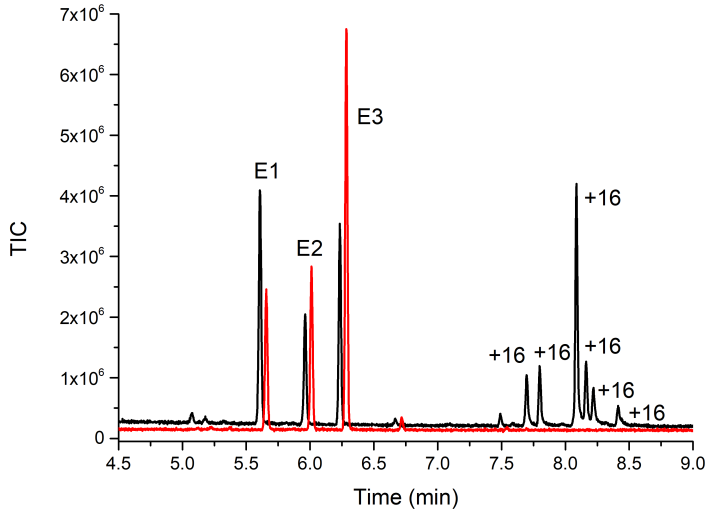

Figure 76: GC-MS analysis of the *in vitro* turnover of ethyl safranate (m/z = 184) with WT-CYP101B1 (black) with substrate control (red). Products at t_R = 7.7, 7.8, 8.1, 8.15, 8.22 and 8.43 min had mass spectra consistent with an addition of an oxygen atom ($\Delta m/z$ = +16). Substrate possessed 3 peaks (E1, E2 and E3) that had similar mass spectra that are likely to be the α, β and γ-isomers of this substrate.[163,164]

The norisoprenoid compounds, α-damascone, δ-damascone, dynascone and α-*iso*-methylionone all displayed high rates of NADH oxidation (495 - 850 min^{-1}). These high rates are in good agreement with the high spin-state shifts observed for these substrates. This further indicates the high complementarity between these substrates and

CYP101B1. The coupling efficiency and levels of product formation were the highest for the damascones (50 - 60 %, Figure 77).

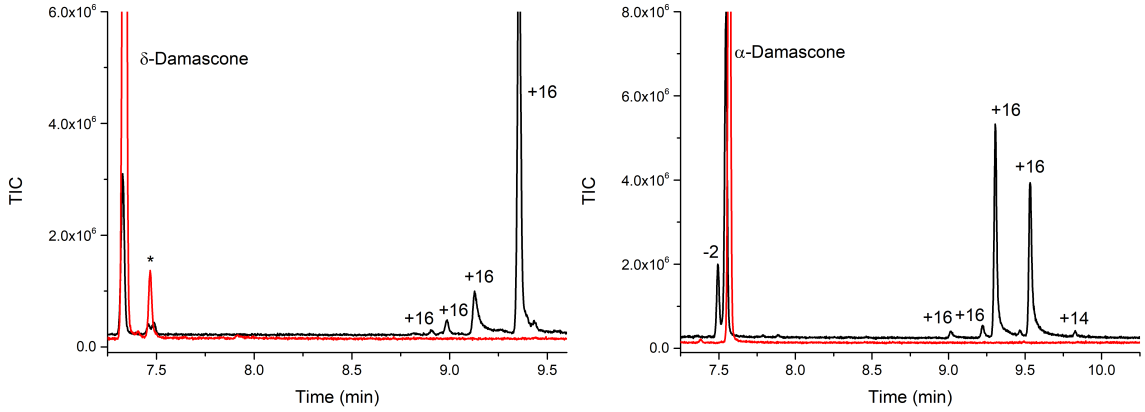

(a) (b)

Figure 77: GC-MS analysis of the *in vitro* turnovers of CYP101B1 (black) with (a) δ-damascone (m/z = 192) where products were identified at t_R = 8.9, 9.0, 9.14, 9.4 min and (b) α-damascone (m/z = 192) with products at t_R = 9.0, 9.25, 9.3, 9.55 min and 9.8 min. Mass spectra for the products of both substrates were consistent with either oxidation (m/z = 208, $\Delta m/z$= +16) or further oxidation (m/z = 206, $\Delta m/z$ = +14) (Appendix C.3 and C.4). The α-damascone may have shown a possible desaturation product at t_R = 7.5 min ($\Delta m/z$ = -2). Substrate controls are shown in red. Impurities are labelled as *. For clarity, chromatograms were offset along the x axis for (b).

δ-Damascone oxidation by CYP101B1 formed four metabolites with one metabolite at t_R = 9.4 min being produced nearly 10-fold higher over the other metabolites (Figure 77a). α-Damascone formed five products upon oxidation by CYP101B1 and was less selective overall compared to the turnover of the δ-derivative, though there were two major metabolites at t_R = 9.3 and 9.55 min (Figure 77b).

The two damascone turnovers contained mainly monooxygenase products (m/z = 208, $\Delta m/z$ = +16). There was also evidence for products, that were present in lower amounts, with m/z = 206 ($\Delta m/z$ = +14), the change in mass by two units compared to the oxidation product would indicate that an oxygen has been added to the compound with an additional abstraction of hydrogen to generate a ketone further oxidation product (Appendix C.3 and C.4). Additionally, it could also arise from epoxidation of a desaturated metabolite. A desaturated metabolite was also present within the α-damascone turnover (m/z= 190, $\Delta m/z$ = -2) at t_R = 7.5 min.

Compared to the damascones, α-*iso*-methylionone and dynascone formed lower amounts of product with CYP101B1. This is reflected in their lower coupling efficiency (32 - 39 %, Table 13). Based on MS analysis, the α-*iso*-methylionone (m/z = 206) turnover formed two oxidation metabolites (m/z = 222, $\Delta m/z$ = +16) as the major products while four other further oxidation products were also observed in smaller amounts (m/z = 220, $\Delta m/z$ = +14) (Figure 78a).

The dynascone (m/z = 192) turnovers formed 3 products (m/z = 208, $\Delta m/z$ = +16) (Figure 78b). One of these at t_R = 9.82 min was formed in significantly higher yield based on its peak area (75 %) than the remaining two products. Mass spectra of the oxidation products for both substrates were detailed in Appendix C.5 and C.6.

These two substrates were also supplied as multiple isomers which were detected via GC-MS analysis and their isomers possessed similar mass spectra (Appendix C.5 and C.6). Dynascone is known to be produced commercially as both its α and β isomers.[165] α-*iso*-Methylionone is also produced alongside a mixture of isomers and the composition depends on the manufacturing route.[163] The two isomers present for these two substrates were likely both oxidised by CYP101B1 to form the multiple products observed.

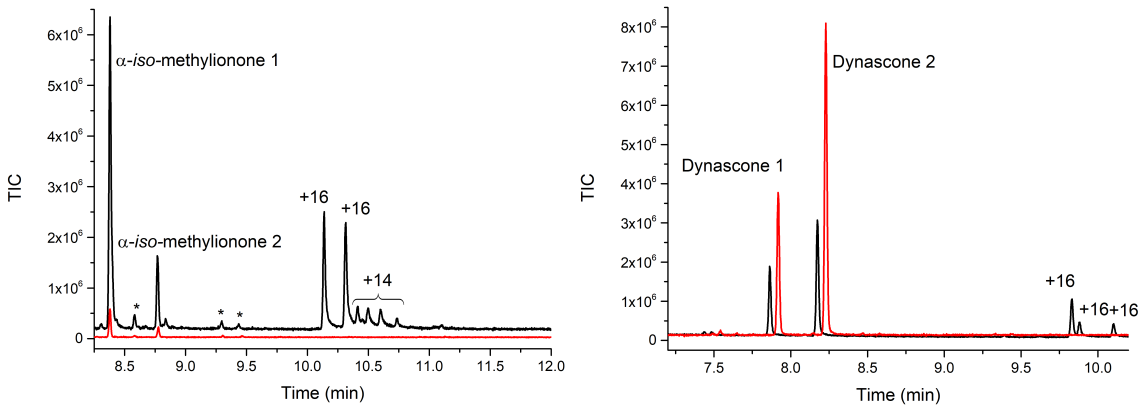

(a) (b)

Figure 78: GC-MS analysis of the *in vitro* turnovers of CYP101B1 (black) with (a) α-*iso*methylionone where products were identified at t_R = 10.1, 10.3, 10.4, 10.5, 10.6 and 10.65 min. (b) Dynascone turnover with products at t_R = 9.82, 9.88 and 10.1 min. Mass spectra for the products of both substrates were consistent with either oxidation ($\Delta m/z$= +16) or further oxidation ($\Delta m/z$ = +14). Substrate controls are shown in red. The substrate controls exhibited two peaks with similar mass spectra. Impurities are labelled as *. For clarity, chromatograms were offset in either the x- or y-axes.

CYP101B1 mediated oxidation of cuminyl acetate resulted in no product formation when analysed by GC-MS, this was despite a moderate NADH oxidation rate of 365 min^{-1} (Table 13). The GVQ mutant of $P450_{BM3}$ is a highly active variant that is capable of oxidising a range of non-natural substrates including alkanes, arenes and branched fatty acids.[166,167] We wished to investigate whether this variant was capable of oxidising the fragrance compounds used here, especially the ones that CYP101B1 could not.

$P450_{BM3}$-GVQ catalysed oxidation of cuminyl acetate (m/z = 192) formed two metabolites (Figure 79) with an NADH oxidation rate of 465 min^{-1}. The major metabolite formed at t_R = 9.3 min had a mass (m/z = 208.1) consistent with oxidation activity ($\Delta m/z$ = +16) (Appendix C.7). The minor metabolite formed (t_R = 8.48 min, m/z

= 190.1) had a mass two units ($\Delta m/z$ = -2) lower than the substrate that agrees with the presence of a desaturation product.

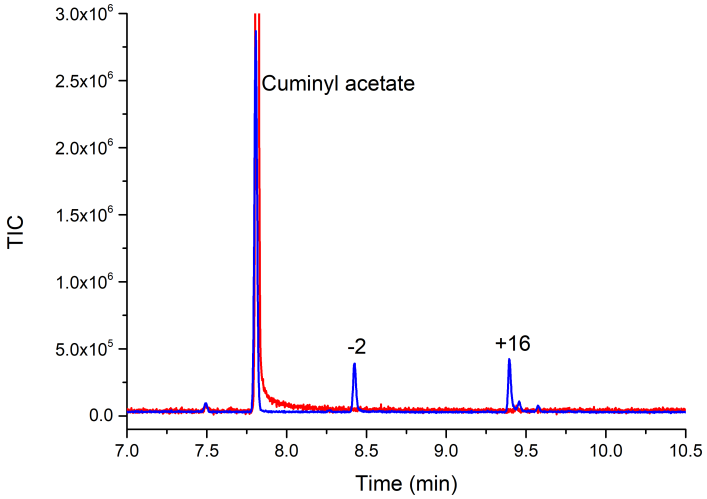

Figure 79: GC-MS analysis of the *in vitro* turnover of cuminyl acetate with $P450_{BM3}$-GVQ (blue) and CYP101B1 (black) with substrate controls (red). Products at t_R= 8.48 and 9.3 min. Mass spectra of the products indicated a desaturation (m/z = 190, $\Delta m/z$ = -2) and oxidation (m/z = 208, $\Delta m/z$ = +16) products.

CYP10B1 and $P450_{BM3}$-GVQ were both capable of oxidising verdyl acetate (m/z = 192). The NADH oxidation rate (Table 13) was faster for CYP101B1 (664 min^{-1}) than it was for $P450_{BM3}$-GVQ (111 min^{-1}). CYP101B1 was selective for the formation of a single product but the $P450_{BM3}$ variant formed two metabolites (Figure 80). All products had mass spectra indicative of a monooxygenase reaction (m/z = 208, $\Delta m/z$ = +16, Figure 81). Despite the similar retention times, the different mass spectra of all three products suggests there were no metabolites formed in common between the CYP101B1 and the $P450_{BM3}$-GVQ systems (Figure 81). Impurities were also present within the verdyl acetate sample that were not identified.

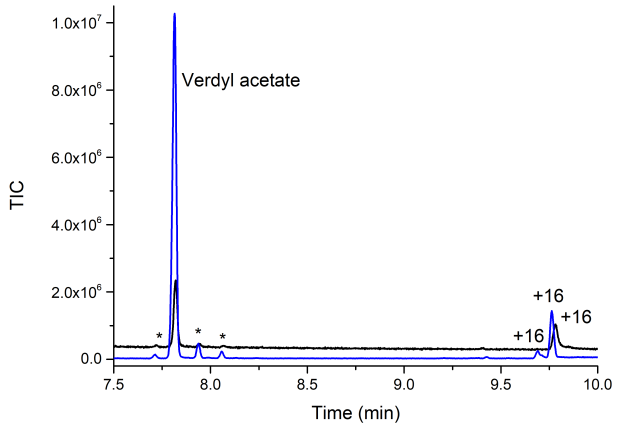

Figure 80: *In vitro* turnover of verdyl acetate with $P450_{BM3}$-GVQ (blue) and CYP101B1 (black). Products at t_R = 9.75 and 9.8 min were identified as oxidation products ($\Delta m/z$ = +16) based on their mass spectra. Impurities are labelled with *.

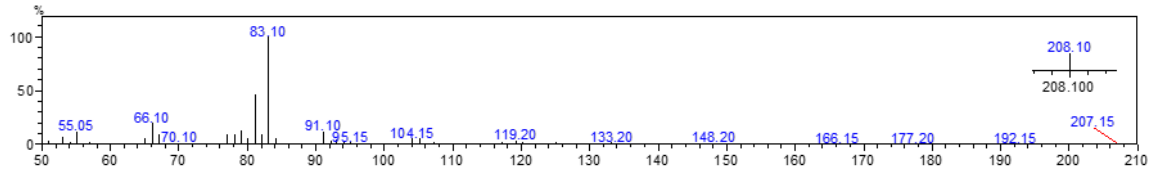

(a) Mass Spectrum of *in vitro* verdyl acetate oxidation product with with $m/z = 208.1$ formed with $P450_{BM3}$-GVQ, $t_R = 9.75$.

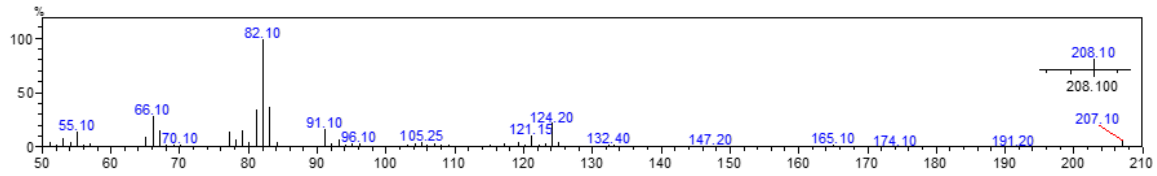

(b) Mass Spectrum of verdyl acetate *in vitro* oxidation product with $m/z = 208.1$ and $t_R = 9.8$ min formed with $P450_{BM3}$-GVQ. Product was identified as 6-hydroxy-verdyl acetate.

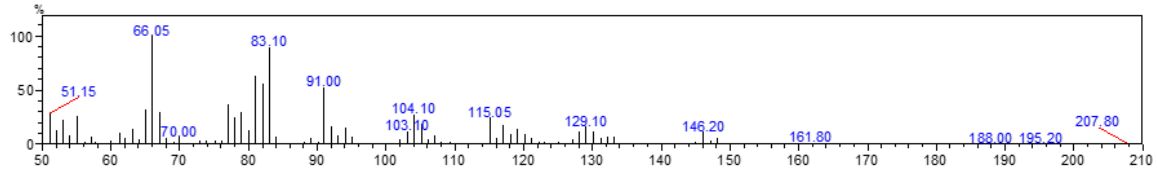

(c) Mass Spectrum of verdyl acetate oxidation product with $m/z = 207.8$, $t_R = 9.85$ min formed with CYP101B1.

Figure 81: Mass Spectrum of verdyl acetate oxidation products formed *in vitro* with different P450 systems.

Table 13: Substrate binding and *in vitro* turnover data for CYP101B1 and $P450_{BM3}$ with different substrates. The data are given as mean ± S.D. with $n \geq 3$. Rates are given as $nmol.nmol_{P450}{}^{-1}.min^{-1}$.

Enzyme	Substrate	NADH	PFR	Coupling Efficiency (%)
CYP101B1	δ-Damascone	705 ± 32	417 ± 35	59 ± 3
	α-Damascone	890 ± 10	457 ± 33	52 ± 3
	Dynascone	495 ± 94	66 ± 20	13 ± 3
	α-Methylionone	850 ± 38	325 ± 9	39 ± 3
	Ethyl Safranate	837 ± 49	264 ± 41	32 ± 4
	Verdyl Acetate	664 ± 100	190 ± 10	29 ± 3
	Dihydroflorate	1235 ± 300	296 ± 70	24 ± 0.01
	Cuminyl acetate	365 ± 25	-[b]	-[b]
$P450_{BM3}$-GVQ[c]	Cuminyl acetate	465 ± 36	76 ± 16	11 ± 2
	Verdyl acetate	111 ± 11	11 ± 2	10 ± 1

[a]No product formation. [b]Not measured. [c]Whole-cell oxidations of $P450_{BM3}$-GVQ with the remaining fragrance compounds tested had low product yield.

5.2.1 Scale up of Product Formation using CYP101 and CYP102 Whole-Cell Oxidation Systems

In vivo whole-cell oxidation systems enable large scale and facile biocatalytic production of metabolites. In order to generate the products from the turnovers in large enough quantities for isolation and identification, enzyme systems of CYP101B1 and $P450_{BM3}$ were used with the fragrance compounds. They were chosen based on the *in vitro* turnovers reported above, whereby δ- and α-damascone, cuminyl acetate, verdyl acetate, α-*iso*-methylionone, ethyl safranate and dihydroflorate had turnovers that gave high levels of metabolite formation with either CYP101B1 or $P450_{BM3}$-GVQ. These were scaled up accordingly with the aim of identifying the metabolites.

The turnovers with α-*iso*-methylionone, ethyl safranate and dihydroflorate displayed multiple product and substrate peaks that caused purification and product isolation to be difficult (Figure 74, 76, 78a). Further study would be needed to isolate these turnovers for characterisation and HPLC separation is likely required to isolate the substrate isomers in a pure form before metabolite formation and identification.

5.2.1.1 Whole-Cell Turnovers of δ-Damascone and α-Damascone

Whole-cell oxidation of δ-damascone showed metabolite formation for CYP101B1 (Figure 82), while the $P450_{BM3}$-GVQ variant did not show any formation of product. One major metabolite was produced in excess at $t_R = 9.4$ min as per the *in vitro* turnover. Two other minor metabolites were formed at $t_R = 8.9$ and 9.0 min that were also present in the *in vitro* turnover as seen in Figure 77a.

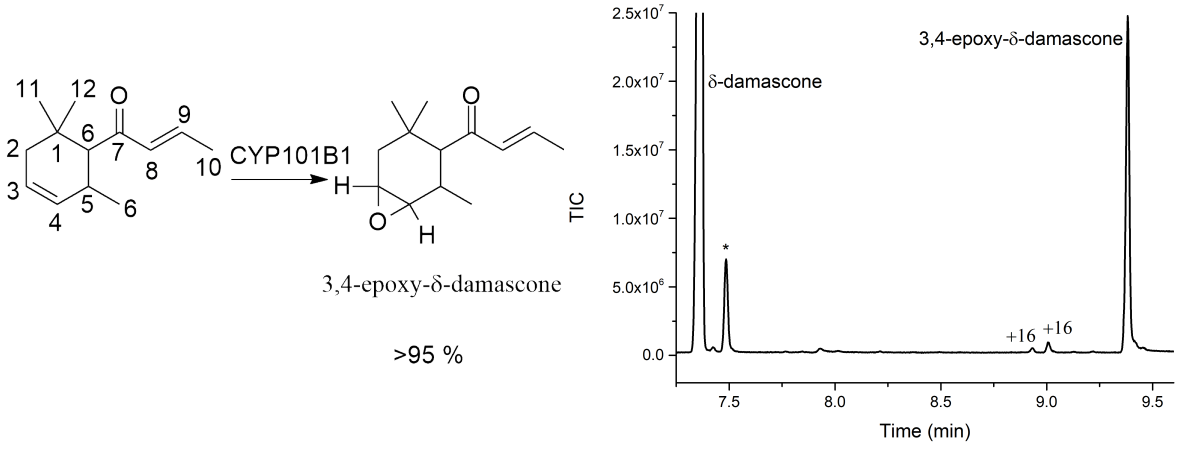

Figure 82: The oxidation of δ-damascone by CYP101B1 alongside the GC-MS analysis of the CYP101B1 whole-cell turnover. Major metabolite produced was 3,4-epoxy-δ-damascone at t_R = 9.4 min. Possible minor oxidation metabolites ($\Delta m/z = +16$) were formed at $t_R = 8.9$ and 9.0 min. Impurities were labelled as *.

The major metabolite was extracted from the whole-cell turnover of CYP101B1. This metabolite was purified by preparative HPLC, analysed by NMR and identified to be 3,4-epoxy-δ-damascone (16 mg isolated yield, Appendix C20). That the metabolite arose from epoxidation was determined via ^{1}H and ^{13}C NMR (Figure 83). The ^{1}H NMR spectrum showed only two alkene hydrogen signals and the presence of two signals with high chemical shifts consistent with epoxide hydrogens (2.87 and 3.19 ppm).[168] This would indicate that alkene oxidation occurred and is confirmed by the loss of two sp^2 carbons in the ^{13}C NMR spectrum.

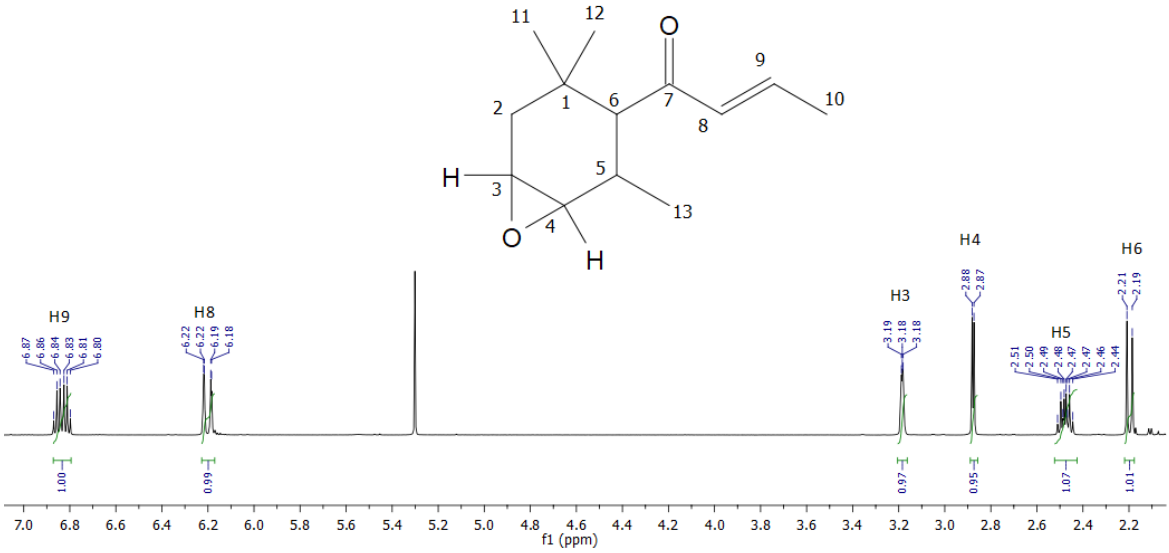

(a)

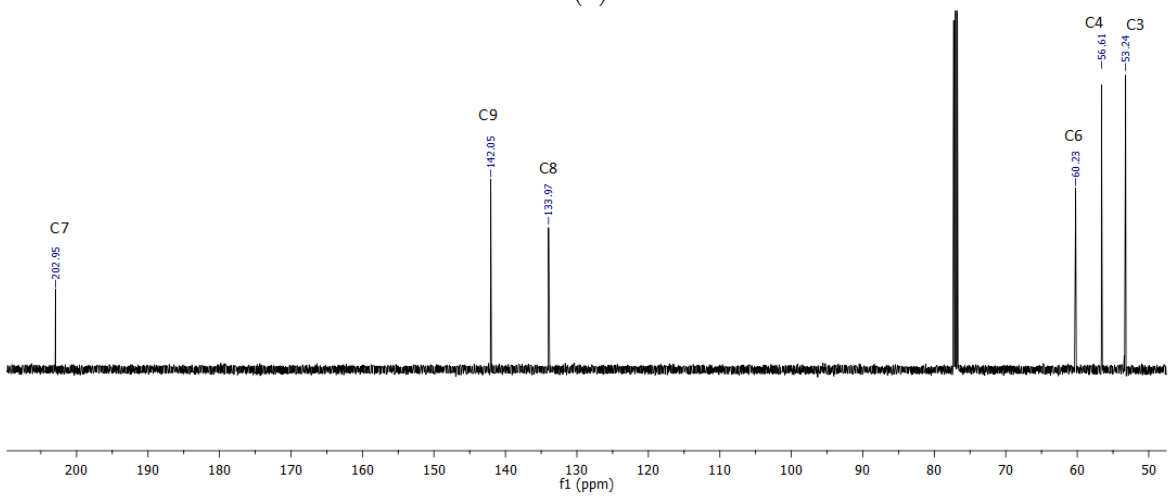

(b)

Figure 83: NMR data for 3,4-epoxy-δ-damascone that shows (a) an expansion of the ^{1}H NMR data, (b) ^{13}C NMR data showing the alkene and epoxide signals for 3,4-epoxy-δ-damascone. Full data in Appendix C20.

HMBC analysis showed the epoxide signals were correlated with signals within the ring structure (C1, C5, C2, C13) indicating that the C3/C4 ring alkene of δ-damascone was oxidised. In addition, the alkene hydrogen signals correlated to the carbonyl group (C7) and the butenone methyl (H10) group (Figure 84), which shows that the alkene retained is located on the butenone side chain.

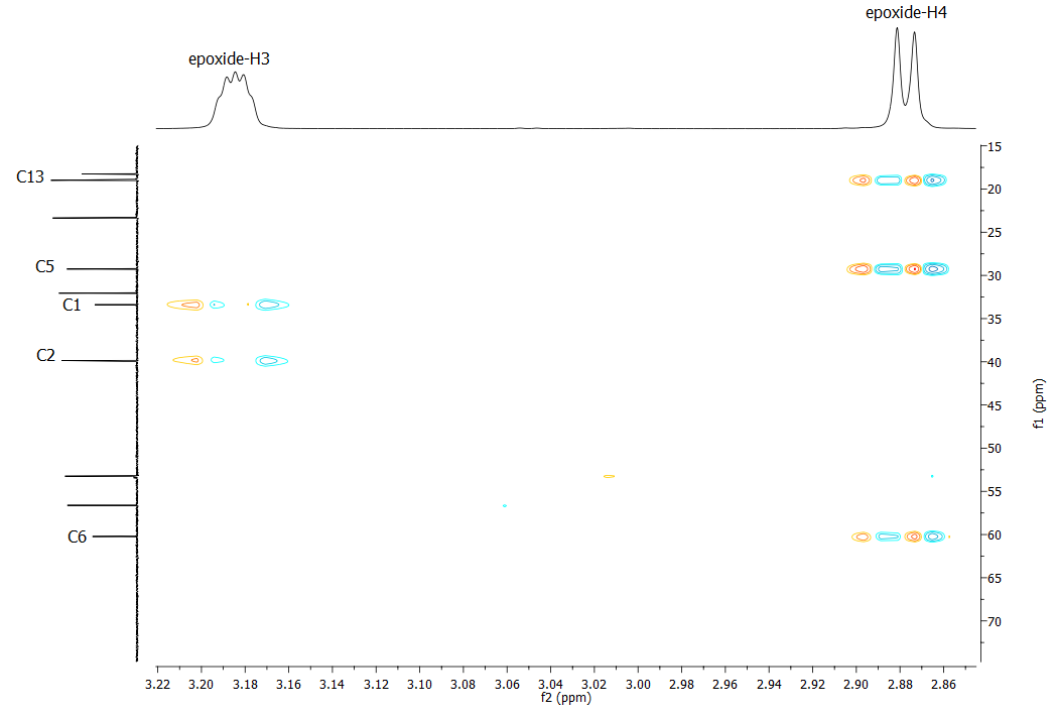

(a)

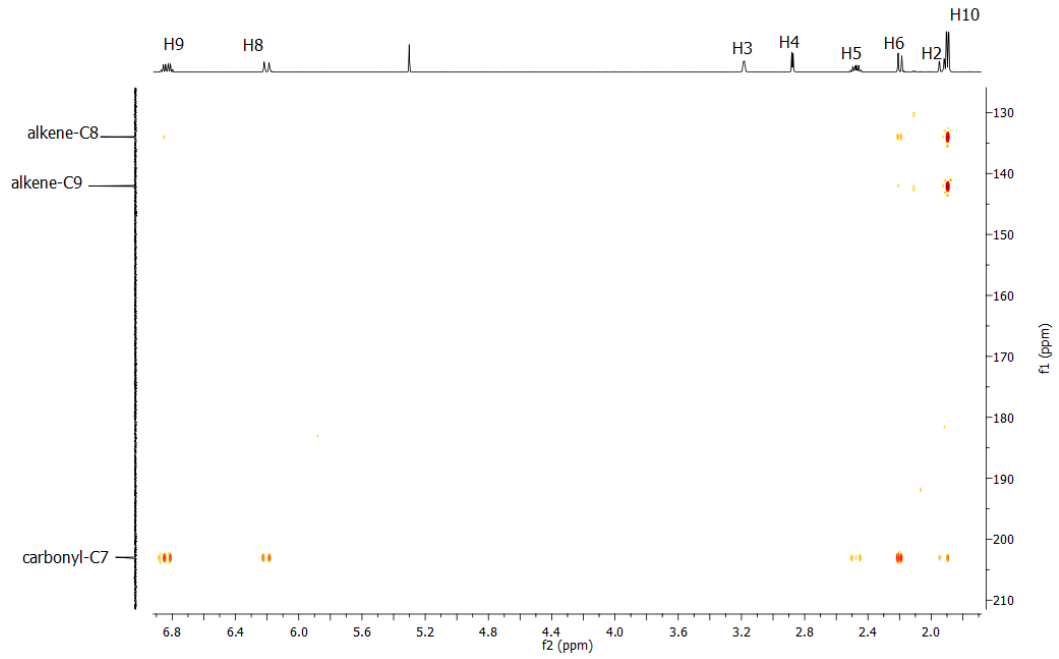

(b)

Figure 84: ^{1}H-^{13}C HMBC NMR data of (a) epoxide and (b) alkene signals for 3,4-epoxy-δ-damascone. Epoxide signals show correlation to ring carbon signals (C1, C2, C5, C6) while the alkene signals show correlation with the carbonyl (C7) and methyl hydrogens (H10) on the butenone side chain. Full data in Appendix C22.

ROESY NMR studies of the purified metabolite showed no through-space correlation between the epoxide hydrogen signals (H3 and H4) and the butenone side chain. Therefore, the epoxidation face cannot be definitively confirmed through the ROESY analysis and further study would be needed to confirm the stereochemistry of the epoxide.

It is also worth noting that the selectivity of CYP101B1 for δ-damascone epoxidation is in agreement with the hydroxylation of β-ionone at C3 or C4 and α-ionone at C3 by this enzyme. The formation of the epoxide was not surprising as P450 alkene epoxidation is an energetically feasible reaction. However, we note that epoxidation in α-ionone is not observed after oxidation by CYP101B1 in any detectable quantity.

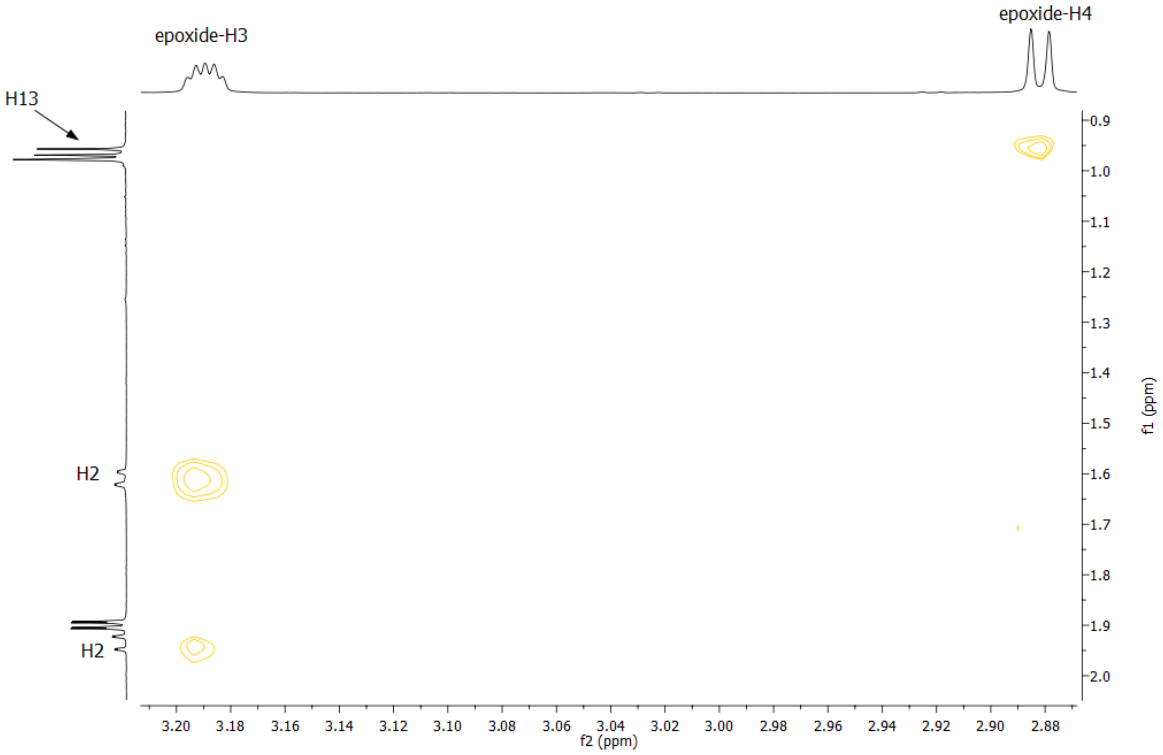

Figure 85: ROESY NMR data of epoxide signals for 3,4-epoxy-δ-damascone.

The whole cell CYP101B1 turnover of α-damascone also generated high levels of product (Figure 86). The $P450_{BM3}$-GVQ variant did not show any product formation with α-damascone.

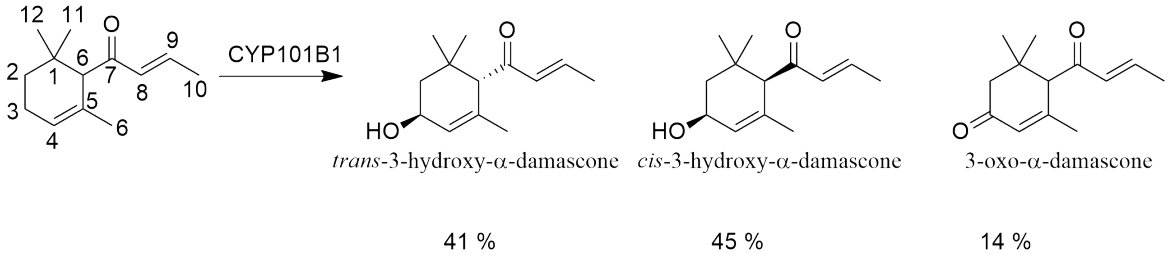

(a)

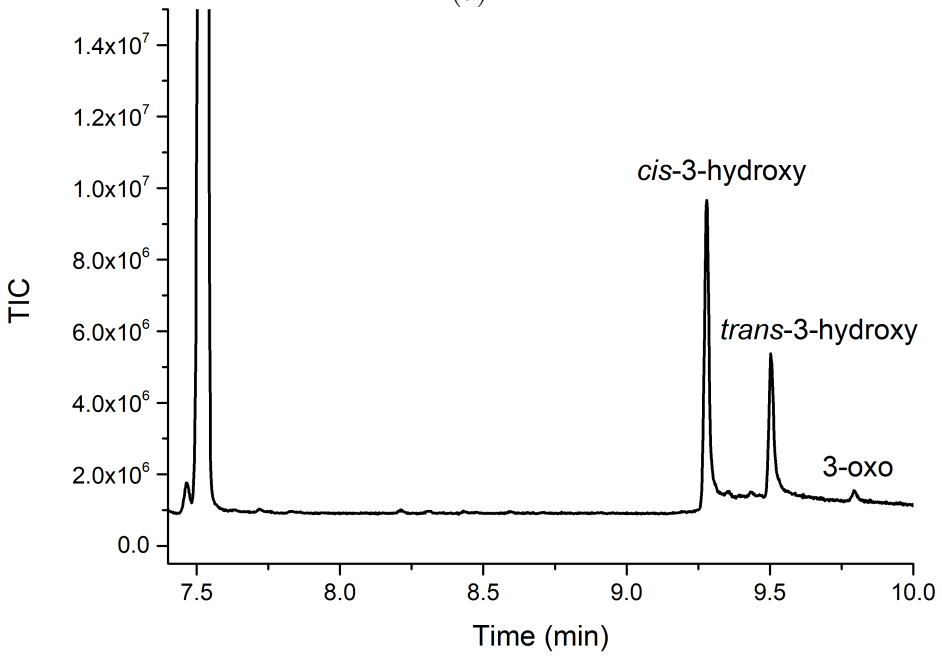

(b)

Figure 86: (a) The oxidation of α-damascone by CYP101B1. (b) GC-MS analysis of the whole-cell turnover of CYP101B1 with α-damascone. Metabolites produced include *cis*-3-hydroxy-α-damascone (t_R = 9.3 min), *trans*-3-hydroxy-α-damascone (t_R = 9.55 min), and 3-oxo-α-damascone (t_R = 9.80 min).

Products were purified using preparative HPLC from a larger scale turnover of CYP101B1 and were characterised via NMR to be *cis*-3-hydroxy-α-damascone (12 mg isolated yield, Appendix C23), *trans*-3-hydroxy-α-damascone (14 mg isolated yield, Appendix C26) and 3-oxo-α-damascone (2 mg isolated yield, Appendix C29). The NMR data for all 3 products matched data in the literature (Appendix C23, C26, C29).[169]

ROESY NMR analysis further confirmed the relative orientation of the two diastereomers via through-space correlations between the H6 and H3 signals. For the *cis* isomer, the H6 and H3 signal were correlated to the same H12 ring methyl group, indicating they were *cis* to each other (Figure 87). The *trans* isomer instead had the H3

and H6 signals correlated with H11 and H12 signals respectively (Figure 88), therefore these two hydrogens are *trans* to each other on the ring.

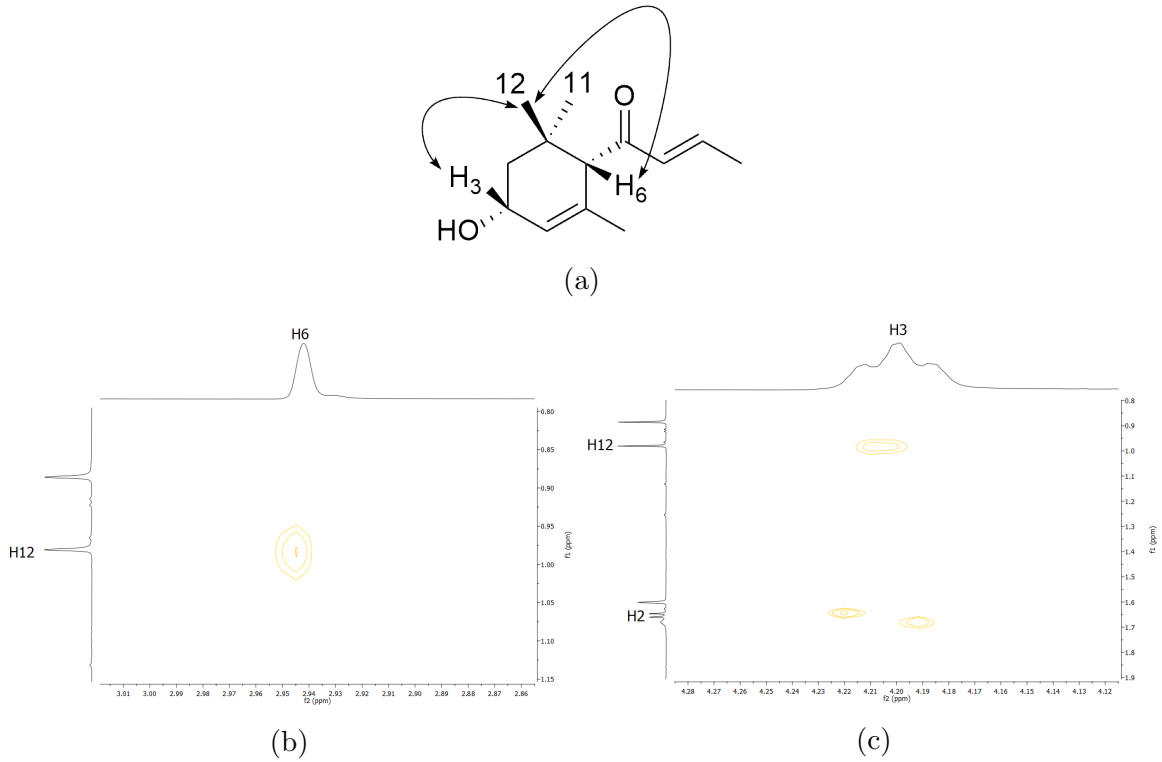

Figure 87: ROESY NMR data for (a) *cis*-3-hydroxy-α-damascone that shows correlations of the (b) H6 and (c) H3 hydrogen signal. Both hydrogen signals show a correlation to the same H12 methyl signal.

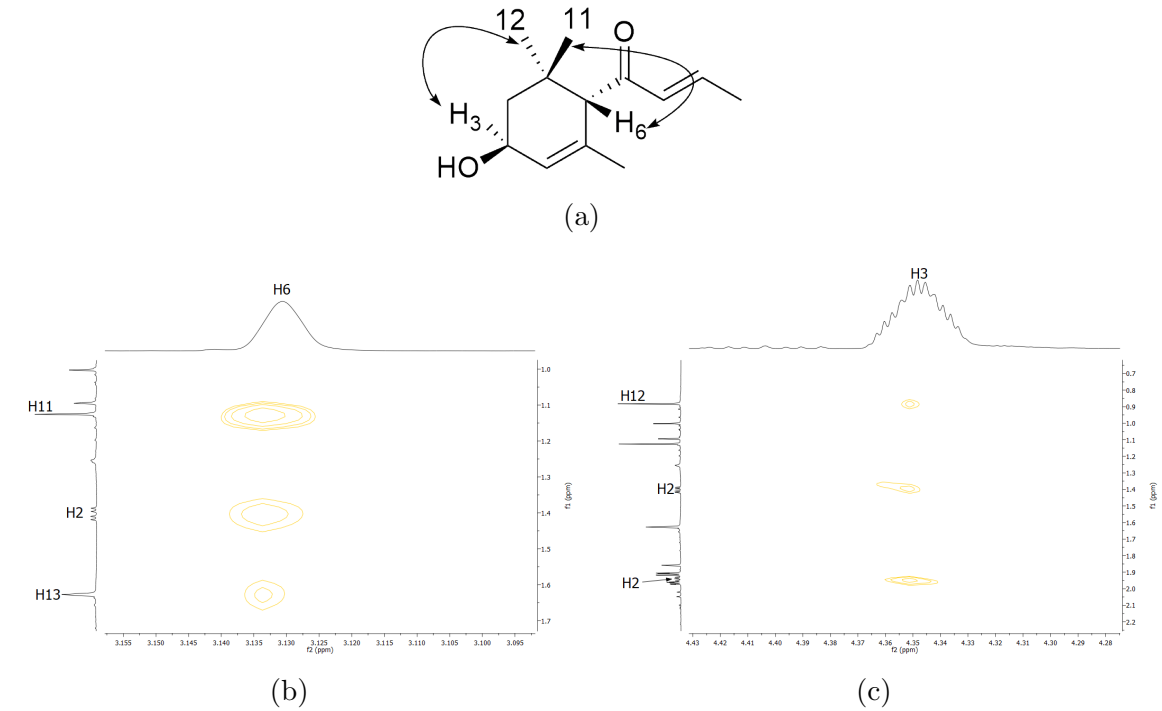

Figure 88: ROESY NMR data for (a) *trans*-3-hydroxy-α-damascone that shows correlations of the (b) H6 and (c) H3 hydrogen signal. H6 is correlated through-space to the H11 methyl hydrogens while H3 is correlated to the H12 signals instead.

The regioselectivity of CYP101B1 for α-damascone was exclusively at the C3 position. This was in agreement with the oxidation of α-ionone by both CYP101B1 and CYP101C1, which also form the *cis*-, *trans*-3-hydroxy and 3-*oxo* derivatives.[61,62] In contrast to δ-damascone, no epoxidation products were formed from the oxidation of α-damascone by CYP101B1.

5.2.1.2 Whole-Cell Turnovers of Cuminyl Acetate and Verdyl Acetate

Cuminyl acetate and verdyl acetate contain acetate groups attached to cyclic structures. Functionalisation of monoterpenes with acetate groups have enabled CYP101B1 to oxidise monoterpenoid derivatives more efficiently.[101] With cuminyl acetate, we wished to assess whether the acetate group can allow efficient oxidation of aromatic compounds by P450 enzymes. CYP101B1 did not show any product formation with cuminyl acetate which was in agreement with the *in vitro* turnover. $P450_{BM3}$-GVQ gave two products with cuminyl acetate (Figure 89).

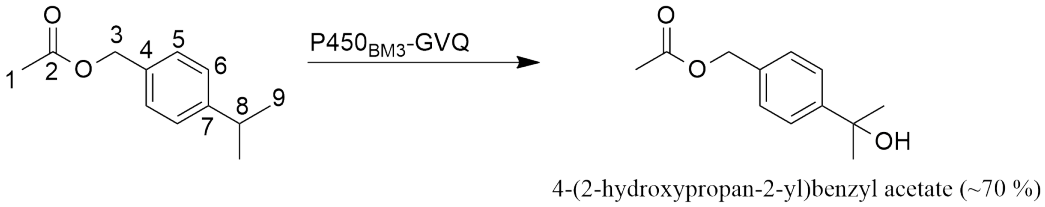

4-(2-hydroxypropan-2-yl)benzyl acetate (~70 %)

(a)

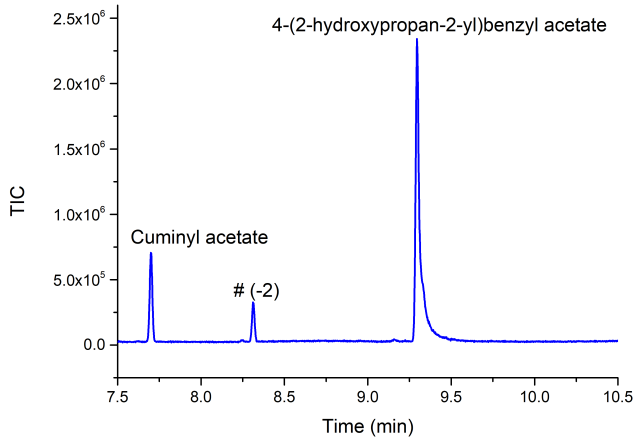

(b)

Figure 89: (a) Oxidation of cuminyl acetate by $P450_{BM3}$-GVQ. (b) GC-MS analysis of the $P450_{BM3}$-GVQ turnover with cuminyl acetate. Major metabolite formed was 4-(2-hydroxypropan-2-yl)benzyl acetate (t_R = 9.3 min). Possible desaturation product with the cuminyl acetate turnover is labelled as # at t_R = 8.30 min (m/z = 190, $\Delta m/z$ = -2).

A larger scale turnover of $P450_{BM3}$-GVQ was carried out with cuminyl acetate and the major product formed was extracted. The product was purified by preparative HPLC

and identified by NMR to be 4-(2-hydroxypropan-2-yl)benzyl acetate (10 mg isolated yield, Appendix C17). The oxidation site was confirmed by the loss of the septuplet signal in the alkyl region within the ^{1}H NMR spectrum (Figure 90). Therefore, the C8 benzylic hydrogen was abstracted by the P450 and this was the site of hydroxylation. The NMR spectrum also indicated that symmetry of the initial substrate was preserved within the oxidation product.

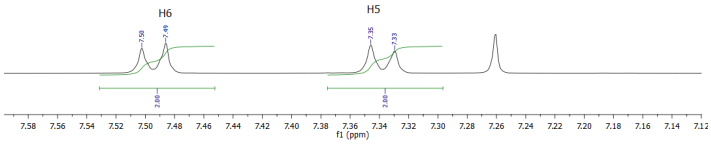

(a)

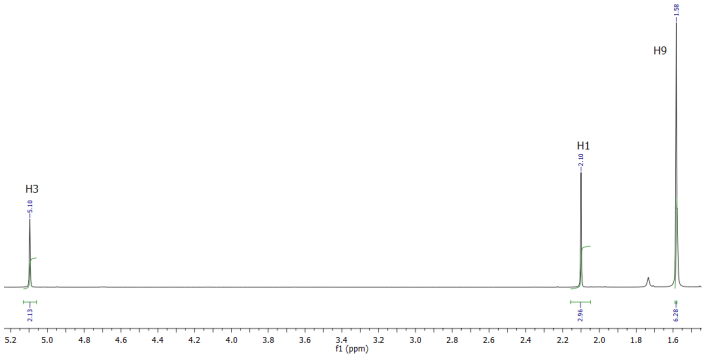

(b)

Figure 90: ^{1}H NMR data of cuminyl acetate that shows the (a) aromatic region and (b) alkyl/benzylic region. Symmetry is present on the molecule and the absence of a septuplet signal indicates the tertiary isopropyl hydrogen on cuminyl acetate was the site of hydroxylation.

A secondary metabolite in the whole-cell turnover (# in Figure 89) that was also present within the *in vitro* turnover was not isolated. This was likely a desaturation product as identified via its mass spectrum (Appendix C.7), whereby compared to the substrate (m/z = 192), the desaturation showed $\Delta m/z$ = -2. The hydroxylation of cuminyl acetate at the isopropyl group by $P450_{BM3}$-GVQ supports the formation of a desaturated metabolite and it is likely that the alkene double bond would be located between the C8 and C9 carbon on the substrate (Figure 91). A similar desaturation activity was observed with the oxidation of 1,4-cineole by $P450_{cam}$ mutants (Chapter 4.2.3.2). The mechanism for desaturation is discussed in Figure 96.

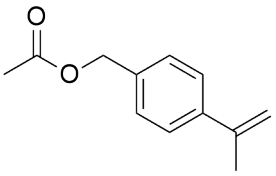

4-(prop-1-en-2-yl)benzyl acetate

Figure 91: Structure of the possible desaturation product formed by CYP101B1 with cuminyl acetate.

Verdyl acetate is tricyclic compound with a structure similar to fenchyl acetate (Chapter 4.2.1) but possesses an additional 5-membered ring which introduces additional steric bulk. CYP101B1 showed metabolite formation *in vitro* with this substrate, it did not produce significant levels of the metabolite with the whole-cell turnovers. The turnover with $P450_{BM3}$-GVQ displayed product formation of a single major product (t_R = 9.8 min) alongside two other minor metabolites (Figure 92). The three metabolites formed were oxidation products based on their MS spectra (Appendix C.8).

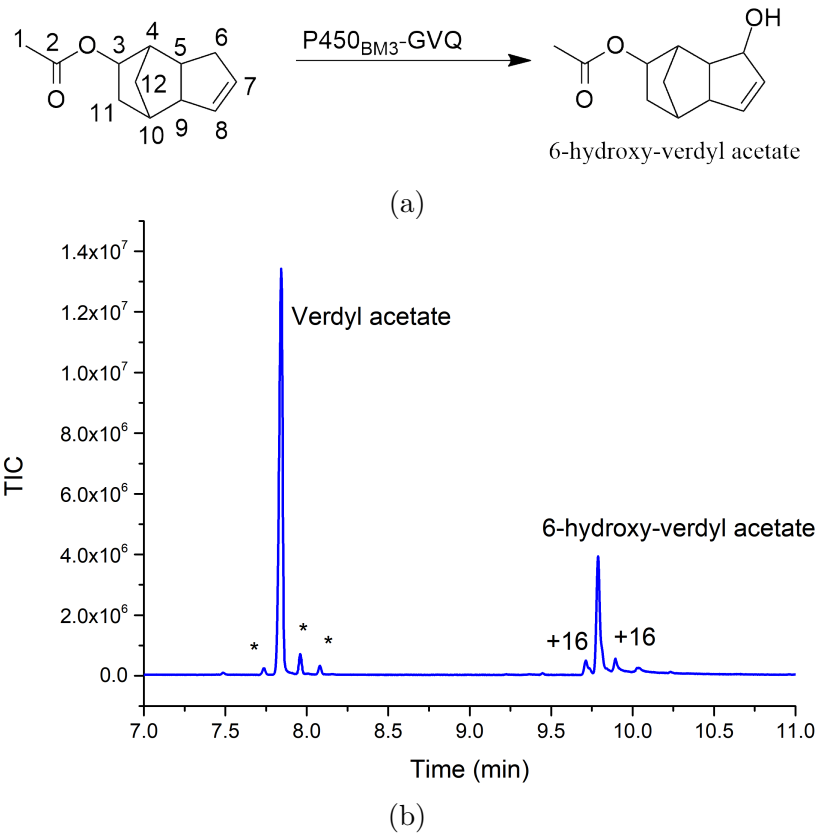

Figure 92: (a) Oxidation of verdyl acetate by $P450_{BM3}$-GVQ. (b) GC-MS analysis of $P450_{BM3}$-GVQ turnover with verdyl acetate. Major metabolite formed was 6-hydroxy-verdyl acetate (t_R = 9.8 min). Minor metabolites with $\Delta m/z$ = +16 at t_R = 9.75 and 9.85 min.

Extraction and purification of the major product with preparative HPLC from a large scale turnover of the GVQ variant with verdyl acetate was successful. The product was characterised via NMR (4 mg isolated yield, Appendix C32). The hydroxylation site was identified from an additional high chemical shift signal (δ_H = 4.34 ppm) with an integration of 1H (Figure 93a). This suggests that a CH_2 group of the substrate was oxidised. There are therefore only three potential oxidation sites (C6, C11, C12) (Figure 92a).

HMBC NMR analysis of the product showed a correlation between the two remaining CH_2 groups (Figure 93b). It is most likely that oxidation at the C6 site results in the CH_2 hydrogens at C11 correlating with the C12 carbon as seen in the HMBC spectrum (Figure 93b). The oxidation at the C6 would be expected as the carbonyl of the ester group would anchor the substrate within the active site and allow it to oxidise regions remote from the acetate group.

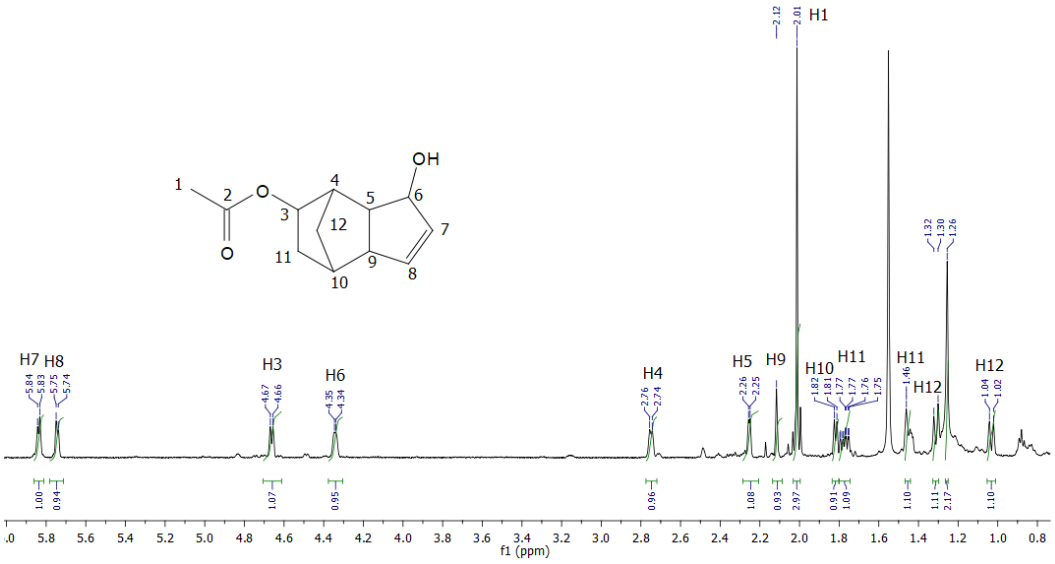

(a)

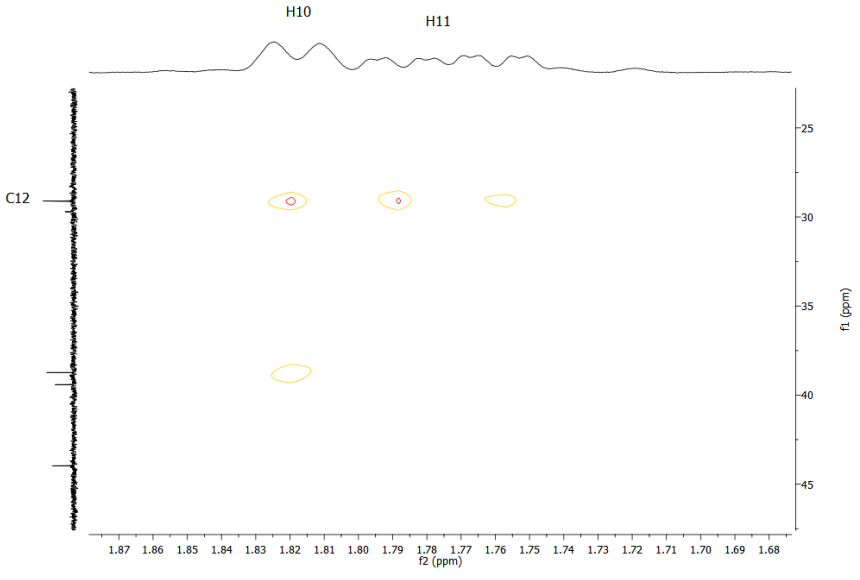

(b)

Figure 93: (a) Expansion of the ^{1}H NMR data for 6-hydroxy verdyl acetate showing the alkene and C-**H**-O signals. (b) HMBC NMR data of the CH_2 signals for 6-hydroxy verdyl acetate, whereby a correlation can be seen between the CH_2 hydrogen of the C11 and the C12 carbon.

To further assess which of the CH_2 groups was hydroxylated, the ^1H NMR spectrum of the initial verdyl acetate starting material was measured (Figure 94a) and the CH_2 groups were identified via ^1H - ^{13}C HSQC analysis (Figure 94b).

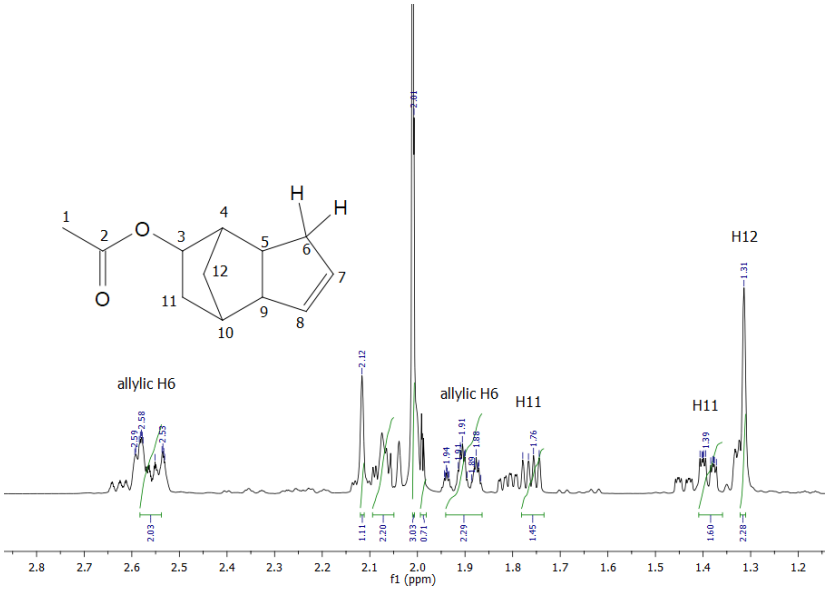

(a)

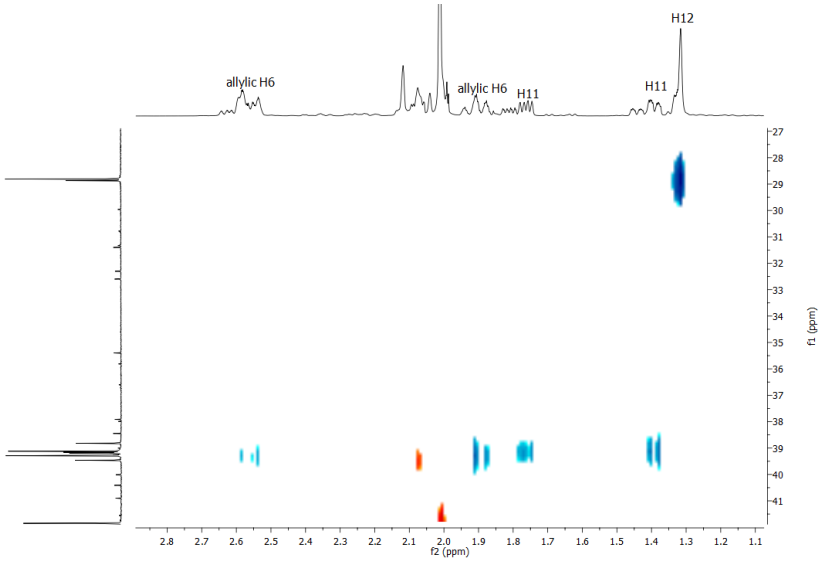

(b)

Figure 94: (a) Expansion of the ^1H NMR data of verdyl acetate that shows the CH_2 groups (C6, C11, C12). (b) ^1H - ^{13}C HSQC NMR data showing the CH_2 groups of verdyl acetate. Blue cross-peaks are the CH_2 groups. Note there is a contamination in the supplied sample which complicates the analyses.

The allylic CH_2 signals for the substrate were identified at $\delta_H = 2.58$ ppm and 1.91 ppm and equivalent signals were not present within the ^1H NMR spectrum of the hydroxy product (Figure 93a). The other two CH_2 signals were at similar chemical shifts. This would indicate that the allylic H6 hydrogens were oxidised by $P450_{BM3}$-GVQ to form 6-hydroxy verdyl acetate.

5.3 Discussion

The screening of a selection of fragrance compounds with the enzymes CYP101B1 and the GVQ variant of $P450_{BM3}$ generated a number of metabolites in good yield. These enzymes have all shown the ability to selectively oxidise fragrance and flavouring compounds.[61,62,79,101] In particular, CYP101B1 can oxidise norisoprenoids selectively and it is unsurprising that this enzyme has oxidation activity and binding affinity with norisoprenoid derivatives such as α-damascone, δ-damascone, dynascone and α-*iso*-methylionone (Table 13). The GVQ variant was able to oxidise cuminyl acetate, which CYP101B1 showed no oxidation activity for.

CYP101B1 exhibited contrasting oxidation activity with α-*iso*-methylionone and dynascone. α-*iso*-Methylionone gave higher product formation *in vitro* compared to the dynascone turnovers. This is likely caused by the higher degree of structural similarity between α-*iso*-methylionone and α-ionone, whereby the ring substituents are identical between the two but the butenone group has been replaced with a longer pentenone in α-*iso*-methylionone. Dynasone showed lower product formation and induced lower spin-state shifts with CYP101B1 likely because its structure was more dissimilar to the ionones by possessing a pentenone side chain with a terminal alkene and lacks an additional ring methyl group.

Ethyl safranate, dihydroflorate and verdyl acetate were among the formate/acetate ester functionalised compounds tested that had moderate to fast NADH oxidation by CYP101B1, though only ethyl safranate exhibited high coupling efficiency and therefore product formation. Ethyl safranate possesses a similar pattern of ring substituents to the ionones but has an additional ring alkene. Its formate ester side chain could mimic the butenone group of the norisoprenoids. These two factors are likely to contribute to its increased activity and greater spin-state shift. The other formate ester tested, dihydroflorate, had poor coupling efficiency despite its fast NADH oxidation rate with CYP101B1. This is most likely due to competing uncoupling pathways. Uncoupling events occur when the electron or proton transfer step occurs too slowly in the P450 catalytic cycle (Chapter 1.2, Figure 1).[13]

$P450_{BM3}$-GVQ displayed moderate product formation rates and coupling efficiencies with cuminyl and verdyl acetate. The whole-cell turnovers of these two substrates with this mutant variant generated product in good yield that would indicate that the oxidation of these substrates was feasible. When compared to the $P450_{BM3}$ variant, CYP101B1 had a higher coupling efficiency with its *in vitro* turnover of verdyl acetate but showed no product formation in the whole-cell turnover. Cuminyl acetate also

displayed no product formation with CYP101B1. This inferred that mere functionalisation of aromatic compounds with a butenone mimicking group is not a viable method to increase the affinity of these compounds to CYP101B1. There are likely additional secondary interactions between the norisoprenoid ring structure and the CYP101B1 active site that play a role in substrate binding. The greater flexibility of the ionone ring and its smaller size when compared to cuminyl and verdyl acetate respectively may be important for its binding to CYP101B1.

The oxidation of α-damascone by CYP101B1 was regioselective for the C3 position forming the *cis* and *trans*-hydroxy metabolites and the further oxidation keto product. This product distribution was similar to that of α-ionone oxidation by CYP101B1. A similar trend in the product distribution was also observed with the oxidation of β-ionone and β-damascone by the same enzyme.[61] The formation of a keto product is indicative of further oxidation of the hydroxy metabolite and was also present in the reaction with α-ionone. It is believed that further oxidation occurs when the amount of initial substrate is limited compared to the hydroxylated products.[61]

The preference for the C3 position despite the changing positions of the ketone and alkene moiety on the butenone side chain suggests their positions has little control on the regioselectivity of CYP101B1. In contrast, the oxidation of β-damascone by CYP260B1 from *Sorangium cellulosum* was exclusively at the C4 site but the regioselectivity was altered slightly with β-ionone, where the C5/C6 alkene underwent epoxidation alongside C4 hydroxylation. This suggests other P450 enzymes are affected by the positions of the alkene and ketone on the butenone side chain.[160] Crystal structure data of the CYP101B1 enzyme with substrate bound could confirm these hypotheses.

The major diastereomer formed by the oxidation of α-ionone by CYP101B1 was the *trans* isomer,[61] while α-damascone oxidation by this enzyme favoured the *cis* isomer instead (Figure 86b). Free-energy related calculations on the stereoselective hydroxylation of α-ionone with $P450_{BM3}$ mutants were carried out by Beer and co-workers to determine the thermodynamic stability of products bound to the enzyme upon oxidation.[170] It was found that *trans*-isomers have the most favourable binding free energies and thus the more favoured isomer. The formation of the *cis*-isomer by CYP101B1 when oxidising α-damascone was nearly 3-fold higher than the *trans* isomer. The changing diastereomer preference between α-ionone and α-damascone oxidation by CYP101 enzymes suggests the positions of the butenone substituents have an effect on the diastereoselectivity of the enzyme. This may arise from the enzyme having a different preference for the enantiomers of each substrate.

Preliminary studies of CYP101B1 mutants, H85F and H85G with α-damascone showed a change in diastereoselectivity from the WT-enzyme by preferentially forming the *trans*-isomer instead, suggesting changing the H85 residue alters the diastereoselectivity (Figure 95).

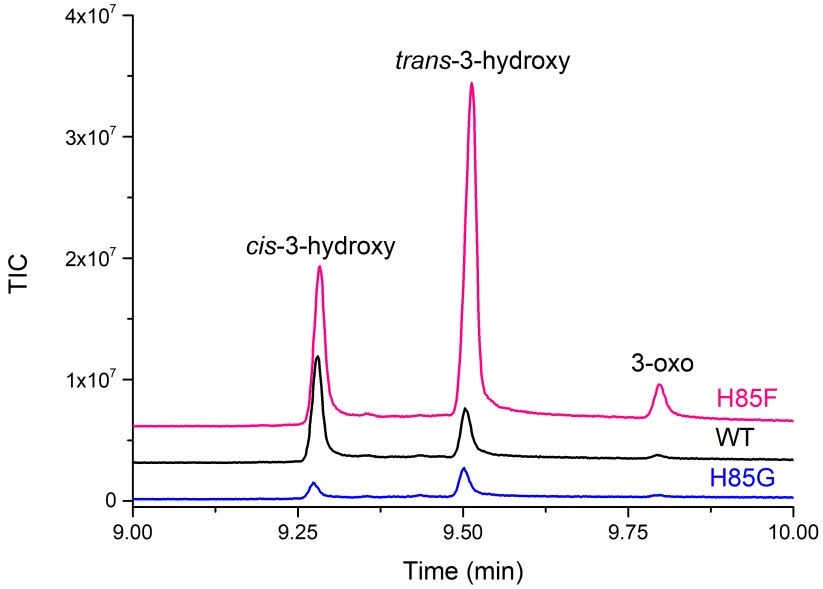

Figure 95: GC-MS analysis of whole-cell turnovers of CYP101B1 mutants with α-damascone. Turnovers include WT-CYP101B1 (black), H85F (pink) and H85G (blue). Metabolites produced include *cis*-3-hydroxy-α-damascone (t_R = 9.3 min), *trans*-3-hydroxy-α-damascone (t_R = 9.4 min), and 3-oxo-α-damascone (t_R = 9.80 min).

The position of the alkene within the norisoprenoid ring plays an important role in determining the type of oxidation reaction carried out by CYP101B1. α-Damascone with its ring alkene at the C4/C5 position formed products that arose exclusively from allylic C3 hydroxylation activity and also small quantities of the C3 keto-product. Biotransformation of α-damascone using bacterial strains of *Botrytis cinerea* formed the same products as CYP101B1, though a slew of other oxy-metabolites were also generated.[169]

δ-Damascone underwent epoxidation at its C3/C4 alkene and has been previously oxidised by CYP260B1 and CYP267B1 from *S. cellulosum* to form 2-hydroxy-δ-damascone.[160] The δ-damascone epoxide formed is therefore unique to CYP101B1. This epoxide would be an ideal intermediate for further chemical or enzymatic ring-opening chemistry that could lead to new flavouring and fragrance compounds with unique sensory properties. For example, epoxidation of the sesquiterpene, ledene and subsequent ring-opening gave ledene derivatives that include an ether, an enol and a diol.[171] These epoxide derived compounds have woody and floral scents.[171] Norisoprenoids that have been hydroxylated at the C3 position have also exhibited allelopathic properties that have garnered interest for possible antifungal and antimicrobial

applications.[172]

Cuminyl and verdyl acetate are both fragrance compounds with woody and floral notes.[173] There does not appear to be any previous biotransformation studies carried out with either of these substrates. The C-H bonds that were oxidised with cuminyl acetate and verdyl acetate were benzylic and allylic C-H bonds respectively.

Cuminyl acetate also displayed the formation of a desaturated product. This is consistent with the oxidation of the tertiary C-H bond within the isopropyl group of cuminyl acetate, whereby an alkene has likely formed on the isopropyl group instead.[174] The GVQ variant produced the major hydroxy metabolite in high yield indicating it was a viable enzyme for this biocatalytic reaction. This variant possesses mutations that are designed to introduce more space and hydrophobicity to the active site of $P450_{BM3}$.

The first step of the desaturation reaction catalysed by P450s is identical to the hydroxylation reaction, whereby hydrogen abstraction first occurs to give the carbon radical.[174] Instead of proceeding with a radical rebound for hydroxylation, desaturation can occur either by (a) transfer of electron from the carbon radical to the iron centre of Cpd I to generate a carbocation and immediate transfer of a proton from said carbocation to the ferryl oxygen or (b) an additional hydrogen abstraction reaction at the carbon radical site to generate the desaturated product (Figure 96).[174,175]

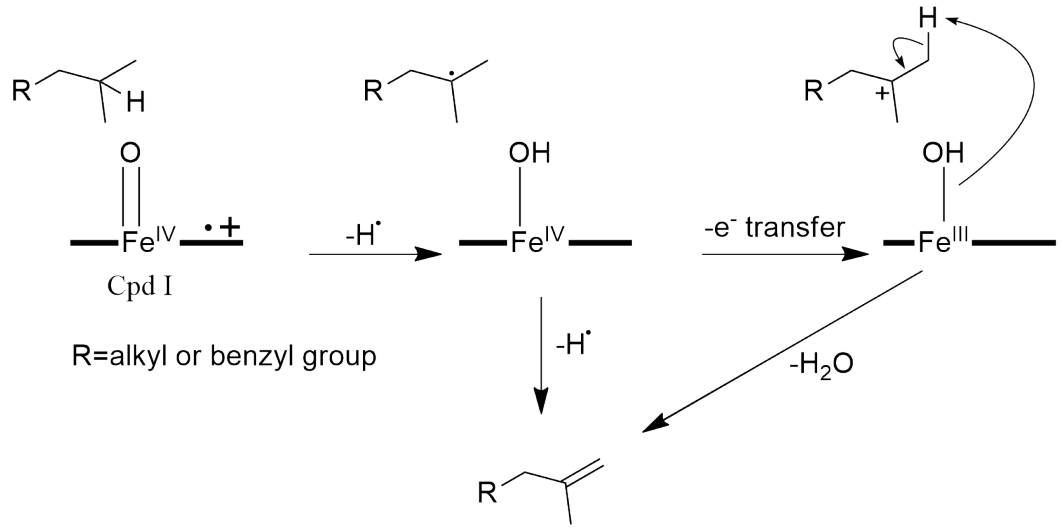

Figure 96: Two possible pathways of how the desaturation reaction can be catalysed by P450s.

The amount of hydroxy product formed was more than 2-fold higher than the desaturated product in the whole-cell turnover of $P450_{BM3}$-GVQ (Figure 89). DFT and QM/MM studies have found that the desaturation pathway has a higher energy barrier that allows the hydroxylation reaction to proceed more favourably.[175] The $P450_{BM3}$ variant tested here may provide a suitable foundation for further mutagenesis studies to

design P450 enzymes that will favour desaturation reactions and it has been suggested that mutations introduced to the binding pocket could alter the binding orientation to suppress the radical rebound pathway, which leads to hydroxylation.[175] It is also possible that the desaturation product could arise from the elimination of water without the involvement of the P450 enzyme.

The P450 catalysed oxidation reactions of the fragrance compounds screened were largely regioselective and different types of reactions were observed including hydroxylations, epoxidations and desaturations. A number of the products identified were also new and expands the "toolbox" towards forming oxidised fragrance compounds with new sensory properties. The engineering of CYP101B1, has not been explored in detail, yet the mutation of a single residue has revealed changes in the diastereoselectivity of α-damascone oxidation. The CYP101B1 mutants may provide useful diastereoselective biocatalytic pathways. The ability to form the desired stereoisomer of a fragrance compound would be useful commercially as a way to tailor perfume formulations with specific olfactory properties.[125] Further studies of these P450 enzymes would be needed to broaden the substrate range and enhance the activity and selectivity of these enzymes. In addition, future work could also involve establishing whether the desaturation products were formed solely by P450 activity.

6 Conclusions and Future Directions

CYP101B1 shows high affinity and oxidation activity for norisoprenoids such as β- and α-ionone but was poor in oxidising hydrophobic substrates. Site-saturation mutagenesis of the CYP101B1 H85 residue was carried out to increase its affinity towards hydrophobic substrates. A total of eleven mutants were made and cloned into pET22 and pRSFDUET vectors for *in vitro* and *in vivo* studies, respectively. Studies were carried out with a selection of substrates that include norisoprenoids, terpenoids and hydrophobic substrates of varying sizes. Whole-cell screening with the CYP101B1 mutants showed altered product selectivity or exhibited small increases in product formation with the substrates tested. The oxidation of hydrophobic substrates by any of the new variants were not significantly improved over the WT enzyme or the previously characterised H85F variant. *In vitro* studies of the H85A and H85G mutants found that it had lower binding affinity and oxidation activity with phenylcyclohexane when compared to the WT enzyme. A range of spin-state shifts measured for biphenyl and naphthalene derivatives for these two variants were consistently lower than 50 % HS. This is indicative of poor substrate to active site complementarity. It is evident that simply changing this histidine residue does not significantly increase the affinity of CYP101B1 towards larger hydrophobic substrates. New mutagenesis approaches could be undertaken with CYP101B1 by altering other active site residues to increase its activity towards non-natural substrates, such as residues Q234 and I237. However, key information regarding how the active site residues interacts with the bound substrate would be useful in rationally designing mutants for biocatalysis. As such, crystal structure data of CYP101B1 could be crucial for further mutagenesis studies with this enzyme.

Rationally designed mutants of $P450_{cam}$ developed for terpene oxidation were screened whole-cell for selective oxidation with fenchone, fenchyl acetate, isophorone, 1,8- and 1,4-cineole. Fenchone and fenchyl acetate oxidation by WT-$P450_{cam}$ and two of its mutants generated hydroxylated products at the C5, C6 and C7 position, with a preference for *exo* hydroxylation. This suggests the carbonyl and acetate within fenchone and fenchyl acetate anchored these two substrates in the active site to favour oxidation on the C5-C6-C7 face. Isophorone was selectively oxidised by mutants WFL (F87W-Y96F-V247L) and WFAL (F87W-Y96F-L244A-V247L) to form two products. The products identified were 4-hydroxyisophorone, as the major metabolite, and 7-hydroxyisophorone as the minor. The C4 position was the preferred hydroxylation site ($>$ 90 %) and the (*R*)-enantiomer was predominantly formed by the $P450_{cam}$ mutants (99 % e.e). 4-Hydroxyisophorone has considerable commercial value as a flavouring

agent and selective biocatalytic processes to produce this compound would be highly desirable.

A number of the $P450_{cam}$ mutants screened altered the regioselectivity of 1,8- and 1,4-cineole oxidations. The oxidation of 1,8-cineole by WT-$P450_{cam}$ formed 6-α-, 5-α- and 5-β-hydroxy-1,8-cineole. Two $P450_{cam}$ mutants altered the selectivity to form either the 5-α- (WFAL) and 6-α- (VFA) hydroxy products in significant excess (> 90 %). 1,4-Cineole oxidation by WT-$P450_{cam}$ unselectively formed 8-hydroxy- and 3α-hydroxy-1,4-cineole in low yield. The 3α-hydroxy product was selectively formed by mutants WFA and WFAL (> 90 %). The 8-hydroxy metabolite was preferentially produced with mutant LF (F87L-Y96F, > 85 %). This metabolite was accompanied by the formation of higher amounts of a desaturated product, whereby the alkene is likely located between the C8 and C9 positions of the isopropyl group. This was consistent with hydroxylation occurring on the same isopropyl group. The oxidation of both cineoles by the $P450_{cam}$ mutants was also enantioselective when this could be assessed. The screening of a small library of $P450_{cam}$ variants has therefore allowed for an impressive range of selective oxidations at different C-H bonds with the two cineoles. This could enable the production of specific cineole hydroxy metabolites that could serve as chiral auxiliaries. This library of enzymes would be a good starting point to develop mutants for other unique C-H bond hydroxylations.

Mutants of $P450_{BM3}$ have also been identified that exhibit selective oxidation towards isophorone and the two cineoles. Whole-cell oxidation of these three substrates were carried out comparing both $P450_{cam}$ and $P450_{BM3}$ enzyme systems to determine how the product formation for both systems varied. Isophorone oxidation gave higher product formation with the $P450_{cam}$ systems. However, the $P450_{BM3}$ systems gave higher metabolite yields for the cineole oxidations. Despite the poorer yield of the $P450_{cam}$ mutants with cineole oxidations, the WT-$P450_{cam}$ whole-cell system converted a majority of the 1,8-cineole added into product. These comparative experiments demonstrated that these P450 whole-cell systems are capable of oxidising the three substrates in higher yield. Scale-up of these systems could be carried out using fermentor systems with higher cell yields and better control of oxygen, pH and substrate levels to generate metabolites on a kilogram scale and may be the first step to using these P450 mutants to produce useful hydroxy-metabolites in good yield.

A selection of fragrance compounds with different molecular architectures were screened with CYP101B1 and a $P450_{BM3}$ mutant, GVQ (A74G-F87V-L188Q). Norisoprenoid compounds such as δ-damascone, α-damascone and α-*iso*-methylionone and an acetate ester, ethyl safranate, induced high spin-state shifts with CYP101B1. The product

formation rates for these four substrates with CYP101B1 were also the fastest and the damascones gave the highest coupling efficiency and levels of product formation. $P450_{BM3}$-GVQ showed product formation with cuminyl acetate and verdyl acetate with moderate product formation and coupling efficiency.

The oxidation of α-damascone by CYP101B1 occurred exclusively at the C3 position to produce diastereomeric metabolites similar to α-ionone oxidation by the same enzyme. This implied that the butenone carbonyl and alkene positions do not influence the regioselectivity of oxidation. The conserved regioselectivity of CYP101B1 for ionones and damascones, even when the butenone side chain is altered is an interesting insight to how this enzyme interacts with different norisoprenoids. WT CYP101B1 preferentially forms the *cis* diastereomer when oxidising α-damascone. Preliminary studies with the mutants of CYP101B1 have shown that the H85F and H85G variants preferentially formed the *trans* isomer rather than the *cis*. In principle, mutagenesis could be used to control the diastereoselectivity of CYP101B1 oxidation. δ-Damascone was epoxidised by CYP101B1 at the C3-C4 position which was in agreement with the regioselectivity of this enzyme with α-damascone and β-damascone. This epoxide is a potential intermediate for ring-opening reactions to generate new norisoprenoid derivatives. The mutant variant of $P450_{BM3}$, GVQ, showed selective oxidations with both cuminyl and verdyl acetate. The oxidation of these two substrates occurred at C-H bonds remote from the acetate group. The oxidation of cuminyl acetate by $P450_{BM3}$-GVQ produced a desaturated metabolite that agreed with the hydroxylation of the isopropyl group within this substrate. Desaturated metabolites were also formed from 1,4-cineole oxidation by $P450_{cam}$ and $P450_{BM3}$ mutants. The mutants tested here provide a suitable starting point for future mutagenesis studies to generate new P450 variants to catalyse and investigate these desaturation reactions.

Overall, the results of this work show that different P450s can be used to generate selective oxidations with a range of substrates. The mutagenesis approach was not successful in increasing the affinity of hydrophobic substrates towards CYP101B1, though the H85F mutant did appear to change the diastereoselectivity of the enzyme when oxidising α-damascone. A number of $P450_{cam}$ and $P450_{BM3}$ mutants were also able to oxidise terpenoid compounds not only with higher yield but also with good selectivity towards different C-H bonds on the substrates tested. Desaturation reactions were also observed with the mutants studied. These results could facilitate larger scale biocatalytic processes to produce specific metabolites. Future work could involve using the enzymes to develop more selective oxidations using further mutagenesis approaches. Additional optimisation of the whole-cell systems could also be carried out to further scale-up the biocatalytic reactions studied here.

References

[1] Garfinkel, D. Studies on pig liver microsomes. I. Enzymic and pigment composition of different microsomal fractions. *Arch. Biochem. Biophys.* **1958**, *77*, 493 – 509.

[2] Klingenberg, M. Pigments of rat liver microsomes. *Arch. Biochem. Biophys.* **1958**, *75*, 376 – 386.

[3] Nelson, D. R. Cytochrome P450 Diversity In The Tree Of Life. *Biochim. Biophys. Acta, Proteins Proteomics* **2018**, *1866*, 141–154.

[4] Poulos, T. L. Heme Enzyme Structure and Function. *Chem. Rev.* **2014**, *114*, 3919–3962.

[5] Nelson, D. R.; Kamataki, T.; Waxman, D. J.; Guengerich, F. P.; Estabrook, R. D.; Feyereisen, R.; Gonzalez, F. J.; Minor J., C.; Gunsalus, I. C.; Gotoh, O.; Okuda, K.; Nebert, D. W. The P450 Superfamily: Update on New Sequences, Gene Mapping, Accession Numbers, Early Trivial Names of Enzymes, and Nomenclature. *DNA Cell Biol.* **1993**, *12*, 1–51.

[6] Katagiri, M.; Ganguli, B. N.; Gunsalus, I. C. A Soluble Cytochrome P-450 Functional in Methylene Hydroxylation. *J. Biol. Chem.* **1968**, *243*, 3543–3546.

[7] Omura, T. Forty Years of Cytochrome P450. *Biochem. Biophys. Res. Commun.* **1999**, *266*, 690 – 698.

[8] Rittle, J.; Green, M. T. Cytochrome P450 Compound I: Capture, Characterization, and C-H Bond Activation Kinetics. *Science* **2010**, *330*, 933–937.

[9] Ortiz de Montellano, P. R.; De Voss, J. J. In *Cytochrome P450: Structure, Mechanism, and Biochemistry*; Ortiz de Montellano, P. R., Ed.; Springer US: Boston, MA, 2005; pp 183–245.

[10] Dawson, J. H.; Sono, M. Cytochrome P-450 and chloroperoxidase: thiolate-ligated heme enzymes. Spectroscopic determination of their active-site structures and mechanistic implications of thiolate ligation. *Chem. Rev.* **1987**, *87*, 1255–1276.

[11] Yoshioka, S.; Takahashi, S.; Hori, H.; Ishimori, K.; Morishima, I. Proximal cysteine residue is essential for the enzymatic activities of cytochrome P450cam. *Eur. J. Biochem.* **2001**, *268*, 252–259.

[12] Makris, T. M.; Denisov, I.; Schlichting, I.; Sligar, S. G. In *Cytochrome P450: Structure, Mechanism, and Biochemistry*; Ortiz de Montellano, P. R., Ed.; Springer US: Boston, MA, 2005; pp 149–182.

[13] Denisov, I. G.; Sligar, S. G. In *Cytochrome P450: Structure, Mechanism, and Biochemistry*; Ortiz de Montellano, P. R., Ed.; Springer International Publishing: Cham, 2015; pp 69–109.

[14] Poulos, T. L.; Johnson, E. F. In *Cytochrome P450: Structure, Mechanism, and Biochemistry*; Ortiz de Montellano, P. R., Ed.; Springer US: Boston, MA, 2005; pp 87–114.

[15] Waskell, L.; Kim, J.-J. P. In *Cytochrome P450: Structure, Mechanism, and Biochemistry*; Ortiz de Montellano, P. R., Ed.; Springer International Publishing: Cham, 2015; pp 33–68.

[16] Hannemann, F.; Bichet, A.; Ewen, K. M.; Bernhardt, R. Cytochrome P450 systems—biological variations of electron transport chains. *Biochim. Biophys. Acta* **2007**, *1770*, 330 – 344.

[17] Paine, M. J. I.; Scrutton, N. S.; Munro, A. W.; Gutierrez, A.; Roberts, G. C. K.; Wolf, C. R. In *Cytochrome P450: Structure, Mechanism, and Biochemistry*; Ortiz de Montellano, P. R., Ed.; Springer US: Boston, MA, 2005; pp 115–148.

[18] Gunsalus, I. C.; Wagner, G. C. Bacterial P-450cam methylene monooxygenase components: Cytochrome m, putidaredoxin, and putidaredoxin reductase. *Methods Enzymol.* **1978**, *52*, 166 – 188.

[19] Bell, S. G.; Dale, A.; Rees, N. H.; Wong, L.-L. A cytochrome P450 class I electron transfer system from Novosphingobium aromaticivorans. *Appl. Microbiol. Biotechnol.* **2010**, *86*, 163–175.

[20] Hawkes, D. B.; Adams, G. W.; Burlingame, A. L.; de Montellano, P. R. O.; Voss, J. J. D. Cytochrome P450cin(CYP176A), Isolation, Expression, and Characterization. *J. Biol. Chem.* **2002**, *277*, 27725–27732.

[21] Narhi, L. O.; Fulco, A. J. Characterization of a catalytically self-sufficient 119,000-dalton cytochrome P-450 monooxygenase induced by barbiturates in Bacillus megaterium. *J. Biol. Chem.* **1986**, *261*, 7160–7169.

[22] Narhi, L. O.; Fulco, A. J. Identification and characterization of two functional domains in cytochrome P-450BM-3, a catalytically self-sufficient monooxygenase

induced by barbiturates in Bacillus megaterium. *J. Biol. Chem.* **1987**, *262*, 6683–6690.

[23] Whitehouse, C. J. C.; Bell, S. G.; Wong, L.-L. P450BM3 (CYP102A1): connecting the dots. *Chem. Soc. Rev.* **2012**, *41*, 1218–1260.

[24] Girhard, M.; Bakkes, P. J.; Mahmoud, O.; Urlacher, V. B. In *Cytochrome P450: Structure, Mechanism, and Biochemistry*; Ortiz de Montellano, P. R., Ed.; Springer International Publishing: Cham, 2015; pp 451–520.

[25] O'Reilly, E.; Kohler, V.; Flitsch, S. L.; Turner, N. J. Cytochromes P450 as useful biocatalysts: addressing the limitations. *Chem. Commun.* **2011**, *47*, 2490–2501.

[26] Carmichael, A. B.; Wong, L.-L. Protein engineering of Bacillus megaterium CYP102. *Eur. J. Biochem.* **2001**, *268*, 3117–3125.

[27] Shinkyo, R.; Kamakura, M.; Ikushiro, S.-i.; Inouye, K.; Sakaki, T. Biodegradation of dioxins by recombinant Escherichia coli expressing rat CYP1A1 or its mutant. *Appl. Microbiol. Biotechnol.* **2006**, *72*, 584–590.

[28] Gillam, E. M. J. Engineering Cytochrome P450 Enzymes. *Chem. Res. Toxicol.* **2008**, *21*, 220–231.

[29] Gillam, E. M. Exploring the potential of xenobiotic-metabolising enzymes as biocatalysts: Evolving designer catalysts from polyfunctional cytochrome P450 enzymes. *Clin. Exp. Pharmacol. Physiol.* **2005**, *32*, 147–152.

[30] Guengerich, F. P. Cytochrome p450 enzymes in the generation of commercial products. *Nat. Rev. Drug Discov.* **2002**, *1*, 359–366.

[31] Urlacher, V. B.; Girhard, M. Cytochrome P450 monooxygenases: an update on perspectives for synthetic application. *Trends Biotechnol.* **2012**, *30*, 26 – 36.

[32] Girvan, H. M.; Munro, A. W. Applications of microbial cytochrome P450 enzymes in biotechnology and synthetic biology. *Curr. Opin. Chem. Biol.* **2016**, *31*, 136–145.

[33] Pylypenko, O.; Schlichting, I. Structural Aspects of Ligand Binding to and Electron Transfer in Bacterial and Fungal P450s. *Annu. Rev. Biochem.* **2004**, *73*, 991–1018.

[34] McLean, K.; Sabri, M.; Marshall, K.; Lawson, R.; Lewis, D.; Clift, D.; Balding, P.; Dunford, A.; Warman, A.; McVey, J.; Quinn, A.-M.; Sutcliffe, M.; Scrutton, N.; Munro, A. Biodiversity of cytochrome P450 redox systems. *Biochem. Soc. Trans.* **2005**, *33*, 796–801.

[35] Dus, K.; Katagiri, M.; Yu, C.-A.; Erbes, D.; Gunsalus, I. Chemical characterization of cytochrome P-450cam. *Biochem. Biophys. Res. Commun.* **1970**, *40*, 1423 – 1430.

[36] Unger, B. P.; Gunsalus, I. C.; Sligar, S. G. Nucleotide sequence of the Pseudomonas putida cytochrome P-450cam gene and its expression in Escherichia coli. *J. Biol. Chem.* **1986**, *261*, 1158–1163.

[37] Yu, C.-A.; Gunsalus, I. C.; Katagiri, M.; Suhara, K.; Takemori, S. Cytochrome P-450cam : I. Crystallization And Properties. *J. Biol. Chem.* **1974**, *249*, 94–101.

[38] Poulos, T. L.; Finzel, B. C.; Gunsalus, I. C.; Wagner, G. C.; Kraut, J. The 2.6-A crystal structure of Pseudomonas putida cytochrome P-450. *J. Biol. Chem.* **1985**, *260*, 16122–30.

[39] Mueller, E. J.; Loida, P. J.; Sligar, S. G. In *Cytochrome P450: Structure, Mechanism, and Biochemistry*; de Montellano, P. R. O., Ed.; Springer US: Boston, MA, 1995; pp 83–124.

[40] Poulos, T. L.; Finzel, B. C.; Howard, A. J. High-resolution crystal structure of cytochrome P450cam. *J. Mol. Biol.* **1987**, *195*, 687 – 700.

[41] Raag, R.; Martinis, S.; Sligar, S.; Poulos, T. Crystal structure of the cytochrome P450cam active site mutant Thr252Ala. *Biochemistry* **1991**, *30*, 11420–11429.

[42] Raag, R.; Poulos, T. L. Crystal structures of cytochrome P450cam complexed with camphane, thiocamphor, and adamantane: factors controlling P450 substrate hydroxylation. *Biochemistry* **1991**, *30*, 2674–2684.

[43] Sakurai, K.; Shimada, H.; Hayashi, T.; Tsukihara, T. Substrate binding induces structural changes in cytochrome P450cam. *Acta Crystallogr., Sect. F: Struct. Biol. Cryst. Commun.* **2008**, *65*, 80–83.

[44] Bell, S. G.; Harford-Cross, C. F.; Wong, L.-L. Engineering the CYP101 system for in vivo oxidation of unnatural substrates. *Protein Eng. Des. Sel.* **2001**, *14*, 797.

[45] Bell, S. G.; Sowden, R. J.; Wong, L.-L. Engineering the haem monooxygenase cytochrome P450 for monoterpene oxidation. *Chem. Commun.* **2001**, 635–636.

[46] Bell, S. G.; Chen, X.; Sowden, R. J.; Xu, F.; Williams, J. N.; Wong, L.-L.; Rao, Z. Molecular Recognition in (+)-α-Pinene Oxidation by Cytochrome P450cam. *J. Am. Chem. Soc.* **2003**, *125*, 705–714.

[47] Poulos, T. L.; Finzel, B. C.; Howard, A. J. Crystal structure of substrate-free Pseudomonas putida cytochrome P-450. *Biochemistry* **1986**, *25*, 5314–5322.

[48] Schrader, J. In *Flavours and Fragrances: Chemistry, Bioprocessing and Sustainability*; Berger, R. G., Ed.; Springer Berlin Heidelberg: Berlin, Heidelberg, 2007; pp 507–574.

[49] Christensen, L. P.; Edelenbos, M.; Kreutzmann, S. In *Flavours and Fragrances: Chemistry, Bioprocessing and Sustainability*; Berger, R. G., Ed.; Springer Berlin Heidelberg: Berlin, Heidelberg, 2007; pp 135–187.

[50] Sullivan, B. In *Pine Bark Beetles*; Tittiger, C., Blomquist, G. J., Eds.; Advances in Insect Physiology; Academic Press, 2016; Vol. 50; pp 129 – 193.

[51] Gomes, B. S.; Neto, B. P.; Lopes, E. M.; Cunha, F. V.; Araújo, A. R.; Wanderley, C. W.; Wong, D. V.; Júnior, R. C. P.; Ribeiro, R. A.; Sousa, D. P.; Medeiros, J. V. R.; Oliveira, R. C.; Oliveira, F. A. Anti-inflammatory effect of the monoterpene myrtenol is dependent on the direct modulation of neutrophil migration and oxidative stress. *Chem. Biol. Interact.* **2017**, *273*, 73 – 81.

[52] Koroch, A. R.; Rodolfo Juliani, H.; Zygadlo, J. A. In *Flavours and Fragrances: Chemistry, Bioprocessing and Sustainability*; Berger, R. G., Ed.; Springer Berlin Heidelberg: Berlin, Heidelberg, 2007; pp 87–115.

[53] Prakash, O.; Chandra, M.; Pant, A.; Rawat, D. In *Essential Oils in Food Preservation, Flavor and Safety*; Preedy, V. R., Ed.; Academic Press: San Diego, 2016; pp 561 – 572.

[54] Crowell, P. L.; Kennan, W. S.; Haag, J. D.; Ahmad, S.; Vedejs, E.; Gould, M. N. Chemoprevention of mammary carcinogenesis by hydroxylated derivatives of d-limonene. *Carcinogenesis* **1992**, *13*, 1261–1264.

[55] Xu, F.; Bell, S. G.; Lednik, J.; Insley, A.; Rao, Z.; Wong, L.-L. The Heme Monooxygenase Cytochrome P450cam Can Be Engineered to Oxidize Ethane to Ethanol. *Angew. Chem. Int. Ed.* **2005**, *44*, 4029–4032.

[56] Fredrickson, J. K.; Brockman, F. J.; Workman, D. J.; Li, S. W.; Stevens, T. O. Isolation and Characterization of a Subsurface Bacterium Capable of Growth on Toluene, Naphthalene, and Other Aromatic Compounds. *Appl. Environ. Microbiol.* **1991**, *57*, 796–803.

[57] Bell, S. G.; Wong, L.-L. P450 enzymes from the bacterium Novosphingobium aromaticivorans. *Biochem. Biophys. Res. Commun.* **2007**, *360*, 666 – 672.

[58] Fredrickson, J. K.; Balkwill, D. L.; Drake, G. R.; Romine, M. F.; Ringelberg, D. B.; White, D. C. Aromatic-degrading Sphingomonas isolates from the deep subsurface. *Appl. Environ. Microbiol.* **1995**, *61*, 1917–22.

[59] Romine, M. F.; Stillwell, L. C.; Wong, K.-K.; Thurston, S. J.; Sisk, E. C.; Sensen, C.; Gaasterland, T.; Fredrickson, J. K.; Saffer, J. D. Complete Sequence of a 184-Kilobase Catabolic Plasmid from Sphingomonas aromaticivorans F199. *J. Bacteriol.* **1999**, *181*, 1585–1602.

[60] Gillam, E. M. J.; Notley, L. M.; Cai, H.; De Voss, J. J.; Guengerich, F. P. Oxidation of Indole by Cytochrome P450 Enzymes. *Biochemistry* **2000**, *39*, 13817–13824.

[61] Hall, E. A.; Bell, S. G. The efficient and selective biocatalytic oxidation of norisoprenoid and aromatic substrates by CYP101B1 from Novosphingobium aromaticivorans DSM12444. *RSC Adv.* **2015**, *5*, 5762–5773.

[62] Ma, M.; Bell, S. G.; Yang, W.; Hao, Y.; Rees, N. H.; Bartlam, M.; Zhou, W.; Wong, L.-L.; Rao, Z. Structural Analysis of CYP101C1 from Novosphingobium aromaticivorans DSM12444. *Chembiochem* **2011**, *12*, 88–99.

[63] Yang, W.; Bell, S. G.; Wang, H.; Zhou, W.; Hoskins, N.; Dale, A.; Bartlam, M.; Wong, L.-L.; Rao, Z. Molecular Characterization of a Class I P450 Electron Transfer System fromNovosphingobium aromaticivoransDSM12444. *J. Biol. Chem.* **2010**, *285*, 27372–27384.

[64] Miura, Y.; Fulco, A. J. (ω–2) Hydroxylation of Fatty Acids by a Soluble System from Bacillus megaterium. *J. Biol. Chem.* **1974**, *249*, 1880–1888.

[65] Matson, R. S.; Stein, R. A.; Fulco, A. J. Hydroxylation of 9-hydroxystearate by a soluble cytochrome P-450-dependent fatty acid hydroxylase from Bacillusmegaterium. *Biochem. Biophys. Res. Commun.* **1980**, *97*, 955 – 961.

[66] Matson, R. S.; Fulco, A. J. Hydroxystearates as inhibitors of palmitate hydroxylation catalyzed by the cytochrome P-450 monooxygenase from Bacillus megaterium. *Biochem. Biophys. Res. Commun.* **1981**, *103*, 531 – 535.

[67] Miura, Y.; Fulco, A. J. ω-1, ω-2 and ω-3 Hydroxylation of long-chain fatty acids, amides and alcohols by a soluble enzyme system from Bacillus megatyerium. *Biochim. Biophys. Acta, Lipids Lipid Metab.* **1975**, *388*, 305 – 317.

[68] Ahmed, F.; L. Avery, K.; M. Cullis, P.; U. Primrose, W.; C. K. Roberts, G. An unusual matrix of stereocomplementarity in the hydroxylation of monohydroxy fatty acids catalysed by cytochrome P450 from Bacillus megaterium with potential application in biotransformations. *Chem. Commun.* **1999**, 2049–2050.

[69] Davis, S.; Sui, Z.; Peterson, J. A.; de Montellano, P. R. Oxidation of ω-Oxo Fatty Acids by Cytochrome P450BM-3(CYP102). *Arch. Biochem. Biophys.* **1996**, *328*, 35 – 42.

[70] Shirane, N.; Sui, Z.; Peterson, J. A.; Ortiz de Montellano, P. R. Cytochrome P450BM-3 (CYP102): Regiospecificity of oxidation of ω-unsaturated fatty acids and mechanism-based inactivation. *Biochemistry* **1993**, *32*, 13732–13741.

[71] Ruettinger, R. T.; Fulco, A. J. Epoxidation of unsaturated fatty acids by a soluble cytochrome P-450-dependent system from Bacillus megaterium. *J. Biol. Chem.* **1981**, *256*, 5728–5734.

[72] Boddupalli, S. S.; Hasemann, C. A.; Ravichandran, K. G.; Lu, J. Y.; Goldsmith, E. J.; Deisenhofer, J.; Peterson, J. A. Crystallization and preliminary x-ray diffraction analysis of P450terp and the hemoprotein domain of P450BM-3, enzymes belonging to two distinct classes of the cytochrome P450 superfamily. *Proc. Natl. Acad. Sci.* **1992**, *89*, 5567–5571.

[73] Li, H.; Poulos, T. L. The structure of the cytochrome p450BM-3 haem domain complexed with the fatty acid substrate, palmitoleic acid. *Nat. Struct. Biol.* **1997**, *4*, 140–6.

[74] Urlacher, V. B.; Makhsumkhanov, A.; Schmid, R. D. Biotransformation of β-ionone by engineered cytochrome P450 BM-3. *Appl. Microbiol. Biotechnol.* **2006**, *70*, 53–59.

[75] Li, Q.-S.; Ogawa, J.; Schmid, R. D.; Shimizu, S. Residue size at position 87 of cytochrome P450 BM-3 determines its stereoselectivity in propylbenzene and 3-chlorostyrene oxidation. *FEBS Lett.* **2001**, *508*, 249–252.

[76] Graham-Lorence, S.; Truan, G.; Peterson, J. A.; Falck, J. R.; Wei, S.; Helvig, C.; Capdevila, J. H. An Active Site Substitution, F87V, Converts Cytochrome P450 BM-3 into a Regio- and Stereoselective (14S,15R)-Arachidonic Acid Epoxygenase. *J. Biol. Chem.* **1997**, *272*, 1127–1135.

[77] van der Schaft, P. H. In *Flavours and Fragrances: Chemistry, Bioprocessing and Sustainability*; Berger, R. G., Ed.; Springer Berlin Heidelberg: Berlin, Heidelberg, 2007; pp 285–301.

[78] Tassaneeyakul, W.; Guo, L.-Q.; Fukuda, K.; Ohta, T.; Yamazoe, Y. Inhibition Selectivity of Grapefruit Juice Components on Human Cytochromes P450. *Arch. Biochem. Biophys.* **2000**, *378*, 356 – 363.

[79] Sowden, R. J.; Yasmin, S.; Rees, N. H.; Bell, S. G.; Wong, L.-L. Biotransformation of the sesquiterpene (+)-valencene by cytochrome P450cam and P450BM-3. *Org. Biomol. Chem.* **2005**, *3*, 57–64.

[80] Seifert, A.; Vomund, S.; Grohmann, K.; Kriening, S.; Urlacher, V. B.; Laschat, S.; Pleiss, J. Rational Design of a Minimal and Highly Enriched CYP102A1 Mutant Library with Improved Regio-, Stereo- and Chemoselectivity. *Chembiochem* **2009**, *10*, 853–861.

[81] Munday, S. D.; Dezvarei, S.; Bell, S. G. Increasing the Activity and Efficiency of Stereoselective Oxidations by using Decoy Molecules in Combination with Rate-Enhancing Variants of P450Bm3. *ChemCatChem* **2016**, *8*, 2789–2796.

[82] Whitehouse, C. J. C.; Bell, S. G.; Tufton, H. G.; Kenny, R. J. P.; Ogilvie, L. C. I.; Wong, L.-L. Evolved CYP102A1 (P450BM3) variants oxidise a range of non-natural substrates and offer new selectivity options. *Chem. Commun.* **2008**, 966.

[83] Whitehouse, C. J. C.; Bell, S. G.; Yang, W.; Yorke, J. A.; Blanford, C. F.; Strong, A. J. F.; Morse, E. J.; Bartlam, M.; Rao, Z.; Wong, L.-L. A Highly Active Single-Mutation Variant of P450BM3(CYP102A1). *ChemBioChem* **2009**, *10*, 1654–1656.

[84] Munday, S. D.; Dezvarei, S.; Lau, I. C.-K.; Bell, S. G. Examination of Selectivity in the Oxidation of ortho- and meta-Disubstituted Benzenes by CYP102A1 (P450 Bm3) Variants. *ChemCatChem* **2017**, *9*, 2512–2522.

[85] Whitehouse, C. J. C.; Yang, W.; Yorke, J. A.; Tufton, H. G.; Ogilvie, L. C. I.; Bell, S. G.; Zhou, W.; Bartlam, M.; Rao, Z.; Wong, L.-L. Structure, electronic properties and catalytic behaviour of an activity-enhancing CYP102A1 (P450BM3) variant. *Dalton Trans.* **2011**, *40*, 10383.

[86] Kraft, P.; Bajgrowicz, J.; Denis, C.; Fráter, G. Odds and Trends: Recent Developments in the Chemistry of Odorants. *Angewandte Chemie* **2000**, *39*, 2980–3010.

[87] Barakat, A.; Brenna, E.; Fuganti, C.; Serra, S. Synthesis, olfactory evaluation and determination of the absolute configuration of the β- and γ-Iralia® isomers. *Tetrahedron: Asymmetry* **2008**, *19*, 2316–2322.

[88] Sell, C. S. On the Unpredictability of Odor. *Angew. Chem. Int. Ed.* **2006**, *45*, 6254–6261.

[89] Azerad, R. *Regio- and Stereoselective Microbial Hydroxylation of Terpenoid Compounds*; CRC Press, 2000; pp 153–180.

[90] Yamazaki, Y.; Hayashi, Y.; Arita, M.; Hieda, T.; Mikami, Y. Microbial Conversion of α-Ionone, α-Methylionone, and α-Isomethylionone. *Appl. Environ. Microbiol.* **1988**, *54*, 2354–2360.

[91] Harrison, P. J.; Bugg, T. D. Enzymology of the carotenoid cleavage dioxygenases: Reaction mechanisms, inhibition and biochemical roles. *Arch. Biochem. Biophys.* **2014**, *544*, 105 – 111, Cofactor Assisted Enzymatic Catalysis.

[92] Cataldo, V. F.; López, J.; Cárcamo, M.; Agosin, E. Chemical vs. biotechnological synthesis of C13-apocarotenoids: current methods, applications and perspectives. *Appl. Microbiol. Biotechnol.* **2016**, *100*, 5703–5718.

[93] Lalko, J.; Lapczynski, A.; Politano, V.; McGinty, D.; Bhatia, S.; Letizia, C.; Api, A. Fragrance material review on α-ionone. *Food Chem. Toxicol.* **2007**, *45*, S235 – S240.

[94] Lapczynski, A.; Lalko, J.; McGinty, D.; Bhatia, S.; Letizia, C.; Api, A. Fragrance material review on trans-β-damascone. *Food Chem. Toxicol.* **2007**, *45*, S199 – S204.

[95] de Carvalho, C. C.; da Fonseca, M. M. R. Biotransformation of terpenes. *Biotechnol. Adv.* **2006**, *24*, 134–142.

[96] Azerad, R. 1,8-Cineole: Chemical and Biological Oxidation Reactions and Products. *ChemPlusChem* **2014**, *79*, 634–655.

[97] Tu, V. A.; Kaga, A.; Gericke, K.-H.; Watanabe, N.; Narumi, T.; Toda, M.; Brueckner, B.; Baldermann, S.; Mase, N. Synthesis and Characterization of Quantum Dot Nanoparticles Bound to the Plant Volatile Precursor of Hydroxy-apo-10-carotenal. *J. Org. Chem.* **2014**, *79*, 6808–6815.

[98] Gerhäuser, C.; Klimo, K.; Hümmer, W.; Hölzer, J.; Petermann, A.; Garreta-Rufas, A.; Böhmer, F.-D.; Schreier, P. Identification of 3-hydroxy-β-damascone and related carotenoid-derived aroma compounds as novel potent inducers of Nrf2-mediated phase 2 response with concomitant anti-inflammatory activity. *Mol. Nutr. Food Res.* **2009**, *53*, 1237–1244.

[99] Ishihara, M.; Tsuneya, T.; Shiota, H.; Shiga, M.; Nakatsu, K. Identification of new constituents of quince fruit flavor. *J. Org. Chem.* **1986**, *51*, 491–495.

[100] Sambrook, J.; Fritsch, E. F.; Maniatis, T. *Molecular Cloning: A Laboratory Manual*; Cold Spring Harbor Laboratory Press: Cold Spring Harbor, NY, USA, 1989.

[101] Hall, E. A.; Sarkar, M. R.; Lee, J. H. Z.; Munday, S. D.; Bell, S. G. Improving the Monooxygenase Activity and the Regio- and Stereoselectivity of Terpenoid Hydroxylation Using Ester Directing Groups. *ACS Catal.* **2016**, *6*, 6306–6317.

[102] Omura, T.; Sato, R. The Carbon Monoxide-binding Pigment of Liver Microsomes. *J. Biol. Chem.* **1964**, *239*, 2370–2378.

[103] Guengerich, F. P.; Martin, M. V.; Sohl, C. D.; Cheng, Q. Measurement of cytochrome P450 and NADPH–cytochrome P450 reductase. *Nat. Protoc.* **2009**, *4*, 1245–1251.

[104] Stok, J. E.; Hall, E. A.; Stone, I. S. J.; Noble, M. C.; Wong, S. H.; Bell, S. G.; De Voss, J. J. In vivo and in vitro hydroxylation of cineole and camphor by cytochromes P450CYP101A1, CYP101B1 and N242A CYP176A1. *J. Mol. Catal. B: Enzym.* **2016**, *128*, 52–64.

[105] Lee, J. H. Z.; Wong, S. H.; Stok, J. E.; Bagster, S. A.; James, J. D. V.; Bell, S. G. Hydroxylation of 1,8- and 1,4-cineole at different C-H bonds using bacterial P450 variants. *Manuscript Being Prepared* **2017**,

[106] Hall, E. A.; Sarkar, M. R.; Bell, S. G. The selective oxidation of substituted aromatic hydrocarbons and the observation of uncoupling via redox cycling during naphthalene oxidation by the CYP101B1 system. *Catal. Sci. Technol.* **2017**, *7*, 1537–1548.

[107] Yang, W.; Bell, S. G.; Wang, H.; Zhou, W.; Bartlam, M.; Wong, L.-L.; Rao, Z. The structure of CYP101D2 unveils a potential path for substrate entry into the active site. *Biochem. J.* **2011**, *433*, 85–93.

[108] Batabyal, D.; Poulos, T. L. Crystal Structures and Functional Characterization of Wild-Type CYP101D1 and Its Active Site Mutants. *Biochemistry* **2013**, *52*, 8898–8906.

[109] Swiss-Model. https://swissmodel.expasy.org/.

[110] England, P. A.; Rouch, D. A.; Westlake, A. C. G.; Bell, S. G.; Nickerson, D. P.; Webberley, M.; Flitsch, S. L.; Wong, L.-L. Aliphatic vs. aromatric C-H bond activation of phenylcyclohexane catalysed by cytochrome P450cam. *Chem. Commun.* **1996**, 357–358.

[111] England, P. A.; Harford-Cross, C. F.; Stevenson, J.-A.; Rouch, D. A.; Wong, L.-L. The oxidation of naphthalene and pyrene by cytochrome P450cam. *FEBS Letters* **1998**, *424*, 271–274.

[112] Fowler, S. M.; England, P. A.; Westlake, A. C. G.; Rouch, D. R.; Nickerson, D. P.; Blunt, C.; Braybrook, D.; West, S.; Wong, L.-L.; Flitsch, S. L. Cytochrome P-450cam monooxygenase can be redesigned to catalyse the regioselective aromatic hydroxylation of diphenylmethane. *J. Chem. Soc., Chem. Commun.* **1994**, 2761.

[113] Bell, S. G.; Yang, W.; Dale, A.; Zhou, W.; Wong, L.-L. Improving the affinity and activity of CYP101D2 for hydrophobic substrates. *Appl. Microbiol. Biotechnol.* **2012**, *97*, 3979–3990.

[114] Sarkar, M. R.; Lee, J. H. Z.; Bell, S. G. The Oxidation of Hydrophobic Aromatic Substrates by Using a Variant of the P450 Monooxygenase CYP101B1. *Chembiochem* **2017**, *18*, 2119–2128.

[115] Sarkar, M. R.; Hall, E. A.; Dasgupta, S.; Bell, S. G. The Use of Directing Groups Enables the Selective and Efficient Biocatalytic Oxidation of Unactivated Adamantyl C-H Bonds. *ChemistrySelect* **2016**, *1*, 6700–6707.

[116] Stevenson, J.-A.; K. Bearpark, J.; Wong, L.-L. Engineering molecular recognition in alkane oxidation catalysed by cytochrome P450cam. *New J. Chem.* **1998**, *22*, 551–552.

[117] French, K. J.; Rock, D. A.; Rock, D. A.; Manchester, J. I.; Goldstein, B. M.; Jones, J. P. Active Site Mutations of Cytochrome P450cam Alter the Binding, Coupling, and Oxidation of the Foreign Substrates (R)- and (S)-2-Ethylhexanol. *Arch. Biochem. Biophys.* **2002**, *398*, 188 – 197.

[118] Baser, K. H. C.; Buchbauer, G. *Handbook of Essential Oils : Science, Technology, and Applications, Second Edition*; CRC Press: New York, United States, 2015.

[119] Ludwiczuk, A.; Skalicka-Woźniak, K.; Georgiev, M. In *Pharmacognosy*; Badal, S., Delgoda, R., Eds.; Academic Press: Boston, 2017; pp 233 – 266.

[120] Ashour, M.; Wink, M.; Gershenzon, J. *Annual Plant Reviews Volume 40: Biochemistry of Plant Secondary Metabolism*; Wiley-Blackwell, 2010; pp 258–303.

[121] Bakkali, F.; Averbeck, S.; Averbeck, D.; Idaomar, M. Biological effects of essential oils – A review. *Food Chem. Toxicol.* **2008**, *46*, 446 – 475.

[122] Chang, M. C. Y.; Keasling, J. D. Production of isoprenoid pharmaceuticals by engineered microbes. *Nat. Chem. Biol.* **2006**, *2*, 674–681.

[123] Schulz, S.; Girhard, M.; Urlacher, V. B. Biocatalysis: Key to Selective Oxidations. *ChemCatChem* **2012**, *4*, 1889–1895.

[124] Brenna, E.; Fuganti, C.; Serra, S. Enantioselective perception of chiral odorants. *Tetrahedron: Asymmetry* **2003**, *14*, 1 – 42.

[125] Serra, S.; Fuganti, C.; Brenna, E. Biocatalytic preparation of natural flavours and fragrances. *Trends Biotechnol.* **2005**, *23*, 193 – 198.

[126] Anwar, F.; Ali, M.; Hussain, A. I.; Shahid, M. Antioxidant and antimicrobial activities of essential oil and extracts of fennel (Foeniculum vulgare Mill.) seeds from Pakistan. *Flavour Fragr. J.* **2009**, *24*, 170–176.

[127] Romagni, J. G.; Allen, S. N.; Dayan, F. E. Allelopathic Effects of Volatile Cineoles on Two Weedy Plant Species. *J. Chem. Ecol.* **2000**, *26*, 303–313.

[128] Barton, A. F. M.; Dell, B.; Knight, A. R. Herbicidal Activity of Cineole Derivatives. *J. Agric. Food. Chem.* **2010**, *58*, 10147–10155, PMID: 20715837.

[129] Kaluzna, I.; Schmitges, T.; Straatman, H.; van Tegelen, D.; Müller, M.; Schürmann, M.; Mink, D. Enabling Selective and Sustainable P450 Oxygenation Technology. Production of 4-Hydroxy-α-isophorone on Kilogram Scale. *Org. Process Res. Dev.* **2016**, *20*, 814–819.

[130] Tarantilis, P. A.; Polissiou, M. G. Isolation and Identification of the Aroma Components from Saffron (Crocus sativus). *J. Agric. Food. Chem.* **1997**, *45*, 459–462.

[131] Zarghami, N.; Heinz, D. Monoterpene aldehydes and isophorone-related compounds of saffron. *Phytochemistry* **1971**, *10*, 2755–2761.

[132] Bellut, H. Process for preparing 3,5,5,-trimethyl-4-hydroxy-2-cyclohexen-1-one. 1990; US Patent 4,898,984.

[133] Hennig, M.; Puntener, K.; Scalone, M. Synthesis of (R)- and (S)-4-hydroxyisophorone by ruthenium-catalysed asymmetric transfer hydrogenation of ketoisophorone. *Tetrahedron: Asymmetry* **2000**, *11*, 1849–1858.

[134] Isler, O.; Lindlar, H.; Montavon, M.; Rüegg, R.; Saucy, G.; Zeller, P. Synthesen in der Carotinoid-Reihe Mitteilung. Totalsynthese von Zeaxanthin und Physalien. *Helv. Chim. Acta* **1956**, *39*, 2041–2053.

[135] Dezvarei, S.; Lee, J. H.; Bell, S. G. Stereoselective hydroxylation of isophorone by variants of the cytochromes P450 CYP102A1 and CYP101A1. *Enzyme Microb. Technol.* **2018**, *10.1016/j.enzmictec.2018.01.002*.

[136] Bell, S.; Chen, X.; Xu, F.; Rao, Z.; Wong, L.-L. Engineering substrate recognition in catalysis by cytochrome P450cam. *Biochem. Soc. Trans.* **2003**, *31*, 558–562.

[137] Nakahashi, H.; Miyazawa, M. Biotransformation of (-)-Camphor by Salmonella typhimurium OY1002/2A6 Expressing Human CYP2A6 and NADPH-P450 Reductase. *J. Oleo Sci.* **2011**, *60*, 545–548.

[138] Gyoubu, K.; ; Miyazawa, M. In Vitro Metabolism of (-)-Camphor Using Human Liver Microsomes and CYP2A6. *Biol. Pharm. Bull.* **2007**, *30*, 230–233.

[139] Miyazawa, M.; Miyamoto, Y. Biotransformation of (1R)-(+)- and (1S)-(-)-camphor by the larvae of common cutworm (Spodoptera litura). *J. Mol. Catal. B: Enzym.* **2004**, *27*, 83–89.

[140] Miyazawa, M.; Gyoubu, K. Metabolism of (+)-Fenchone by CYP2A6 and CYP2B6 in Human Liver Microsomes. *Biol. Pharm. Bull.* **2006**, *29*, 2354–2358.

[141] Joe, Y. A.; Goo, Y. M.; Lee, Y. Y. Microbiological oxidation of isophorone to 4-hydroxyisophorone and chemical transformation of 4-hydroxyisophorone to 2,3,5-trimethyl-p-benzoquinone. *Arch. Pharmacal Res.* **1989**, *12*, 73–78.

[142] Tavanti, M.; Parmeggiani, F.; Castellanos, J. R. G.; Mattevi, A.; Turner, N. J. One-Pot Biocatalytic Double Oxidation of α-Isophorone for the Synthesis of Ketoisophorone. *ChemCatChem* **2017**, *9*, 3338–3348.

[143] Bell, S. G.; Tan, A. B. H.; Johnson, E. O. D.; Wong, L.-L. Selective oxidative demethylation of veratric acid to vanillic acid by CYP199A4 from Rhodopseudomonas palustris HaA2. *Mol. BioSyst.* **2009**, *6*, 206–214.

[144] Rosazza, J. P. N.; Steffens, J. J.; Sariaslani, F. S.; Goswami, A.; Beale, J. M.; Reeg, S.; Chapman, R. Microbial Hydroxylation of 1,4-Cineole. *Appl. Environ. Microbiol.* **1987**, *53*, 2482–2486.

[145] Asakawa, Y.; Matsuda, R.; Tori, M.; Hashimoto, T. Preparation of biologically active substances and animal and microbial metabolites from menthols, cineoles and kauranes. *Phytochemistry* **1988**, *27*, 3861–3869.

[146] Carman, R.; Rayner, A. 2-,4-Dihydroxy-1,8-cineole. A New Possum Urinary Metabolite. *Aust. J. Chem.* **1994**, *47*, 2087.

[147] Miyazawa, M.; Yamamoto, Y. N. K.; Kameoka, H. Biotransformation of 1,4-Cineole to 3-endo-hydroxy-1,4-cineole by Aspergillus Niger. *Chem. Express* **1992**, *7*, 125–128.

[148] Asakawa, Y.; Toyota, M.; Ishida, T. Biotransformation of 1,4-Cineole, a Monoterpene Ether. *Xenobiotica* **1988**, *18*, 1129–1134.

[149] Miyazawa, M.; Miyamoto, Y. Biotransformation of (+)-(1R)- and (-)-(1S)-fenchone by the larvae of common cutworm (Spodoptera litura). *J. Mol. Catal. B: Enzym.* **2005**, *32*, 123–130.

[150] Nakahashi, H.; Yagi, N.; Miyazawa, M. Biotransformation of (+)-Fenchone by Salmonella typhimurium OY1002/2A6 Expressing Human CYP2A6 and NADPH-P450 Reductase. *J. Oleo Sci.* **2013**, *62*, 293–296.

[151] Slessor, K. E.; Stok, J. E.; Cavaignac, S. M.; Hawkes, D. B.; Ghasemi, Y.; Voss, J. J. D. Cineole biodegradation: Molecular cloning, expression and characterisation of (1R)-6β-hydroxycineole dehydrogenase from Citrobacter braakii. *Bioorg. Chem.* **2010**, *38*, 81–86.

[152] Miyazawa, M.; Shindo, M. Biotransformation of 1,8-Cineole by Human Liver Microsomes. *Nat. Prod. Lett.* **2001**, *15*, 49–53.

[153] Miyazawa, M.; Kameoka, H.; Morinaga, K.; Negoro, K.; Mura, N. Hydroxycineole: four new metabolites of 1,8-cineole in rabbits. *J. Agric. Food. Chem.* **1989**, *37*, 222–226.

[154] Meharenna, Y. T.; Slessor, K. E.; Cavaignac, S. M.; Poulos, T. L.; Voss, J. J. D. The Critical Role of Substrate-Protein Hydrogen Bonding in the Control of Regioselective Hydroxylation in P450cin. *J. Biol. Chem.* **2008**, *283*, 10804–10812.

[155] Boddupalli, S. S.; Estabrook, R. W.; Peterson, J. A. Fatty acid monooxygenation by cytochrome P-450BM-3. *J. Biol. Chem.* **1990**, *265*, 4233–4239.

[156] Roome, P. W.; Peterson, J. A. The reduction of putidaredoxin reductase by reduced pyridine nucleotides. *Arch. Biochem. Biophys.* **1988**, *266*, 32–40.

[157] Brumaghim, J. L.; Li, Y.; Henle, E.; Linn, S. Effects of Hydrogen Peroxide upon Nicotinamide Nucleotide Metabolism in *Escherichia coli*. *J. Biol. Chem.* **2003**, *278*, 42495–42504.

[158] Neeli, R.; Roitel, O.; Scrutton, N. S.; Munro, A. W. Switching Pyridine Nucleotide Specificity in P450 BM3. *J. Biol. Chem.* **2005**, *280*, 17634–17644.

[159] Branco, R. J.; Seifert, A.; Budde, M.; Urlacher, V. B.; Ramos, M. J.; Pleiss, J. Anchoring effects in a wide binding pocket: The molecular basis of regioselectivity in engineered cytochrome P450 monooxygenase from B. megaterium. *Proteins: Struct., Funct., Bioinf.* **2008**, *73*, 597–607.

[160] Litzenburger, M.; Bernhardt, R. Selective oxidation of carotenoid-derived aroma compounds by CYP260B1 and CYP267B1 from Sorangium cellulosum So ce56. *Appl. Microbiol. Biotechnol.* **2016**, *100*, 4447–4457.

[161] Schmit, C. Deodorant compositions having antibacterial and odor blocking properties and related methods. 2015; WO Patent App. PCT/US2014/071,025.

[162] Lambrecht, S.; Dilk, E.; Worner, P. Perfume compositions comprising 4,8-dimethyl-3,7-nonadien-2-one. 2001; US Patent App. 09/736,599.

[163] Sell, C. S. *Chemistry and the Sense of Smell*; John Wiley & Sons, Inc., 2014; pp 237–295.

[164] Surburg, H.; Panten, J. *Common Fragrance and Flavor Materials : Preparation, Properties and Uses*; John Wiley & Sons, Incorporated: Berlin, Germany, 2016.

[165] Camps, A. *Perfumery: Techniques in Evolution*, 2nd ed.; Allured Pub Corp, 2008.

[166] Appel, D.; Lutz-Wahl, S.; Fischer, P.; Schwaneberg, U.; Schmid, R. D. A P450 BM-3 mutant hydroxylates alkanes, cycloalkanes, arenes and heteroarenes. *J. Biotechnol.* **2001**, *88*, 167 – 171.

[167] Budde, M.; Morr, M.; Schmid, R. D.; Urlacher, V. B. Selective Hydroxylation of Highly Branched Fatty Acids and their Derivatives by CYP102A1 from Bacillus megaterium. *Chembiochem* **2006**, *7*, 789–794.

[168] Xia, W.; Budge, S. M.; Lumsden, M. D. New 1H NMR-Based Technique To Determine Epoxide Concentrations in Oxidized Oil. *J. Agric. Food. Chem.* **2015**, *63*, 5780–5786.

[169] Schoch, E.; Benda, I.; Schreier, P. Bioconversion of α-Damascone by Botrytis cinerea. *Appl. Environ. Microbiol.* **1991**, *57*, 15–18.

[170] de Beer, S. B.; Venkataraman, H.; Geerke, D. P.; Oostenbrink, C.; Vermeulen, N. P. Free Energy Calculations Give Insight into the Stereoselective

Hydroxylation of α-Ionones by Engineered Cytochrome P450 BM3 Mutants. *J. Chem. Inf. Model.* **2012**, *52*, 2139–2148.

[171] Gaydou, E. M.; Smadja, J.; Lageot, C.; Faure, R. Sesquiterpene Epoxidation: Rearrangement of (+)-Ledene Epoxy Compounds. *J. Agric. Food. Chem.* **1996**, *44*, 1840–1846.

[172] Walter, M. H.; Strack, D. Carotenoids and their cleavage products: Biosynthesis and functions. *Nat. Prod. Rep.* **2011**, *28*, 663.

[173] McGinty, D.; Letizia, C.; Api, A. Fragrance material review on p-isopropylbenzyl acetate. *Food Chem. Toxicol.* **2012**, *50*, S394–S397.

[174] de Montellano, P. R. O. Hydrocarbon Hydroxylation by Cytochrome P450 Enzymes. *Chem. Rev.* **2010**, *110*, 932–948.

[175] Ji, L.; Faponle, A. S.; Quesne, M. G.; Sainna, M. A.; Zhang, J.; Franke, A.; Kumar, D.; van Eldik, R.; Liu, W.; de Visser, S. P. Drug Metabolism by Cytochrome P450 Enzymes What Distinguishes the Pathways Leading to Substrate Hydroxylation Over Desaturation. *Chem. Eur. J* **2015**, *21*, 9083–9092.

Appendix A Data for Chapter 3

In Vitro Assays of CYP101B1 Mutants

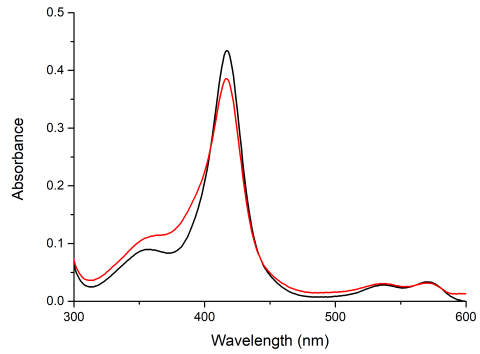

(a) 1,8-Cineole

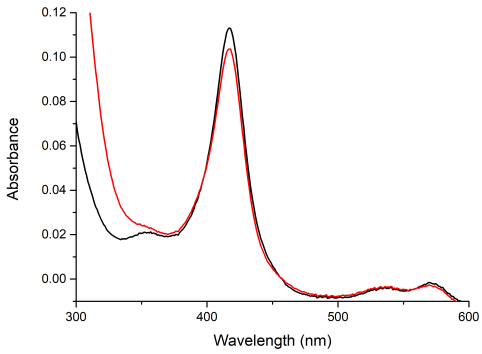

(b) *cis*-Jasmone

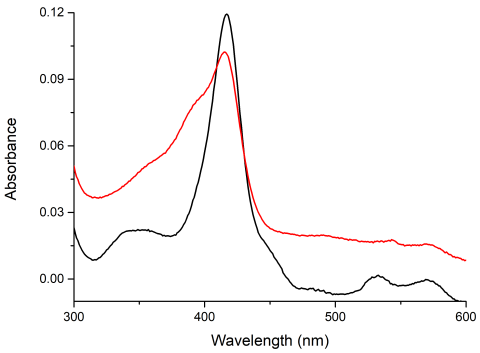

(c) Fenchyl Acetate

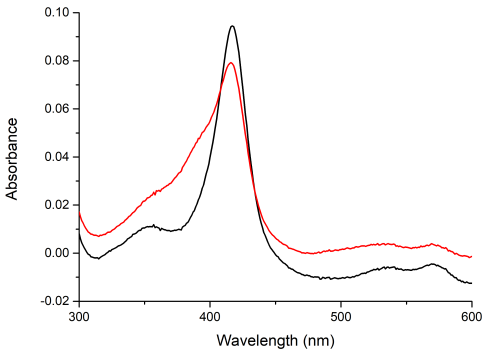

(d) Isobornyl Acetate

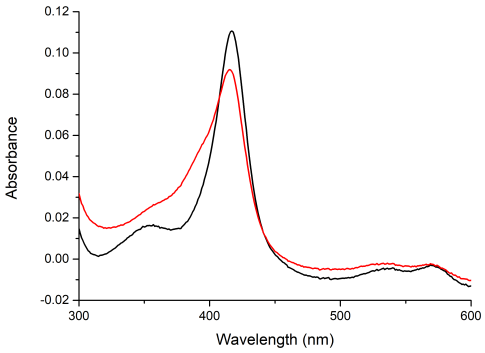

(e) (*R*)-nopol.

Figure A1: Spin-State Shift Studies of H85G-CYP101B1 with various terpenoids and norisoprenoids.

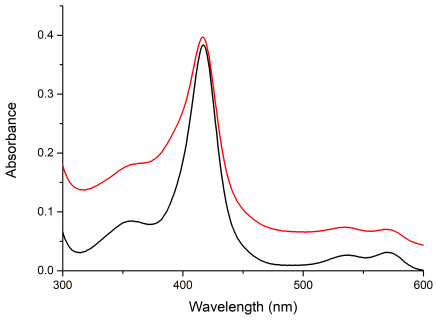

(a) Cyclodecane.

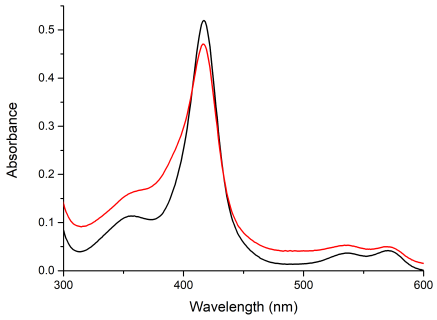

(b) Cyclododecane

Figure A2: Spin-State shift studies of H85G-CYP101B1 with cycloalkanes.

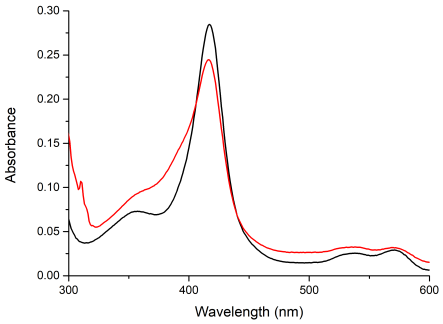

(a) Naphthalene.

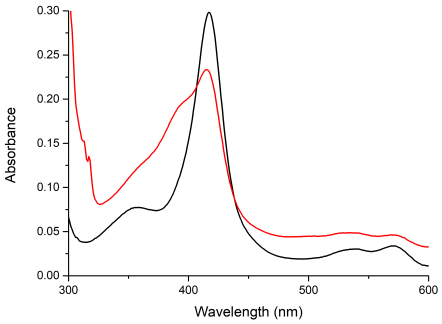

(b) 1-Methylnaphthalene.

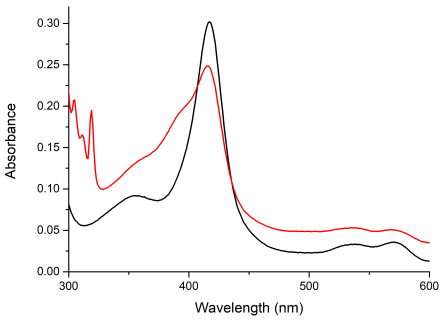

(c) 2-Methylnaphthalene.

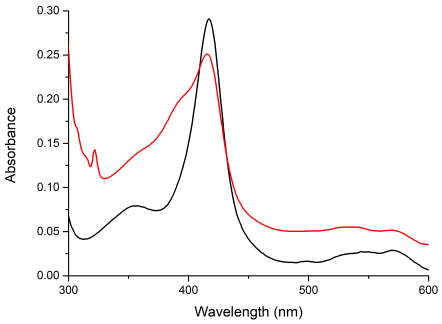

(d) 1,2-Diethylnaphthalene.

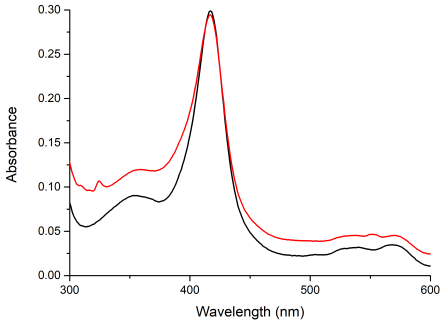

(e) 3,6-Dimethylnaphthalene.

Figure A3: Spin-State Shift Studies of H85A-CYP101B1 with Napthalene Variants.

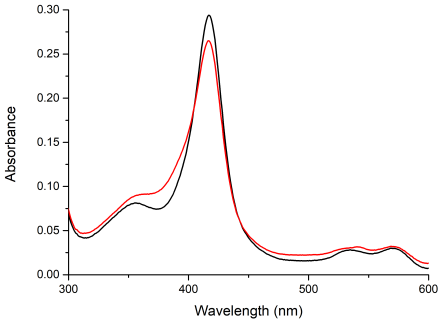

(a) 3-phenyltoluene

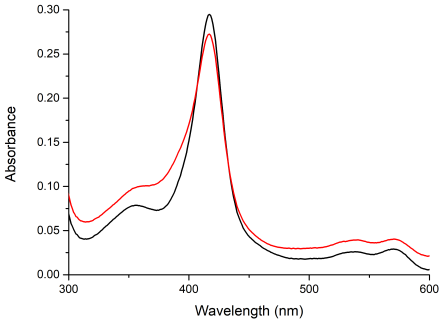

(b) 4-phenyltoluene

Figure A4: Spin-State Shift Studies of H85A-CYP101B1 with Toluene Variants.

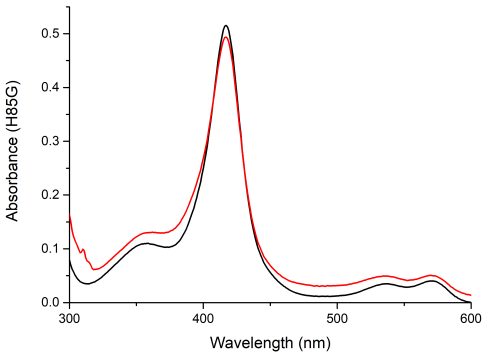

(a) Naphthalene.

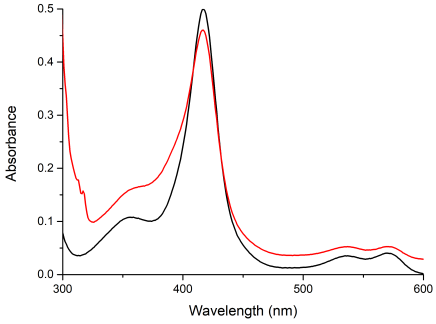

(b) 1-Methylnaphthalene.

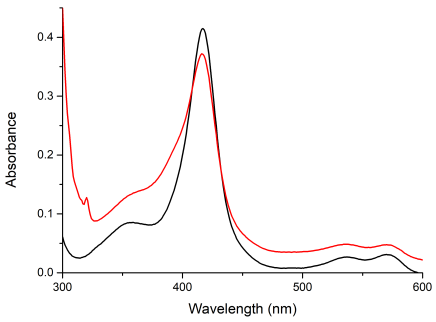

(c) 1,5-Dimethylnaphthalene.

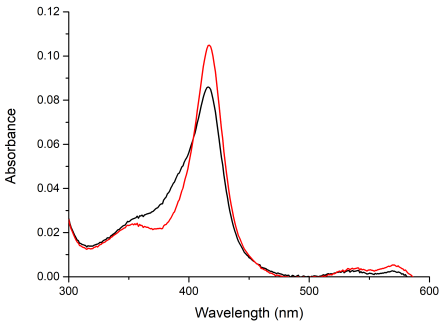

(d) Sclareolide

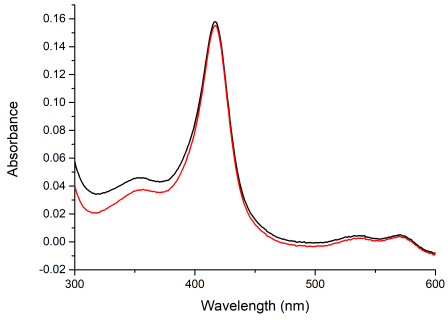

(e) Valencene

Figure A5: Spin-State Shift Studies of H85G-CYP101B1 with various hydrophobic substrates.

Appendix B Data for Chapter 4

Cell Biomass and P450 Concentrations.

Table B1: The concentration of P450 enzyme and cell wet weight (cell biomass) for enzymes used in the whole-cell oidation of terpenoids. Cell biomass is given as given as mean ± S.D. with $n = 2$.

Enzyme	**P450 Concentration (nM)**	**Cell Biomass (g/L)**
$P450_{BM3}$-WT	183	16 ± 0.3
$P450_{BM3}$-GVQ	88	13 ± 0.3
$P450_{BM3}$-RLYFFAIP	108	14 ± 0.3
$P450_{BM3}$-RLYGVQ	86	14 ± 0.4
$P450_{cam}$-WT	25	13 ± 0.3
$P450_{cam}$-WFAL	54	13 ± 0.6
$P450_{cam}$-WFL	15	17 ± 2
$P450_{cam}$-VFL	10	17 ± 3
$P450_{cam}$-LF	98	14 ± 0.4

NMR Analysis of Fenchyl Acetate Oxidation Products

5-*exo*-hydroxyfenchyl acetate ^{1}H NMR (500 MHz, $CDCl_3$) δ 4.32 (d, J = 1.8 Hz, 1H, *exo* H2), 4.18 (d, J = 6.7 Hz, 1H, *endo* H5), 2.25 (ddd, J = 13.8, 6.7, 2.5 Hz, 1H, *endo* H6), 2.06 (s, 3H, H12), 1.73 (s, 1H, H4), 1.62 (dd, J = 10.8, 1.5 Hz, 1H, H7a), 1.48 (d, J = 10.8 Hz, 1H, H7b), 1.14 (s, 3H, H9), 1.07 (s, 3H, H10), 1.00 (ddd, J = 13.8, 2.9, 1.6 Hz, 1H, *exo* H6), 0.76 (s, 3H, H8). ^{13}C NMR (126 MHz, $CDCl_3$) δ 171.4 (C11), 84.6 (C2), 71.3 (C5), 55.9 (C4), 47.6 (C3), 39.6 (C6), 39.0 (C1), 37.0 (C7), 29.7 (C9), 20.9 (C12), 19.3 (C8), 18.8 (C10).

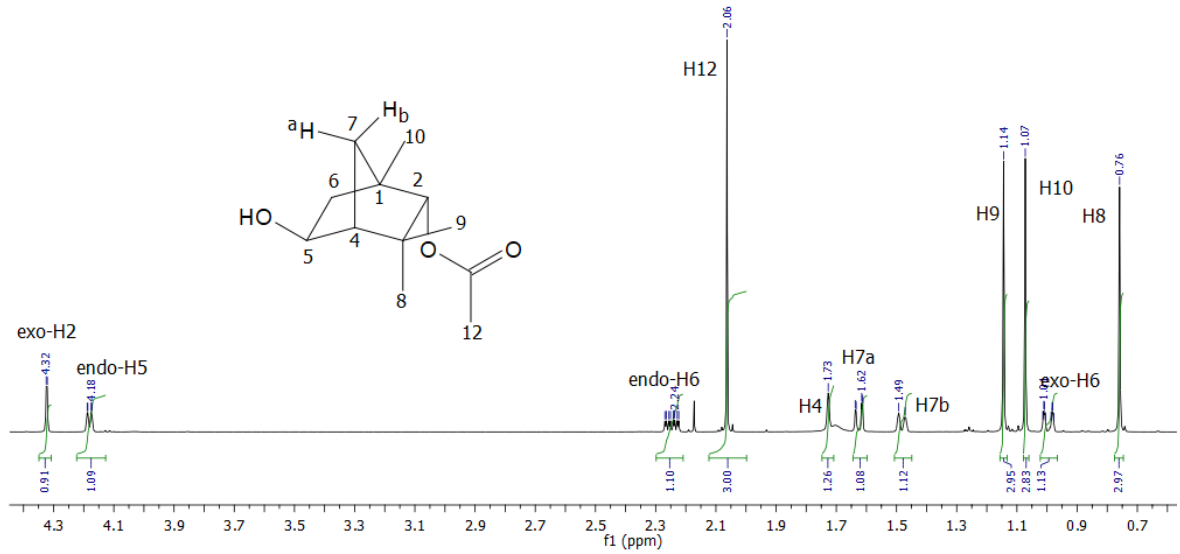

(a)

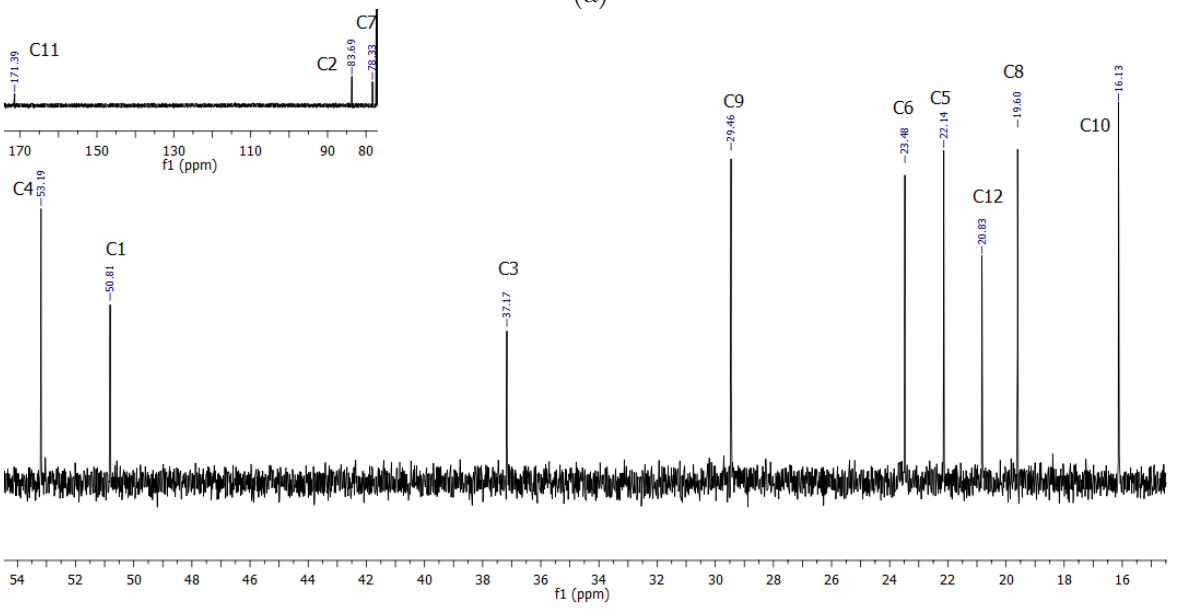

(b)

Figure B1: ^{1}H NMR (a) and ^{13}C NMR (b) spectrum spectrum of 5-*exo*-hydroxyfenchyl acetate. Data matched previously reported literature.[101]

Table B2: Comparison of Experimental NMR data of 5-*exo*-hydroxyfenchyl acetate to the literature.[101]

Position	Experimental δ_H (ppm)	Literature[101] δ_H (ppm)
exo-H2	4.32	4.32
endo-H5	4.18	4.18
endo-H6	2.25	2.24
H12	2.06	2.06
H4	1.73	1.72
$H7_a$	1.62	1.61
$H7_b$	1.48	1.48
H9	1.14	1.14
H10	1.07	1.07
exo-H6	1.00	0.99
H8	0.76	0.75

(7*S*)-hydroxyfenchyl acetate ^{1}H NMR (500 MHz, $CDCl_3$) δ 4.39 (d, J = 1.2 Hz, 1H, H2), 3.86 (s, 1H, H7), 2.08 (s, 3H, H12), 1.87 – 1.57 (m, 4H, H4/H5/H6), 1.27 (m, 1H, H6), 1.12 (s, 3H, H9), 0.99 (s, 3H, H10), 0.80 (s, 3H, H8). ^{13}C NMR (126 MHz, $CDCl_3$) δ 171.4 (C11), 83.7 (C2), 78.3 (C7), 53.2 (C4), 50.8 (C1), 37.2 (C3), 29.5 (C9), 23.5 (C6), 22.1 (C5), 20.8 (C12), 19.6 (C8), 16.1 (C10).

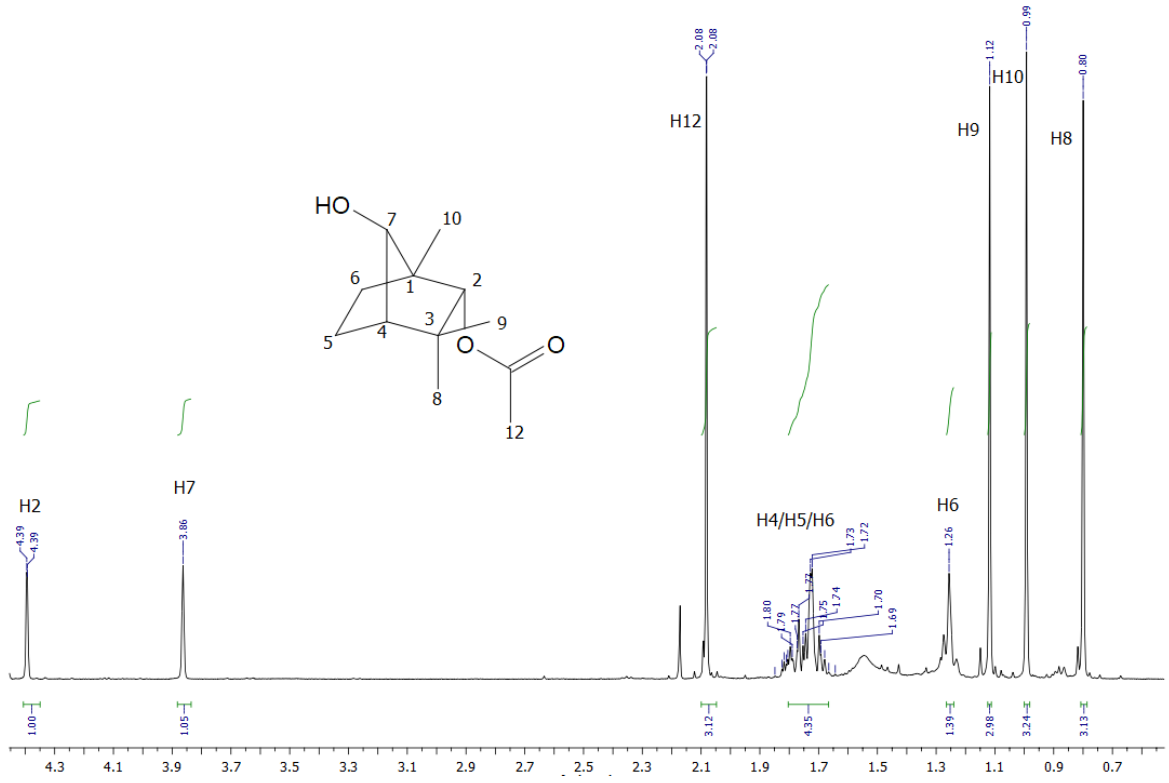

(a)

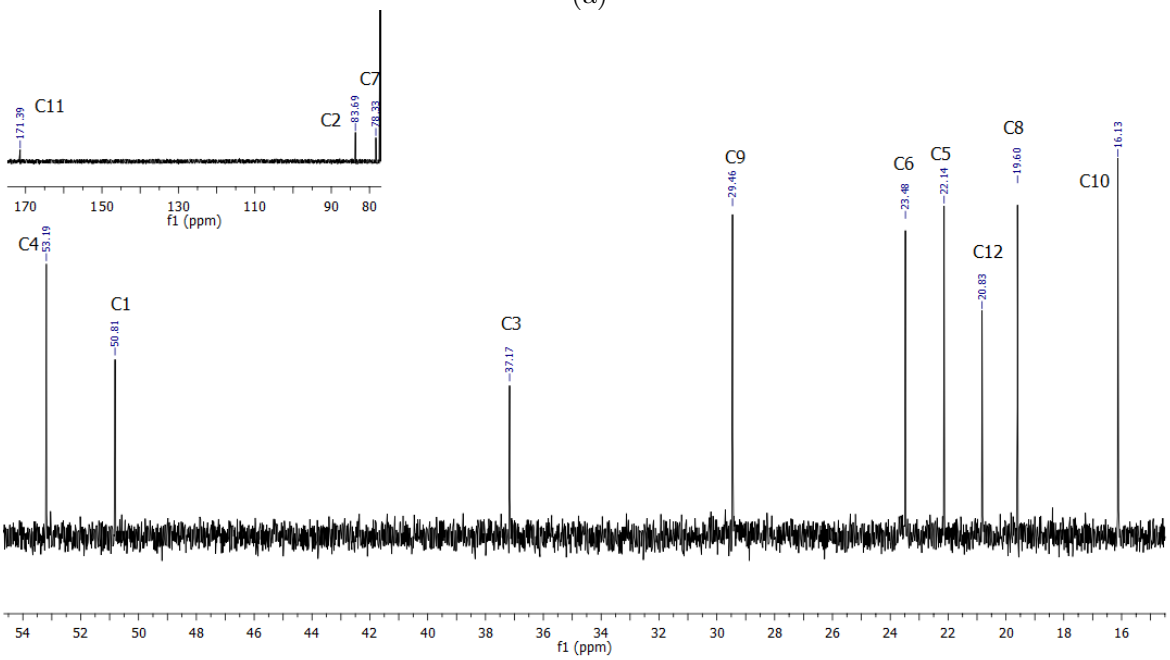

(b)

Figure B2: ^{1}H NMR (a) and ^{13}C NMR (b) spectrum spectrum of (7*S*)-hydroxyfenchyl acetate.

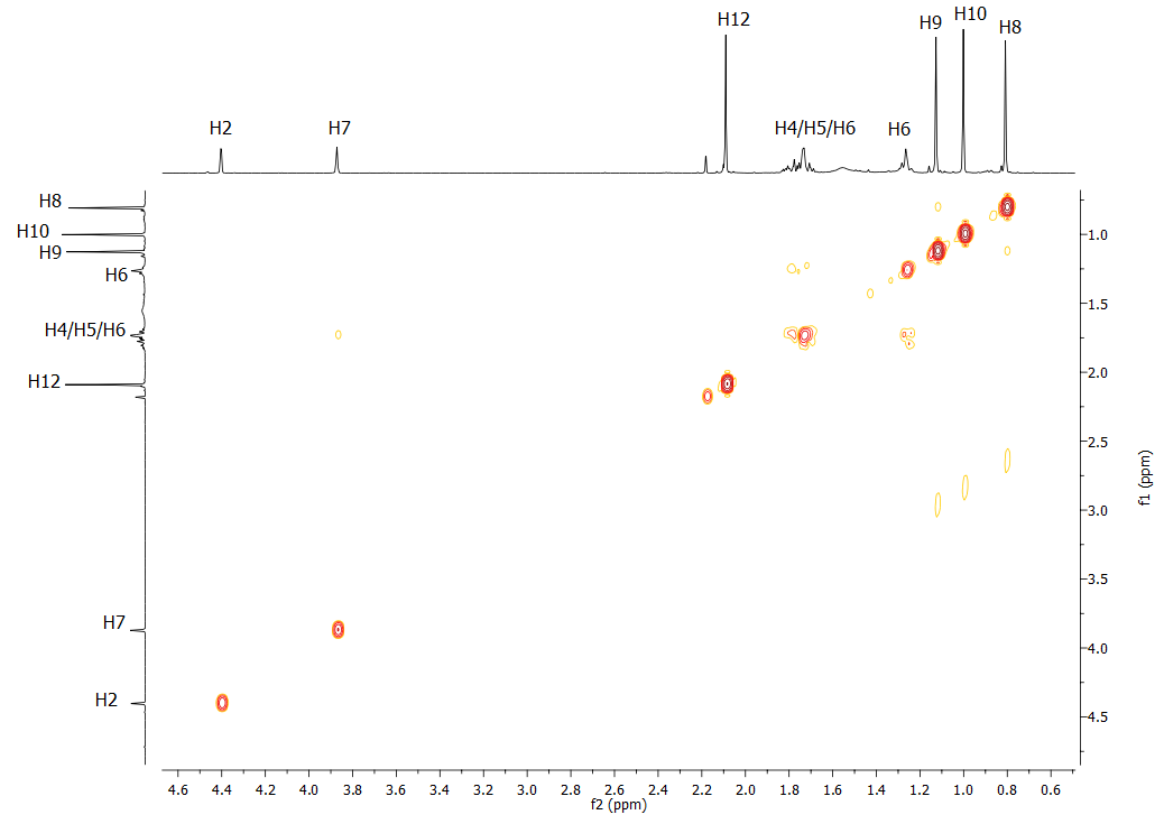

(a)

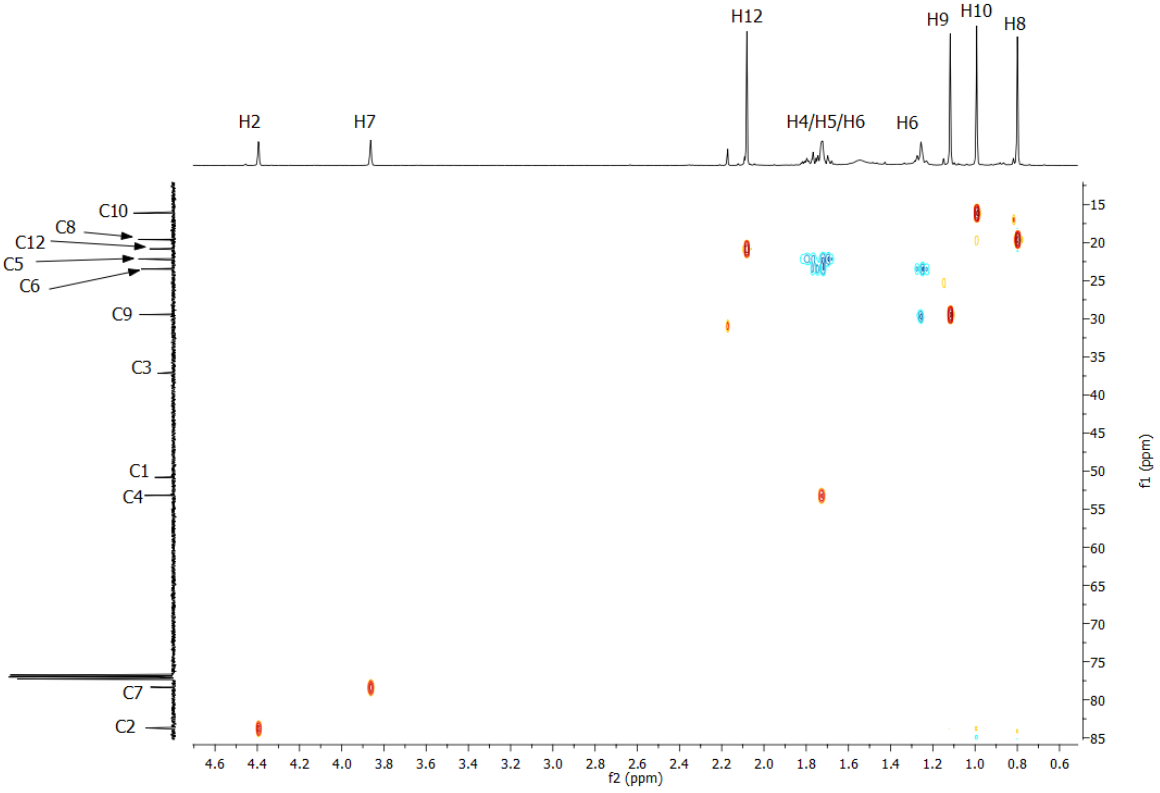

(b)

Figure B3: (a)^{1}H-^{1}H COSY and (b) ^{1}H-^{13}C HSQC NMR data for (7*S*)-hydroxyfenchyl acetate.

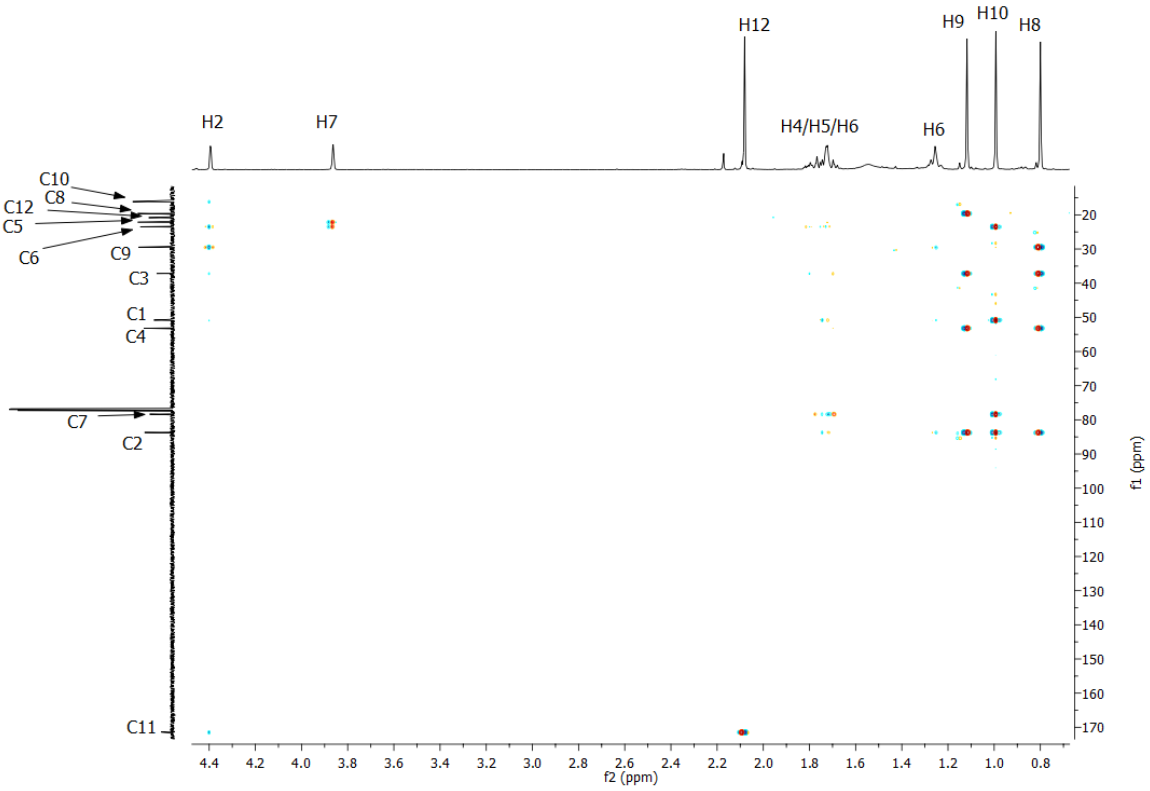

Figure B4: ^{1}H-^{13}C HMBC for (7*S*)-hydroxyfenchyl acetate.

Mass Spectra Analysis of Fenchyl Acetate Oxidation Products

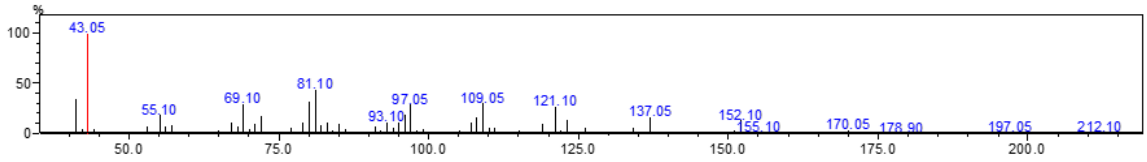

(a) Mass spectra of 5-*exo*-hydroxyfenchyl acetate with $m/z = 212.1$ and $t_R = 6.55$ min.

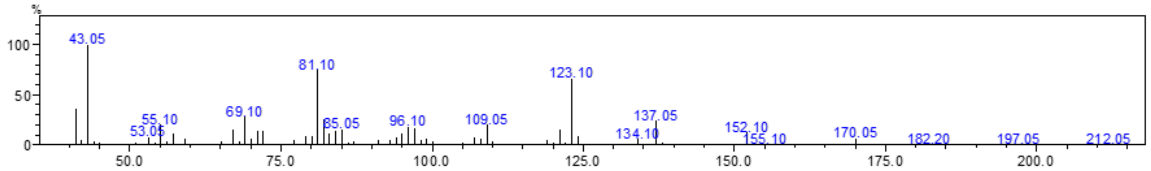

(b) Mass spectra of (7*S*)-hydroxyfenchyl acetate with $m/z = 212.1$ and $t_R = 6.72$ min.

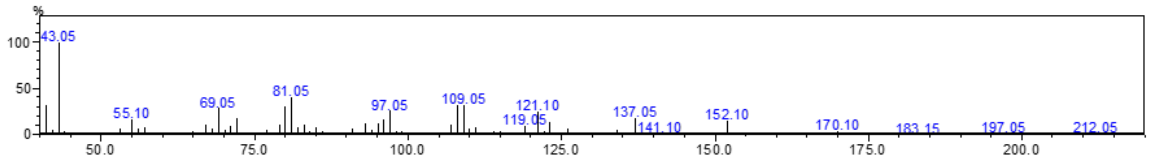

(c) Mass spectra of 5-*exo*-/6-*exo*hydroxyfenchyl acetate with $m/z = 212.1$ and $t_R = 6.55$ min.

Figure B5: Mass spectra of oxidation products of fenchyl acetate by $P450_{cam}$-Y96A and WT-$P450_{cam}$.

NMR Analysis of Fenchone Oxidation Products

5-*exo*-hydroxyfenchone ^{1}H NMR (500 MHz, $CDCl_3$) δ 4.38 (d, J = 6.4 Hz, 1H, *endo*-H5), 2.14 (s, 1H, H4), 2.07 (dd, J = 10.9, 1.9 Hz, 1H, H7b), 1.89 (ddd, J = 14.2, 6.5, 2.3 Hz, 1H, *exo*-H6), 1.74 (d, J = 10.8 Hz, 1H, H7a), 1.46 (d, J = 14.1 Hz, 1H, *endo*-H6), 1.15 (s, 3H, H10), 1.06 (s, 3H, H8/H9), 1.03 (s, 3H, H8/H9). ^{13}C NMR (126 MHz, $CDCl_3$) δ 222.0 (C2), 70.7 (C5), 53.6 (C1), 53.2 (C4), 45.3 (C3), 43.2 (C6), 37.5 (C7), 23.7 (C8/C9), 21.3 (C8/C9), 14.2 (C10).

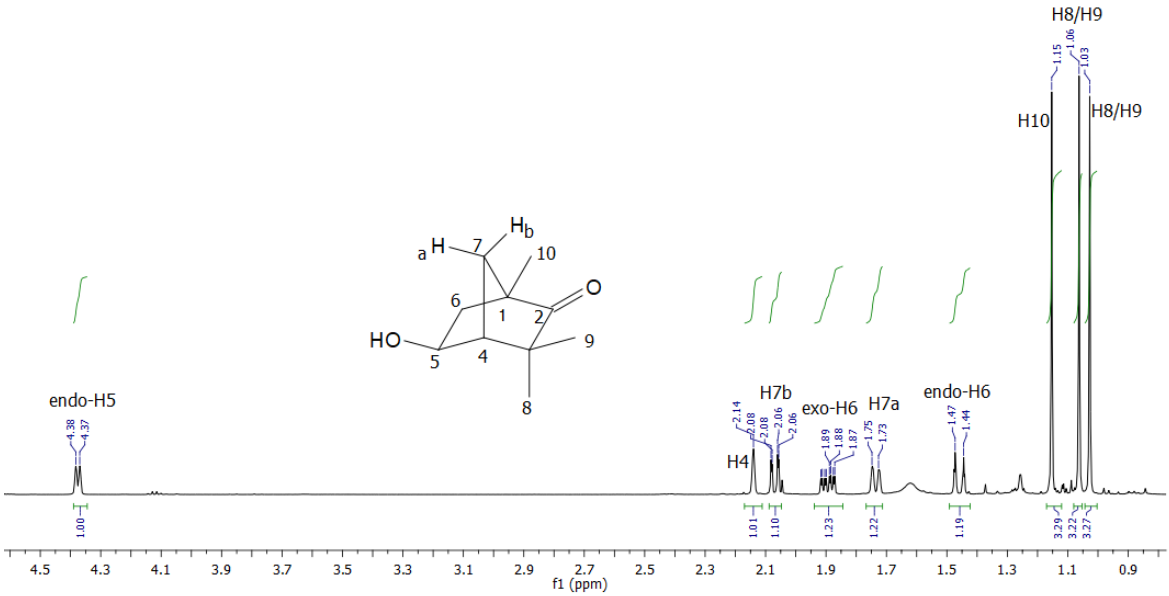

(a)

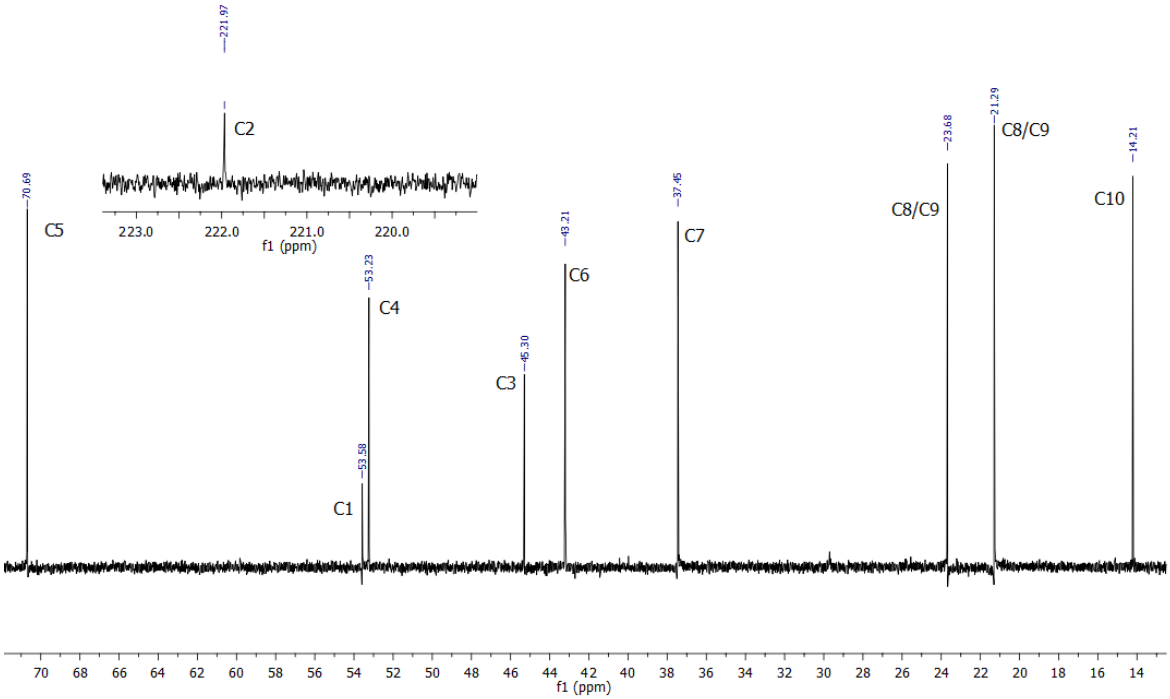

(b)

Figure B6: (a) ^{1}H and (b) ^{13}C NMR spectrum of 5-*exo*-hydroxyfenchone. Data matched previously reported literature.[101]

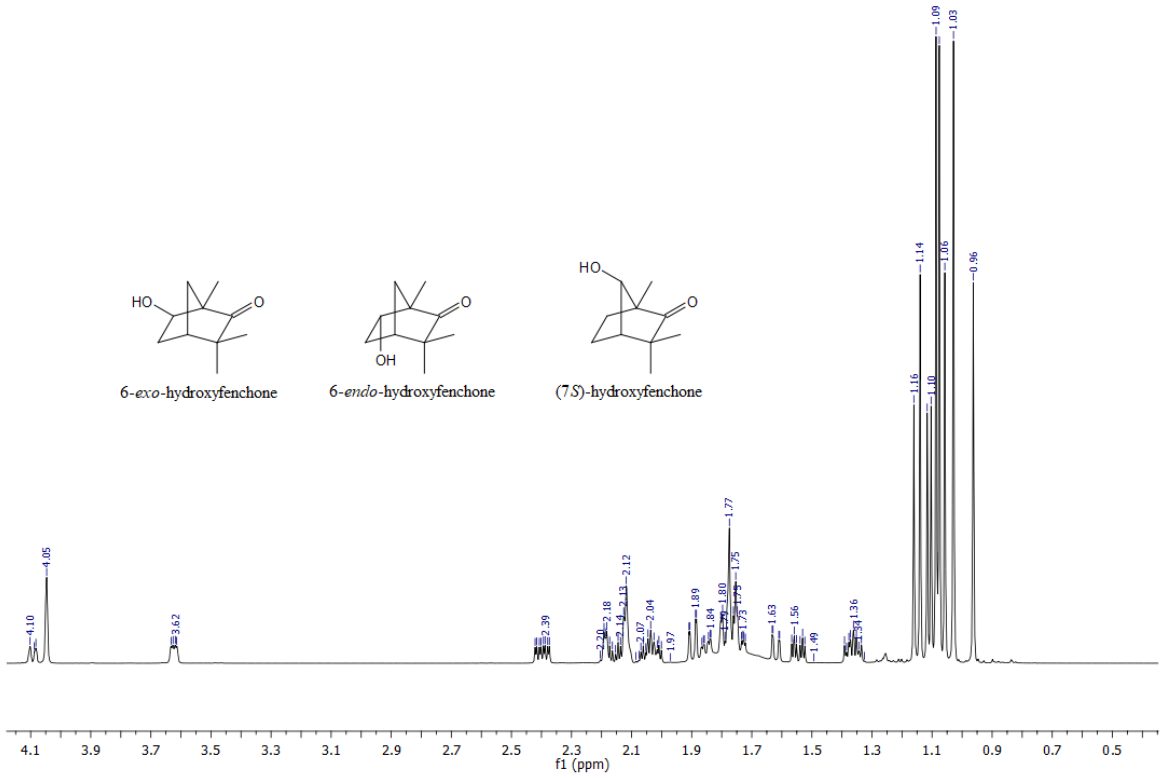

Figure B7: ^{1}H NMR spectrum of the isolated mixture from the Y96F and (+)-Fenchone enzyme turnover that contains 6-*endo*-, 6-*exo*- and (7S)-hydroxyfenchone.

Table B3: Comparison of Experimental NMR data of 5-*exo*-hydroxyfenchone to the literature.[101]

Position	Experimental δ_H (ppm)	Literature[101] δ_H (ppm)
endo-H5	4.38	4.37
H4	2.14	2.14
$H7_b$	2.07	2.07
exo-H6	1.89	1.89
$H7_a$	1.74	1.74
endo-H6	1.46	1.46
H10	1.15	1.15
H9	1.06	1.06
H10	1.03	1.03

Literature Data for Fenchone Oxidation Products

6-*endo*-hydroxyfenchone[140] ^{1}H NMR ($CDCl_3$) δ 1.10 (3H, s, H8), 1.12 (3H, s ,H9), 1.16 (3H, s, H10), 1.62 (1H, dd, J = 1.7, 11.0 Hz, $H7_b$), 1.74 (1H, ddd, J = 2.6, 3.7, 13.8, *endo*-H5), 1.85 (1H, ddd, J = 1.7 , 2.6 , 11.0, $H7_a$), 2.10 - 2.12 (1H, m, H4), 2.15 (1H, ddd, J = 4.3, 9.6, 13.8 Hz, *exo*-H5), 4.09 (1H, ddd, J = 1.7, 3.7, 9.6 Hz,*exo*-H6.)

EI-MS, *m/z* (rel. intensity): 168 $[M]^+$ (2), 153 $[M\text{-}CH_3]^+$ (1), 140 (1), 124 (8), 109 (4), 107 (5), 97 (9), 88 (35), 81 (100), 69 (21), 55 (7), 53 (6), 43 (6), 41 (19).

6-*exo*-hydroxyfenchone[140] ^{1}H NMR ($CDCl_3$) δ 0.96 (3H, s, H9), 1.06 (3H, s, H8), 1.14 (3H, s, H10), 1.55 (1H, ddd, J = 3.5, 4.5, 13.8 Hz, *exo*-H5), 1.76 (1H, dddd, J = 1.2, 1.5, 2.9 , 10.9 Hz, $H7_a$), 1.90 (1H, dd, J = 1.7, 10.9 Hz, $H7_b$), 2.18 - 2.20 (1H, m, H4), 2.40 (1H, ddd, J = 2.9, 6.9, 13.8 Hz), *endo*-H5), 3.62 (1H, ddd, J = 1.5, 3.5, 6.9 Hz, *emdo*-H6).

EI-MS, *m/z* (rel. intensity): 168 $[M]^+$ (18), 153 $[M\text{-}CH_3]^+$ (3), 140 (3), 124 (41), 109 (16), 107 (11), 97 (55), 96 (35), 88 (34), 81 (100), 70 (37), 69 (30), 55 (12), 53 (10), 43 (12), 41 (33).

Mass Spectra Analysis of Fenchone Oxidation Products

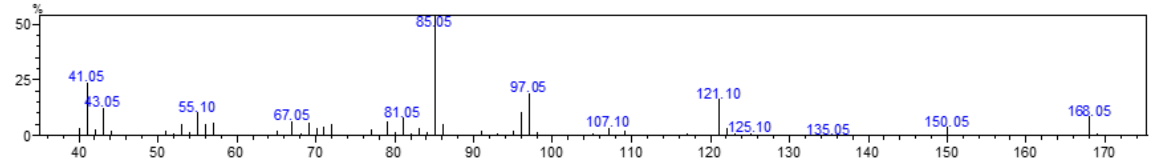

(a) Mass spectra of 5-*exo*-hydroxyfenchone with m/z = 168.05 and t_R = 8.85 min.

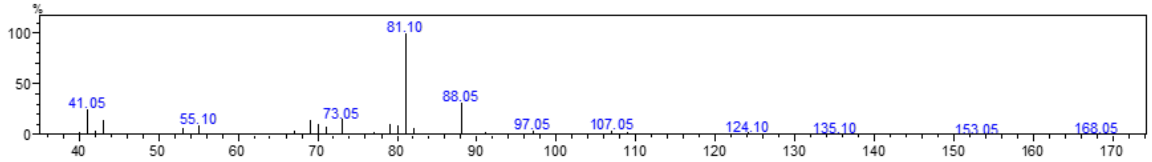

(b) Mass spectra of 6-*endo*-hydroxyfenchone with m/z = 168.05 and t_R = 8.53 min.

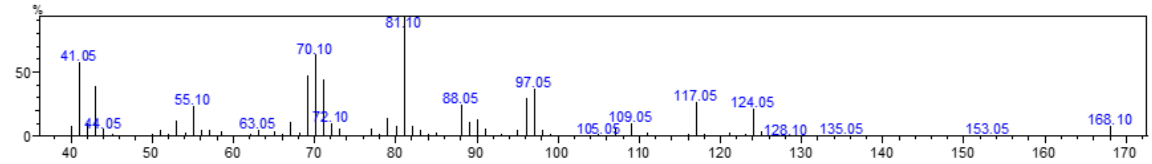

(c) Mass spectra of 6-*exo*-hydroxyfenchone with m/z = 168.05 and t_R = 8.69 min.

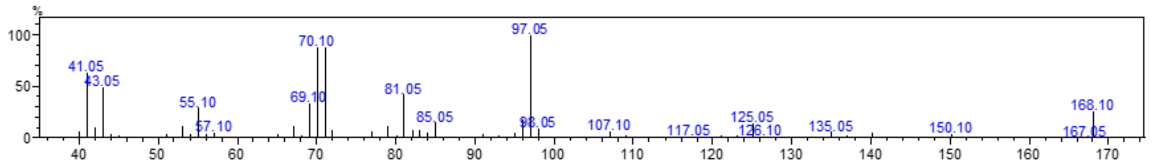

(d) Mass spectra of (7*S*)-hydroxyfenchone with m/z = 168.05 and t_R = 8.95 min.

Figure B8: Mass spectra of oxidation products of fenchone by $P450_{cam}$-Y96F. Data for 5-*exo*-, 6-*endo*-, 6-*exo*-hydroxyfenchone is in good agreement with what was previously reported in the literature. [101,140]

NMR Analysis of Isophorone Oxidation Products

4-hydroxyisophorone ^{1}H NMR (500 MHz, $CDCl_3$) δ 5.86 (s, 1H, H2), 4.03 (s, 1H, H4), 2.41 (d, J = 16.3 Hz, 1H, H6), 2.21 (d, J = 16.3 Hz, 1H, H6), 2.06 (s, 3H, H7), 1.07 (s, 3H, H8/H9), 1.02 (s, 3H, H8/H9). ^{13}C NMR (126 MHz, $CDCl_3$) δ 202.12 (C1), 164.61 (C3), 128.64 (C2), 79.28 (C4), 51.62 (C6), 41.17 (C5), 29.57 (C8/C9), 24.24 (C8/C9), 24.01 (C7). $[\alpha]_D^{20}$ = +113.2 (c= 1.00, MeOH)

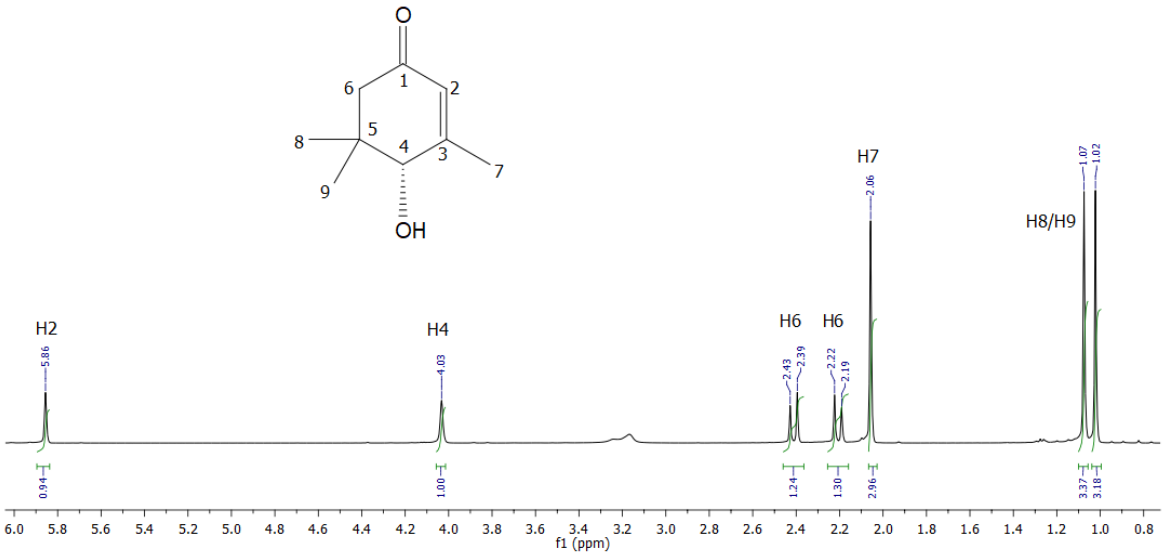

(a)

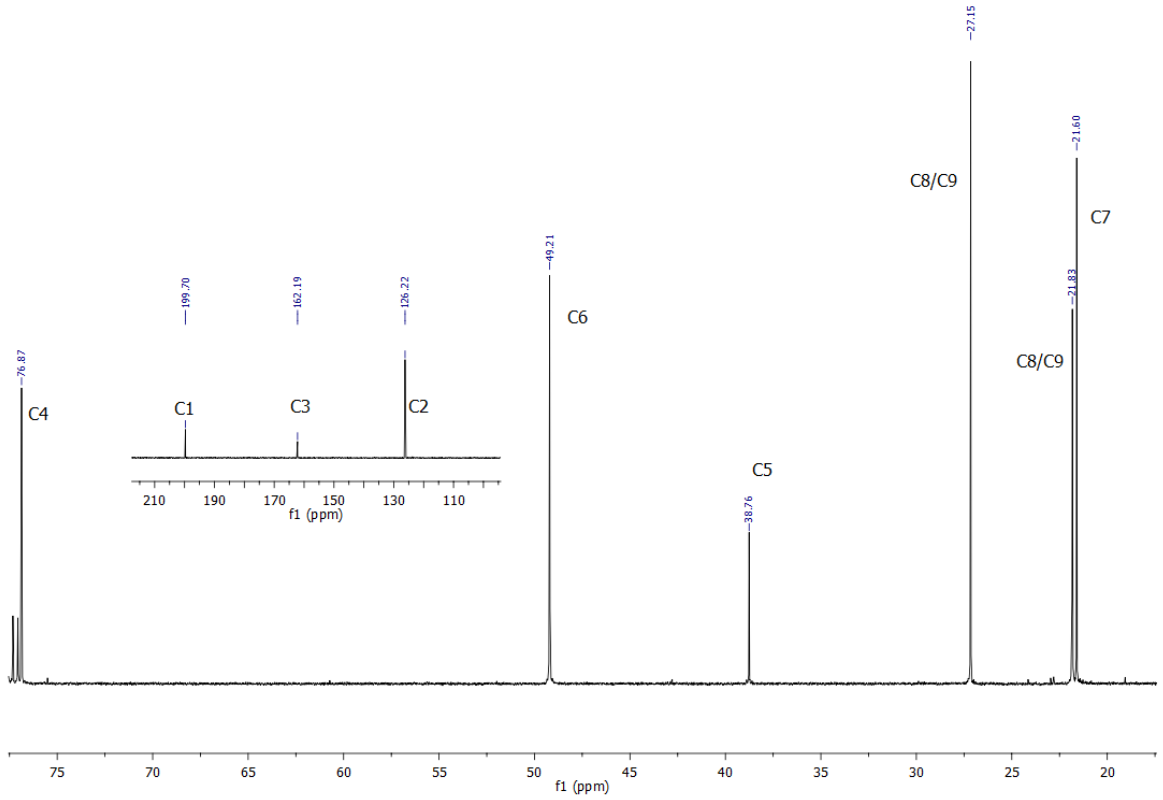

(b)

Figure B9: (a) ^{1}H NMR and (b) ^{13}C NMR spectrum spectrum for 4-hydroxyisophorone.

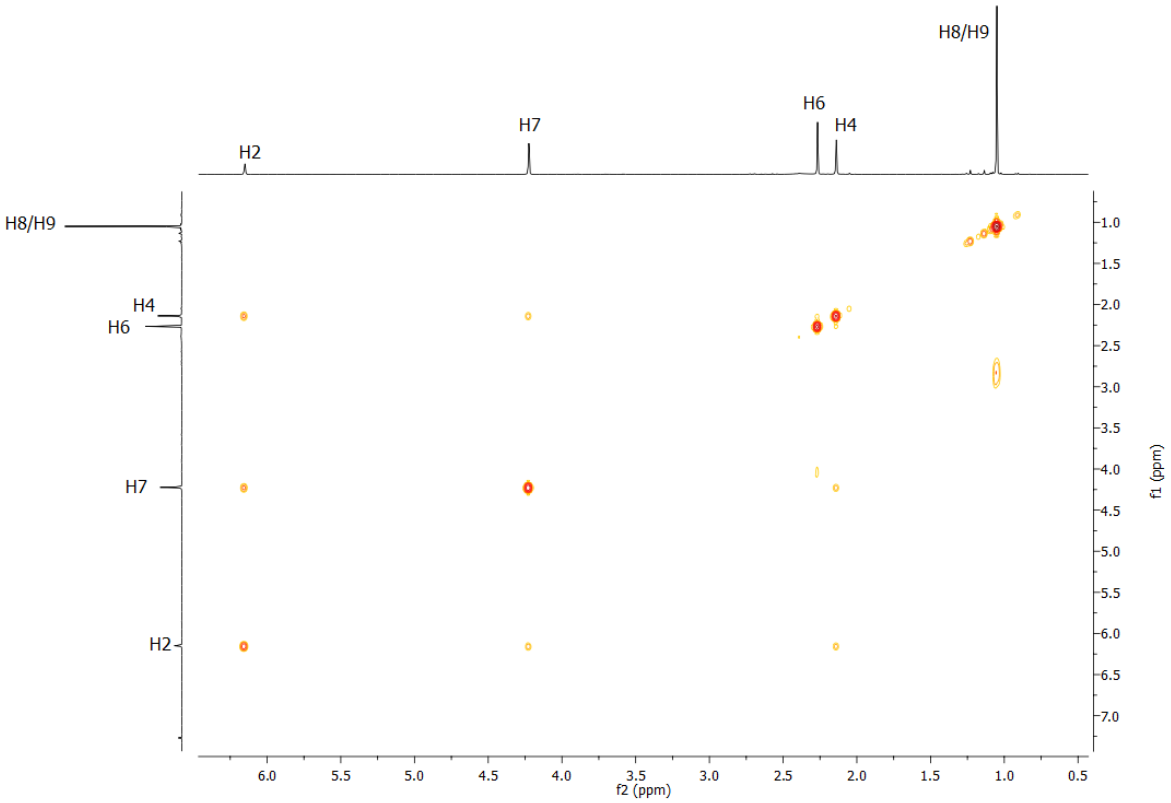

(a)

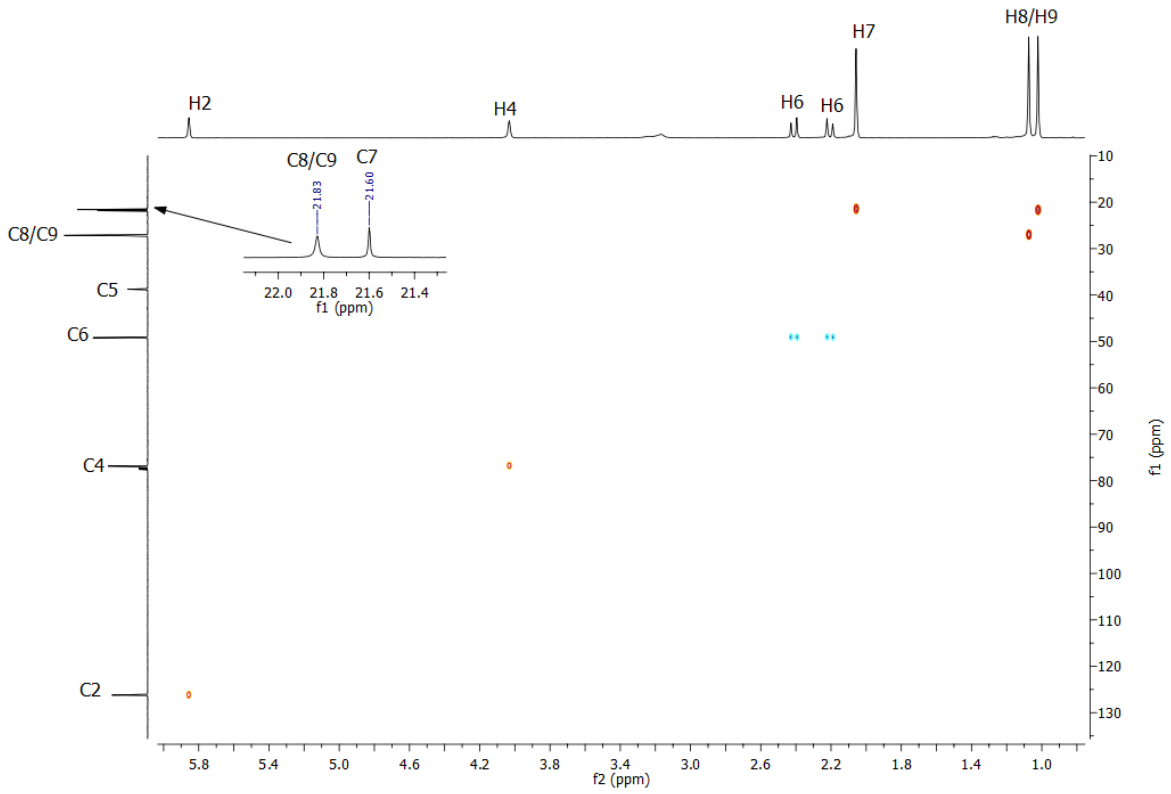

(b)

Figure B10: (a)^{1}H-^{1}H COSY and (b) ^{1}H-^{13}C HSQC NMR data for 4-hydroxyisophorone.

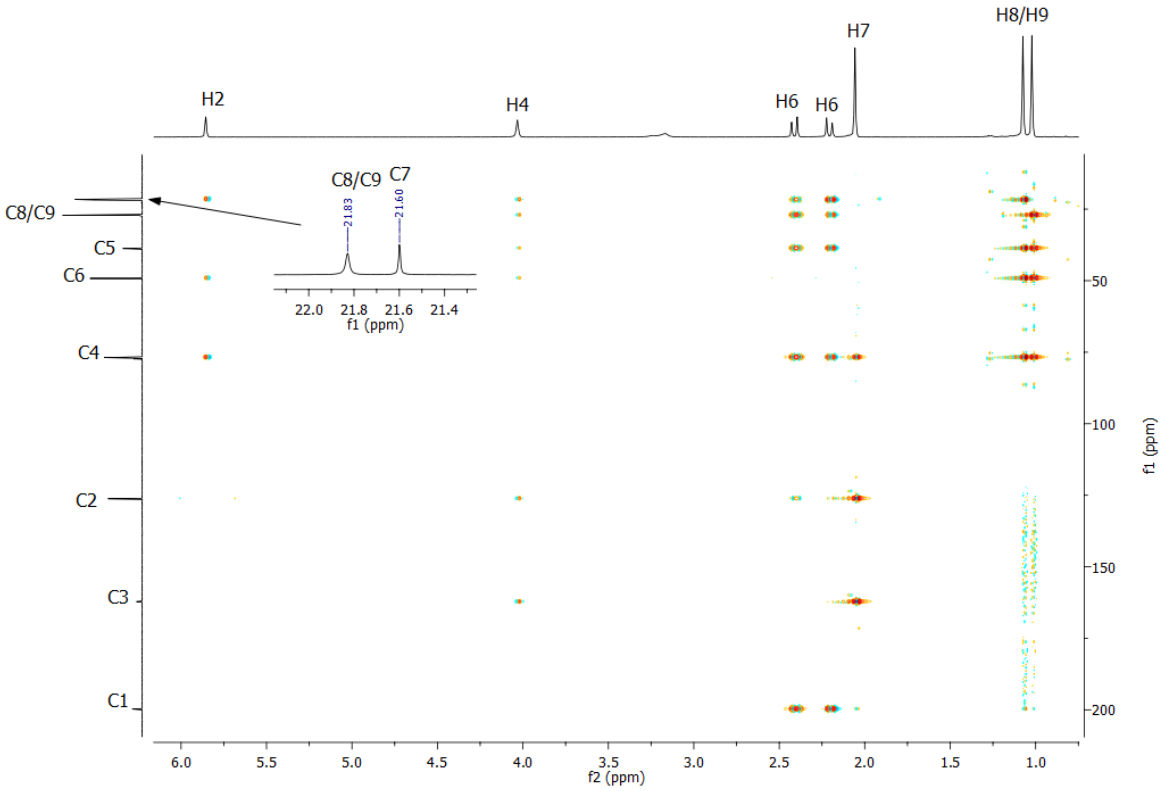

Figure B11: ^{1}H-^{13}C HMBC for 4-hydroxyisophorone.

7-hydroxyisophorone ^{1}H NMR (500 MHz, $CDCl_3$) δ 6.15 (s, 1H, H2), 4.22 (s, 2H, H7), 2.27 (s, 3H, H6), 2.14 (s, 2H, H4), 1.05 (s, 6H, H8/H9). ^{13}C NMR (126 MHz, $CDCl_3$) δ 200.09 (C1), 162.22 (C3), 122.11 (C2), 65.03 (C7), 51.56 (C6), 40.26 (C4), 33.66 (C5), 28.23 (C8/C9).

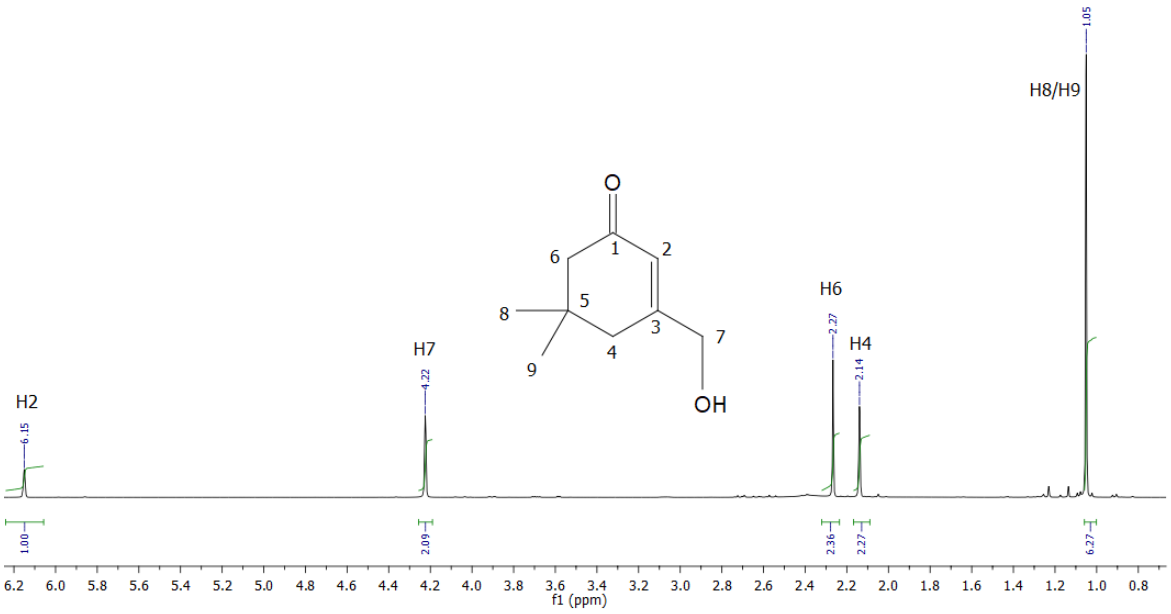

(a)

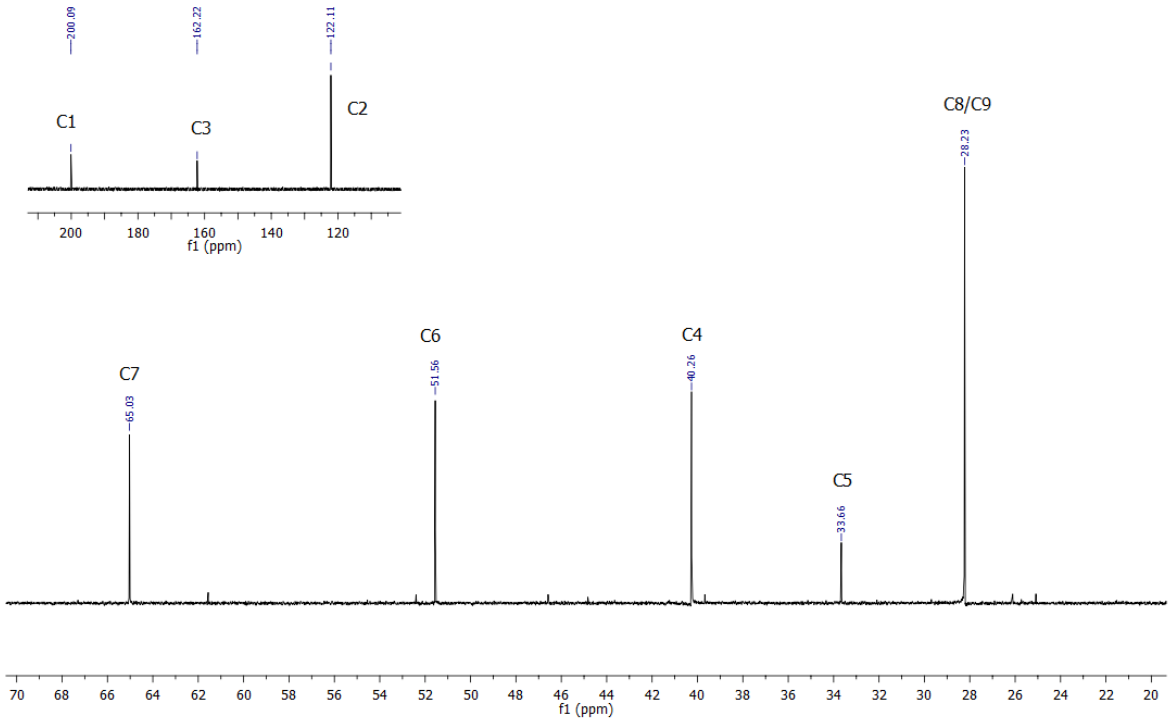

(b)

Figure B12: (a) ^{1}H NMR and (b) ^{13}C NMR spectrum spectrum for 7-hydroxyisophorone.

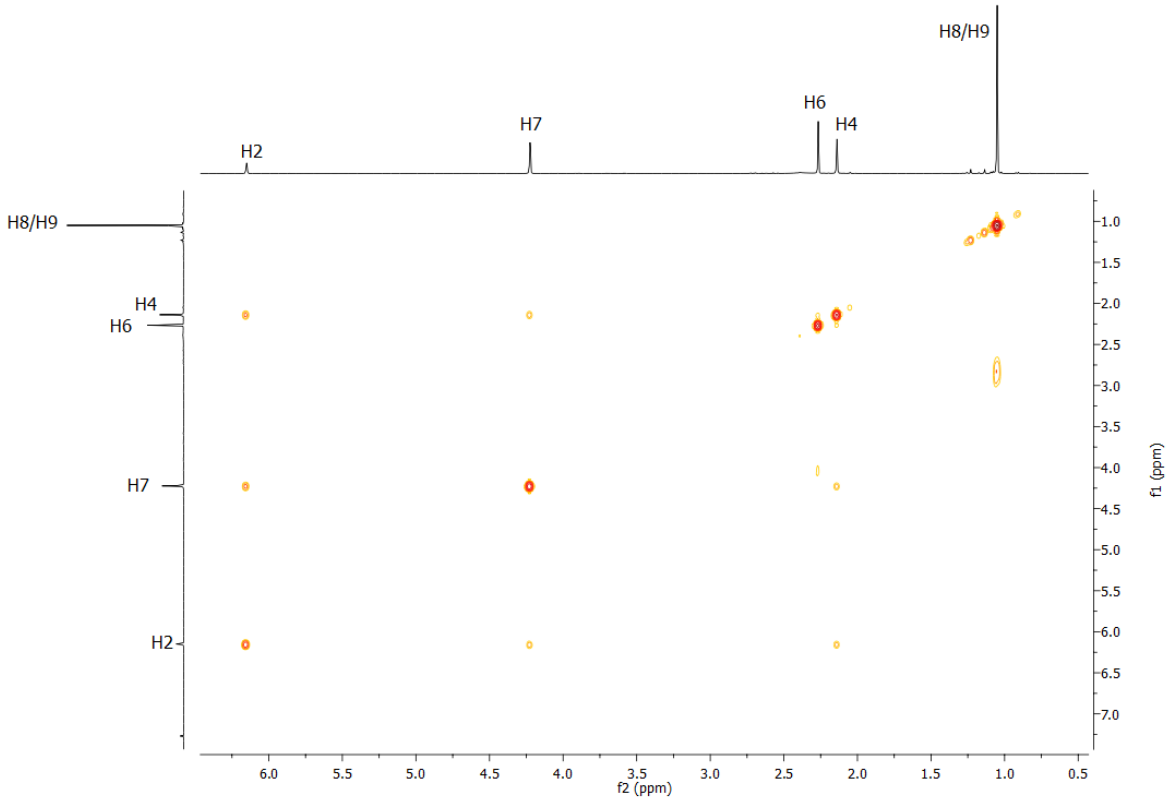

(a)

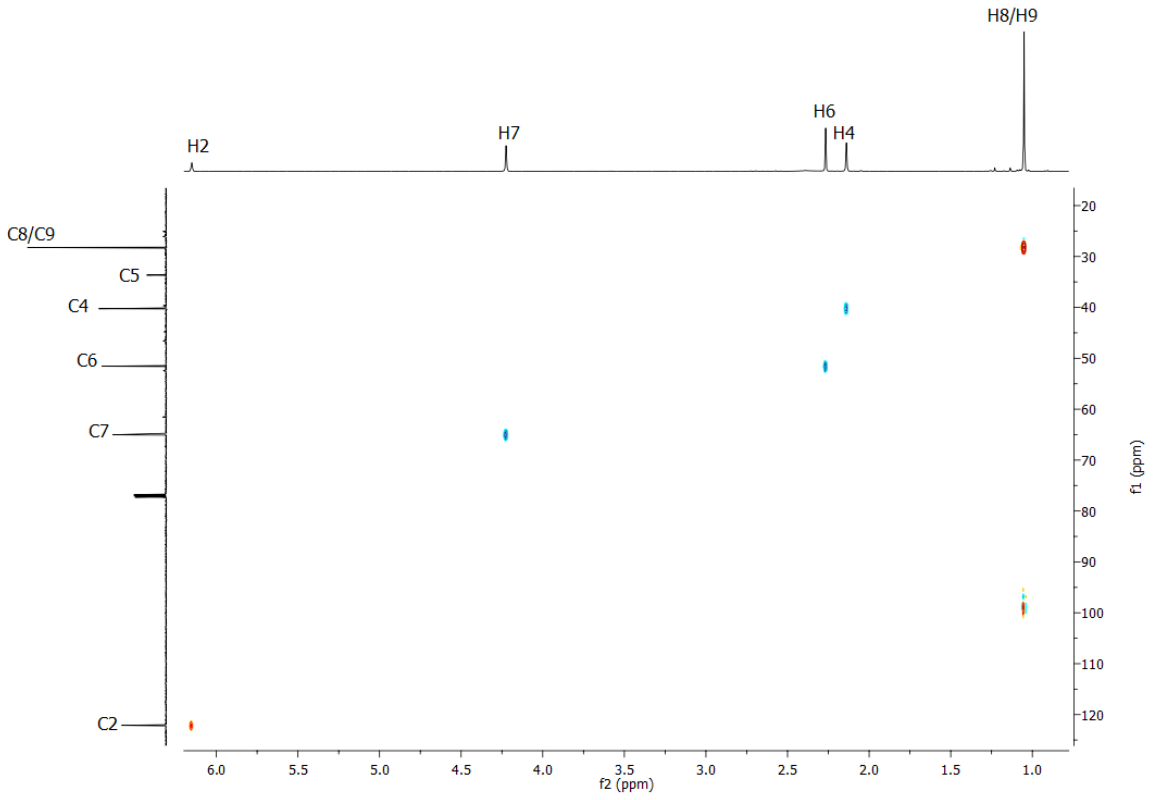

(b)

Figure B13: (a)^{1}H-^{1}H COSY and (b) ^{1}H-^{13}C HSQC NMR data for 7-hydroxyisophorone.

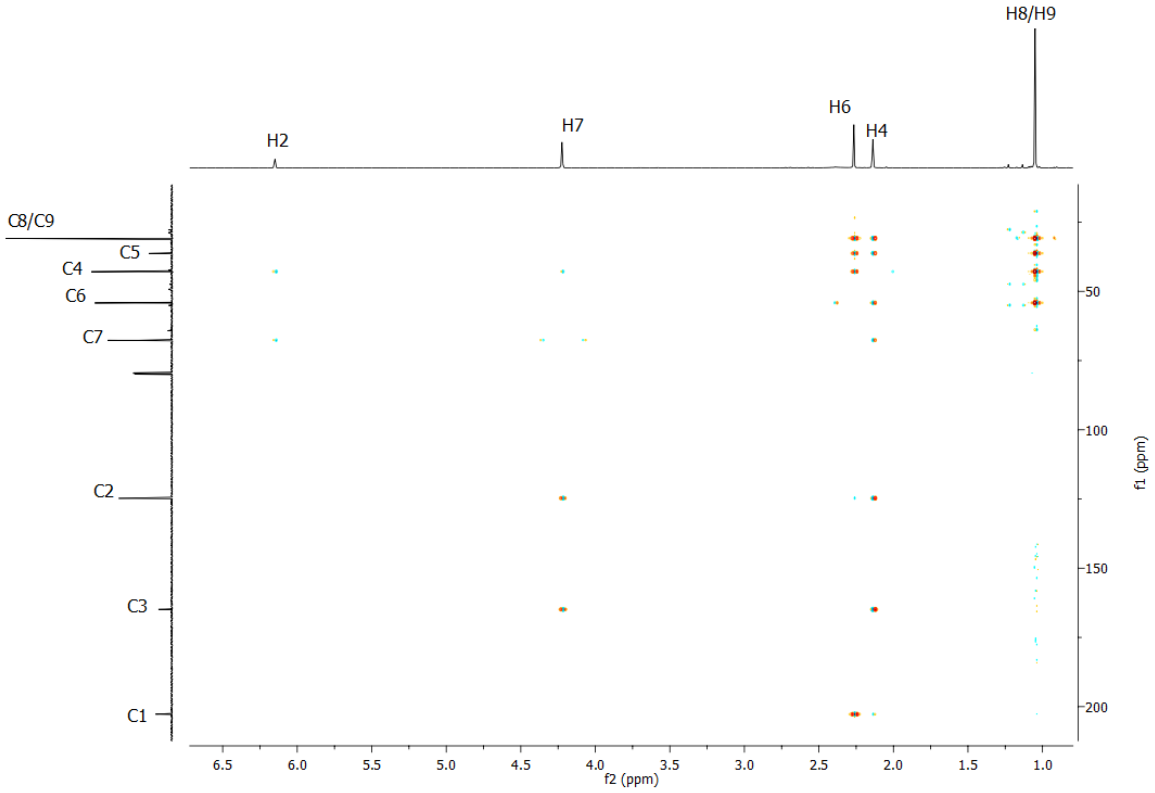

Figure B14: ^{1}H-^{13}C HMBC for 7-hydroxyisophorone.

Mass Spectra Analysis of Isophorone Oxidation Products

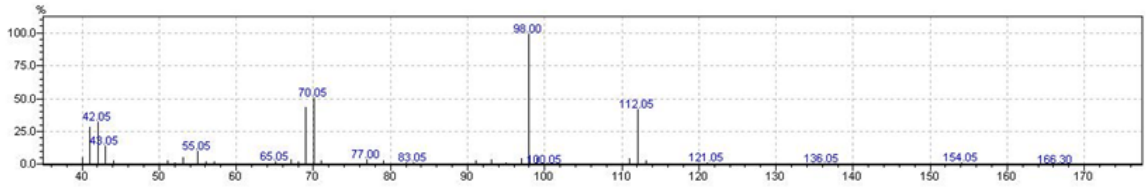

(a) Mass spectra of 4-hydroxyisophorone with $m/z = 154.05$ with $t_R = 9.15$ min.

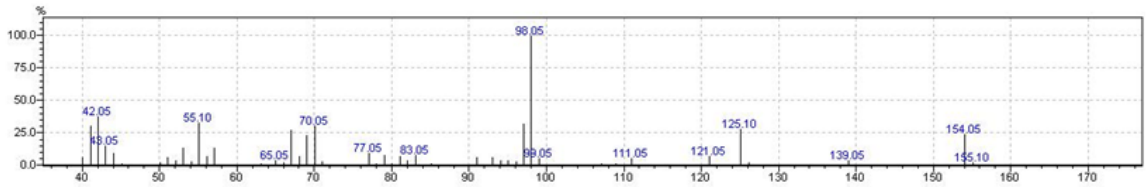

(b) Mass spectra of 7-hydroxyisophorone with $m/z = 154.05$ with $t_R = 10.6$ min.

Figure B15: Mass spectra of (a) 4-hydroxyisophorone and (b) 7-hydroxyisophorone.

Mass Spectra Analysis of 1,8-Cineole Oxidation Products

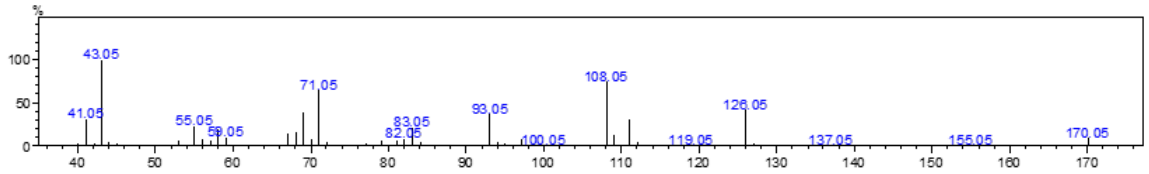

(a) Mass spectra of 6α-hydroxy-1,8-cineole with $m/z = 170.05$ and $t_R = 7.7$ min.

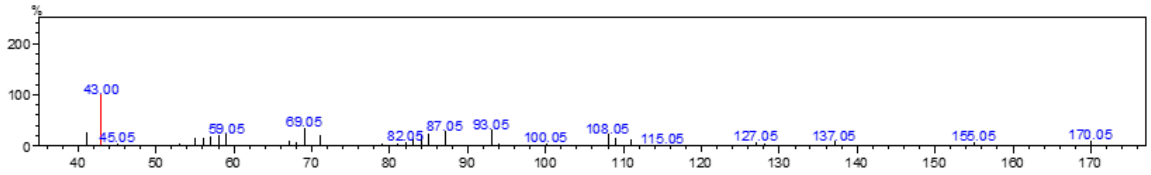

(b) Mass spectra of 5-α-hydroxy-1,8-cineole with $m/z = 170.05$ and $t_R = 8.5$ min.

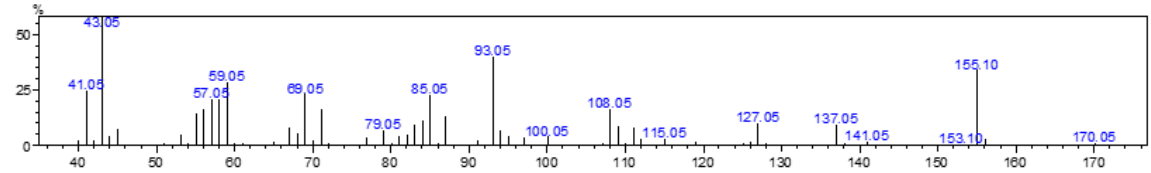

(c) Mass spectra of 5-β-hydroxy-1,8-cineole with $m/z = 168.05$ and $t_R = 8.2$ min.

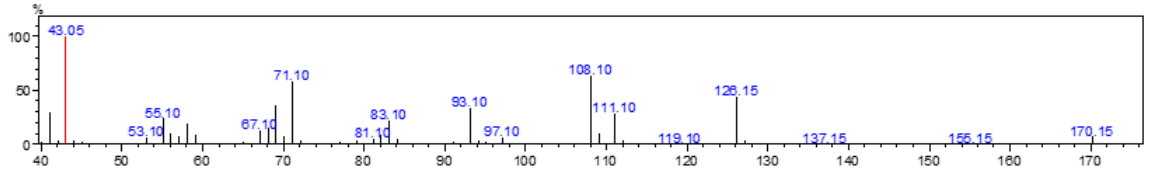

(d) Mass spectra of 6-β-hydroxy-1,8-cineole with $m/z = 170.15$ and $t_R = 7.5$ min.

Figure B16: Mass spectra of (a) 6-α-hydroxy-1,8-cineole, (b) 5-α-hydroxy-1,8-cineole and (c) 5-β-hydroxy-1,8-cineole and (d) 6-β-hydroxy-1,8-cineole

Literature Data for 1,4-Cineole Oxidation Products

8-hydroxy-1,4-cineole[145] ^{1}H NMR ($CDCl_3$, 400 MHz) δ 1.25 (s, 6H, CH_3, H9 and H10), 1.43 (s, 3H, CH_3, H7). ^{13}C NMR ($CDCl_3$, 100 MHz) δ 21.1, 25.3 (2 × CH_3), 31.9 (2 × CH_2), 37.5 (2 × CH_2), 71.6, 83.9, 91.7. GC-MS (*m/z*): 170 (M+, 7), 155 (4), 137 (7), 112 (13), 111 (39), 110 (18), 109 (12), 97 (10), 95 (9), 93 (15), 85 (13), 83 (8), 79 (9), 69 (17), 67 (12), 59 (100), 55 (19), 43 (96).

2-β-hydroxy-1,4-cineole[145] ^{1}H NMR ($CDCl_3$, 400 MHz) δ 0.94 and 0.95 (2 × d, J = 6.9 Hz, 2 × 3H, CH_3, H9 and H10), 1.40 (s, 3H, CH_3, H7), 2.04 (m, 2H), 3.73 (t, J = 7.5 Hz, 1H). ^{13}C NMR ($CDCl_3$, 100 MHz) δ 16.4, 18.18, 18.21, 32.60, 32.63, 32.9, 45.2, 76.9, 85.6, 88.8. GC-MS (*m/z*): 170 (M+, 4), 153 (4), 137 (2), 127 (6), 125 (9), 112 (17), 109 (10), 97 (13), 95 (10), 86 (10), 83 (19), 71 (23), 43 (100).

3-β-hydroxy-1,4-cineole[145] ^{1}H NMR ($CDCl_3$, 400 MHz) δ 0.91 and 1.00 (2 × dd, J = 6.9 and 0.7 Hz, 2 × 3H, H9 and H10), 1.45 (s, 3H, CH_3, H7), 1.70 (td, J = 12.2 and 3.4 Hz, 1H), 2.18 (dd, J = 13.3 and 6.9 Hz, 1H), 2.36 (septet, J = 6.9 Hz, 1H), 3.89 (ddd, J = 9.3, 6.8 and 2.0 Hz, 1H). GC-MS (*m/z*): 170 (M+, 7), 155 (1), 139 (1), 137 (3), 127 (8), 125 (6), 111 (8), 109 (8), 86 (54), 84 (43), 71 (58), 43 (100).

3-α-hydroxy-1,4-cineole[147] ^{1}H NMR ($CDCl_3$, 500 MHz) δ 0.98 and 0.99 (2 × d, J = 6.9 Hz, 2 × 3H, CH_3, H9 and H10), 1.34 (s, 3H, CH_3, H7), 1.38 (dd, J = 12.5 and 3.1 Hz, 1H, H2), 1.46 – 1.59 (m, 3H, OH, 2 × 1H, H5 and H6), 1.75 (m, 1H, H6), 1.98 – 2.06 (m, 2H, H8 and H2), 2.25 (ddd, J = 11.8, 9.4 and 4.3 Hz, 1H, H5), 4.17 (dddd, J = 9.6, 4.6, 3.1 and 1.6 Hz, 1H, H3). 13C NMR (CDCl3, 125 MHz) δ 17.9, 18.3, 21.7, 25.3, 32.3, 37.3, 47.9, 74.9, 83.0, 90.4. GC-MS (*m/z*): 170 (M+, 8), 137 (2), 128 (1), 127 (8), 125 (9), 111 (9), 109 (7), 97 (6), 95 (4), 87 (22), 86 (55), 71 (55), 43 (100).

9-hydroxy-1,4-cineole[145] ^{1}H NMR ($CDCl_3$, 400 MHz) δ 0.83 (d, J = 7.0 Hz, 3H, CH_3, H10), 1.43 (s, 3H, 3H, CH_3, H7), 3.48 (dd, J = 11.2 and 4.2 Hz, 1H), 3.70 (dd, J = 11.1 and 9.6 Hz, 1H). GC-MS (*m/z*): 170 (M+, 14), 155 (1), 141 (11), 139 (12), 137 (3), 123 (13), 111 (38), 97 (10), 95 (18), 93 (17), 91 (7), 87 (35), 83 (15), 81 (13), 79 (19), 69 (29), 67 (28), 55 (52), 43 (100).

Mass Spectra Analysis of 1,4-Cineole Oxidation Products

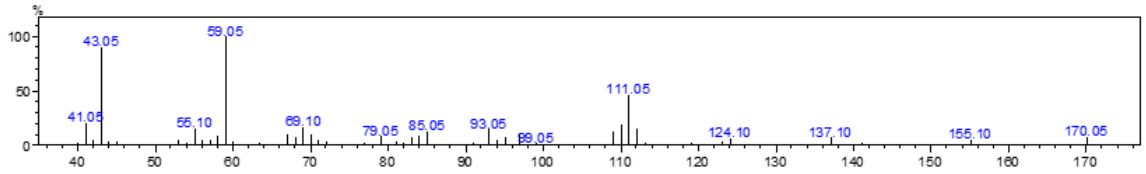

(a) Mass spectra of 8-hydroxy-1,4-cineole with $m/z = 170.05$ and $t_R = 6.0$ min.

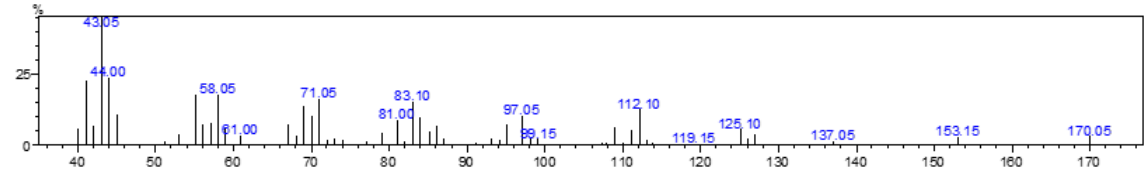

(b) Mass spectra of 2-β-hydroxy-1,4-cineole with $m/z = 170.05$ and $t_R = 7.15$ min.

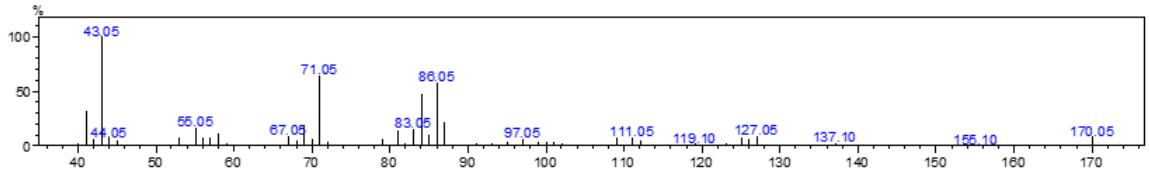

(c) Mass spectra of 3-β-hydroxy-1,4-cineole with $m/z = 170.05$ and $t_R = 6.85$ min.

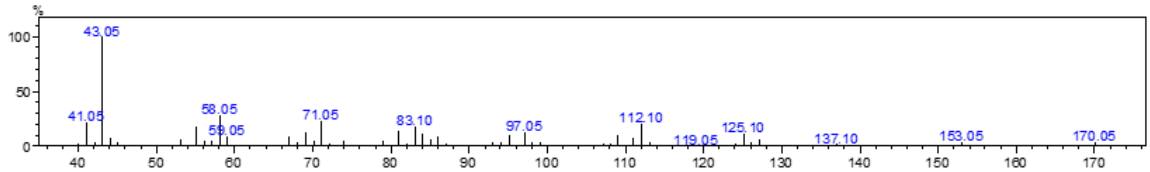

(d) Mass spectra of 2-α-hydroxy-1,4-cineole with $m/z = 170.05$ and $t_R = 7.65$ min.

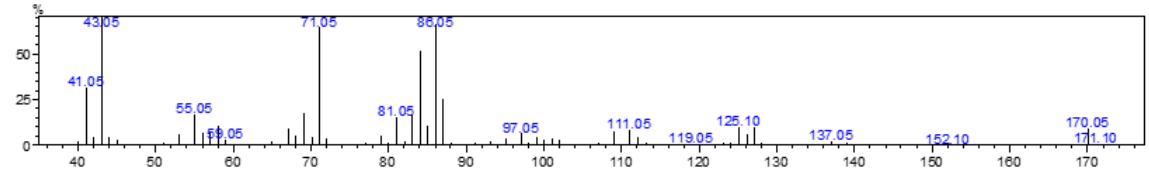

(e) Mass spectra of 3-α-hydroxy-1,4-cineole with $m/z = 170.05$ and $t_R = 7.3$ min.

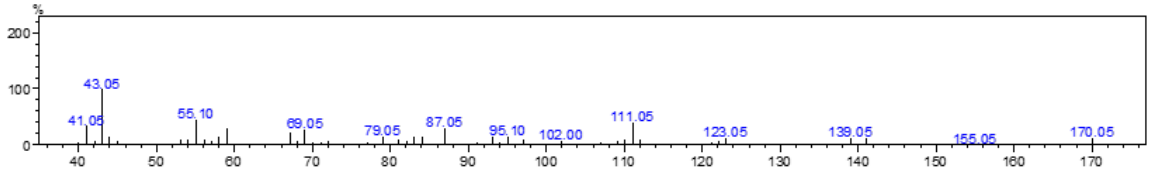

(f) Mass spectra of 9-hydroxy-1,4-cineole with $m/z = 170.05$ and $t_R = 8.25$ min.

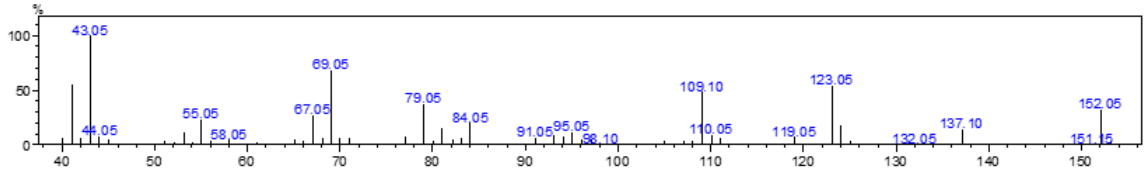

(g) Mass spectra of Desaturation Product A with $m/z = 152.05$ and $t_R = 4.15$ min.

Figure B17: Mass spectra of (a) 8-hydroxy-1,4-cineole, (b) 2β-hydroxy-1,4-cineole and (c) 3β-hydroxy-1,4-cineole, (d) 2α-hydroxy-1,4-cineole, (e) 3α-hydroxy-1,4-cineole, (f) 9-hydroxy-1,4-cineole and (g) Desaturation product **A**.

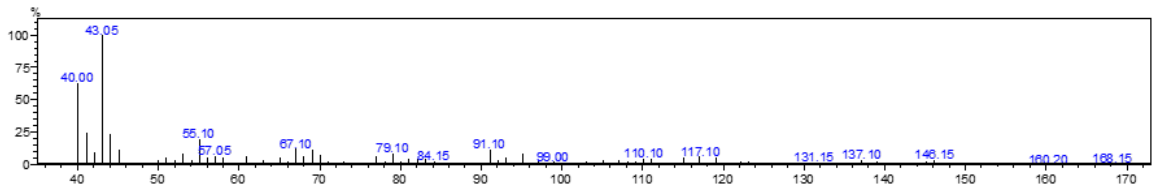

(a) Mass spectra of unknown 1,4-cineole further oxidation product (#) with m/z = 168.15 and t_R = 7.49 min.

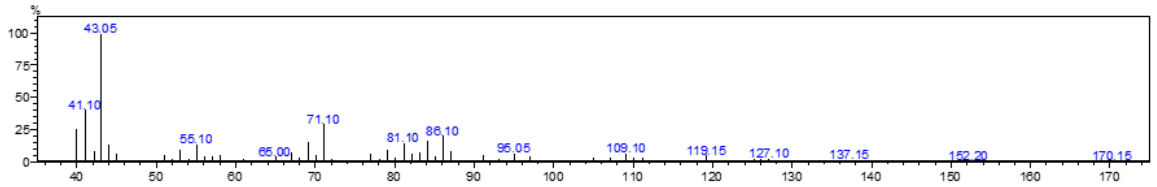

(b) Mass spectra of unknown 1,4-cineole oxidation product ($) and m/z = 170.15 with t_R = 7.23 min.

Figure B18: Mass spectra of unknown oxidation products of 1,4-cineole by $P450_{cam}$ and $P450_{BM3}$ mutants.

Appendix C Data for Chapter 5

C.1 Mass Spectra Analysis: Dihydroflorate

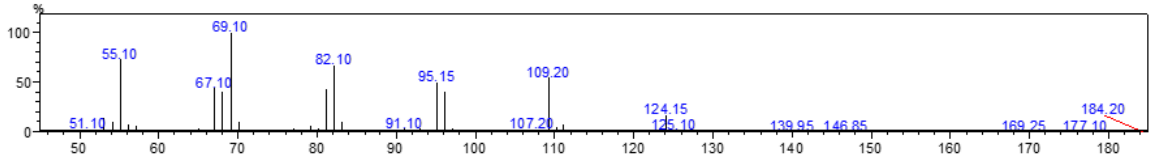

(a) Mass spectra of dihydroflorate isomer, D1, with m/z = 184.2 and t_R = 5.60 min)

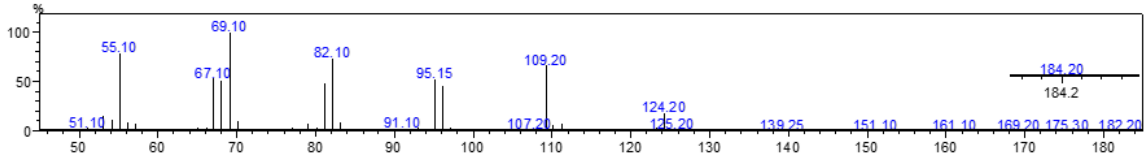

(b) Mass spectra of dihydroflorate isomer, D2 with m/z = 184.2 and t_R = 5.95 min)

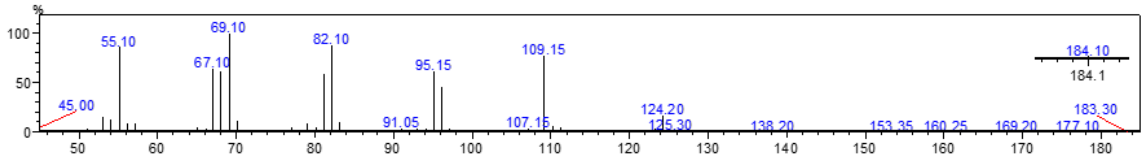

(c) Mass spectra of dihydroflorate isomer, D3 with m/z = 184.1 and t_R = 6.23 min)

Figure C1: Mass spectra of dihydroflorate isomers.

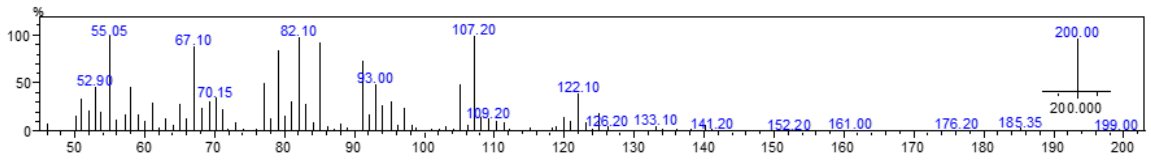

(a) Mass spectrum of dihydroflorate oxidation product with m/z = 200 and t_R = 7.75 min.

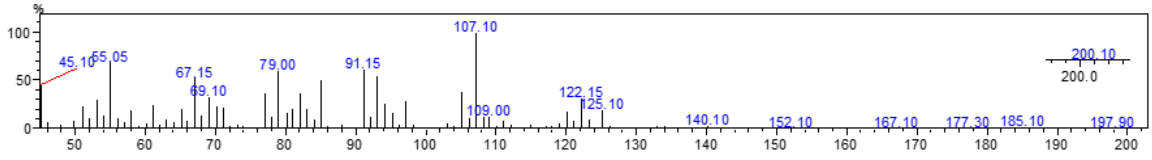

(b) Mass spectrum of dihydroflorate oxidation product with m/z = 200.1 and t_R = 7.85 min.

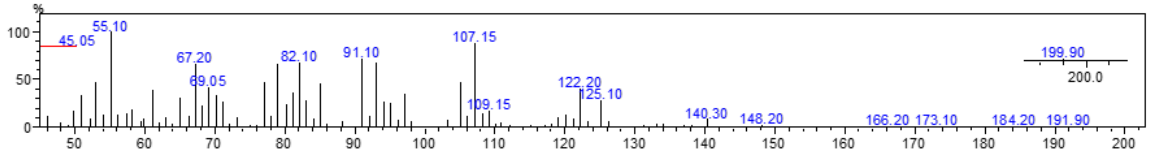

(c) Mass spectrum of dihydroflorate oxidation product with m/z = 199.9 and t_R = 8.08 min.

Figure C2: Mass spectra of dihydroflorate oxidation products.

C.2 Mass Spectra Analysis: Ethyl Safranate

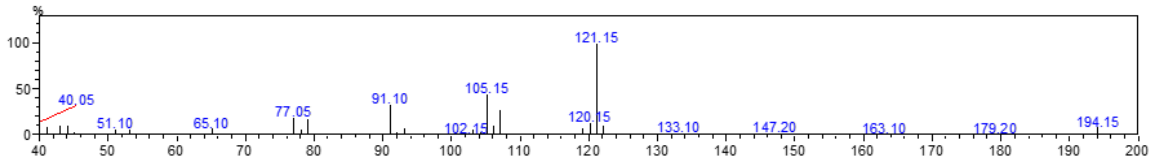

(a) Mass spectrum of ethyl safranate isomer, E1 with $m/z = 194.15$ and $t_R = 5.60$ min.

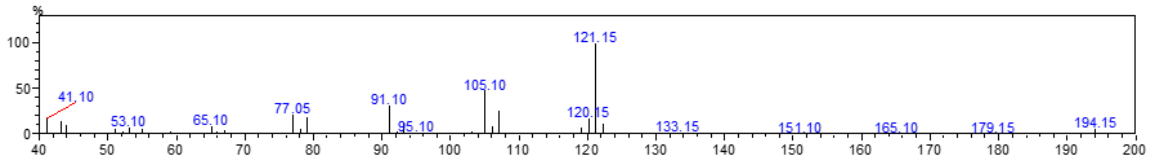

(b) Mass spectrum of ethyl safranate isomer, E2 with $m/z = 194.15$ and $t_R = 5.95$ min.

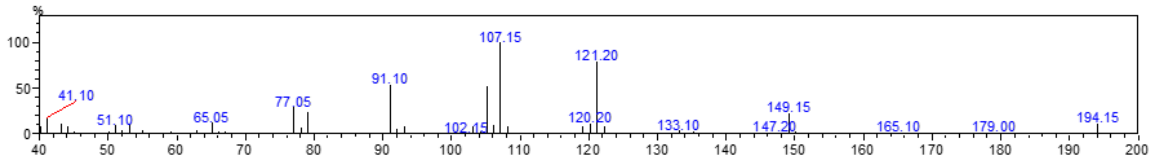

(c) Mass spectrum of ethyl safranate isomer, E3 with $m/z = 194.15$ and $t_R = 6.23$ min.

Figure C3: Mass spectra of ethyl safranate isomers.

Mass Spectra Analysis: Ethyl Safranate (continued)

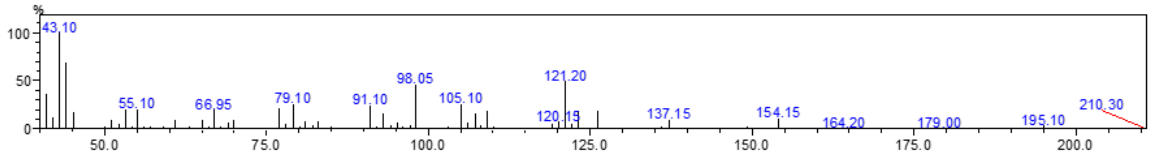

(a) Mass spectrum of ethyl safranate oxidation product with m/z = 210.3, t_R = 7.7 min.

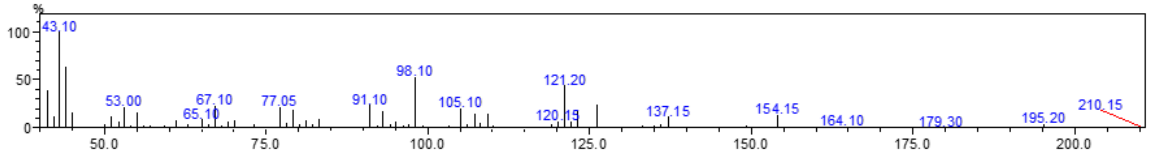

(b) Mass spectrum of ethyl safranate oxidation product with m/z = 210.15, t_R = 7.8 min.

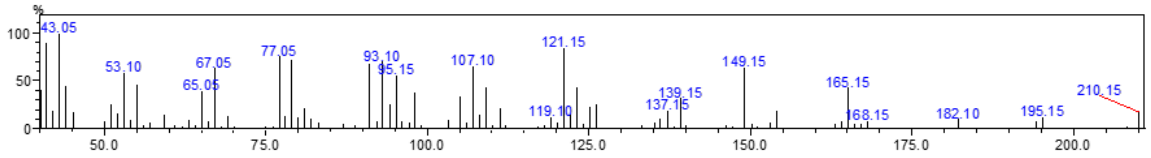

(c) Mass spectrum of ethyl safranate oxidation product with m/z = 210.15, t_R = 8.1 min.

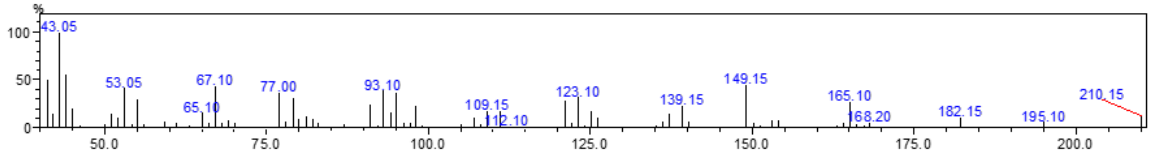

(d) Mass spectrum of ethyl safranate oxidation product with m/z = 210.15, t_R = 8.15 min.

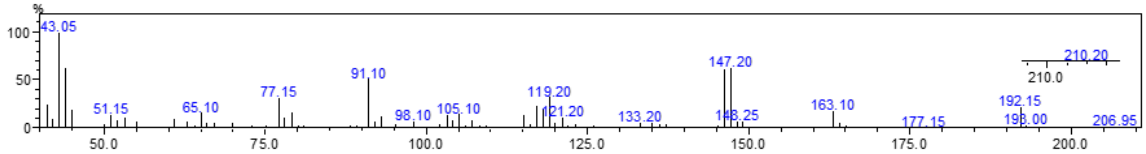

(e) Mass spectrum of ethyl safranate oxidation product with m/z = 210.2, t_R = 8.22 min.

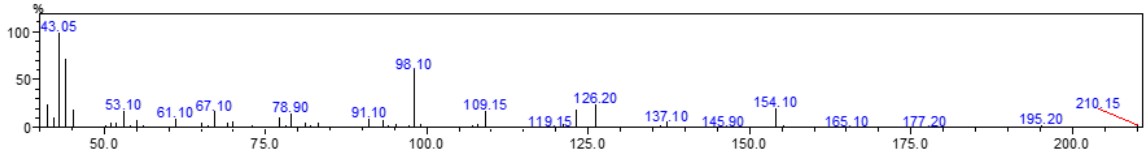

(f) Mass spectrum of ethyl safranate oxidation product with m/z = 210.15, t_R = 8.43 min.

Figure C4: Mass spectra of ethyl safranate oxidation products.

C.3 Mass Spectra Analysis: δ-Damascone

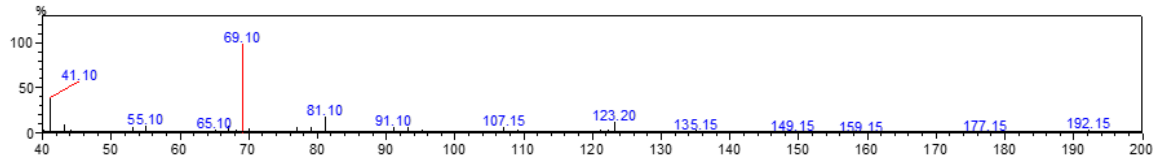

Figure C5: Mass Spectrum of δ-damascone with m/z = 192.15, t_R= 7.34 min.

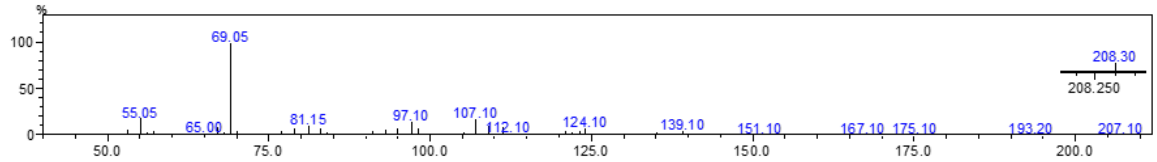

(a) Mass spectra of δ-damascone oxidation product formed *in vivo* and *in vitro* with m/z = 208.3, t_R= 8.9 min.

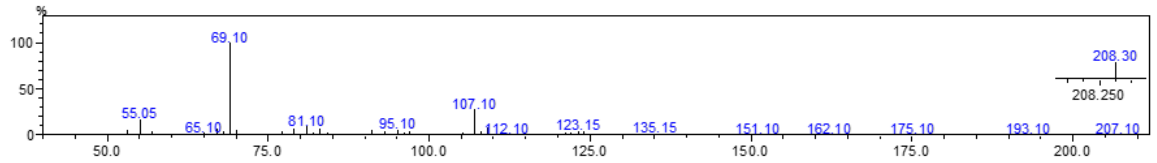

(b) Mass spectra of δ-damascone oxidation product formed *in vivo* and *in vitro* with m/z = 208.3, t_R= 9.0 min.

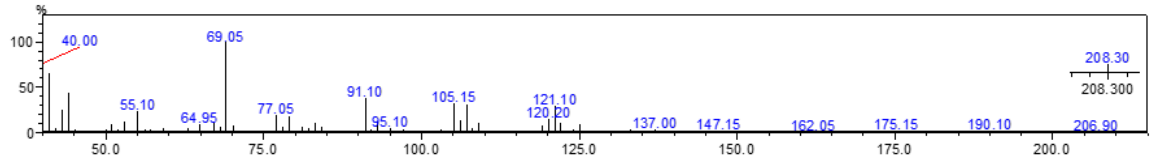

(c) Mass spectra of δ-damascone oxidation product formed *in vitro* with m/z = 208.3, t_R= 9.14 min. This product was not observed in the whole-cell turnover.

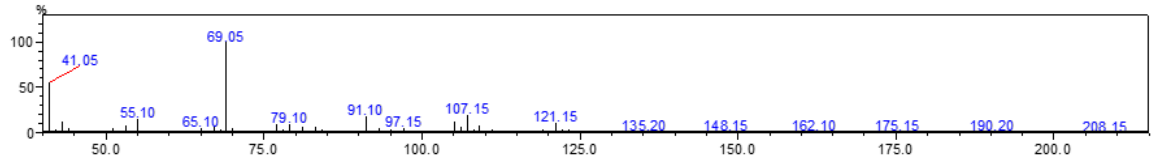

(d) Mass spectra of δ-damascone oxidation product formed both *in vivo* and *in vitro* with m/z = 208.15, t_R= 9.4 min. Product is identified as 3,4-epoxy-δ-damascone.

Figure C6: Mass spectra of δ-damascone oxidation products.

C.4 Mass Spectra Analysis: α-Damascone

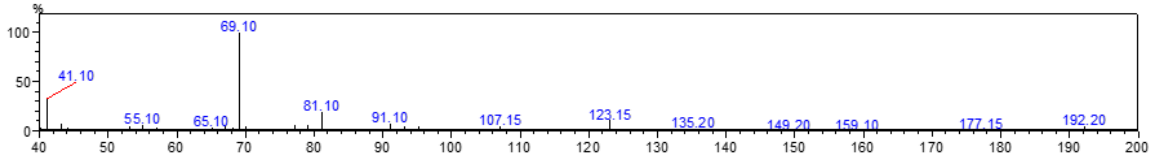

Figure C7: Mass Spectrum of α-damascone with m/z = 192, t_R= 7.51 min.

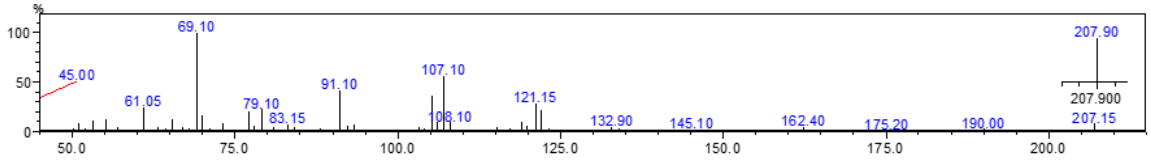

(a) Mass spectra of α-damascone oxidation product with m/z = 207.9, t_R = 9.0 min. This product was only observed in the *in vitro* turnover.

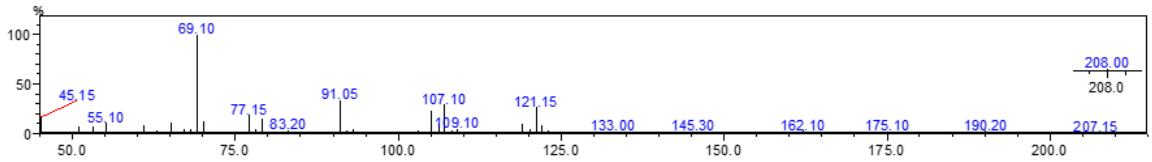

(b) Mass spectra of α-damascone oxidation product with m/z = 208, t_R = 9.25 min. This product was only observed in the *in vitro* turnover.

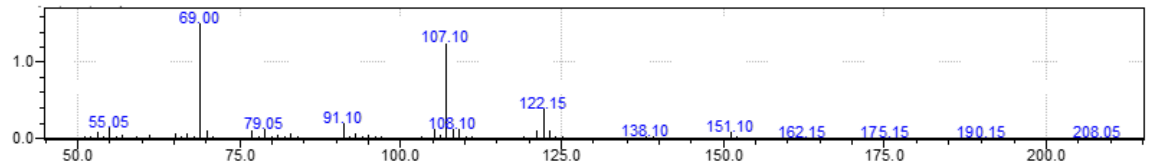

(c) Mass spectra of α-damascone oxidation product with m/z = 208.05, t_R = 9.3 min. Product was identified as *cis*-3-hydroxy-α-damascone.

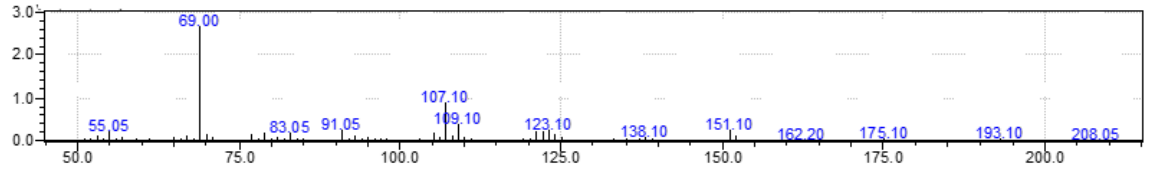

(d) Mass spectra of α-damascone oxidation product with m/z = 208.05, t_R = 9.4 min. Product was identified as *trans*-3-hydroxy-α-damascone.

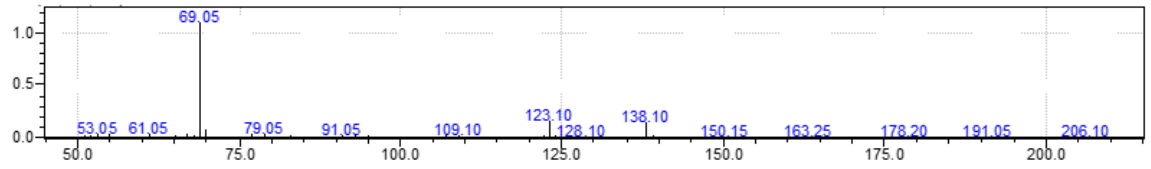

(e) Mass spectra of α-damascone oxidation product with m/z = 206.1, t_R = 9.8 min. Product was identified as 3-oxo-α-damascone.

Figure C8: Mass spectra of α-damascone oxidation products.

C.5 Mass Spectra Analysis: α-*iso*-methylionone

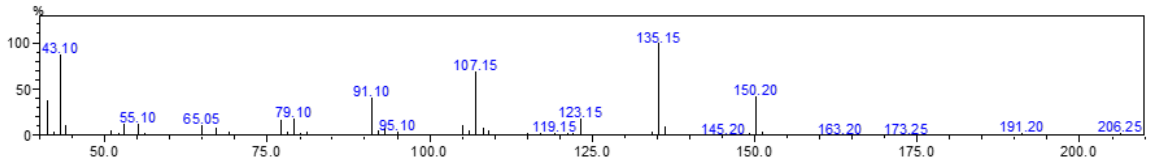

(a) Mass spectra of α-*iso*-methylionone isomer 1 with m/z =206.25, t_R= 8.40 min.

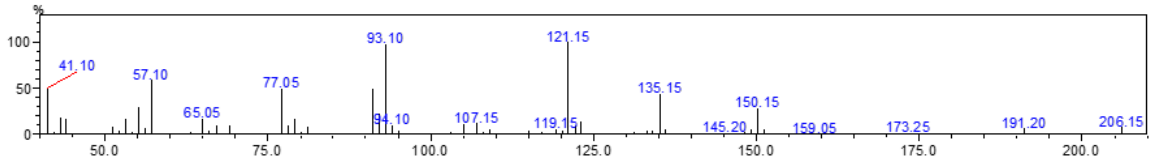

(b) Mass spectra of α-*iso*-methylionone isomer 2 with m/z =206.15, t_R= 8.77 min.

Figure C9: Mass spectra of α-*iso*-methylionone isomers.

Mass Spectra Analysis: α-*iso*-methylionone (continued)

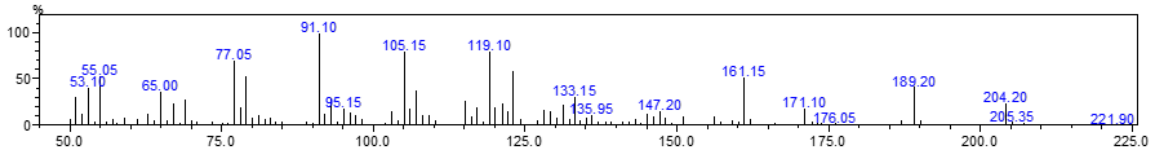

(a) Mass spectra of α-*iso*-methylionone oxidation product with m/z = 221.9, t_R = 10.13 min.

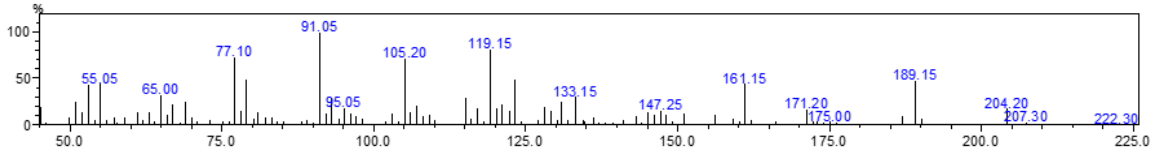

(b) Mass spectra of α-*iso*-methylionone oxidation product with m/z = 222.3, t_R = 10.3 min.

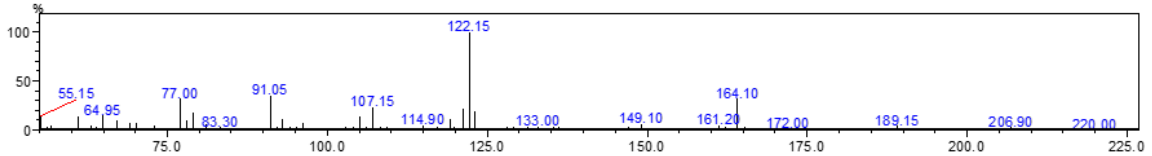

(c) Mass spectra of α-*iso*-methylionone oxidation product with m/z = 220, t_R = 10.4 min.

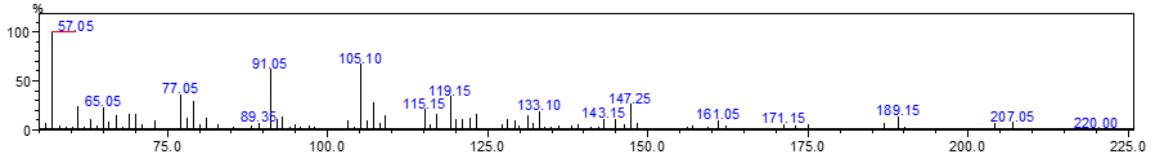

(d) Mass spectra of α-*iso*-methylionone oxidation product with m/z = 220, t_R = 10.5 min.

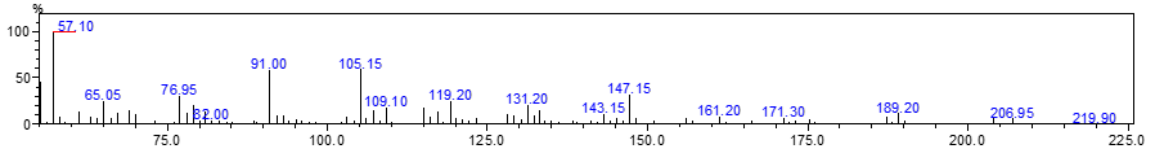

(e) Mass spectra of α-*iso*-methylionone oxidation product with m/z = 219.9, t_R = 10.6 min.

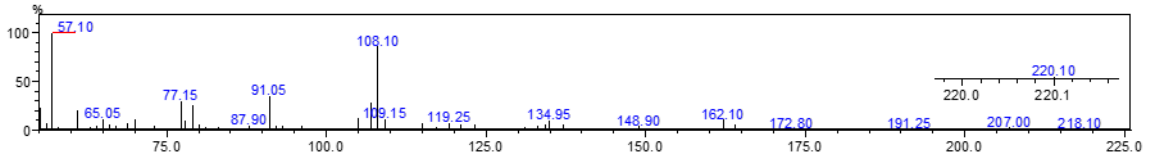

(f) Mass spectra of α-*iso*-methylionone oxidation product with m/z = 220.1, t_R = 10.65 min.

Figure C10: Mass spectra of α-*iso*-methylionone oxidation products.

C.6 Mass Spectra Analysis: Dynascone

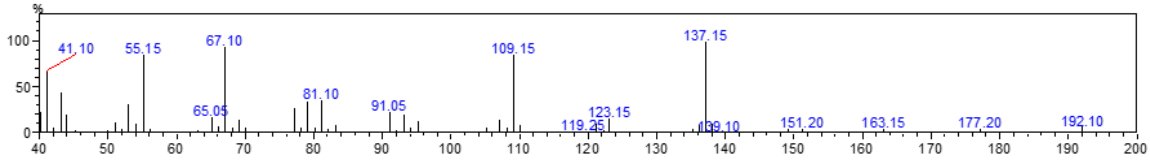

(a) Mass spectra of dynascone isomer 1 with m/z = 192.1, t_R = 7.9 min.

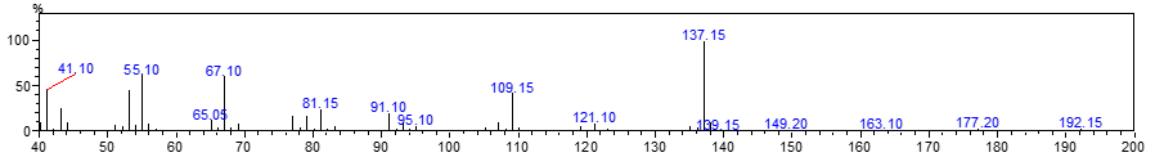

(b) Mass spectra of dynascone isomer 1 with m/z = 192.15, t_R = 8.23 min.

Figure C11: Mass spectra of dynascone isomers.

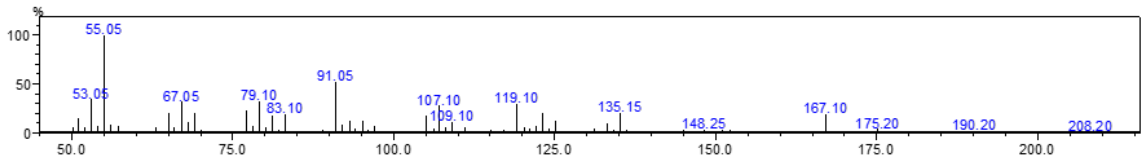

(a) Mass spectra of dynascone oxidation product with m/z = 208.2, t_R = 9.82 min.

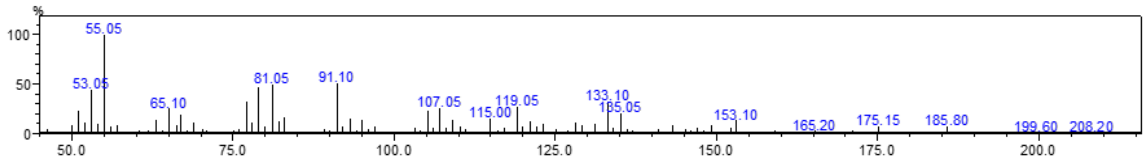

(b) Mass spectra of dynascone oxidation product with m/z = 208.2, t_R = 9.88 min.

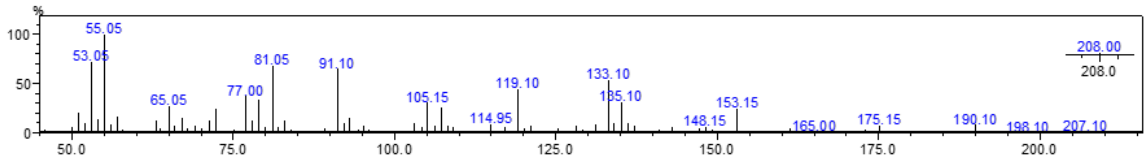

(c) Mass spectra of dynascone oxidation product with m/z = 208, t_R = 10.1 min.

Figure C12: Mass spectra of dynascone oxidation products.

C.7 Mass Spectra Analysis: Cuminyl Acetate

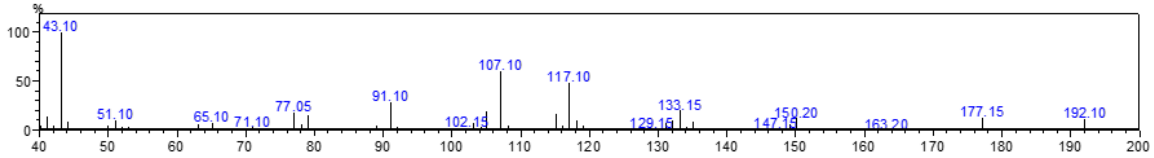

Figure C13: Mass Spectrum of cuminyl acetate with m/z = 192.1 and t_R= 7.81 min.

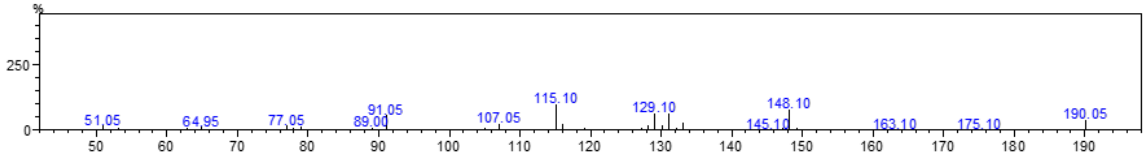

(a) Mass spectra of cuminyl acetate desaturation product with m/z = 190.05, t_R = 8.48 min.

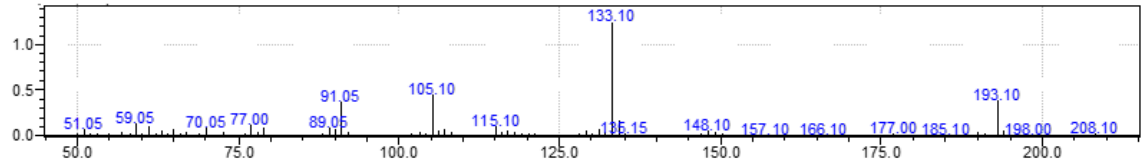

(b) Mass spectra of cuminyl acetate oxidation product with m/z = 208.1, t_R = 9.3 min. Product identified as 4-(2-hydroxypropan-2-yl)benzyl acetate.

Figure C14: Mass spectra of cuminyl cetate turnover products.

C.8 Mass Spectra Analysis: Verdyl Acetate

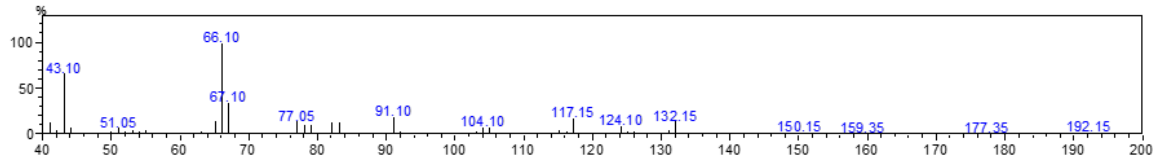

Figure C15: Mass Spectrum of verdyl acetate with m/z = 192.15 and t_R= 7.84 min.

In Vivo Products

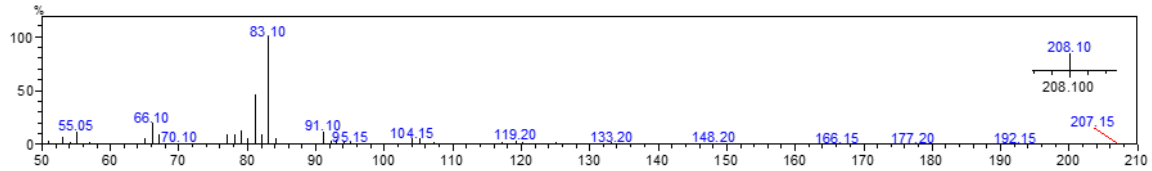

(a) Mass Spectrum of *in vitro* verdyl acetate oxidation product with with m/z = 208.1 and t_R = 9.75 formed with $P450_{BM3}$-GVQ.

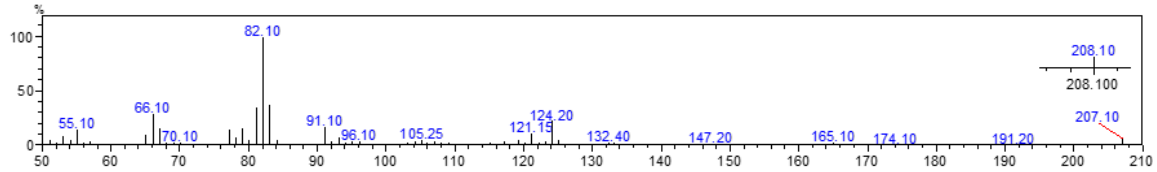

(b) Mass Spectrum of verdyl acetate *in vitro* oxidation product with m/z = 208.1 and t_R = 9.8 min formed with $P450_{BM3}$-GVQ. Product was identified as 6-hydroxy-verdyl acetate.

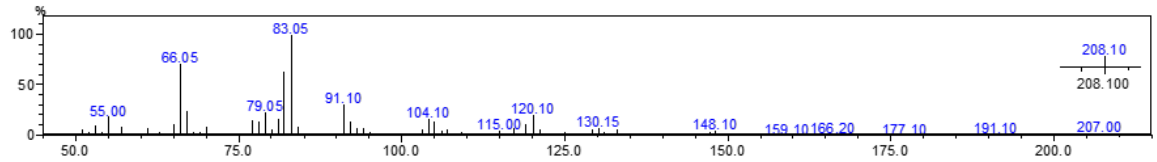

(c) Mass Spectrum of verdyl acetate oxidation product with m/z = 208.1, t_R = 9.82 min formed with $P450_{BM3}$-GVQ.

Figure C16: Mass Spectrum of verdyl acetate oxidation products formed *in vivo* with $P450_{BM3}$-GVQ.

NMR Analysis

4-(2-hydroxypropan-2-yl)benzyl acetate ^{1}H NMR (500 MHz, $CDCl_3$) δ 7.49 (d, J = 8.2 Hz, 1H, H6), 7.34 (d, J = 8.1 Hz, 1H, H5), 5.10 (s, 1H, H3), 2.10 (s, 1H, H1), 1.58 (s, 6H, H9). ^{13}C NMR (126 MHz, $CDCl_3$) δ 170.93 (C2), 149.28 (C7), 134.31 (C4), 128.27 (C7), 124.67 (C6), 72.46 (C8), 66.06 (C3), 31.77 (C9), 21.04 (C1).

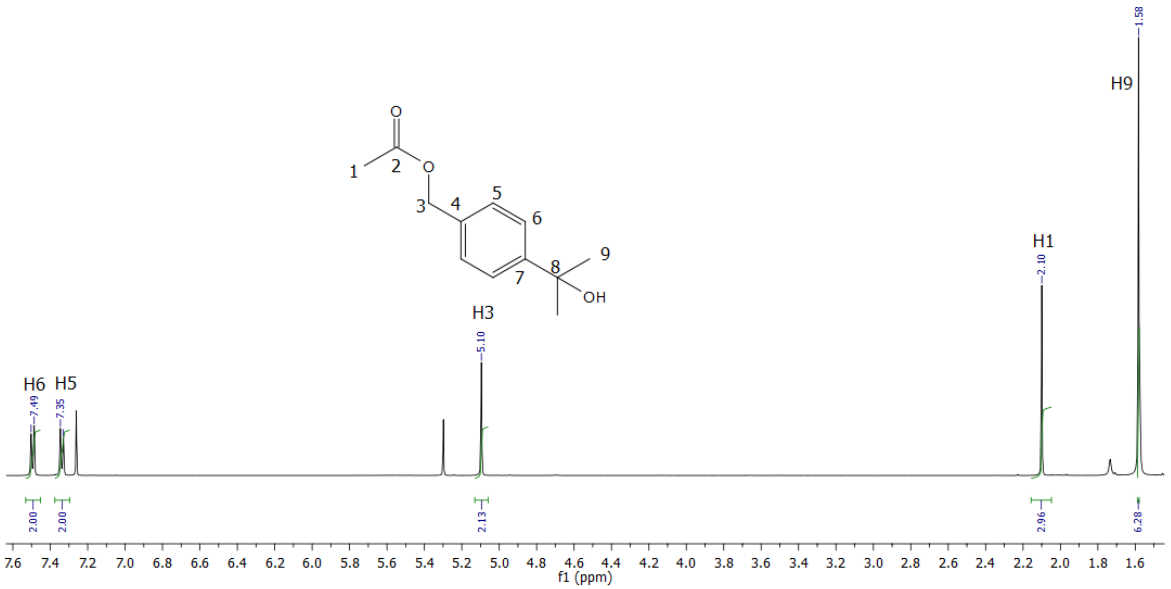

(a)

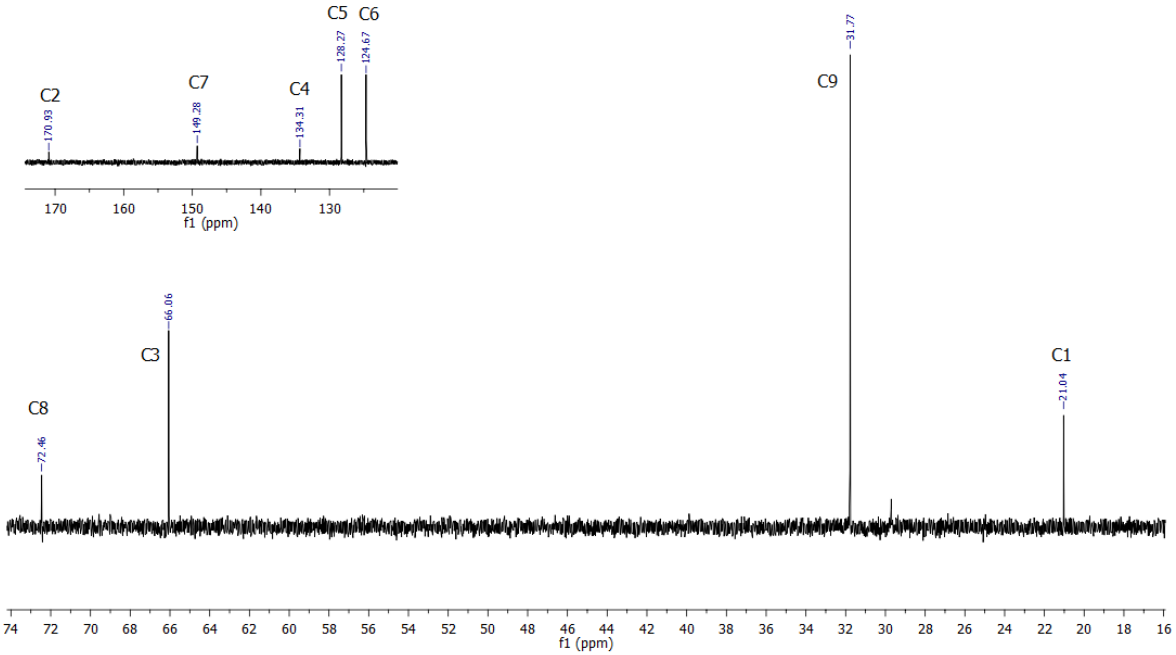

(b)

Figure C17: ^{1}H NMR (a) and ^{13}C NMR (b) spectrum spectrum of 4-(2-hydroxypropan-2-yl)benzyl acetate.

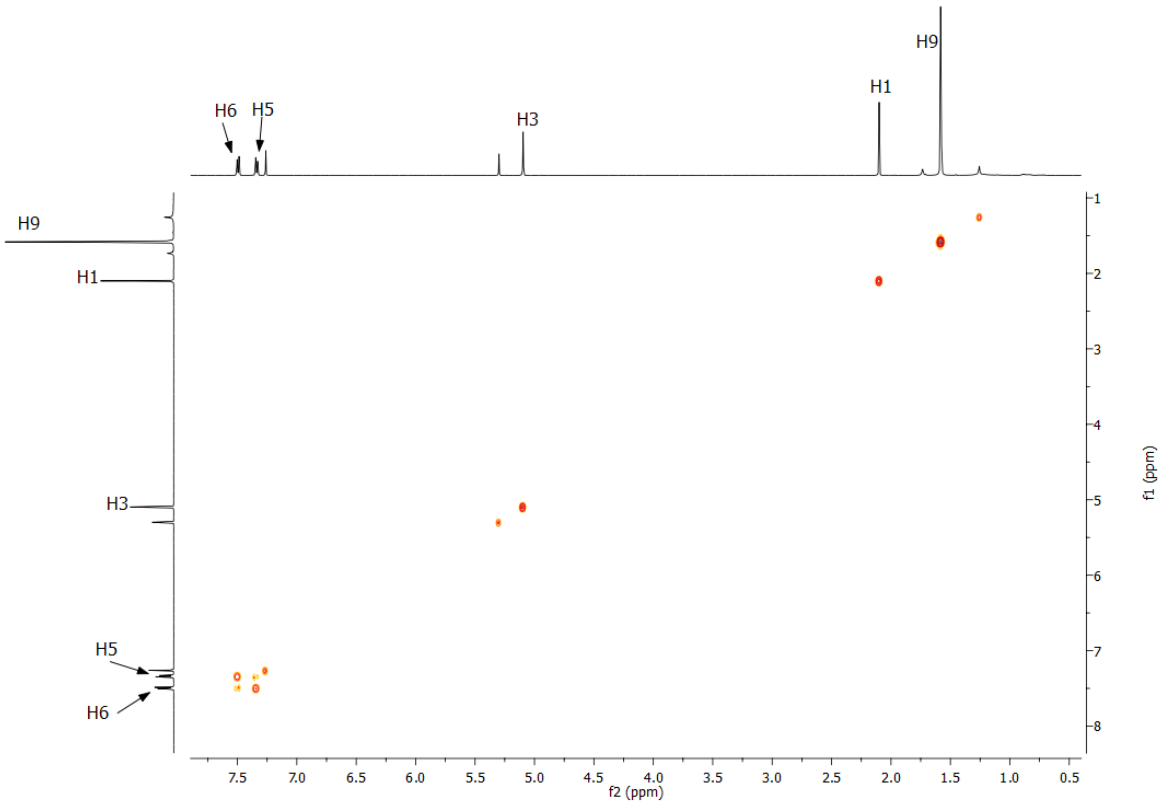

(a)

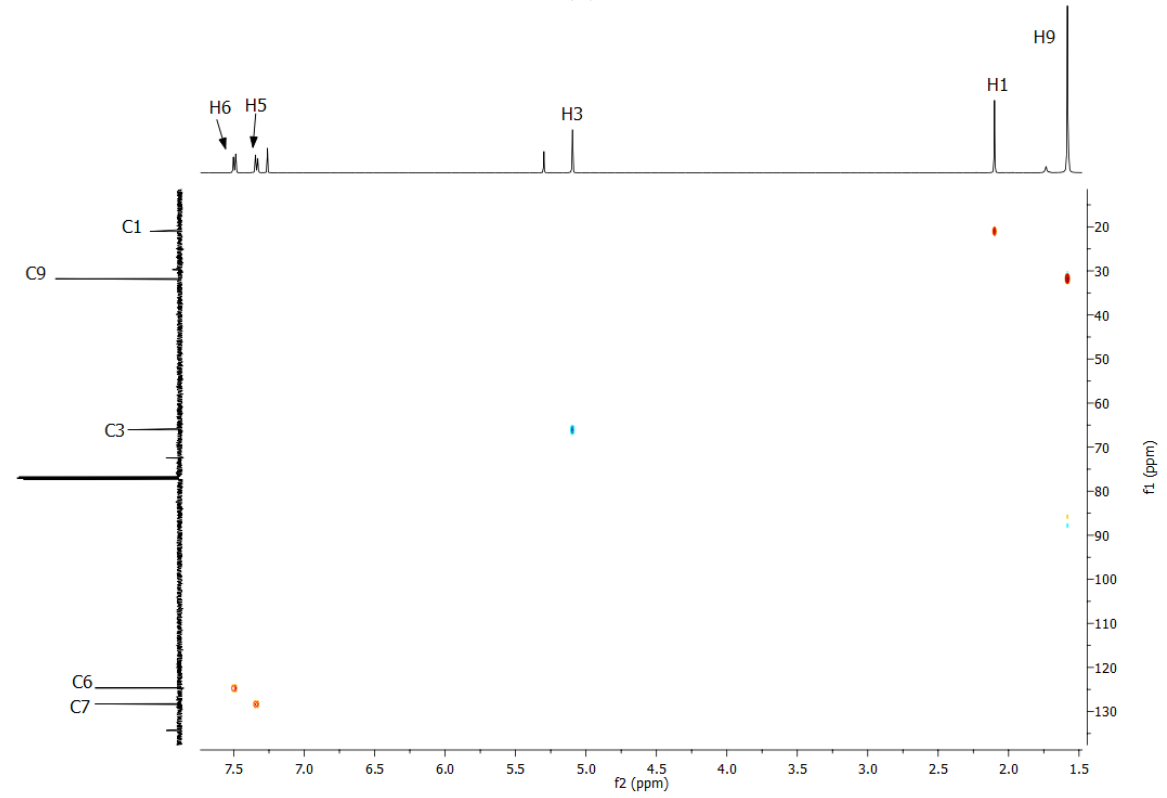

(b)

Figure C18: (a)^{1}H-^{1}H COSY and (b) ^{1}H-^{13}C HSQC NMR data for 4-(2-hydroxypropan-2-yl)benzyl acetate.

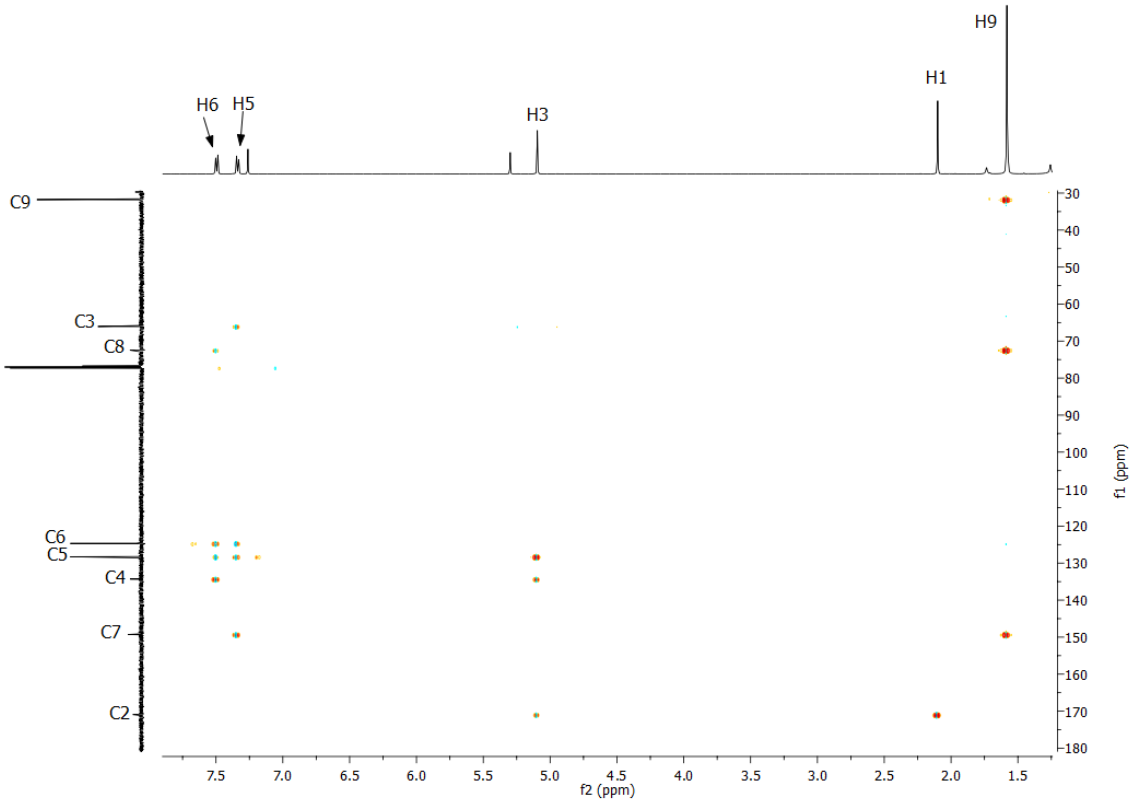

Figure C19: ^{1}H-^{13}C HMBC for 4-(2-hydroxypropan-2-yl)benzyl acetate.

3,4-epoxy-δ-damascone ^{1}H NMR (500 MHz, $CDCl_3$) δ 6.83 (dq, J = 13.8, 6.9 Hz, 1H, H9), 6.20 (dd, J = 15.5, 1.6 Hz, 1H, H8), 3.21 – 3.18 (m, 1H, H3), 2.88 (d, J = 4.0 Hz, 1H, H4), 2.48 (dq, J = 11.6, 7.2 Hz, 1H, H5), 2.20 (d, J = 11.5 Hz, 1H, H6), 1.93 (dd, J = 15.2, 1.3 Hz, 1H, H2), 1.90 (dd, J = 6.9, 1.6 Hz, 3H, H10), 1.59 (d, J = 1.6 Hz, 1H, H2), 0.98 (s, 3H, H11/H12), 0.96 (d, J = 7.2 Hz, 3H, H13), 0.86 (s, 3H, H11/H12). ^{13}C NMR (126 MHz, $CDCl_3$) δ 203.0 (C7), 142.1 (C9), 134.0 (C8), 60.2 (C6), 56.6 (C4), 53.2 (C3), 39.9 (C2), 33.4 (C1), 32.1 (C11/C12), 29.3 (C5), 23.4 (C11/C12), 19.0 (C13), 18.3 (C10).

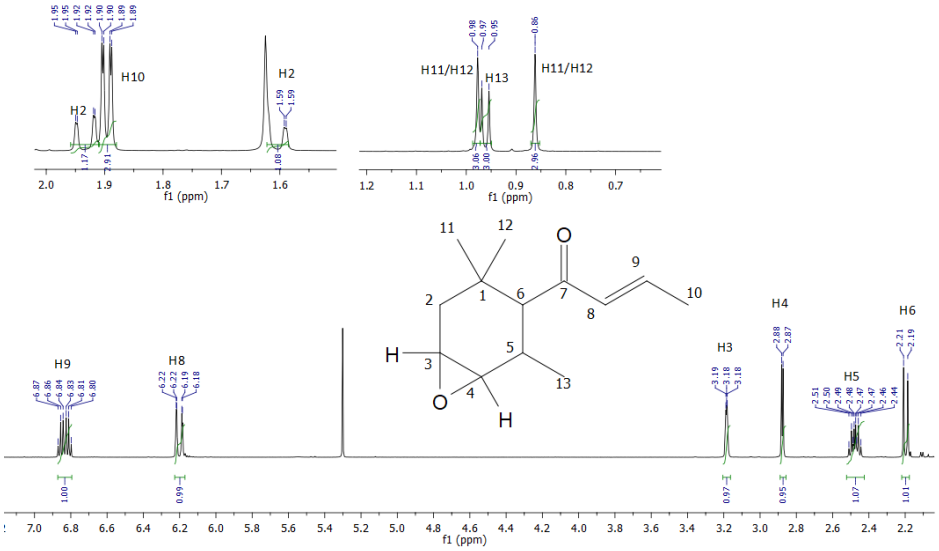

(a)

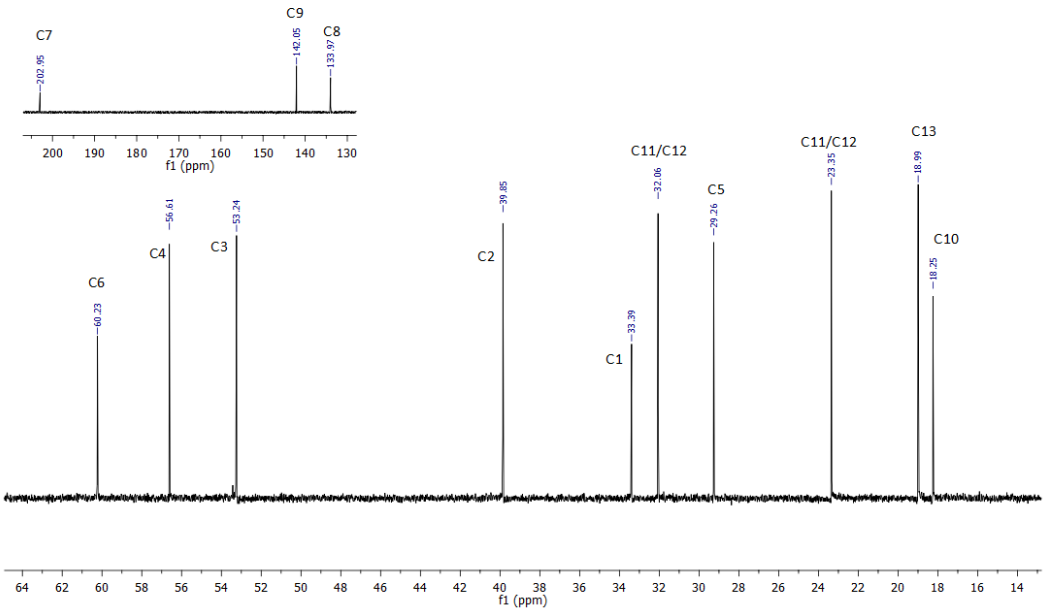

(b)

Figure C20: ^{1}H NMR (a) and ^{13}C NMR (b) spectrum spectrum of 3,4-epoxy-δ-damascone.

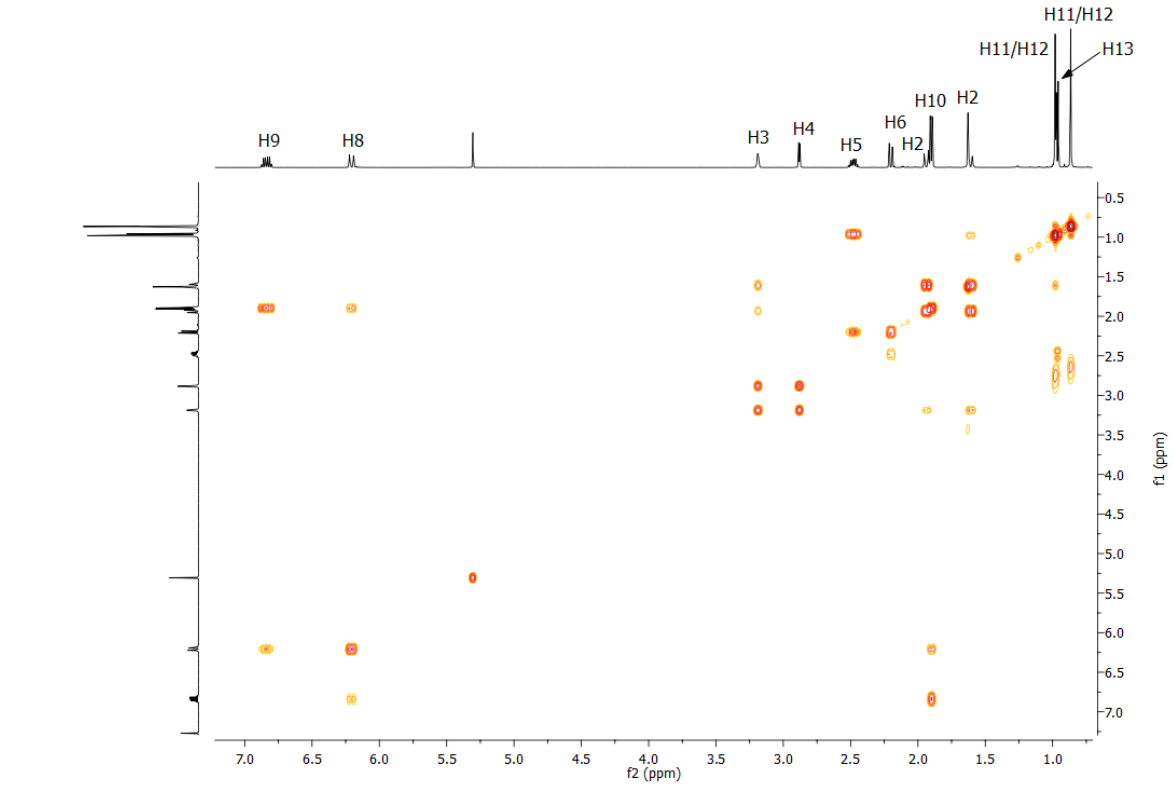

(a)

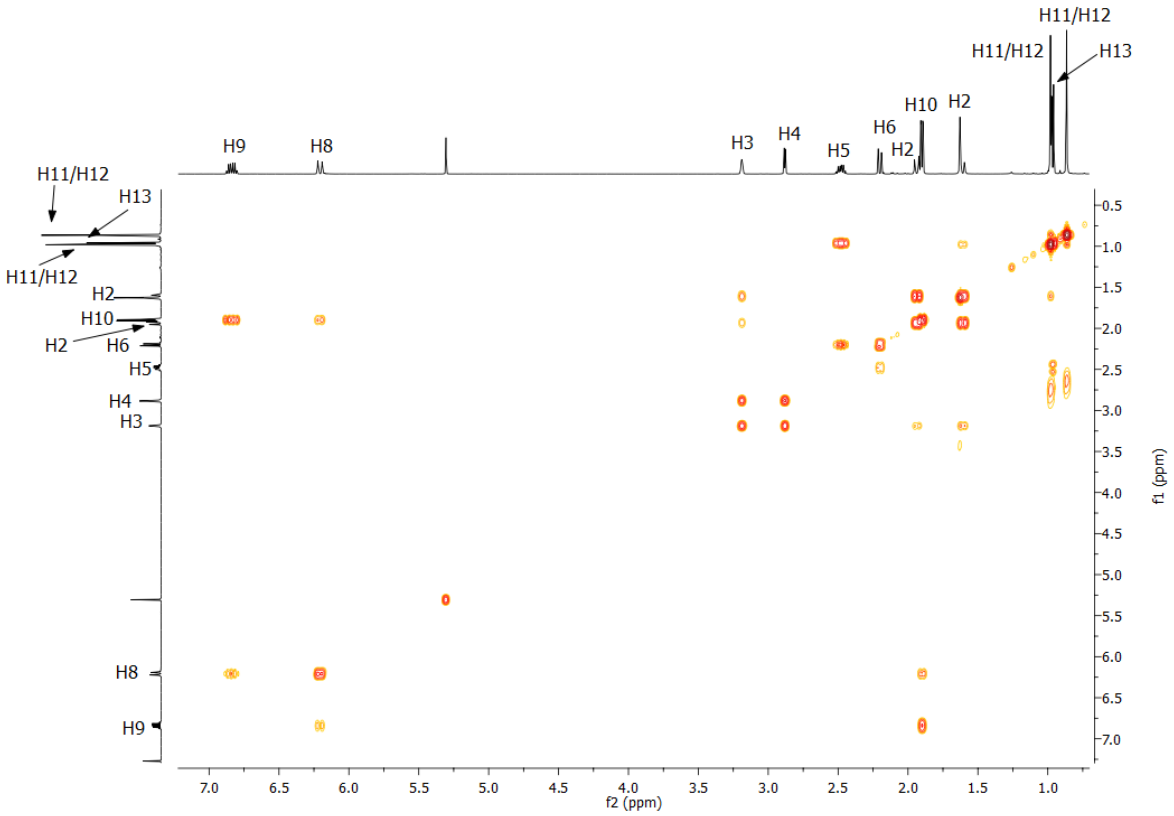

(b)

Figure C21: (a)^{1}H-^{1}H COSY and (b) ^{1}H-^{13}C HSQC NMR data for 3,4-epoxy-δ-damascone.

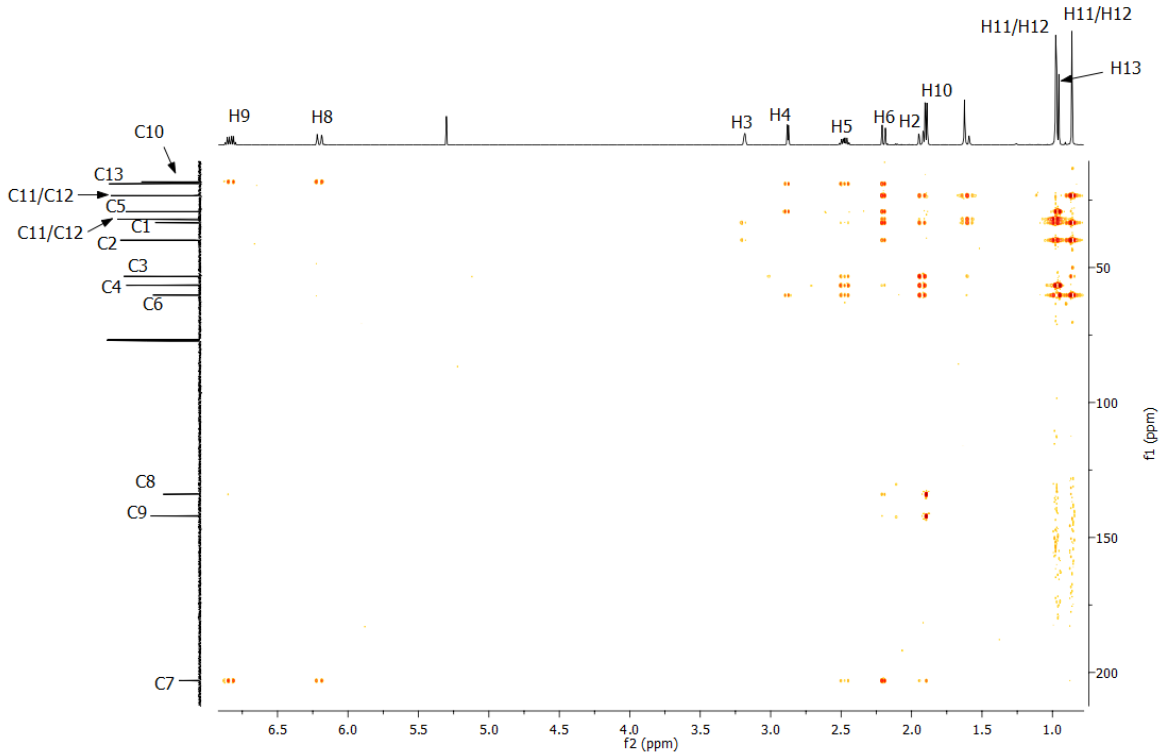

Figure C22: ^{1}H-^{13}C HMBC for 3,4-epoxy-δ-damascone.

***cis*-3-hydroxy-α-damascone** ^{1}H NMR (500 MHz, $CDCl_3$) δ 6.91 (dq, J = 13.8, 6.9 Hz, 1H, H9), 6.32 (dd, J = 15.5, 1.4 Hz, 1H, H8), 5.69 (s, 1H, H4), 4.20 (s, 1H, H3), 2.94 (s, 1H, H6), 1.92 (dd, J = 6.8, 1.4 Hz, 3H, H10), 1.66 (d, 1H, H2), 1.65 (d, 1H, H2), 1.60 (s, 3H, H13), 0.98 (s, 3H, H12), 0.89 (s, 3H, H11). ^{13}C NMR (126 MHz, $CDCl_3$) δ 201.2 (C7), 143.3 (C9), 133.5 (C5), 132.4 (C8), 127.6 (C4), 66.2 (C3), 60.8 (C6), 40.9 (C2), 34.9 (C1), 28.6 (C11), 28.3 (C12), 23.0 (C13), 18.3 (C10).

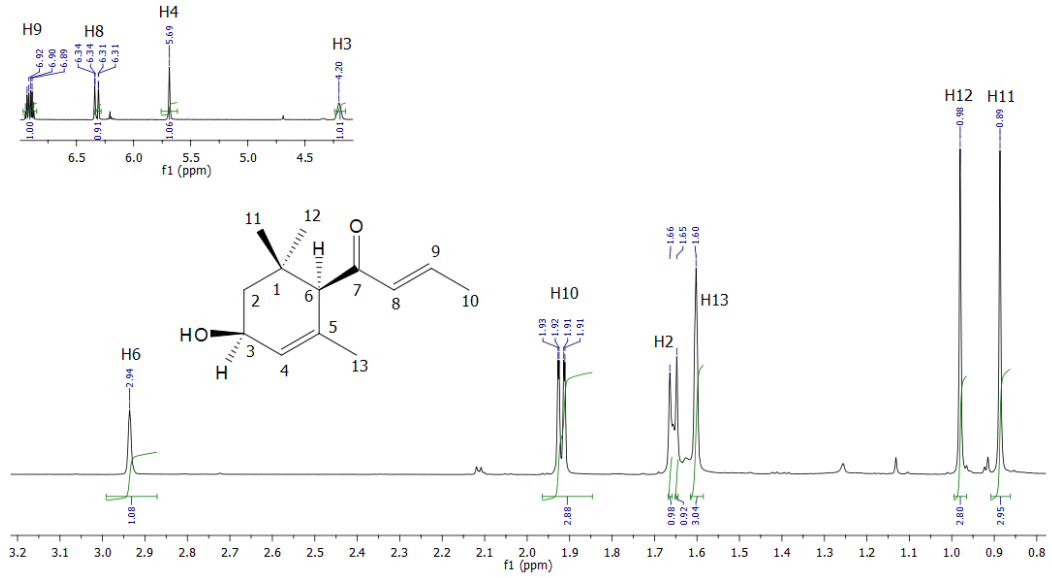

(a)

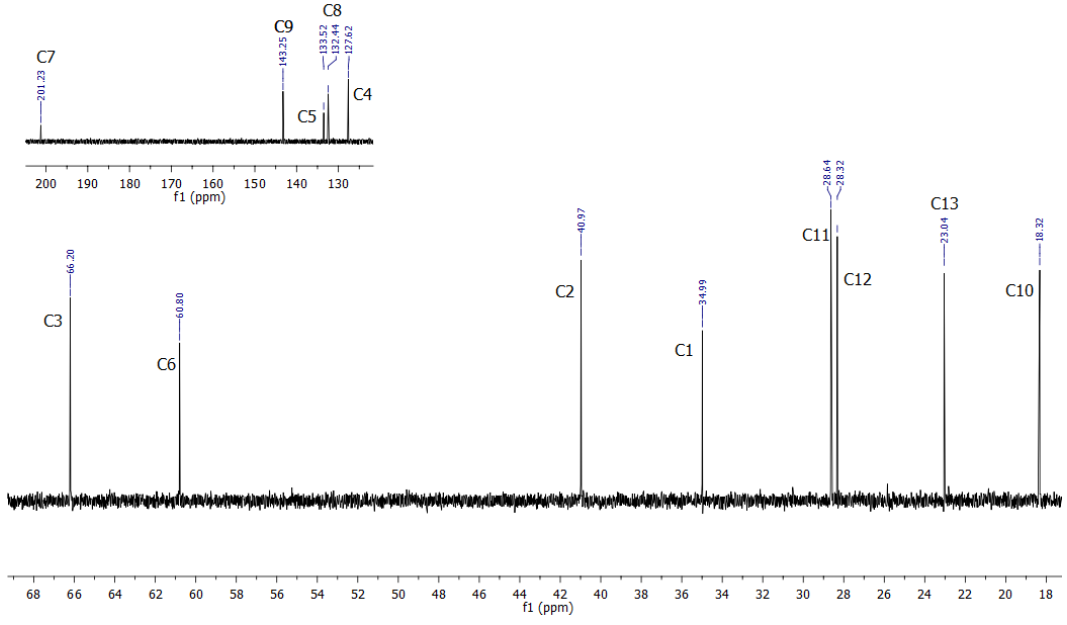

(b)

Figure C23: ^{1}H NMR (a) and ^{13}C NMR (b) spectrum spectrum of *cis*-3-hydroxy-α-damascone.

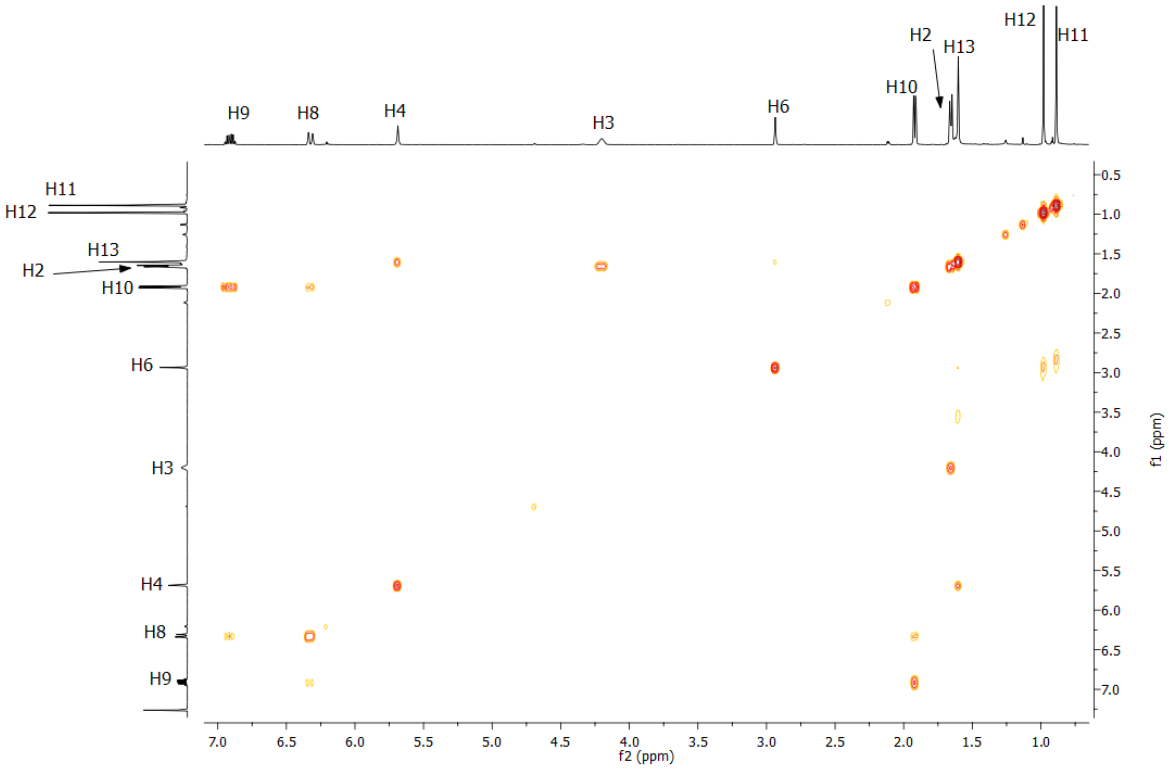

(a)

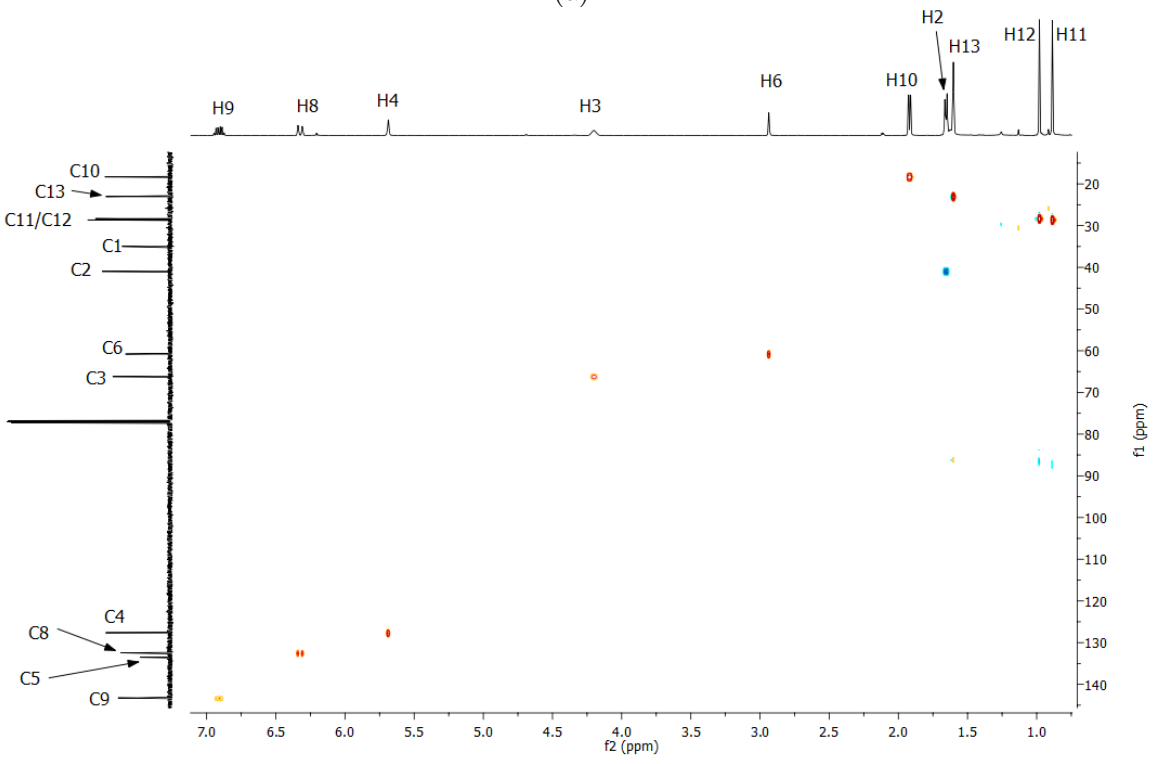

(b)

Figure C24: (a)^{1}H-^{1}H COSY and (b) ^{1}H-^{13}C HSQC NMR data for *cis*-3-hydroxy-α-damascone.

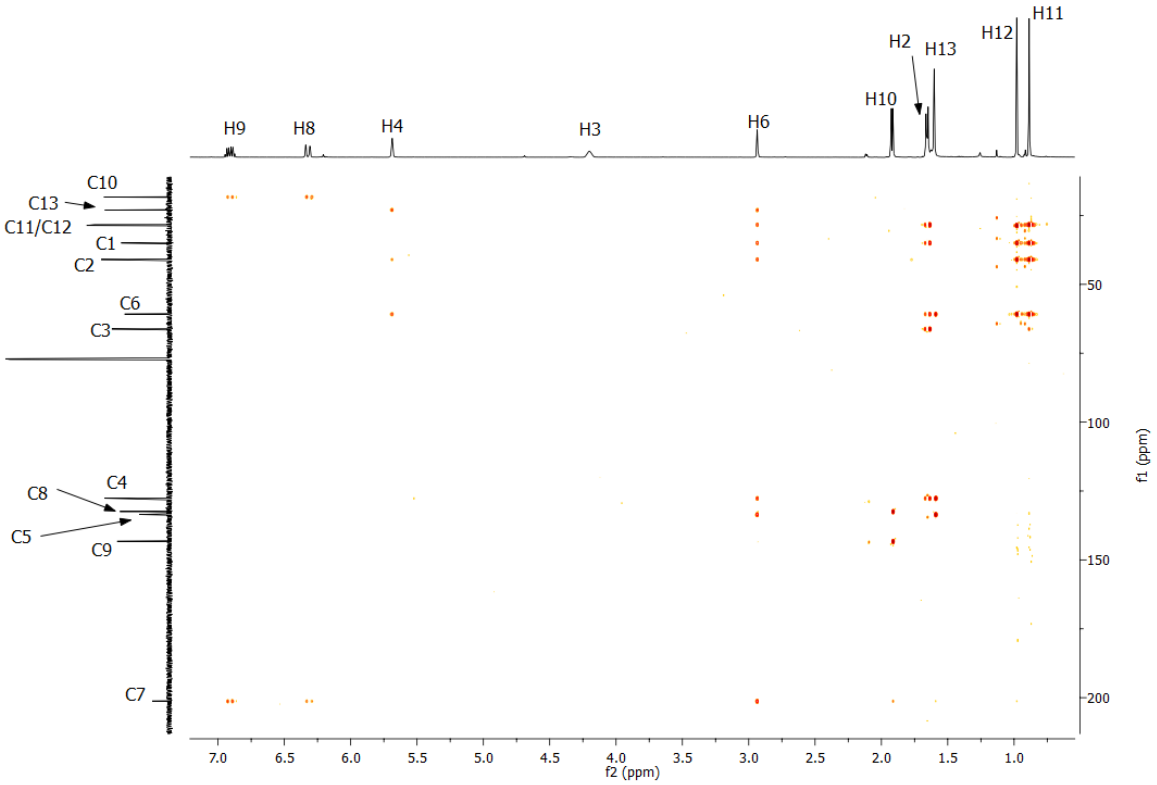

Figure C25: ^{1}H-^{13}C HMBC for *cis*-3-hydroxy-α-damascone.

***trans*-3-hydroxy-α-damascone** ^{1}H NMR (500 MHz, $CDCl_3$) δ 6.89 (dq, J = 13.8, 6.9 Hz, 1H, H9), 6.23 (dd, J = 15.5, 1.6 Hz, 1H, H8), 5.90 – 5.60 (m, 1H, H4), 4.34 (s, 1H, H3), 3.13 (s, 1H, H6), 1.95 (dd, J = 13.6, 5.9 Hz, 1H, H2), 1.91 (dd, J = 6.9, 1.6 Hz, 2H, H10), 1.63 (s, 2H, H13), 1.42 (d, J = 5.4 Hz, 1H, H2), 1.39 (d, J = 5.4 Hz, 1H, H2), 1.13 (s, 3H, H11), 0.88 (s, 3H, H12). ^{13}C NMR (126 MHz, $CDCl_3$) δ 200.43 (C7), 142.83 (C9), 134.21 (C5), 132.64 (C8), 126.69 (C4), 65.49 (C3), 61.04 (C6), 43.63 (C2), 33.33 (C1), 30.54 (C11), 25.87 (C12), 22.73 (C13), 18.28 (C10).

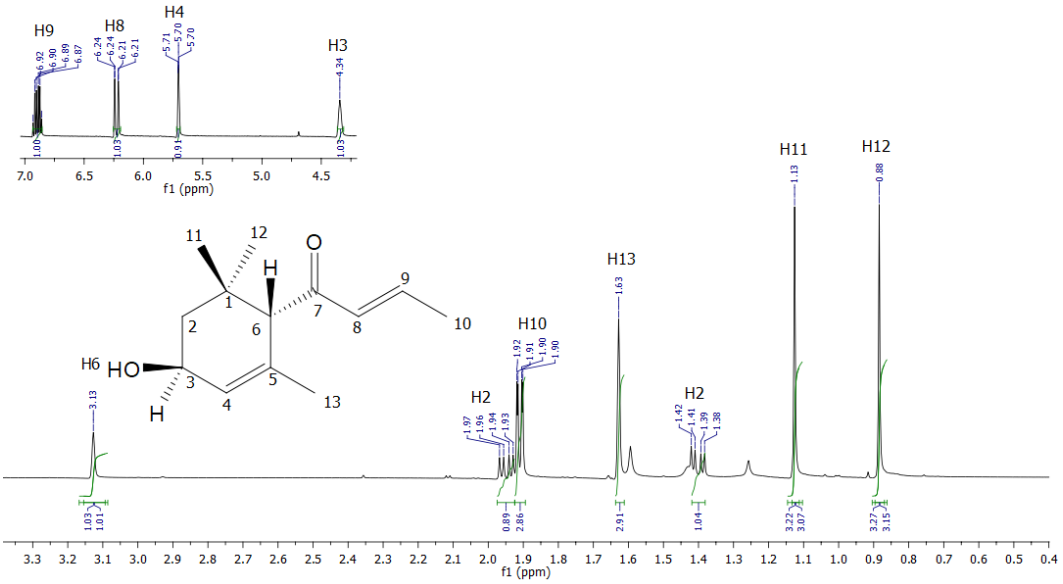

(a)

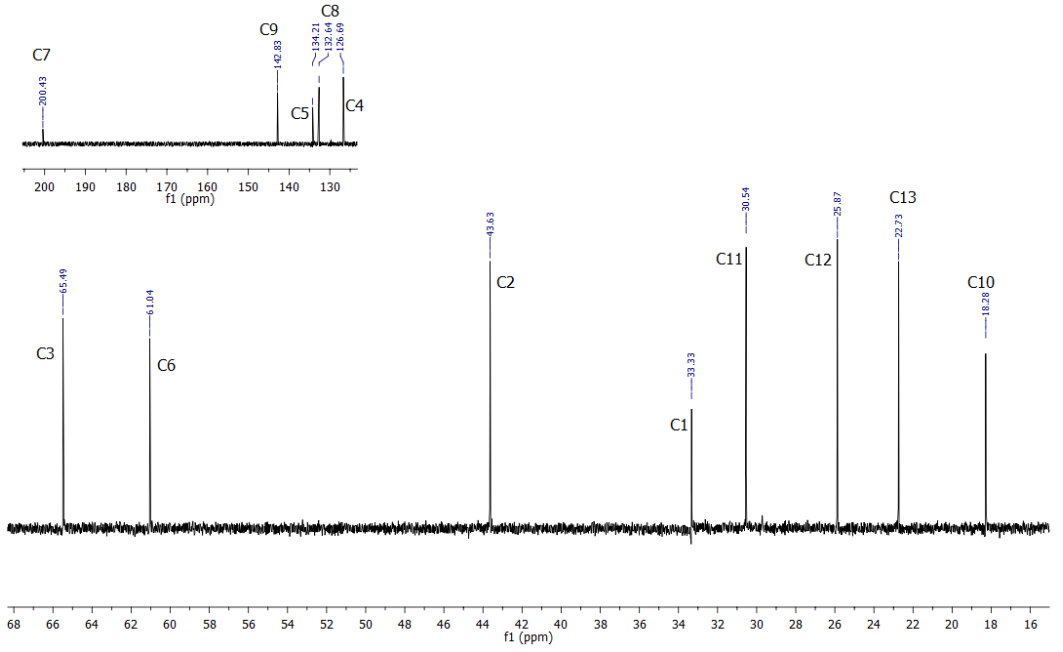

(b)

Figure C26: ^{1}H NMR (a) and ^{13}C NMR (b) spectrum spectrum of *trans*-3-hydroxy-α-damascone.

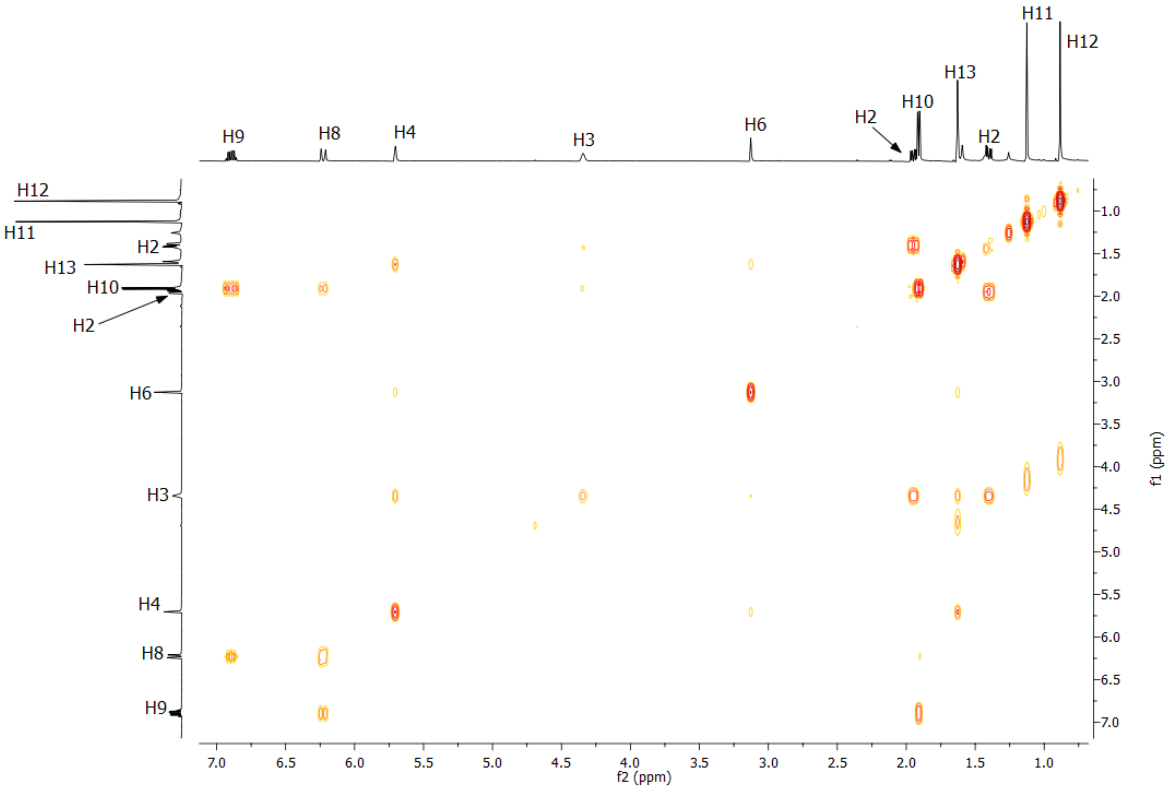

(a)

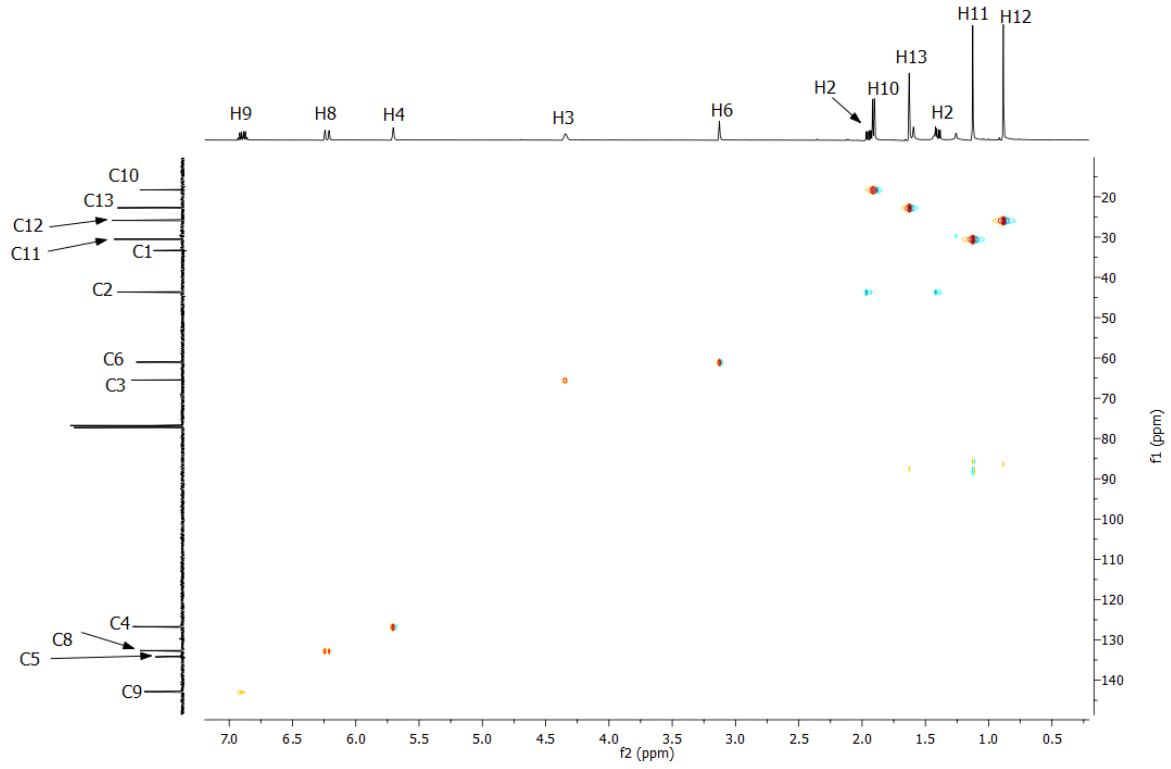

(b)

Figure C27: (a)^{1}H-^{1}H COSY and (b) ^{1}H-^{13}C HSQC NMR data for *trans*-3-hydroxy-α-damascone.

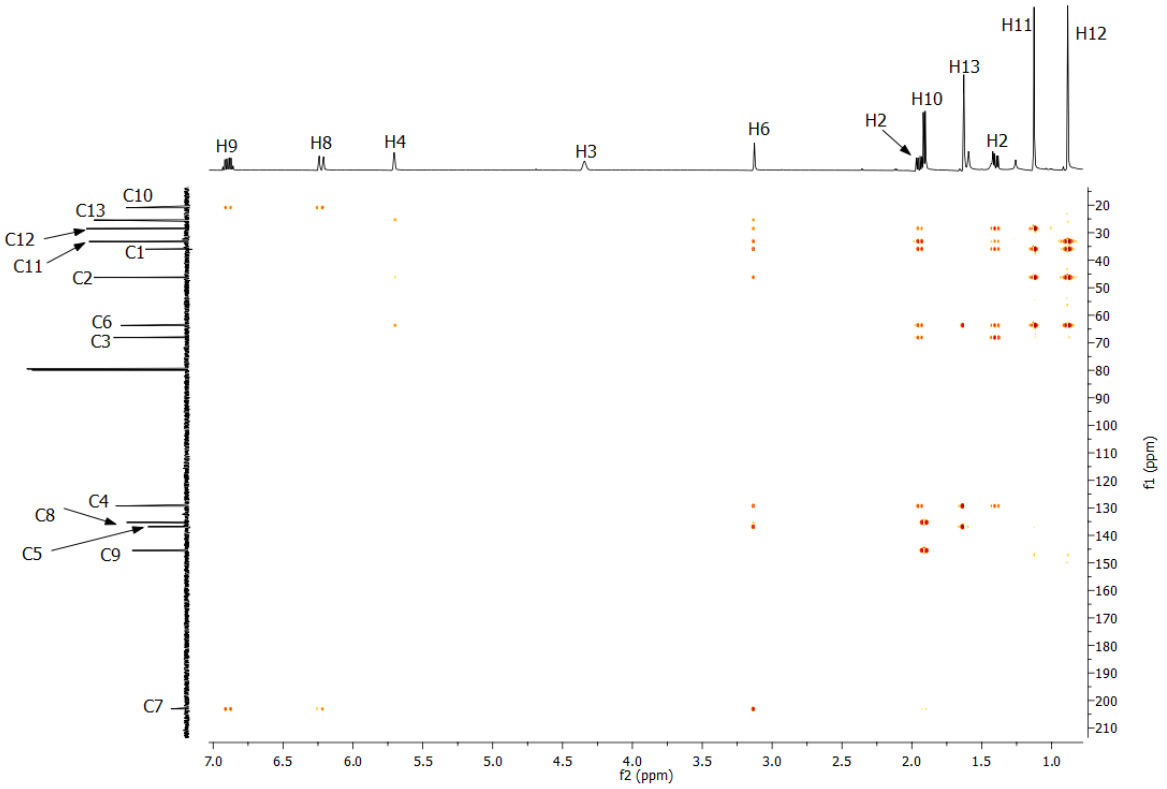

Figure C28: ^{1}H-^{13}C HMBC for *trans*-3-hydroxy-α-damascone.

3-*oxo*-α-damascone ^{1}H NMR (500 MHz, $CDCl_3$) δ 6.99 (dq, J = 13.8, 6.9 Hz, 1H, H9), 6.30 (dd, J = 15.5, 1.7 Hz, 1H, H8), 6.01 (s, 1H, H4), 3.37 (s, 1H, H6), 2.68 (d, J = 16.6 Hz, 1H, H2), 2.03 (d, J = 16.6 Hz, 1H, H2), 1.96 (dd, J = 6.9, 1.7 Hz, 3H, H10), 1.86 (d, J = 1.0 Hz, 3H, H13), 1.09 (s, 3H, H11/H12), 1.00 (s, 3H, H11/H12). ^{13}C NMR (126 MHz, $CDCl_3$) δ 199.17 (C3), 197.73 (C7), 156.07 (C5), 144.89 (C9), 132.35 (C8), 127.62 (C4), 61.77 (C6), 47.02 (C2), 36.66 (C1), 29.17 (C11/C12), 27.56 (C11/C12), 23.97 (C13), 18.46 (C10).

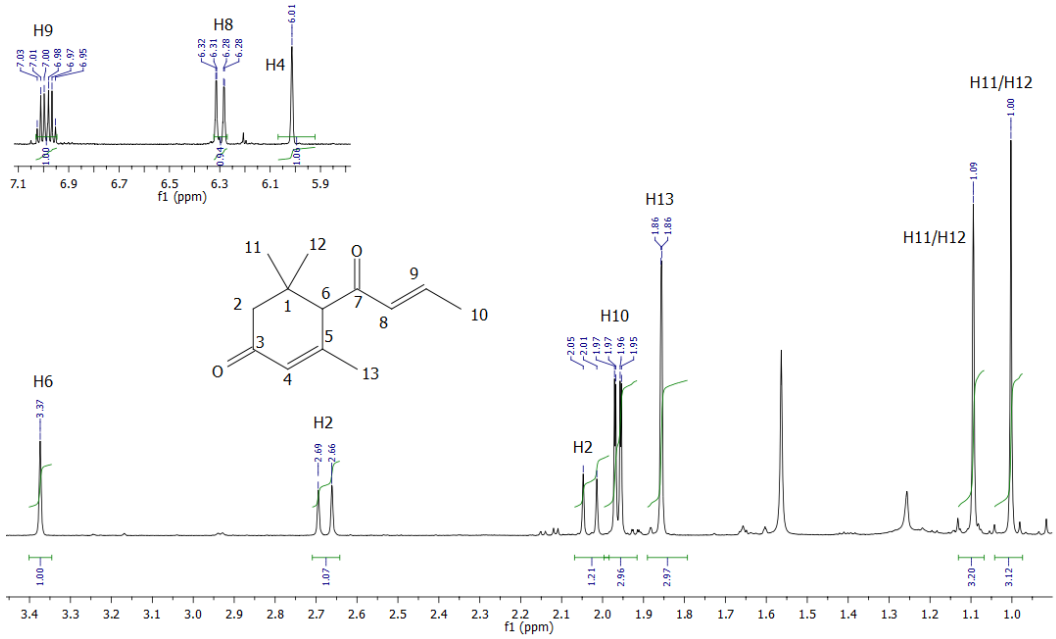

(a)

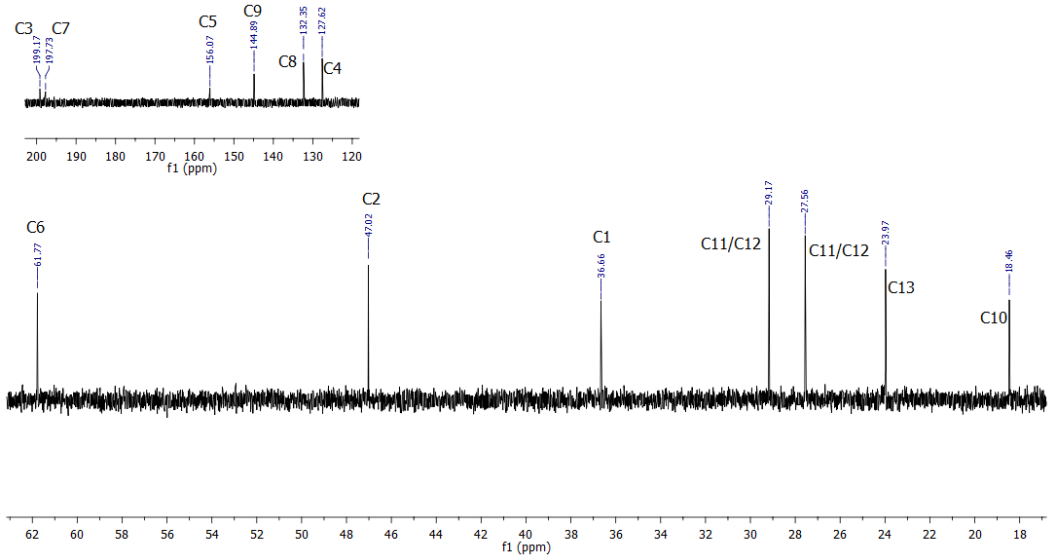

(b)

Figure C29: ^{1}H NMR (a) and ^{13}C NMR (b) spectrum spectrum of 3-*oxo*-α-damascone.

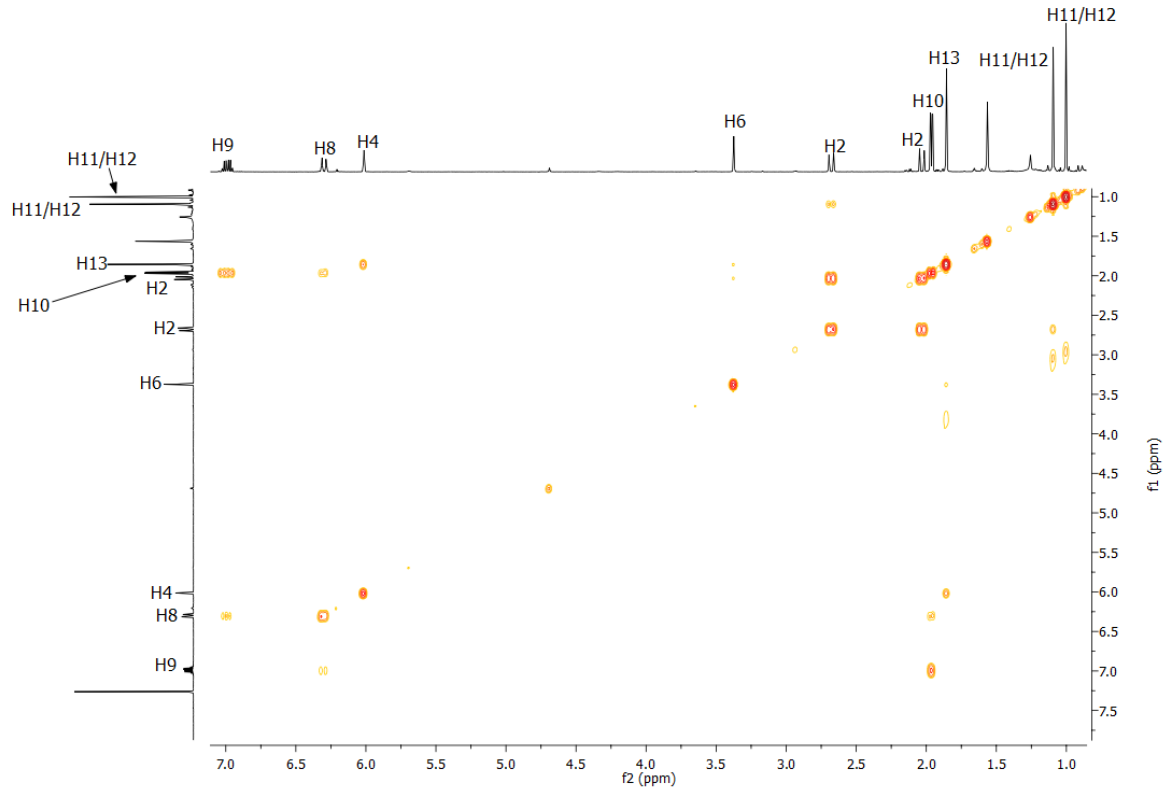

(a)

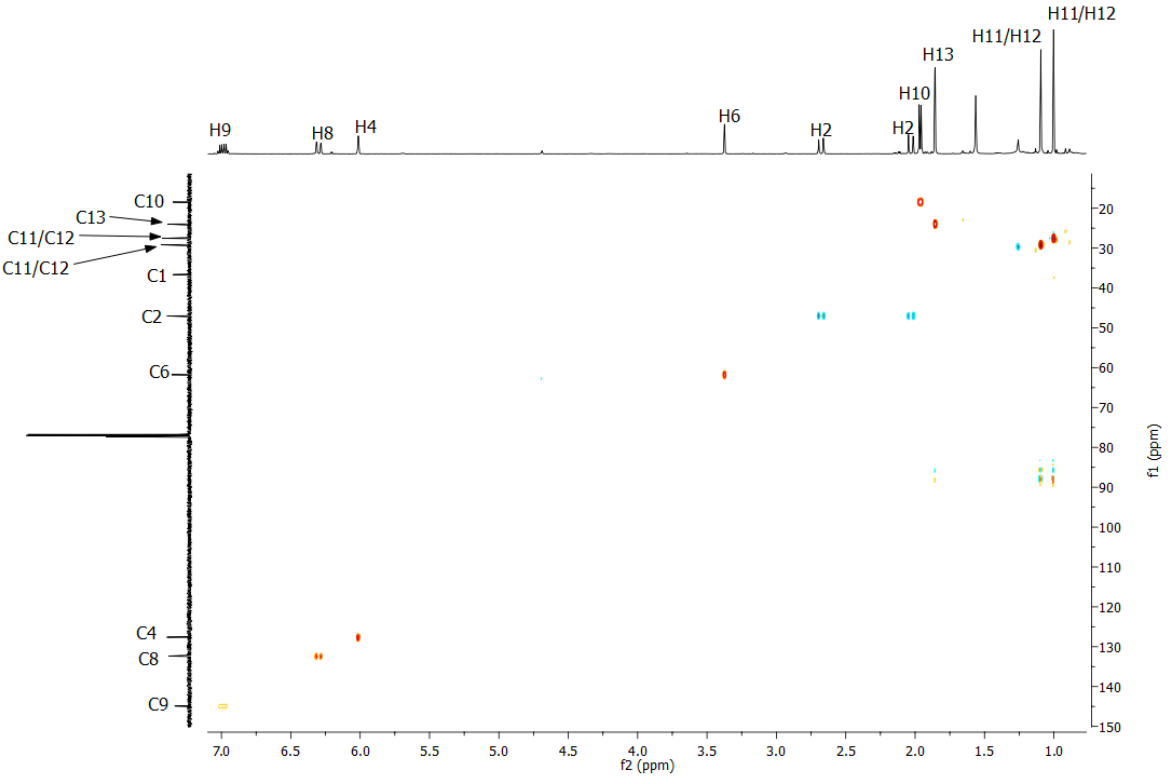

(b)

Figure C30: (a)^{1}H-^{1}H COSY and (b) ^{1}H-^{13}C HSQC NMR data for 3-*oxo*-α-damascone.

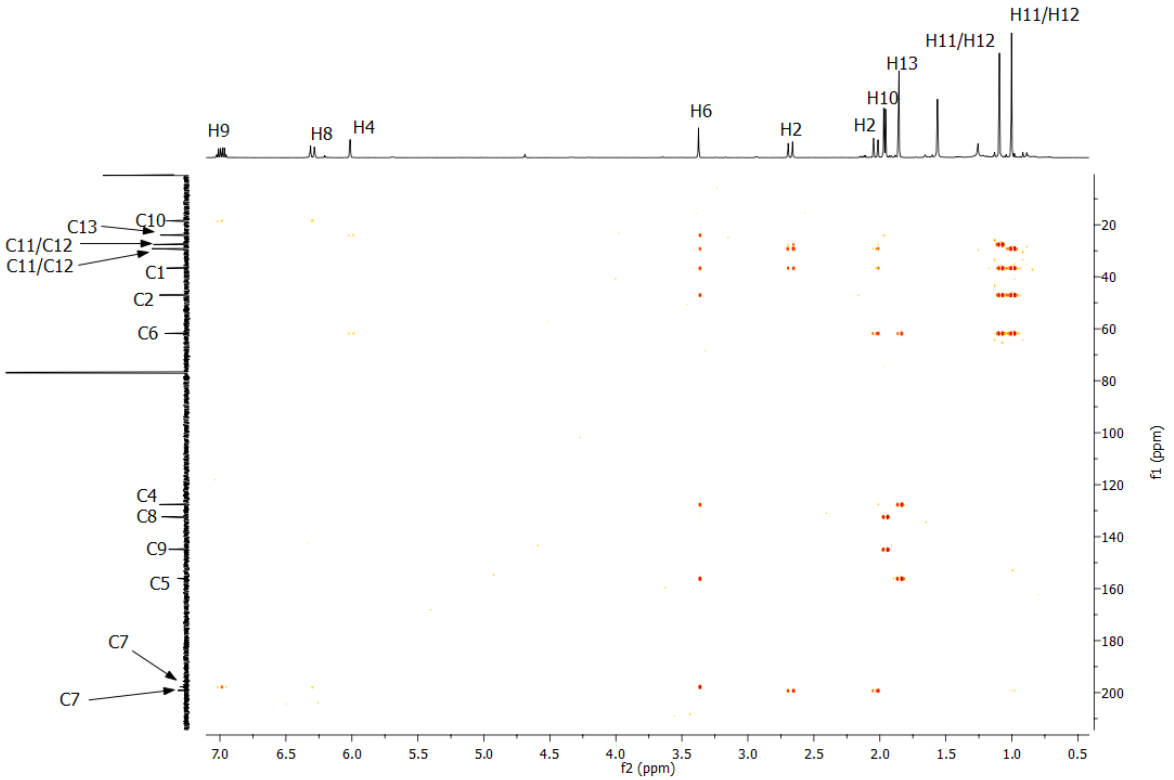

Figure C31: ^{1}H-^{13}C HMBC for 3-*oxo*-α-damascone.

Table C1: Comparison of Experimental NMR data of *cis*-, *trans*- and 3-oxo-α-damascone to the literature.[169]

Metabolite	Position	Experimental δ_C (ppm, 126 MHz, $CDCl_3$)	Literature[169] δ_C (ppm, 200 MHz, $CDCl_3$)
cis-3-hydroxy	C7	201.2	201.4
	C9	143.3	143.3
	C5	133.5	133.3
	C8	132.4	132.4
	C4	127.6	127.7
	C3	66.2	66.1
	C6	60.8	60.8
	C2	40.9	40.9
	C1	34.9	34.9
	C11	28.6	28.6
	C12	28.3	28.3
	C13	23.0	23.0
	C10	18.3	18.3
trans-3-hydroxy	C7	200.43	200.4
	C9	142.83	142.7
	C5	134.21	134.0
	C8	132.64	132.6
	C4	126.69	126.7
	C3	65.49	65.4
	C6	61.04	61.0
	C2	43.63	43.6
	C1	33.33	33.3
	C11	30.54	30.5
	C12	25.87	25.8
	C13	22.73	22.6
	C10	18.28	18.2
3-oxo	C3	199.17	199.1
	C7	197.73	197.7
	C5	156.07	156.1
	C9	144.89	144.8
	C8	132.35	132.4
	C4	127.62	127.5
	C6	61.77	61.7
	C2	47.02	47.0
	C1	36.66	36.6
	C11/C12	29.17	29.1
	C11/C12	27.56	27.5
	C13	23.97	23.8
	C10	18.46	18.3

6-hydroxy-verdyl acetate ^{1}H NMR (500 MHz, $CDCl_3$) δ 5.84 (d, J = 5.5 Hz, 1H), 5.74 (d, J = 5.4 Hz, 1H), 4.66 (d, J = 6.7 Hz, 1H), 4.34 (d, J = 3.8 Hz, 1H), 2.75 (d, J = 6.5 Hz, 1H), 2.25 (d, J = 3.9 Hz, 1H), 2.12 (s, 1H), 2.01 (s, 3H), 1.82 (d, J = 6.7 Hz, 1H), 1.77 (ddd, J = 13.5, 7.0, 2.1 Hz, 1H), 1.46 (s, 1H), 1.31 (d, J = 10.5 Hz, 1H), 1.03 (d, J = 10.5 Hz, 1H). ^{13}C NMR (126 MHz, $CDCl_3$) δ 170.84 (C2), 136.07 (C8), 135.17 (C7), 82.69 (C6), 77.18 (C3), 54.34 (C10), 50.29 (C4), 43.97 (C9), 39.41 (C5), 38.73 (C11), 29.11 (C12), 21.35 (C1).

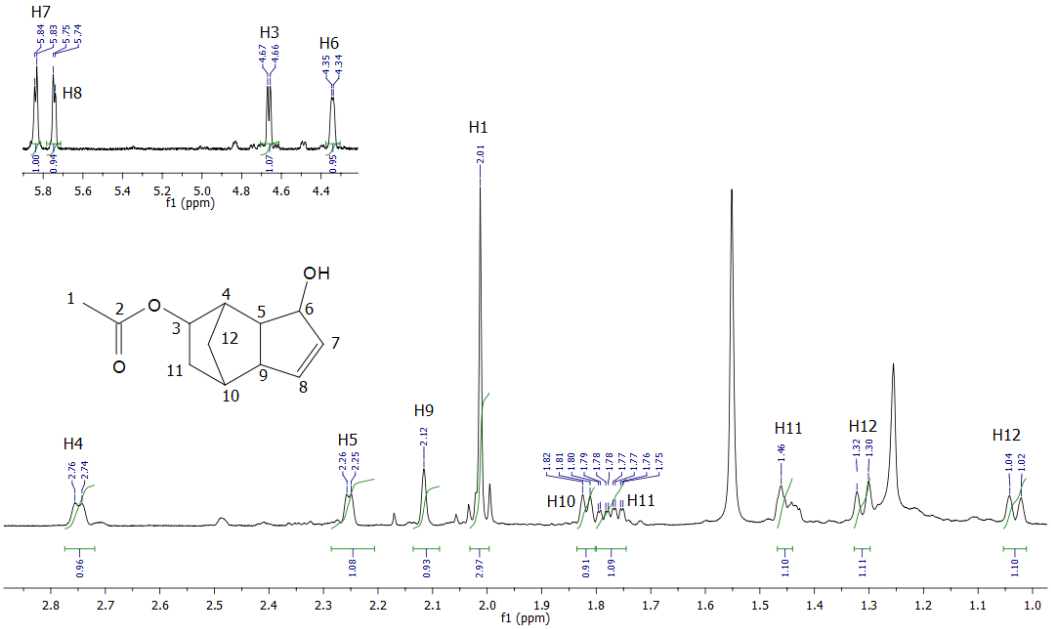

(a)

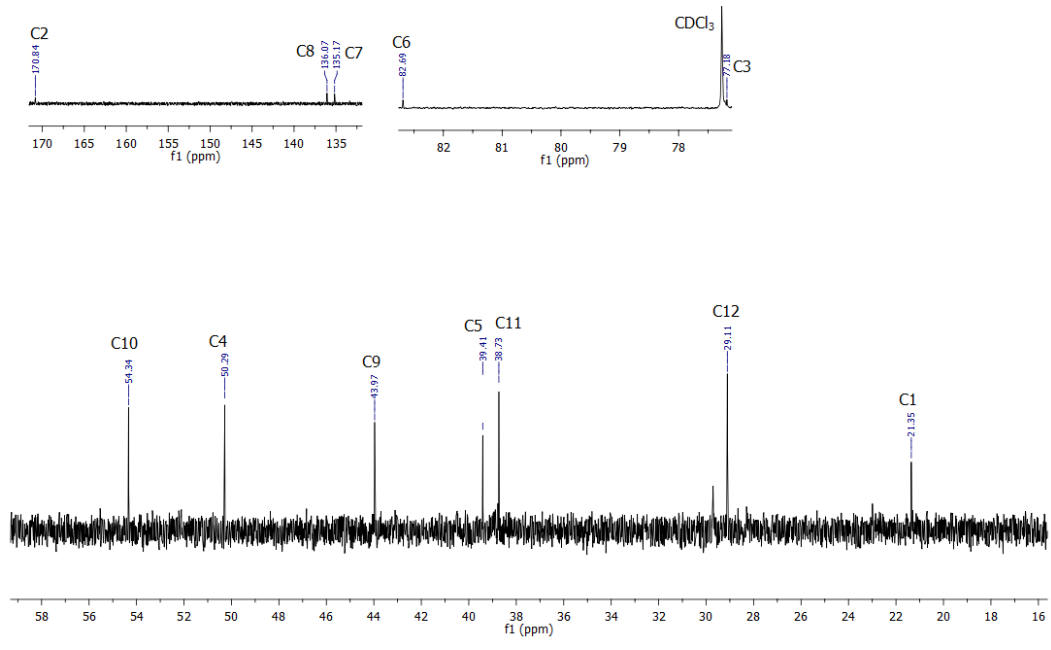

(b)

Figure C32: ^{1}H NMR (a) and ^{13}C NMR (b) spectrum spectrum of 6-hydroxy-verdyl acetate.

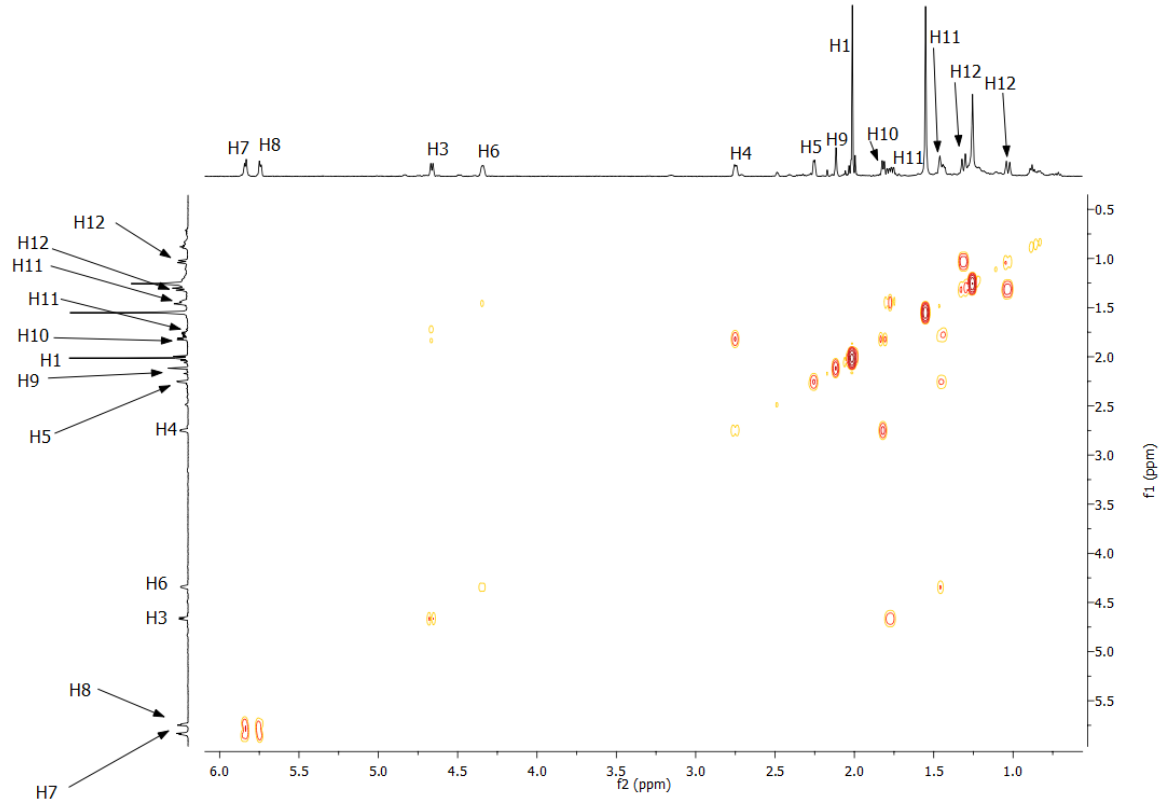

(a)

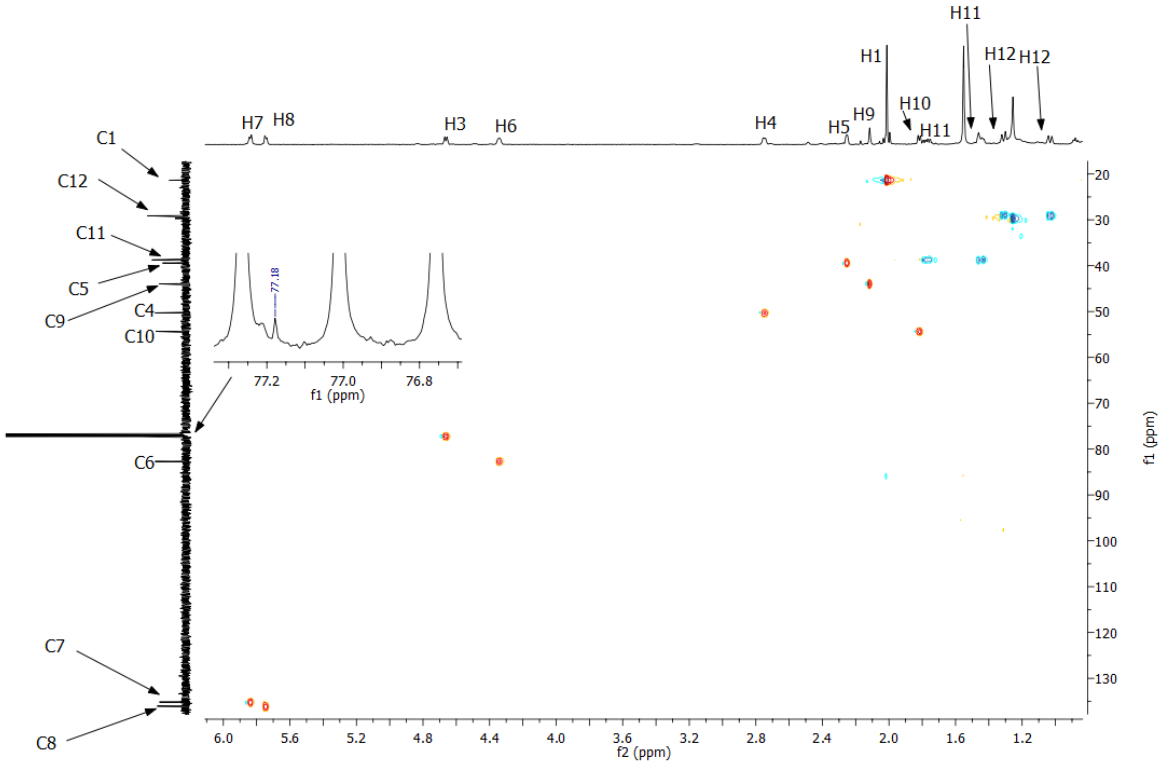

(b)

Figure C33: (a)^{1}H-^{1}H COSY and (b) ^{1}H-^{13}C HSQC NMR data for 6-hydroxy-verdyl acetate.

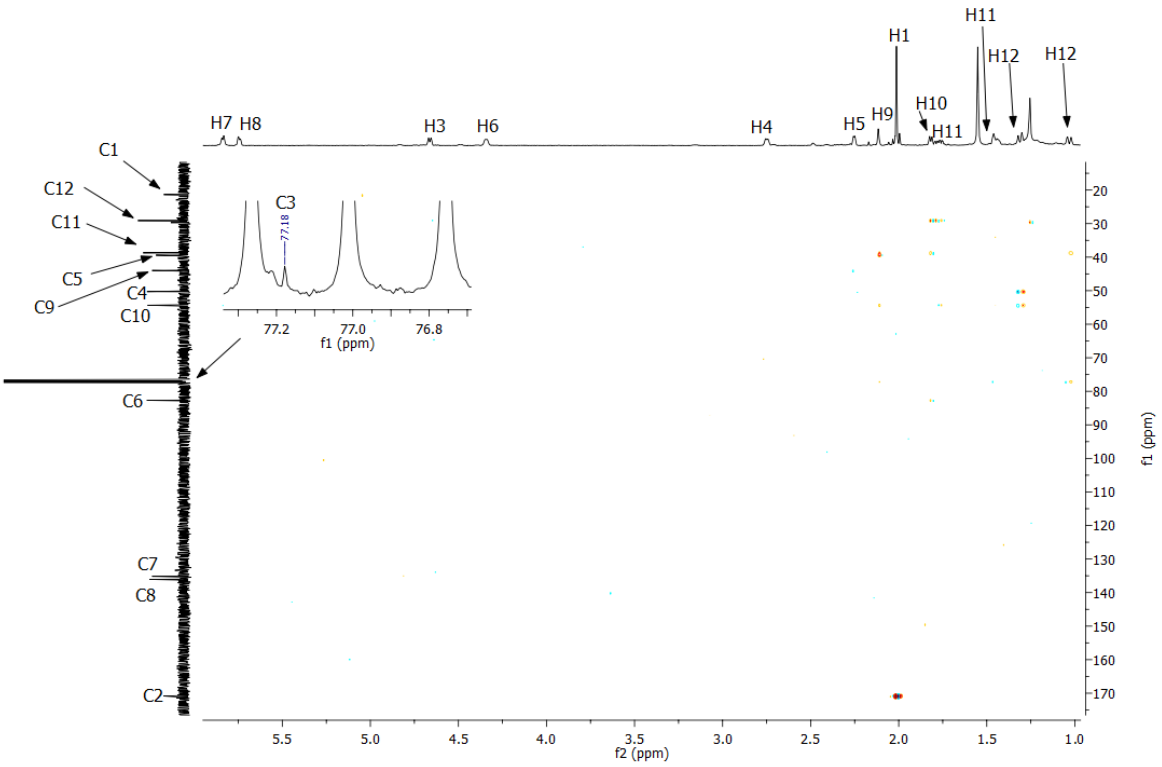

Figure C34: ^{1}H-^{13}C HMBC for 6-hydroxy-verdyl acetate.

Table C2: HMBC correlation data for 6-hydroxy verdyl acetate.

Position	δ_C (ppm)	δ_H (ppm)	HMBC Correlation Positions
11	38.73 (CH_2)	1.77 (ddd), 1.46 (m)	12, 10, 4
12	29.11 (CH_2)	1.31 (d), 1.03 (d)	11, 10
10	54.34 (CH)	1.81 (d)	9, 11, 12
9	43.94 (CH)	2.12 (s)	5, 10
5	39.41 (CH)	2.25 (d)	9
4	50.29 (CH)	2.75 (d)	11
1	21.35 (CH_3	2.01 (s)	2